

**EFFECT OF CHROMIUM CONTENT ON HEAT
TREATMENT BEHAVIOR AND ABRASIVE WEAR
RESISTANCE OF MULTI-ALLOYED WHITE CAST IRON**

Mr. Jatupon Opapaiboon



**A Dissertation Submitted in Partial Fulfillment of the Requirements
for the Degree of Doctor of Engineering in Metallurgical and Materials**

Engineering

Department of Metallurgical Engineering

Faculty of Engineering

Chulalongkorn University

Academic Year 2018

Copyright of Chulalongkorn University

ผลของปริมาณโครเมียมต่อพฤติกรรมของกรรมวิธีทางความร้อนและความต้านทานการสึกหรอ
แบบขัดสีของเหล็กหล่อขาวธาตุผสมหลายธาตุ



วิทยานิพนธ์นี้เป็นส่วนหนึ่งของการศึกษาตามหลักสูตรปริญญาวิศวกรรมศาสตรดุษฎีบัณฑิต
สาขาวิชาวิศวกรรมโลหการและวัสดุ ภาควิชาวิศวกรรมโลหการ
คณะวิศวกรรมศาสตร์ จุฬาลงกรณ์มหาวิทยาลัย
ปีการศึกษา 2561
ลิขสิทธิ์ของจุฬาลงกรณ์มหาวิทยาลัย

Thesis Title	EFFECT OF CHROMIUM CONTENT ON HEAT TREATMENT BEHAVIOR AND ABRASIVE WEAR RESISTANCE OF MULTI-ALLOYED WHITE CAST IRON
By	Mr. Jatupon Opapaiboon
Field of Study	Metallurgical and Materials Engineering
Thesis Advisor	Assistant Professor MAWIN SUPRADIST NA AYUDHAYA, Ph.D.
Thesis Co Advisor	Associate Professor Prasonk Sricharoenchai, D.Eng. Professor Yasuhiro Matsubara, Dr.Eng.

Accepted by the Faculty of Engineering, Chulalongkorn University in Partial Fulfillment of the Requirement for the Doctor of Engineering

..... Dean of the Faculty of Engineering
(Associate Professor SUPOT
TEACHAVORASINSKUN, D.Eng.)

DISSERTATION COMMITTEE

..... Chairman
(Professor GOBBOON LOTHONGKUM, Dr.Eng.)

..... Thesis Advisor
(Assistant Professor MAWIN SUPRADIST NA
AYUDHAYA, Ph.D.)

..... Thesis Co-Advisor
(Associate Professor Prasonk Sricharoenchai, D.Eng.)

..... Thesis Co-Advisor
(Professor Yasuhiro Matsubara, Dr.Eng.)

..... Examiner
(Associate Professor EKASIT NISARATANAPORN,
Ph.D.)

..... External Examiner
(Associate Professor Sudsakorn Inthidech, D.Eng.)

..... External Examiner
(Associate Professor Paritud Bhandhubanyong, D.Eng.)

จตุพล โอภาไพบูลย์ : ผลของปริมาณ โครเมียมต่อพฤติกรรมของกรรมวิธีทางความร้อนและความต้านทานการสึกหรอแบบขัดสีของเหล็กหล่อขาวธาตุผสมหลายธาตุ.

(EFFECT OF CHROMIUM CONTENT ON HEAT TREATMENT BEHAVIOR AND ABRASIVE WEAR RESISTANCE OF MULTI-ALLOYED WHITE CAST IRON) อ.ที่ปรึกษา

หลัก : ศศ. ดร.มาวิน สุประดิษฐ์ ณ อยู่ธยา, อ.ที่ปรึกษาร่วม : รศ. ดร.ประสงค์ ศรีเจริญชัย, ศ. ดร.ยาสุอิโร มัตสึบาระ

เพื่อตรวจสอบผลของปริมาณ โครเมียมต่อพฤติกรรมของกรรมวิธีทางความร้อนและความต้านทานการสึกหรอแบบขัดสีของเหล็กหล่อขาวธาตุผสมหลายธาตุที่มีส่วนประกอบทางเคมีพื้นฐาน ได้เตรียมเหล็กหล่อที่แปรผันปริมาณโครเมียมจาก 3-9% ได้ชุบแข็งชิ้นงานที่อบอ่อนจากอุณหภูมิ ออสเทนไนท์ 1323 เคลวินและ 1373 เคลวินแล้วอบคืนตัวที่อุณหภูมิ 673 เคลวินถึง 873 เคลวิน ด้วยช่วงห่าง 50 เคลวิน โครงสร้างจุลภาคของชิ้นงานแต่ละชิ้นประกอบด้วยเฟสโครต์ไพไรต์หรืออสเทนไนต์ (γ_p) กับยูเทกติก ($\gamma+MC$) และ ($\gamma+M_2C$) ในชิ้นงานที่มีปริมาณโครเมียม 3 และ 5% ในทางกลับกันยูเทกติก ($\gamma+M_7C_3$) ปรากฏในชิ้นงานที่มีปริมาณโครเมียม 6% และมากกว่า เนื้อพื้นในสภาพหล่อส่วนมากเป็นอสเทนไนต์เหลือค้าง แต่เนื้อพื้นในสภาพชุบแข็งประกอบด้วยคาร์ไบด์ทุติยภูมิที่ตกตะกอน มาร์เทนไซต์และอสเทนไนต์เหลือค้าง

ในส่วนพฤติกรรมของกรรมวิธีทางความร้อน ความแข็งในสภาพชุบแข็งเพิ่มขึ้นถึงค่าสูงสุดที่ปริมาณโครเมียม 5% และต่อมาลดลงตามปริมาณโครเมียมที่เพิ่มขึ้น สัดส่วนเชิงปริมาตรของอสเทนไนต์เหลือค้าง (V_γ) แสดงแนวโน้มเดียวกับความแข็ง อุณหภูมิออสเทนไนท์สูงกว่าทำให้ความแข็งต่ำกว่าแต่ค่า V_γ สูงกว่า ในสภาพอบคืนตัว ความแข็งและการแข็งขึ้นทุติยภูมิบ้างขึ้นกับอุณหภูมิออสเทนไนท์สูงและปริมาณโครเมียม ระดับของการแข็งขึ้นทุติยภูมิมีค่าสูงในชิ้นงานชุบแข็งจากอุณหภูมิออสเทนไนท์สูง ความแข็งอบคืนตัวสูงสุด (H_{Tmax}) ได้จากอุณหภูมิ 773 เคลวินถึง 798 เคลวินและอุณหภูมิออสเทนไนท์สูงให้ค่า H_{Tmax} ที่สูงกว่า ค่า V_γ ลดลงอย่างช้าๆเมื่ออุณหภูมิอบคืนตัวเพิ่มขึ้น ค่า V_γ ที่ H_{Tmax} มีค่าต่ำกว่า 5% ในชิ้นงานทุกชิ้น ค่าสูงสุดของ H_{Tmax} ได้จากชิ้นงานที่มีปริมาณโครเมียม 5% โดยไม่คำนึงถึงอุณหภูมิออสเทนไนท์สูง

ในส่วนความต้านทานการสึกหรอแบบขัดสี ได้ประเมินความต้านทานการสึกหรอแบบขัดสีชิ้นงานในสภาพชุบแข็ง (As-H) H_{Tmax} อุณหภูมิต่ำกว่าและสูงกว่า H_{Tmax} ($L-H_{Tmax}$ และ $H-H_{Tmax}$) โดยการทดสอบการสึกหรอแบบขัดสีซูเกะ (Suga) และการทดสอบการสึกหรอแบบขัดสีด้วยล้อ ความสัมพันธ์ระหว่างน้ำหนักที่สูญเสีย (W_l) และระยะการสึกหรอ (W_d) เป็นเส้นตรงในชิ้นงานทุกชิ้น อัตราการสึกหรอ (R_w) แปรผันขึ้นอยู่กับการสภาวะของกรรมวิธีทางความร้อนและปริมาณโครเมียม ได้ค่า R_w ค่าสุดในชิ้นงาน As-H และตามด้วยชิ้นงาน H_{Tmax} ค่า R_w สูงสุดในชิ้นงาน $L-H_{Tmax}$ หรือชิ้นงาน $H-H_{Tmax}$ โดยไม่คำนึงถึงปริมาณโครเมียมและอุณหภูมิออสเทนไนท์สูง ในการทดสอบการสึกหรอแบบขัดสีทั้ง 2 แบบค่า R_w ลดลงอย่างต่อเนื่องจนถึงปริมาณโครเมียม 6% หลังจากนั้นเพิ่มขึ้นอย่างช้าๆตามการเพิ่มขึ้นของปริมาณโครเมียม อุณหภูมิออสเทนไนท์สูงให้ค่า R_w ต่ำกว่าอุณหภูมิออสเทนไนท์ต่ำตลอดช่วงของปริมาณโครเมียม ค่า R_w ลดลงตามการเพิ่มขึ้นของความแข็ง ในช่วงที่ V_γ น้อยกว่า 5% ค่า R_w กระจายในช่วงกว้างขึ้นอยู่กับความแข็ง เมื่อค่า V_γ มากกว่า 5% ค่า R_w ลดลงอย่างต่อเนื่องตามการเพิ่มขึ้นของค่า V_γ ผิวที่สึกหรอประกอบด้วยเกิดการกัดกร่อน การครูดและการเกิดรอยร้าวในชิ้นงานทุกชิ้น ได้พบการเกิดรอยร้าวในบริเวณยูเทกติกในขณะที่ได้ตรวจพบการกัดกร่อนและการครูดในเนื้อพื้น

สาขาวิชา วิศวกรรมโลหการและวัสดุ
ปีการศึกษา 2561

ลายมือชื่อนิสิต
ลายมือชื่อ อ.ที่ปรึกษาหลัก
ลายมือชื่อ อ.ที่ปรึกษาร่วม
ลายมือชื่อ อ.ที่ปรึกษาร่วม

5871402421 : MAJOR METALLURGICAL AND MATERIALS ENGINEERING

KEYWORD: MULTI-ALLOYED WHITE CAST IRON, HEAT TREATMENT, HARDNESS,
VOLUME FRACTION OF RETAINED AUSTENITE, ABRASIVE WEAR
RESISTANCE, CHROMIUM EFFECT

Jatupon Opapaiboon : EFFECT OF CHROMIUM CONTENT ON HEAT
TREATMENT BEHAVIOR AND ABRASIVE WEAR RESISTANCE OF MULTI-
ALLOYED WHITE CAST IRON. Advisor: Asst. Prof. MAWIN SUPRADIST NA
AYUDHAYA, Ph.D. Co-advisor: Assoc. Prof. Prasonk Sricharoenchai, D.Eng., Prof.
Yasuhiro Matsubara, Dr.Eng.

The effect of Cr content on heat treatment behavior and abrasive wear resistance of multi-alloyed white cast irons with basic composition was investigated. The cast irons with varying Cr content from 3-9% were prepared. The annealed specimens were hardened from 1323K and 1373K austenitizing and then, tempered at 673K to 873K with 50K intervals. The microstructure of each specimen consisted of primary austenite dendrite (γ_p) and ($\gamma+MC$) and ($\gamma+M_2C$) eutectics in specimens with 3 and 5%Cr. By contrast, ($\gamma+M_7C_3$) eutectic appeared in specimens with 6%Cr and more. The matrix in as-cast state was mostly retained austenite but that in as-hardened specimens composed of precipitated secondary carbide, martensite and retained austenite.

As for heat treatment behavior, hardness in as-hardened state increased to highest value at 5%Cr and subsequently, decreased as Cr content rose. The volume fraction of retained austenite (V_g) displayed similar trend to the hardness. The higher austenitizing temperature contributed to lower the hardness but increase the V_g values. In the tempered state, the hardness showed more or less secondary hardening depending on austenitizing temperature and Cr content. The degree of secondary hardening was greater in the specimen hardened from higher austenitizing temperature. The maximum tempered hardness (H_{Tmax}) was obtained at 773K to 798K tempering and high austenitizing temperature offered higher H_{Tmax} . The V_g decreased gradually as the tempering temperature was elevated. The V_g value at H_{Tmax} was less than 5% in all the specimens. The highest value of H_{Tmax} was obtained in 5%Cr specimen regardless of austenitizing temperature.

In order to evaluate the abrasive wear resistance, the as-hardened (As-H), H_{Tmax} , lower and higher than H_{Tmax} ($L-H_{Tmax}$ and $H-H_{Tmax}$) specimens were evaluated using Suga abrasion test and rubber wheel abrasion test. A linear relation between wear loss (W_l) and wear distance (W_d) was obtained in all the specimens. The wear rate (R_w) varied depending on heat treatment condition and Cr content. The lowest R_w value or highest wear resistance was obtained in the As-H specimen followed by H_{Tmax} specimen. The highest R_w value or lowest abrasive wear resistance was obtained in $L-H_{Tmax}$ or $H-H_{Tmax}$ specimen, regardless of Cr content and austenitizing temperature. In both abrasive wear tests, the R_w decreased continuously until 6%Cr and after that, it increased gradually with a rise of Cr content. The high austenitizing temperature provided lower R_w value than low austenitizing temperature in all range of Cr content. The R_w decreased with an increase in hardness. In the region of V_g less than 5%, the R_w values scattered in a wide range depending on the hardness. When the V_g got over 5%, the R_w value decreased continuously increasing of V_g value. The worn surface consisted of grooving, scratching and pitting in all the specimens. The pitting was found in eutectic area while the grooving and scratching were observed in matrix.

Field of Study:	Metallurgical and Materials Engineering	Student's Signature
Academic Year:	2018	Advisor's Signature
		Co-advisor's Signature
		Co-advisor's Signature

ACKNOWLEDGEMENTS

First of all, I would like to thank my thesis advisor, Assistant Professor Mawin Supradist Na Ayuthaya for his kind advice and caring about the scholarship. I also thank Associate Professor Prasonk Srichareonchai, who has given me a great opportunity to join in the collaboration group of Professor Yasuhiro Matsubara at National Institute of Technology, Kurume College.

This research could not have done without supporting and guidance by many people. I would like to express extreme appreciation to my thesis co-advisor, Professor Yasuhiro Matsubara, for his kindness, guidance and valuable comments since the first until the last year. I would like to thank Associate Professor Sudsakorn Inthidech for his guidance and support since I started my experiment at Faculty of Engineering, Mahasarakham University. I would also like to appreciate Professor Nobuya Sasaguri and Professor Kaoru Yamamoto from the Department of Materials Science and Engineering of National Institute of Technology, Kurume College, for their advice and taking care of me during my staying and working there. Moreover, I truly thank to Mr.Kiyoshi Nanjo, technician of Cast Metals Laboratory, for his lessons to use equipments in the laboratory which I was supposed to avail experiments in Japan.

I would like to thank Dr.Yuzo Yokomizo, Director of Kawara Steel Works Co.,Ltd., for his helping to cast my specimens. I also thank Mr.Masaki Isobe, Managing Director of Isobe Iron Works Co., Ltd., for providing rubber wheel abrasive wear test.

I appreciate to Graduate School, Chulalongkorn University, for scholarship “The 100th Anniversary Chulalongkorn University Fund for Doctoral Student” and “Overseas Research Experience Scholarship for Graduate Student”.

Finally, I would like to express my appreciation to my family for their affording and supporting with economic assistance since I decided to study the doctoral course. I could not carry out whole works without their encouragement.

Jatupon Opaiboon

TABLE OF CONTENTS

	Page
ABSTRACT (THAI)	iii
ABSTRACT (ENGLISH)	iv
ACKNOWLEDGEMENTS	v
TABLE OF CONTENTS	vi
LIST OF TABLES	x
LIST OF FIGURES	xii
Chapter I Introduction	1
1.1 Background	1
1.2 Objectives	5
1.3 Scopes of research	5
1.4 Advantages of research	6
Chapter II Literature Reviews	7
2.1 History of wear resistant materials	7
2.2 Alloy designing	9
2.3 Type and morphology of carbides in multi-alloyed white cast iron	14
2.3.1 Effect of alloying elements on type and morphology of carbide	19
2.3.2 Influence of solidification rate on type and morphology of carbide	23
2.4 Solidification sequence of multi-alloyed white cast iron	24
2.5 Matrix of multi-alloyed white cast iron	27
2.6 Matrix transformation of multi-alloyed white cast iron	28
2.7 Heat treatment of multi-alloyed white cast iron	29
2.8 Abrasive wear resistance	31
2.9 Abrasive wear resistance of alloyed white cast irons	34
Chapter III Experimental Procedures	42
3.1 Preparation of test specimens	42

3.2 Heat treatment process.....	46
3.2.1 Heat treatment condition to investigate heat treatment behavior	46
3.2.2 Heat treatment condition of test piece to perform carry out abrasive .. wear test	47
3.3 Observation of microstructure	49
3.3.1 Optical microscope (OM).....	49
3.3.2 Scanning electron microscope (SEM)	50
3.4 Hardness measurement	50
3.5 Measurement of volume fraction of austenite	50
3.6 Abrasive wear test.....	54
3.6.1 Mechanism of abrasive wear	54
3.6.2 Preparation of surface of wear test piece.....	55
3.6.3 Suga abrasive wear tester	56
3.6.4 Rubber wheel abrasive wear tester.....	57
Chapter IV Experimental Results	60
4.1 Microstructures of specimens in as-cast state.....	60
4.1.1 Effect of Cr content on as-cast microstructure.....	60
4.1.2 Effect of Cr content on amount of primary austenite (γ_P) and eutectic structures	64
4.1.3 Effect of Cr content on macro- and micro-hardness in as-cast state	67
4.2 Effect of Cr content on heat treatment behavior.....	68
4.2.1 Relationship between heat treatment condition and variation of matrix structure	68
4.2.1.1 As-hardened state	68
4.2.2 Relationship between macro-hardness and volume fraction of retained austenite (V_γ)	75
4.2.2.1 As-hardened state	75
4.2.2.2 Tempered state.....	77
4.3 Effect of Cr content and heat treatment conditions on abrasive wear resistance	85

4.3.1 Suga abrasive wear test (two-body-type).....	89
4.3.1.1 Wear test results of specimens tempered after hardening from 1323K austenitizing.....	90
4.3.1.2 Wear test results of specimens tempered after hardening from 1373K austenitizing.....	97
4.3.2 Rubber wheel abrasive wear test (three-body-type).....	105
4.3.2.1 Wear test results of specimens tempered after hardening from 1323K austenitizing.....	106
4.3.2.2 Wear test results of specimens tempered after hardening from 1373K austenitizing.....	113
Chapter V Discussions.....	121
5.1 Effect of Cr content on heat treatment behavior.....	121
5.1.1 Effect of Cr content on hardness and volume fraction of retained austenite (V_γ).....	121
5.1.1.1 As-hardened state.....	121
5.1.1.2 Tempered state.....	127
5.1.1.2.1 Relationship between hardness and tempering temperature.....	127
5.1.1.2.2 Relationship between hardness and volume fraction of retained austenite (V_γ) in tempered state....	135
5.1.2 Variation of maximum tempered hardness (H_{Tmax}), volume fraction of retained austenite (V_γ) and Cr content.....	140
5.1.2.1 Effect of Cr content on maximum tempered hardness (H_{Tmax}) and volume fraction of retained austenite at H_{Tmax} ($V_{\gamma-H_{Tmax}}$).....	140
5.1.2.2 Relationship between maximum tempered hardness (H_{Tmax}) and volume fraction of retained austenite (V_γ).....	145
5.1.3 Degree of secondary hardening (ΔH_s).....	148
5.1.3.1 Effect of Cr content on degree of secondary hardening (ΔH_s) ..	149
5.1.3.2 Effect of volume fraction of retained austenite (V_γ) in as-hardened state on degree of secondary hardening (ΔH_s).....	151
5.1.3.3 Relationship between maximum tempered hardness (H_{Tmax}) and degree of secondary hardening (ΔH_s).....	153

5.2 Abrasive wear resistance	155
5.2.1 Severity of abrasive wear between Suga and rubber wheel abrasive wear tests.....	155
5.2.2 Effect of Cr content on wear rate (R_w).....	157
5.2.3 Effect of macro-hardness on wear rate (R_w).....	164
5.2.4 Relationship between wear rate (R_w) and volume fraction of retained austenite (V_γ) in heat-treated state.....	168
5.2.5 Observation of worn surface	178
Chapter VI Conclusions.....	192
6.1 Effect of Cr content on heat treatment behavior.....	192
6.1.1 Effect of Cr content on microstructure.....	192
6.1.1.1 As-cast state.....	192
6.1.1.2 As-hardened state	193
6.1.2 Effect of Cr content on hardness and volume fraction of retained austenite (V_γ)	193
6.1.2.1 As-hardened state	193
6.1.2.2 Tempered state.....	194
6.2 Effect of Cr content on abrasive wear behavior	195
6.2.1 Behavior of abrasive wear.....	196
6.2.2 Observation of worn surface	197
REFERENCES	198
Appendix.....	206
VITA.....	221

LIST OF TABLES

	Page
Table 2-1 Hardness of carbides and matrix phases of multi-alloyed white cast iron ..	10
Table 2-2 Alloy concentration in carbides and matrix of multi-alloyed white cast iron with basic chemical composition	15
Table 2-3 Solidification sequence of multi-alloyed white cast irons with several chemical compositions.....	26
Table 2-4 Hardness of some abrasive materials and matrix phase	33
Table 3-1 Chemical composition of charge materials	43
Table 3-2 Target chemical compositions of test specimens	44
Table 3-3 Chemical compositions of the ingot	44
Table 3-4 Conditions of heat treatment	46
Table 3-5 Heat treatment conditions.....	48
Table 3-6 Etchant, etching method and observation point	49
Table 3-7 X-ray diffraction conditions for measurement of volume fraction of retained austenite (V_{γ})	53
Table 3-8 Test condition for Rubber wheel abrasive wear test	59
Table 4-1 Area fractions of primary austenite (γ_P) and eutectic structures	65
Table 4-2 Macro- and micro-hardness of as-cast specimens.....	67
Table 4-3 Macro-, micro-hardness and volume fraction of retained austenite (V_{γ}) of as-hardened specimens.....	75
Table 4-4 Selected tempering temperatures for $L-H_{T_{max}}$, $H_{T_{max}}$ and $H-H_{T_{max}}$ in each specimen	86

Table 4-5 Macro-hardness and volume fraction of retained austenite (V_γ) of heat-treated test pieces for abrasive wear test. Austenitizing : 1323K	87
Table 4-6 Macro-hardness and volume fraction of retained austenite (V_γ) of heat-treated test pieces for abrasive wear test. Austenitizing : 1373K	88
Table 4-7 Total wear losses at wear distance of 192 m of specimens hardened from 1323K and tempered. Suga abrasive wear test under a load of 9.8N (1 kgf)	89
Table 4-8 Wear rates (R_w) of specimens hardened from 1323K and tempered. Suga abrasive wear test under a load of 9.8N (1 kgf)	97
Table 4-9 Wear rates (R_w) of specimens hardened from 1373K and tempered. Suga abrasive wear test under a load of 9.8N (1 kgf)	105
Table 4-10 Wear rates (R_w) of specimens hardened from 1323K and tempered. Rubber wheel abrasive wear test under a load of 85.3N (8.7 kgf). Austenitizing : 1323K.....	113
Table 4-11 Wear rates (R_w) of specimens hardened from 1323K and tempered. Rubber wheel abrasive wear test under a load of 85.3N (8.7 kgf). Austenitizing : 1373K.....	119
Table 5-1 The difference in hardness between macro-hardness and micro-hardness in tempered state	133
Table 5-2 Degree of secondary hardening (ΔH_s) of tempered specimens.....	149
Table 5-3 Wear loss per unit area of 5%Cr specimen with different heat treatment condition (Hardening : 1373K austenitizing)	157
Table 5-4 Micro-hardness of matrix in heat-treated specimens used for abrasive wear test.....	164

LIST OF FIGURES

	Page
Fig.1-1 The transition of alloyed white cast iron for rolling and pulverizing mill rolls	2
Fig.2-1 Trend of materials and manufacturing processes of rolls	8
Fig.2-2 Comparison of deeply etched microstructures of M_3C eutectic carbides in the as-cast state of cast iron 5%Cr-3.6%C and M_7C_3 eutectic carbides in the as-cast state of cast iron 30%Cr-2.4%C	11
Fig.2-3 The schematic drawing of discontinuous eutectic M_7C_3 carbides	11
Fig.2-4 Comparison of two-dimensional and three-dimensional microstructures of MC carbide in multi-alloyed white cast iron by OM and SEM.....	16
Fig.2-5 Comparison of two-dimensional and three-dimensional microstructures of M_2C carbide in multi-alloyed white cast iron by OM and SEM.....	17
Fig.2-6 Comparison of two-dimensional and three-dimensional microstructures of M_7C_3 carbide in multi-alloyed white cast iron by OM and SEM	18
Fig.2-7 Influence of V and C contents on type and morphology of carbides crystallized from the melt of multi-alloyed white cast iron.....	20
Fig.2-8 Influence of W_{eq} value and C content on type and morphology of carbides crystallized from the melt of multi-alloyed white cast iron.....	21
Fig.2-9 Influence of Co and C contents on type and morphology of carbides crystallized from the melt of multi-alloyed white cast iron.....	22

Fig.2-10 Type of carbide corresponding to solidification rate and C content	23
Fig.2-11 Solidification of multi-alloyed white cast iron with basic chemical composition (Fe-5%Cr-5%Mo-5%W-5%V-5%Co-2%C).....	25
Fig.2-12 Quasi-binary section diagram of multi-alloyed white cast iron with alloy system of M (Fe-5%Cr-5%Mo-5%W-5%V-5%Co)-C.....	27
Fig.2-13 CCT diagrams of multi-alloyed white cast iron with different C contents in basic chemical composition (Fe-5%Cr-5%Mo-5%W-5%V-2%Co-C alloys).....	29
Fig.2-14 Tempered hardness curve and variation of volume fraction of retained austenite (V_γ) of multi-alloyed white cast iron with basic chemical composition.....	30
Fig.2-15 Schematic drawing of wearing of cast iron with too small carbides (a), carbides in effective size (b) and continuous carbides (c).....	31
Fig.2-16 Classification of abrasive wear	32
Fig.2-17 Effect of carbide volume fraction on (a) hardness and (b) volume wear rate of high Cr white cast irons.....	35
Fig.2-18 Relationship between wear loss and testing time of multi-alloyed white cast iron in Fe-M-C alloys in (a) as-cast, (b) as-hardened and (c) hardened-tempered states. ($M_{No.1}$: 9.95%Cr-0.01%V-5.14%Mo-4.87%W, $M_{No.2}$: 0.04%Cr-10.21%V-5.21%Mo-4.84%W and $M_{No.3}$: 17.54%Cr-3.14%V-0.01%Mo-0.02%W)	36
Fig.2-19 Effect of Co content on wear rate (R_w) of multi-alloyed white cast irons heat-treated with different conditions	37
Fig.2-20 Effect of tempering temperature on wear rate (R_w) of multi-alloyed white cast irons heat-treated with different Cr content.....	38

Fig.2-21 Effect of alloying elements content on hot abrasive wear resistance of multi-alloyed white cast iron with the basic chemical composition in relations of C and another carbide formers of V, Cr, Mo and W	40
Fig.2-22 Relationship between wear depth and wear load of conventional rolls and CPC type roll made of multi-alloyed white cast iron	41
Fig.3-1 Schematic drawing of CO ₂ mold for round-bar ingot	45
Fig.3-2 Schematic drawings of processes for making test pieces of abrasive wear tests from ingots	45
Fig.3-3 Schematic illustration showing how to determine three tempering temperatures from tempered hardness curve	48
Fig.3-4 Schematic drawing of model showing abrasive wear by single grit with cone shape [49].....	54
Fig.3-5 Schematic drawing of Suga abrasive wear tester	57
Fig.3-6 Photo and schematic drawing of rubber wheel abrasive wear tester.....	58
Fig.4-1 Microstructures of as-cast specimens with different Cr contents	63
Fig.4-2 Effect of Cr content on area fraction of primary austenite and eutectic structures	66
Fig.4-3 Matrix microstructures of as-hardened specimens with different Cr contents. Austenitizing : 1323K.....	71
Fig.4-4 Matrix microstructures of as-hardened specimens with different Cr contents. Austenitizing : 1373K.....	74

Fig.4-5 Relationship between macro-hardness, volume fraction of retained austenite (V_{γ}) and tempering temperature of specimen No.1. Austenitizing : (a) 1323K and (b) 1373K.....	79
Fig.4-6 Relationship between macro-hardness, volume fraction of retained austenite (V_{γ}) and tempering temperature of specimen No.2. Austenitizing : (a) 1323K and (b) 1373K.....	80
Fig.4-7 Relationship between macro-hardness, volume fraction of retained austenite (V_{γ}) and tempering temperature of specimen No.3. Austenitizing : (a) 1323K and (b) 1373K.....	81
Fig.4-8 Relationship between macro-hardness, volume fraction of retained austenite (V_{γ}) and tempering temperature of specimen No.4. Austenitizing : (a) 1323K and (b) 1373K.....	83
Fig.4-9 Relationship between macro-hardness, volume fraction of retained austenite (V_{γ}) and tempering temperature of specimen No.5. Austenitizing : (a) 1323K and (b) 1373K.....	84
Fig.4-10 Relationship between wear loss (W_l) and wear distance (W_d) of specimen No.1 with 3%Cr hardened from 1323K austenitizing. Suga abrasive wear test under a load of 9.8N (1 kgf)	91
Fig.4-11 Relationship between wear loss (W_l) and wear distance (W_d) of specimen No.2 with 5%Cr hardened from 1323K austenitizing. Suga abrasive wear test under a load of 9.8N (1 kgf)	92

Fig.4-12 Relationship between wear loss (W_1) and wear distance (W_d) of specimen No.3 with 6%Cr hardened from 1323K austenitizing. Suga abrasive wear test under a load of 9.8N (1 kgf)	94
Fig.4-13 Relationship between wear loss (W_1) and wear distance (W_d) of specimen No.4 with 7%Cr hardened from 1323K austenitizing. Suga abrasive wear test under a load of 9.8N (1 kgf)	95
Fig.4-14 Relationship between wear loss (W_1) and wear distance (W_d) of specimen No.5 with 9%Cr hardened from 1323K austenitizing. Suga abrasive wear test under a load of 9.8N (1 kgf)	96
Fig.4-15 Relationship between wear loss (W_1) and wear distance (W_d) of specimen No.1 with 3%Cr hardened from 1373K austenitizing. Suga abrasive wear test under a load of 9.8N (1 kgf)	99
Fig.4-16 Relationship between wear loss (W_1) and wear distance (W_d) of specimen No.2 with 5%Cr hardened from 1373K austenitizing. Suga abrasive wear test under a load of 9.8N (1 kgf)	100
Fig.4-17 Relationship between wear loss (W_1) and wear distance (W_d) of specimen No.3 with 6%Cr hardened from 1373K austenitizing. Suga abrasive wear test under a load of 9.8N (1 kgf)	101
Fig.4-18 Relationship between wear loss (W_1) and wear distance (W_d) of specimen No.4 with 7%Cr hardened from 1373K austenitizing. Suga abrasive wear test under a load of 9.8N (1 kgf)	103

Fig.4-19 Relationship between wear loss (W_1) and wear distance (W_d) of specimen No.5 with 9%Cr hardened from 1373K austenitizing. Suga abrasive wear test under a load of 9.8N (1 kgf)	104
Fig.4-20 Relationship between wear loss (W_1) and wear distance (W_d) of specimen No.1 with 3%Cr hardened from 1323K. Rubber wheel abrasive wear test under a load of 85.3N (8.7 kgf)	107
Fig.4-21 Relationship between wear loss (W_1) and wear distance (W_d) of specimen No.2 with 5%Cr hardened from 1323K. Rubber wheel abrasive wear test under a load of 85.3N (8.7 kgf)	108
Fig.4-22 Relationship between wear loss (W_1) and wear distance (W_d) of specimen No.3 with 6%Cr hardened from 1323K. Rubber wheel abrasive wear test under a load of 85.3N (8.7 kgf)	110
Fig.4-23 Relationship between wear loss (W_1) and wear distance (W_d) of specimen No.4 with 7%Cr hardened from 1323K. Rubber wheel abrasive wear test under a load of 85.3N (8.7 kgf)	111
Fig.4-24 Relationship between wear loss (W_1) and wear distance (W_d) of specimen No.5 with 9%Cr hardened from 1323K. Rubber wheel abrasive wear test under a load of 85.3N (8.7 kgf)	112
Fig.4-25 Relationship between wear loss (W_1) and wear distance (W_d) of specimen No.1 with 3%Cr hardened from 1373K. Rubber wheel abrasive wear test under a load of 85.3N (8.7 kgf)	114

Fig.4-26 Relationship between wear loss (W_l) and wear distance (W_d) of specimen No.2 with 5%Cr hardened from 1373K. Rubber wheel abrasive wear test under a load of 85.3N (8.7 kgf)	116
Fig.4-27 Relationship between wear loss (W_l) and wear distance (W_d) of specimen No.3 with 6%Cr hardened from 1373K. Rubber wheel abrasive wear test under a load of 85.3N (8.7 kgf)	117
Fig.4-28 Relationship between wear loss (W_l) and wear distance (W_d) of specimen No.4 with 7%Cr hardened from 1373K. Rubber wheel abrasive wear test under a load of 85.3N (8.7 kgf)	118
Fig.4-29 Relationship between wear loss (W_l) and wear distance (W_d) of specimen No.5 with 9%Cr hardened from 1373K. Rubber wheel abrasive wear test under a load of 85.3N (8.7 kgf)	120
Fig.5-1 Relationship between micro-hardness and Cr content of as-hardened specimens.....	122
Fig.5-2 Relationship between macro-hardness, volume fraction of retained austenite (V_γ) and Cr content of as-hardened specimens.....	123
Fig.5-3 Relationship between micro-hardness and volume fraction of retained austenite (V_γ) of as-hardened specimens	126
Fig.5-4 Relationship between macro-hardness, micro-hardness and tempering temperature of 3%Cr specimens. Austenitizing : (a) 1323K and (b) 1373K.....	128
Fig.5-5 Relationship between macro-hardness, micro-hardness and tempering temperature of 5%Cr specimens. Austenitizing : (a) 1323K and (b) 1373K.....	129

Fig.5-6 Relationship between macro-hardness, micro-hardness and tempering temperature of 6%Cr specimens. Austenitizing : (a) 1323K and (b) 1373K.....	130
Fig.5-7 Relationship between macro-hardness, micro-hardness and tempering temperature of 7%Cr specimens. Austenitizing : (a) 1323K and (b) 1373K.....	131
Fig.5-8 Relationship between macro-hardness, micro-hardness and tempering temperature of 9%Cr specimens. Austenitizing : (a) 1323K and (b) 1373K.....	132
Fig.5-9 Relationship between hardness and volume fraction of retained austenite (V_γ) in tempered state. (a) Macro-hardness and (b) Micro-hardness	136
Fig.5-10 Relationship between micro-hardness and tempering temperature of tempered specimens with volume fraction of retained austenite (V_γ) less than 2% ..	139
Fig.5-11 Relationship between maximum tempered hardness (H_{Tmax}), volume fraction of retained austenite at H_{Tmax} ($V_{\gamma-H_{Tmax}}$) and Cr content.....	141
Fig.5-12 SEM microphotographs of specimens with H_{Tmax} . Austenitizing : 1323K.	145
Fig.5-13 Relationship between maximum tempered hardness (H_{Tmax}) and volume fraction of retained austenite at H_{Tmax} ($V_{\gamma-H_{Tmax}}$).....	146
Fig.5-14 Relationship between maximum tempered hardness (H_{Tmax}) and volume fraction of retained austenite (V_γ) in as-hardened state	147
Fig.5-15 Relationship between degree of secondary hardening (ΔH_s) and Cr content	150
Fig.5-16 Relationship between degree of secondary hardening (ΔH_s) and volume fraction of retained austenite (V_γ) in as-hardened state	151

Fig.5-17 Relationship between degree of secondary hardening (ΔH_s) and difference between volume fraction of retained austenite in as-hardened state and that at H_{Tmax} ($\Delta V_{\gamma-H_{Tmax}}$)	152
Fig.5-18 Relationship between maximum tempered hardness (H_{Tmax}) and degree of secondary hardening (ΔH_s).....	154
Fig.5-19 Cross-sectional structure of SiC abrasive paper fixed on aluminum wheel in Suga abrasive wear test.....	155
Fig.5-20 Schematic explanation of wear mechanism by rubber wheel abrasive wear test.....	156
Fig.5-21 Relationship between wear rate (R_w) and Cr content of specimens by Suga abrasive wear test. Load : 9.8N (1 kgf).....	159
Fig.5-22 Relationship between wear rate (R_w) and Cr content of specimens by rubber wheel abrasive wear test. Load : 85.3N (8.7 kgf)	161
Fig.5-23 Relationship between wear rate (R_w) and macro-hardness of specimens for Suga abrasive wear test.....	165
Fig.5-24 Relationship between wear rate (R_w) and macro-hardness of specimens for rubber wheel abrasive wear test.....	165
Fig.5-25 Relationship between wear rate (R_w) and volume fraction of retained austenite (V_γ) of all the specimens (Suga abrasive wear test)	169
Fig.5-26 Relationship between wear rate (R_w) and volume fraction of retained austenite (V_γ) of all the specimens (Rubber wheel abrasive wear test).....	169

Fig.5-27 Relationship between wear rate (R_w) and macro-hardness of specimens with volume fraction of retained austenite (V_γ) less than 5% (Suga abrasive wear test) ..	170
Fig.5-28 Relationship between wear rate (R_w) and macro-hardness of specimens with volume fraction of retained austenite (V_γ) less than 5% (Rubber wheel abrasive wear test).....	172
Fig.5-29 Relationship between wear rate (R_w) and volume fraction of retained austenite (V_γ) in as-hardened state (Suga abrasive wear test).....	173
Fig.5-30 Relationship between wear rate (R_w) and volume fraction of retained austenite (V_γ) in as-hardened state (Rubber wheel abrasive wear test)	173
Fig.5-31 Relationship between wear rate (R_w) and volume fraction of retained austenite at H_{Tmax} ($V_{\gamma-HTmax}$) (Suga abrasive wear test)	175
Fig.5-32 Relationship between wear rate (R_w) and volume fraction of retained austenite at H_{Tmax} ($V_{\gamma-HTmax}$) (Rubber wheel abrasive wear test).....	175
Fig.5-33 Relationship between volume fraction of retained austenite (V_γ) and distance from surface of specimen No.3 in as-hardened state for (a) Suga and (b) rubber wheel abrasive wear tests (Austenitizing: 1373K)	177
Fig.5-34 SEM microphotographs of worn surface after Suga abrasive wear test in 3%Cr specimen hardened from 1373K austenitizing	181
Fig.5-35 SEM microphotographs of worn surface after Suga abrasive wear test in 6%Cr specimen hardened from 1373K austenitizing	183
Fig.5-36 SEM microphotographs of worn surface after Suga abrasive wear test in 9%Cr specimen hardened from 1373K austenitizing	185

- Fig.5-37 SEM microphotographs of worn surface after rubber wheel abrasive wear test in 3%Cr specimen hardened from 1373K austenitizing..... 187
- Fig.5-38 SEM microphotographs of worn surface after rubber wheel abrasive wear test in 6%Cr specimen hardened from 1373K austenitizing..... 189
- Fig.5-39 SEM microphotographs of worn surface after rubber wheel abrasive wear test in 9%Cr specimen hardened from 1373K austenitizing..... 191



Chapter I

Introduction

1.1 Background

Alloyed white cast irons have been widely used more than a century as parts and components of machines in steel, cement, mining industries and thermal power plants. The surface of such machine is worn by hard abrasive materials under the services. Therefore, alloyed white cast irons with high hardness and good resistance to abrasive wear have been developed.

The transition of alloyed white cast irons as roll materials in rolling and pulverizing mills is shown in Fig.1-1. The first composition starts with low-alloyed white irons. However, the toughness and abrasive wear resistance are quite low due to the precipitation of ledeburite as eutectic in continuous network configuration and pearlite matrix. Therefore, the low-alloyed white iron was replaced by Ni-hard cast iron which contains more Cr and additional Ni. The wear resistance of Ni-hard cast iron is greatly improved because the Cr and Ni prevent the matrix from pearlite transformation and promote martensite transformation in the as-cast matrix. However, the toughness was not improved because the morphology of eutectic carbide cannot be modified. In 1970's, an outstanding development of abrasive wear resistance was carried out in the cast iron with a large amount of Cr that is called as high Cr cast iron. In the cast iron, the excellent performances of abrasive wear resistance as well as good heat and corrosion resistance were obtained. Even so, a large volume fraction of eutectic carbide or ledeburite in high Cr cast iron tends to reduce the toughness. In order to improve the quality or performance, a new type of alloyed white cast iron

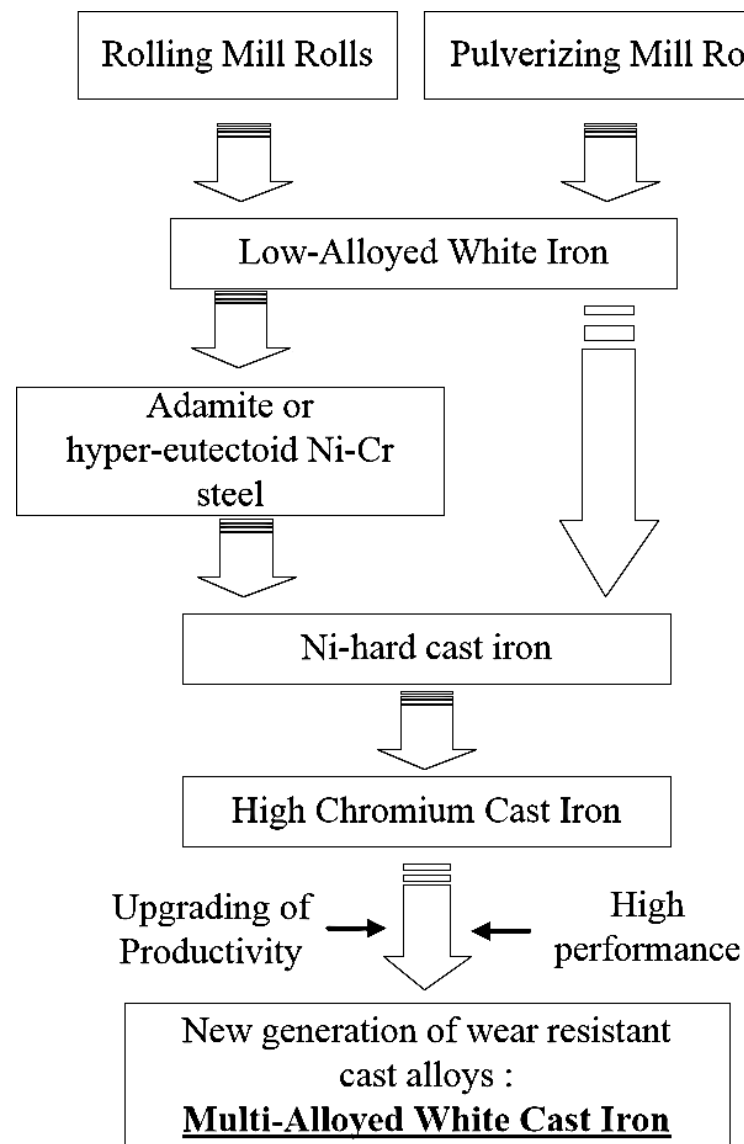


Fig.1-1 The transition of alloyed white cast iron for rolling and pulverizing mill rolls

[1].

with high toughness and considerable wear resistance has been developed and it was named as “multi-alloyed white cast iron”.

The multi-alloyed white cast irons contain strong carbide forming elements such as chromium (Cr), molybdenum (Mo), tungsten (W) and vanadium (V). These elements combine with carbon (C) to form MC, M₂C, M₆C, M₇C₃ and M₂₃C₆

carbides with extremely high hardness. Besides, the alloying elements dissolved in the matrix promoted the secondary hardening by precipitation of carbides during heat treatment. The basic alloy composition of multi-alloyed white cast irons contains 5 mass% (hereafter shown by %) for each element of Cr, Mo, W and V [1, 2]. Moreover, cobalt (Co) was added to improve high temperature properties. It was reported that the rolls made by multi-alloyed white cast iron showed much higher quality and longer service life than that made of high Cr white cast iron [1, 3, 4].

It is known that the Cr is a strong carbide former and improves hardness as well as abrasive wear resistance in high Cr cast iron. This is because Cr combines with C to form hard eutectic carbides of the M_7C_3 type with discontinuous and interconnected morphology, and this morphology give suitable toughness and excellent abrasive wear resistance [5, 6]. The residual Cr dissolves into the matrix and increases hardenability of the cast iron by suppressing the pearlite transformation. Therefore, it can be said that Cr is an important element and it should be adopted as a basic alloying element of multi-alloyed white cast iron.

The multi-alloyed white cast iron with hypoeutectic composition is preferred in the viewpoint of toughness. The solidification sequence starts with the crystallization of primary austenite (γ_P), following by the eutectic reaction of ($L \rightarrow \gamma +$ eutectic carbides). The morphology, microstructure, size and amount of carbides are controlled by the chemical composition and cooling rate [2]. Moreover, the heat treatment process is another factor to control the mechanical properties [7].

The heat treatment process for multi-alloyed white cast iron is the same way as the high Cr cast iron or tool steel [8]. The specimen is held at the austenitizing

temperature to destabilize the retained austenite in the as-cast condition. During quenching, the matrix is transformed to bainite or martensite. The tempering is generally used for reducing the residual stress and the retained austenite formed in the hardening process. Consequently, the matrix with high hardness improves the wear resistance.

In the industrial applications, abrasive wear resistance is an important factor for machine parts so as to avoid the failure due to load or stress during operation. Even under the normal condition, the parts or components of machines undergo wear by abrasive particles [7, 9-11]. The abrasive wear can be classified into two groups; two-body and three-body-types. In the case of two-body-type abrasive wear, the wear occurs when abrasive particles provide the high stress on the surface of machine parts and heavy plastic deformation is caused there. Such a wear can be seen in the frames of jaw and impact crushers. In the laboratory test, the Suga abrasive wear tester is suitable to evaluate this type of wear resistance.

In the case of three-body-type abrasive wear, the abrasive particles moving freely on the surface of machine parts. The typical examples can be seen in the ball mills or tube mills to pulverize the cement clinkers, coals and blast furnace slags. In this case, the wear stress is usually lower than that in two-body-type wear test. The rubber wheel abrasive wear tester is suitable to test equipment for evaluation of the three-body-type wear [6-7]. However, the test results in the laboratory cannot be used directly for the industrial applications because the actual wear behavior is complex and depends on many factors [9, 12].

Nevertheless, the systematic research on the heat treatment and the related wear resistance of multi-alloyed white cast iron is a few. Recently, the solidification sequence, the effects of C and Mo contents on heat treatment behavior of multi-alloyed white cast iron with basic alloy composition have been reported [13-15]. However, the systematic research of Cr content on the heat treatment behavior and abrasive wear resistance of multi-alloyed white cast iron has not been found.

From the reasons as mentioned above, therefore, systematic and more accurate researches for abrasive wear are demanded now.

1.2 Objectives

In the research, the effect of Cr content on heat treatment and abrasive wear behaviors of multi-alloyed white cast iron with basic alloy composition was clarified. On the heat treatment behavior, the relationship between macro- and micro-hardness, volume fraction of retained austenite (V_γ) and tempering temperature in the different austenitizing temperatures was investigated using multi-alloyed white cast iron varying Cr content widely. On the other side, the abrasive wear resistance will be evaluated using Suga abrasive wear tester for two-body-type wear and rubber wheel abrasive wear tester for three-body-type wear. Then, correlation between hardness, V_γ , Cr content and abrasive wear resistance was clarified.

1.3 Scopes of research

The experiments are carried out by the following.

1. Preparation of specimens with 3 to 9%Cr.

2. Heat treatment of annealing at 1123K, hardening from 1323 and 1373K, and tempering at 673-873K by 50K intervals.
3. Observation of microstructure in the as-cast and heat-treated states.
4. Measurement of macro- and micro- hardness in the as-cast and heat-treated states.
5. Measurement of V_γ in the heat-treated states.
6. Evaluations of abrasive wear resistance using Suga and rubber wheel abrasive wear tests.
7. Clarification of correlation between hardness, V_γ , abrasive wear resistance and Cr content.

1.4 Advantages of research

1. This research clarifies the effect of Cr content on heat treatment behavior and abrasive wear resistance of multi-alloyed white cast iron with basic chemical composition.
2. This research reveals the correlation between hardness, volume fraction of retained austenite (V_γ), abrasive wear resistance and Cr content of multi-alloyed white cast iron.
3. The results of this research can offer the useful guidelines for the suitable heat treatment to improve the abrasive wear resistance of multi-alloyed white cast iron.

Chapter II

Literature Reviews

2.1 History of wear resistant materials

During the past half-century, the trend of materials and their manufacturing processes for rolling and pulverizing mill rolls can be shown in Fig.2-1. In 1950's, low alloyed white cast iron or chill cast iron had been used as abrasive wear resistant materials as well as roll materials. It is usually produced by chill mold casting. The microstructure consists of eutectic ledeburite and pearlite matrix. Hence, this cast iron has low toughness and abrasive wear resistance. The hardness of cast iron can be improved by the addition of Cr to promote carbide formation and refine the pearlite structure. However, this cast iron cannot be used over 600°C because the cementite (Fe_3C) could decompose to graphite. Therefore, low-alloyed white cast iron is limited to use under the severe wear and low-temperature applications. Then, the alloyed cast iron with higher wear resistance and higher toughness was developed. Responding to such a demand, International Nickel Company (INCO) developed Ni-hard cast iron. The Ni-hard cast iron containing high Cr and Ni produces austenite and martensite matrix in the as-cast state, and so, it showed better abrasive wear resistance than the low-alloyed white cast iron. However, it formed the connectivity of eutectic carbide made poor impact toughness. To conquer this problem, the high Cr white cast iron with low connectivity of eutectic carbides was developed in 1900's. The cast irons containing Cr over 12% produce hard eutectic carbide of the M_7C_3 type with discontinuous but interconnected configuration. Hence, high Cr cast iron showed higher abrasion and corrosion wear resistance than Ni-hard cast iron. The matrix

of high Cr cast iron could be controlled by the heat treatment. Since then, the high Cr cast iron has been widely used as the abrasive wear resistant cast alloys especially for rolls of rolling and pulverizing mill. However, there still remained the problem that a large volume fraction of Cr carbide deteriorated the toughness under an impact loading. For that reason, the development of a new type of alloys which has more toughness and higher wears resistance has been requiring. To achieve this purpose, the white cast iron containing plural types of carbides with higher hardness than the M_7C_3 carbides were developed.

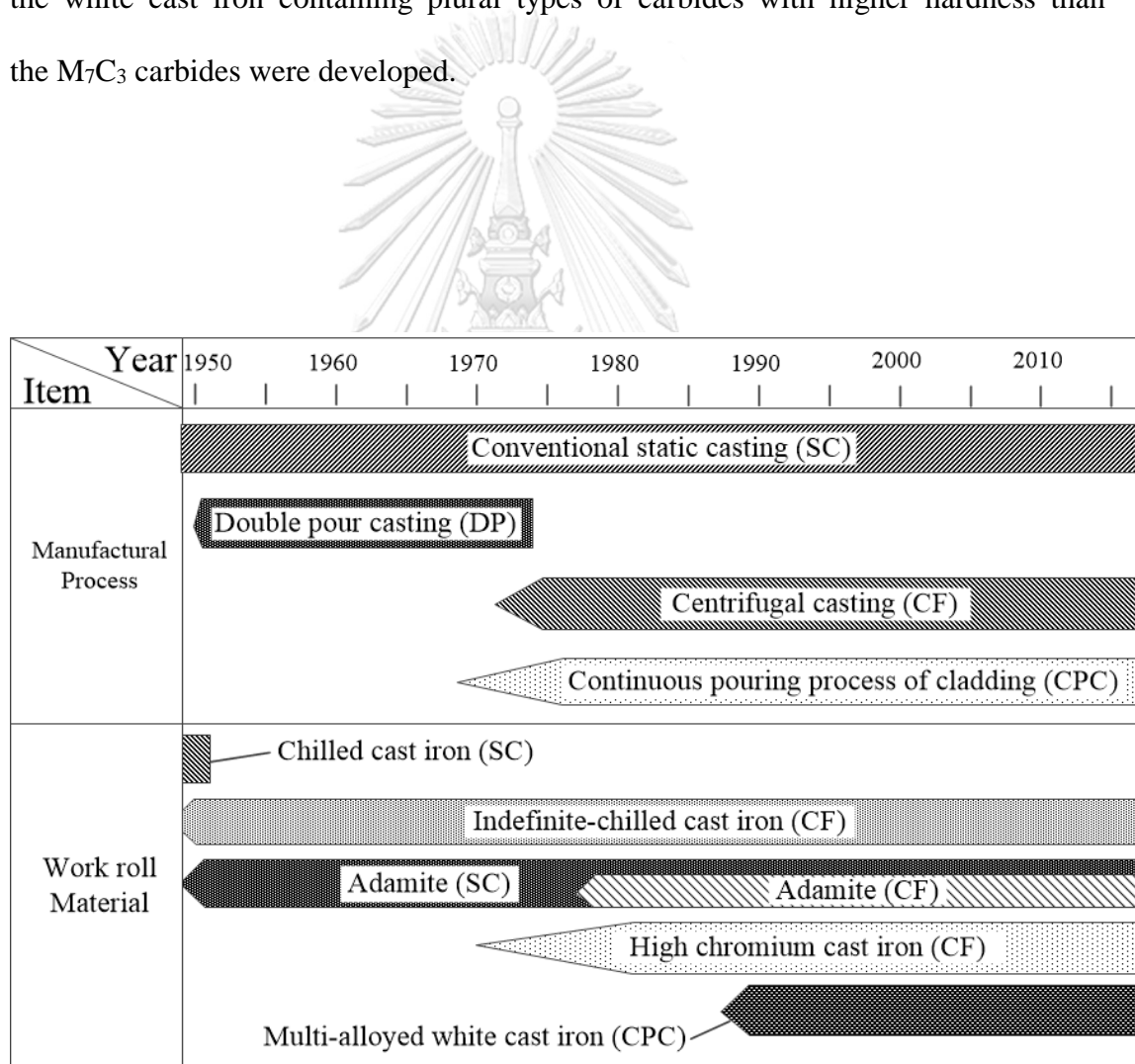


Fig.2-1 Trend of materials and manufacturing processes of rolls [1].

2.2 Alloy designing

The multi-alloyed white cast iron has been researched and developed for 30 years ago in Japan. It contains the strong carbide forming elements such as Cr, Mo, W and V. The basic chemical composition of multi-alloyed white cast iron is set at total 20% of strong carbide forming elements that are 5% of Cr, Mo, V and W each. During solidification, each element forms its special carbides such as MC, M_2C , M_6C , M_7C_3 and $M_{23}C_6$ which has high hardness. Additionally, the residual elements dissolve in matrix and promote the secondary hardening. As a result, the matrix is strengthened [13]. The hardness of the special carbides are shown in Table 2-1 [13, 16].

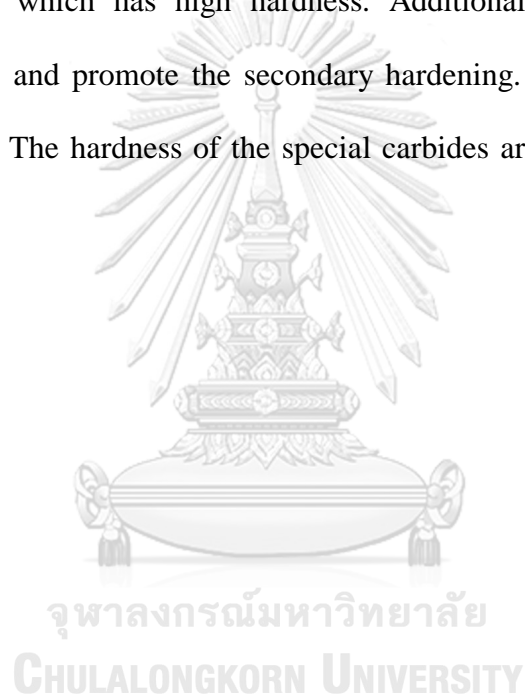


Table 2-1 Hardness of carbides and matrix phases of multi-alloyed white cast iron [9, 13].

Carbide or matrix	Hardness (HV)
$\text{Fe}_3\text{C} / \text{M}_3\text{C}$	800-1000
$(\text{Cr,Fe})_7\text{C}_3 / \text{M}_7\text{C}_3$	1200-1800
$(\text{Cr,Fe})_{23}\text{C}_6 / \text{M}_{23}\text{C}_6$	1100
$(\text{Mo,Fe})_2\text{C} / \text{M}_2\text{C}$	1800
$(\text{Mo,Fe})_6\text{C} / \text{M}_6\text{C}$	1800-2000
WC / MC	2400
$(\text{W,Fe})_2\text{C} / \text{M}_2\text{C}$	3000
$(\text{W,Fe})_6\text{C} / \text{M}_6\text{C}$	1900-2100
$(\text{V,Fe})\text{C} / \text{MC}$	2800
Ferrite	200-270
Pearlite	250-450
Austenite	250-500
Martensite	300-800

It is well known that Cr combines with C to form M_7C_3 carbide type [where M is (Cr,Fe)] during solidification. This carbide type has high hardness and improves wear resistance due to the discontinuous morphology of the eutectic carbides [7-11]. In addition, Cr can dissolve into matrix and increases hardenability. Powell [5] found that the eutectic carbide of cast iron changed from continuous M_3C carbide to finer and discontinuous M_7C_3 carbide when the Cr/C content increased. The Cr/C value is a significant factor for the formation of M_7C_3 carbide [6]. The comparison of M_3C with M_7C_3 carbide morphologies is shown in Fig 2-4 and the schematic drawing of

the discontinuous structure of eutectic M_7C_3 carbides is illustrated in Fig.2-5. The crystal lattice of the M_3C carbide is orthorhombic, while the M_7C_3 is hexagonal. From Table 2-1, the hardness of M_3C and M_7C_3 carbides are 800 to 1,000 HV and 1,200 to 1,800 HV, respectively.

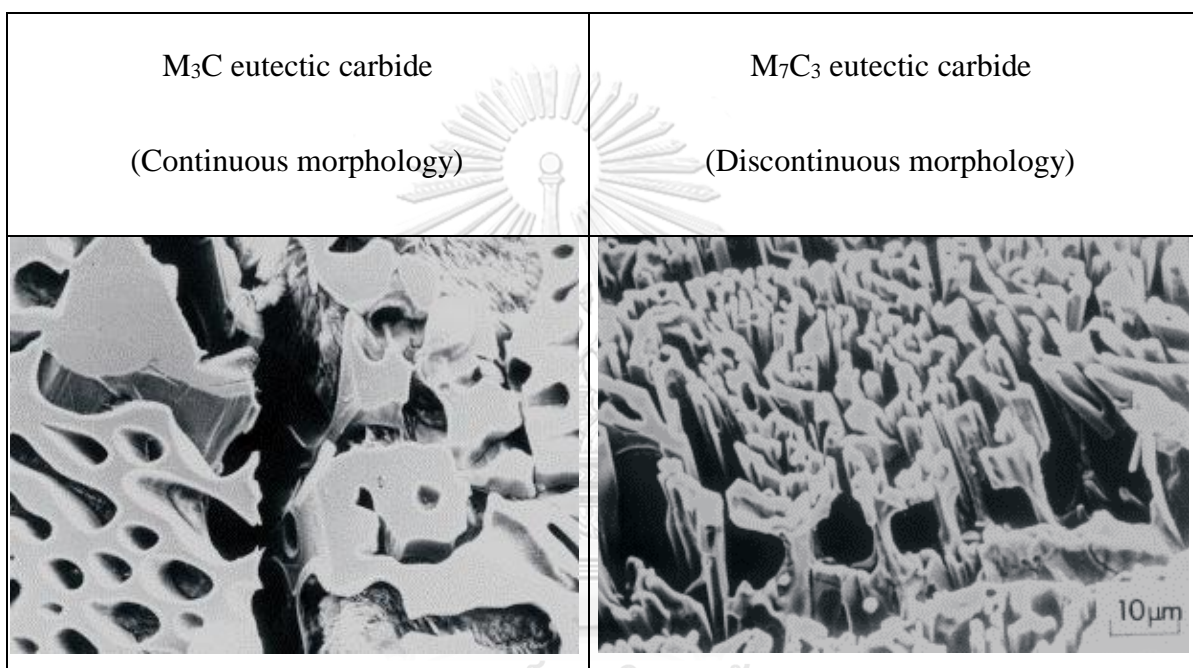


Fig.2-2 Comparison of deeply etched microstructures of M_3C eutectic carbides in the as-cast state of cast iron 5%Cr-3.6%C and M_7C_3 eutectic carbides in the as-cast state of cast iron 30%Cr-2.4%C [17, 18].

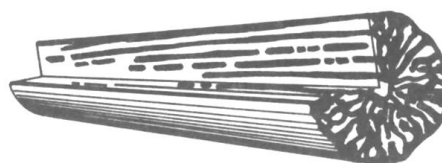


Fig.2-3 The schematic drawing of discontinuous eutectic M_7C_3 carbides [19].

It is well known that Mo and W are strong carbide formers. They form as a complex carbide of M_2C [(Mo,Fe)₂C] or M_6C [(Mo,Fe)₆C] types. These carbides have a higher hardness than Cr carbide of M_7C_3 . In addition, Mo and W also dissolve into the matrix and improve hardenability. Moreover, Mo improves high temperature wear resistance and it has more effect than W in the improvement of hardenability [8, 11, 20, 21]. Although W has the ability to form carbide similar to Mo, Mo has higher diffusivity than W. This means that Mo has more efficiency than W. Therefore, the parameter of W equivalent (W_{eq}), which defined a simultaneous effect of both elements, is introduced using the following equation.

$$W_{eq} = \%W + 2*\%Mo \dots\dots\dots(2-1)$$

V is one of strong carbide former and the ability of carbide formation is stronger than that of Mo, W and Cr. The V forms the MC [(V,Fe)C] type of carbide. This carbide has the highest hardness as shown in Table 2-1. It is well known that V is a grain refiner because it acts as nuclei of carbides during solidification [2, 8, 14, 21]. V decreases hardenability but it greatly promotes the secondary hardening during tempering.

Co does not form any carbide and the Co is not generally used in alloyed steel and cast iron because of reduction of hardenability. However, the Co is added to multi-alloyed white cast iron in order to improve the corrosion, oxidation and wear resistance of at elevated temperature. It was reported that Co increased the hardness in the tempering by promoting the martensite transformation [2, 20-25].

It is natural that the C combines with carbide forming elements to form special carbides during solidification. Subsequently, the remaining C dissolves into the matrix and takes part in phase transformation in matrix and it will be to the heat treatment as well. In the multi-alloyed cast iron, the plural kinds of carbides are expected to crystallize as eutectic. In order to explain the effect of C on heat treatment behavior, a parameter of carbon balance (C_{bal}) is introduced to express the behavior of C dissolved in the matrix. The equation of C_{bal} is shown by the next equation [13, 14, 26].

$$C_{bal} = \%C \text{ in cast iron} - \%C_{stoich} \dots\dots\dots(2-2)$$

Where %C is total C content in the cast iron and $\%C_{stoich}$ is the amount of C which combines with strong carbide forming elements. The C_{stoich} depends on the type of eutectic carbide when eutectic M_7C_3 carbide does not exist in the solidification structure of multi-alloyed white cast iron, the C_{stoich} is obtained from equation (2-3).

$$\%C_{stoich} = (0.060*\%Cr) + (0.063*\%Mo) + (0.033*\%W) + (0.235*\%V) \dots\dots\dots(2-3)$$

When eutectic M_7C_3 carbide exists in the cast iron, next equation is available.

$$\%C_{stoich} = (0.099*\%Cr) + (0.063*\%Mo) + (0.033*\%W) + (0.235*\%V) \dots\dots\dots(2-4)$$

The C_{bal} is one of important parameters to define carbide and matrix structure. In case that the C_{bal} is positive values means that it remains an excess carbon in the matrix, while a negative value means that carbon is unsaturated in matrix [14, 26]. However, the C_{bal} calculated from above equations may be not accurate because the calculation is done using the theoretical equation in equilibrium condition for

the alloy design. It was reported that the C_{bal} value is an important parameter to determine the condition of heat treatment. Hashimoto [26] reported that martensitic matrix was obtained when the C_{bal} value was -1 to +1%.

2.3 Type and morphology of carbides in multi-alloyed white cast iron

There are many kinds of carbide precipitated in multi-alloyed white cast iron. Type and morphology of carbide are specified by the chemical composition and cooling rate [13]. As the C content of cast iron rises, the eutectic carbide increases and more uniform microstructure is obtained [13, 24, 27]. Moreover, fine carbide structure reveals at high cooling rate while the coarse structure will appear at low cooling rate [28].

Table 2-2 shows the alloy concentration in carbides and matrix. It was found that the MC carbide is mainly formed by V. The major elements dissolved in M_2C carbide are Mo and W and those in the M_7C_3 carbide are Cr and Fe. The matrix is mostly composed of Fe [9, 29-33]. Typical morphologies of MC, M_2C and M_7C_3 carbide are displayed two and three-dimensional in Fig.2-4 to Fig.2-6, respectively.

The MC carbide contains more than 50% V and it precipitates as a eutectic during solidification. This carbide can be classified into petal-like, nodular and coral-like morphologies as shown in Fig.2-4. The petal-like MC carbide precipitates in a low C cast iron and nodular MC carbide is observed in the cast iron with high C content. Coral-like MC carbide precipitates in the cast iron with high V content and sometimes it co-exists with M_7C_3 or M_2C carbide depending on the C content.

The hardness of MC carbide is about 2800 HV. It was reported that the MC carbide improved the wear resistance and the nodular morphology of MC carbide may also improve the toughness due to less notch effect [24].

Table 2-2 Alloy concentration in carbides and matrix of multi-alloyed white cast iron with basic chemical composition [13].

Carbides and matrix	Elements (%)					
	Cr	Mo	W	V	Co	Fe
MC	3.0 ~ 4.1	4.2 ~ 10	4.3 ~ 8.3	49 ~ 65	0.6 ~ 1.0	16 ~ 18
M ₂ C	10 ~ 15	26 ~ 30	19 ~ 22	6.4 ~ 12	0.8 ~ 1.3	20 ~ 26
M ₇ C ₃	17 ~ 24	5.3 ~ 9.0	3.6 ~ 5.4	3.2 ~ 6.2	2.2 ~ 3.2	59 ~ 66
Matrix	3.5 ~ 4.2	0.2 ~ 1.3	1.8 ~ 3.1	1.0 ~ 2.4	0 ~ 14	82 ~ 85

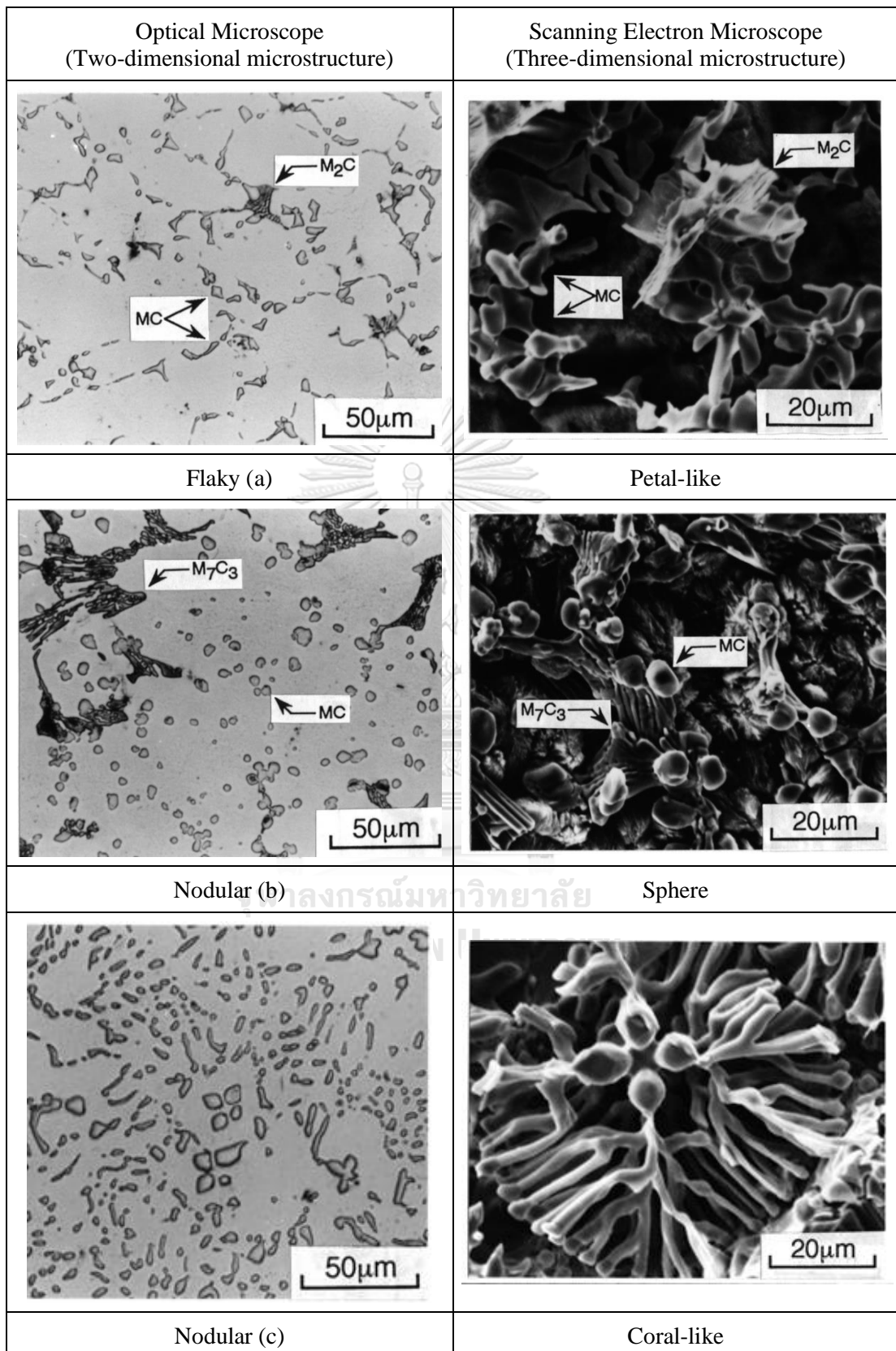


Fig.2-4 Comparison of two-dimensional and three-dimensional microstructures of MC carbide in multi-alloyed white cast iron by OM and SEM [13].

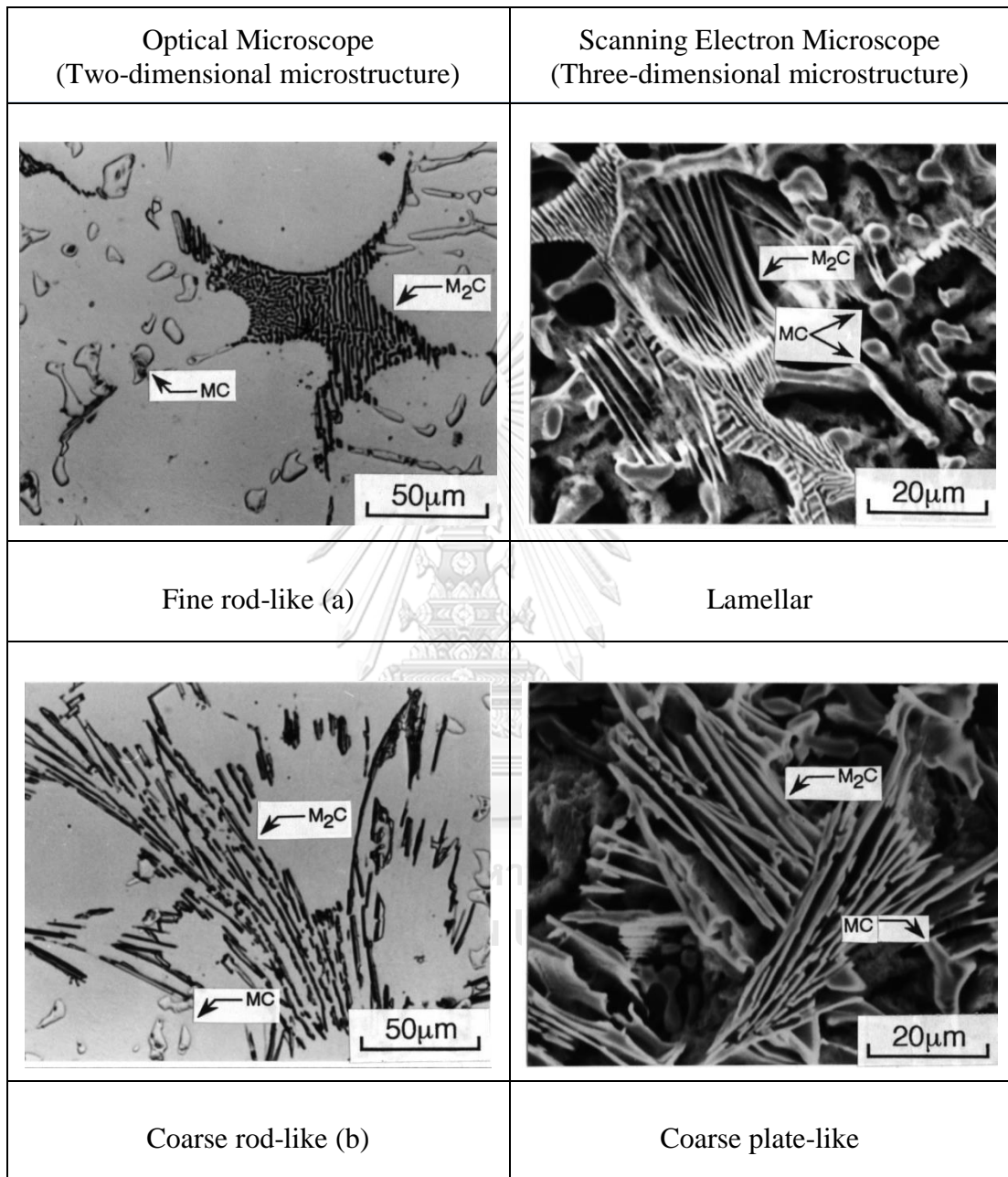
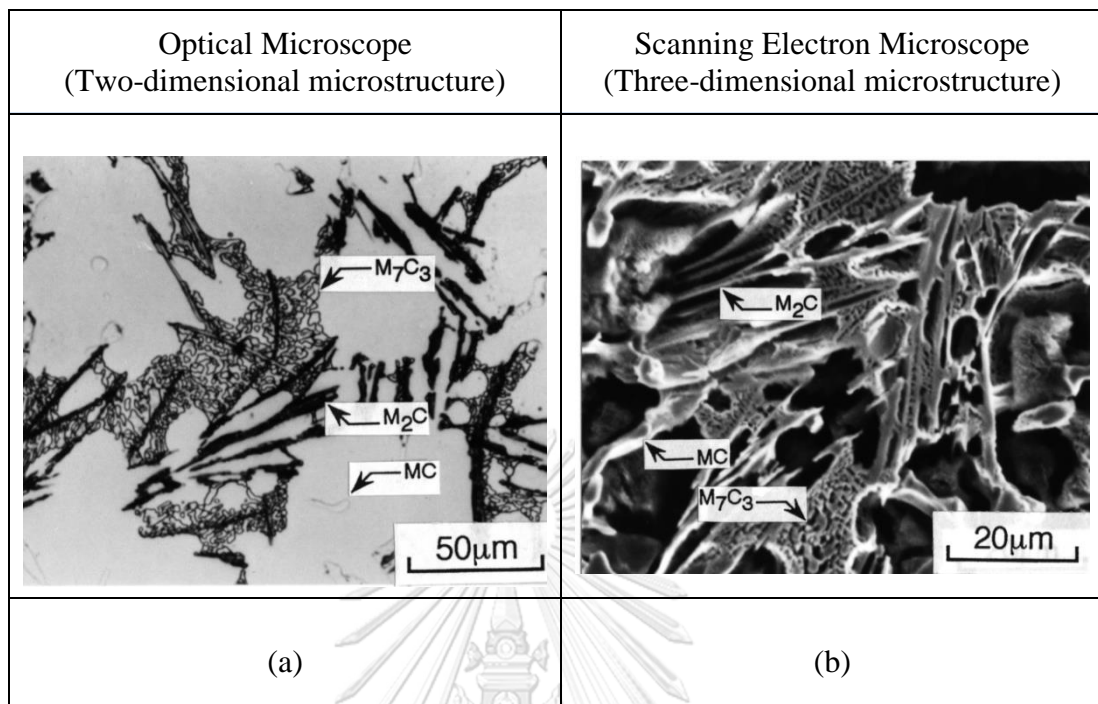


Fig.2-5 Comparison of two-dimensional and three-dimensional microstructures of M_2C carbide in multi-alloyed white cast iron by OM and SEM [13].



(Rod-like or ledeburitic)

Fig.2-6 Comparison of two-dimensional and three-dimensional microstructures of M_7C_3 carbide in multi-alloyed white cast iron by OM and SEM [13].

The optical and SEM microstructures of M_2C carbides are shown in Fig.2-5. The Mo and W-rich carbides precipitate in fine lamellar and/or coarse plate-like morphologies which depend on the chemical composition of the cast iron. The plate-like M_2C carbide can be seen in the cast iron with high W_{eq} value. However, it is reported that the M_2C carbide could transform to M_6C carbide by heat treatment [34]. The lamellar eutectic M_2C carbide exists in isolation and this indicates that the eutectic M_2C carbides crystallize in the last stage of solidification. The fine or coarse rod-like carbides are discovered in two-dimensional microstructure but it is found that they are fine or coarse plates in the three-dimensional microstructure. The hardness of M_2C carbides is 1800 HV.

The microphotographs of M_7C_3 carbide in rod-like or ledeburitic morphology are shown in Fig.2-6 and they can be seen in the cast irons with high W_{eq} value and high C content. The eutectic M_7C_3 carbide sometimes appears co-existing with MC and M_2C carbides. The hardness of M_7C_3 carbide is in the range of 1200-1800 HV.

2.3.1 Effect of alloying elements on type and morphology of carbide

The influence of V and C contents on type and morphology of carbides in multi-alloyed white cast iron is shown in Fig.2-7. It is found that the MC carbide crystallizes in all the composition areas, but it differs in the morphology. The nodular MC carbide appears in the area over 1.4 %C and in 1-6 %V. On the other hand, the flaky MC carbide is observed in the region of C and V contents less than 2 and 10%, respectively. The coral-like MC carbide appears in high V range of 8-15%. In case of the rod-like M_7C_3 carbide, it is seen in a wide range of high C content and low V content [13, 29, 35].

The influence of W_{eq} and C content on type and morphology of carbide is shown in Fig.2-8. From the diagram, the MC carbide exists in all of composition area but the nodular MC carbides are limited in the area of W_{eq} 3 to 11% and C content from 1.7 to 3.2%. By contrast, the flaky MC carbide appears in the area of W_{eq} more than 15% and C content more than 1.8%. The morphology of M_2C carbides is clearly separated under the straight line. The lamellar M_2C carbides are found in the W_{eq} less than 15% and the plate-like M_2C carbides are in the W_{eq} more than 15%. The rod-like M_7C_3 carbides can be observed in the same region of nodular MC carbides.

The influence of Co and C content on type and morphology of carbides in multi-alloyed white cast iron is shown in Fig.2-9. It is clear that Co content does not effect on the type and morphology of carbide. This is reasonable because Co does not form any carbide.

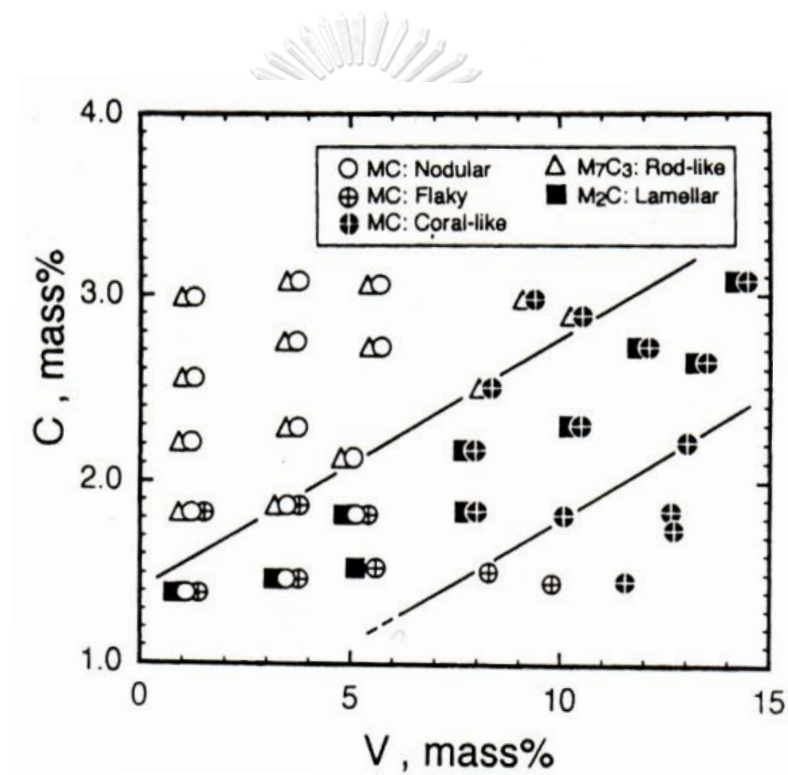


Fig.2-7 Influence of V and C contents on type and morphology of carbides crystallized from the melt of multi-alloyed white cast iron [13].

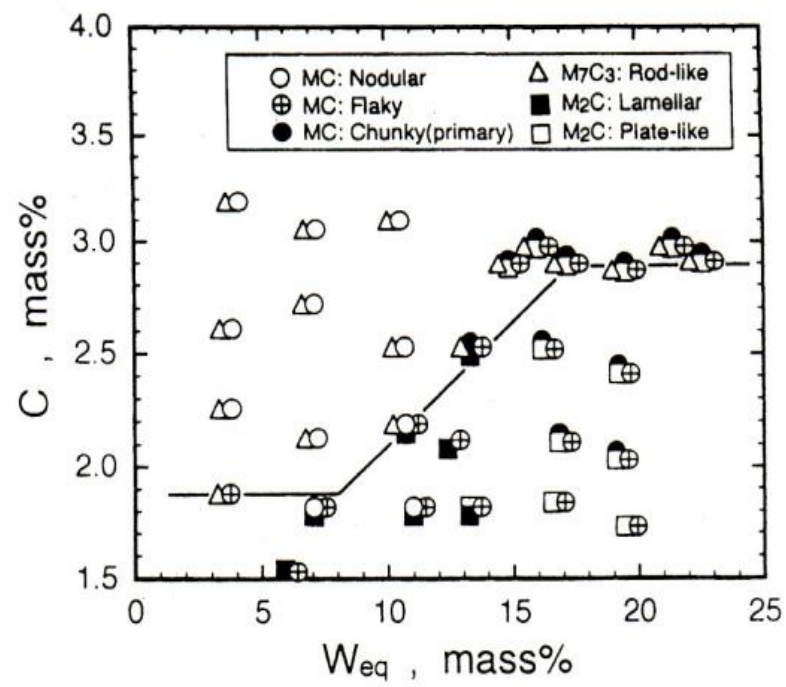


Fig.2-8 Influence of W_{eq} value and C content on type and morphology of carbides crystallized from the melt of multi-alloyed white cast iron [13].

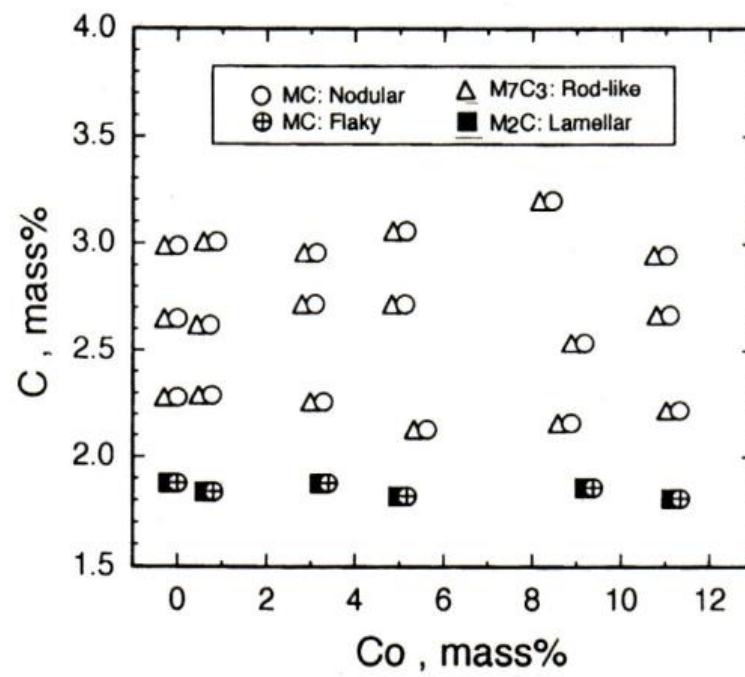


Fig.2-9 Influence of Co and C contents on type and morphology of carbides crystallized from the melt of multi-alloyed white cast iron [13].

2.3.2 Influence of solidification rate on type and morphology of carbide

The influence of solidification rate on the type and morphology of carbide in multi-alloyed white cast iron is shown in Fig.2-10. The MC and M_2C carbides are found in all the regions of the diagram but different in morphology. The M_7C_3 appears at high C content and low solidification rate. The M_3C can be observed in the narrow area of the diagram at low solidification rate and high C content. Boccalini et al. [28] studied the effect of cooling rate on the microstructure of multi-alloyed white cast iron with niobium. It was reported that an increase in the cooling rate from 0.15 to 1.5 K/s refined the eutectic carbide.

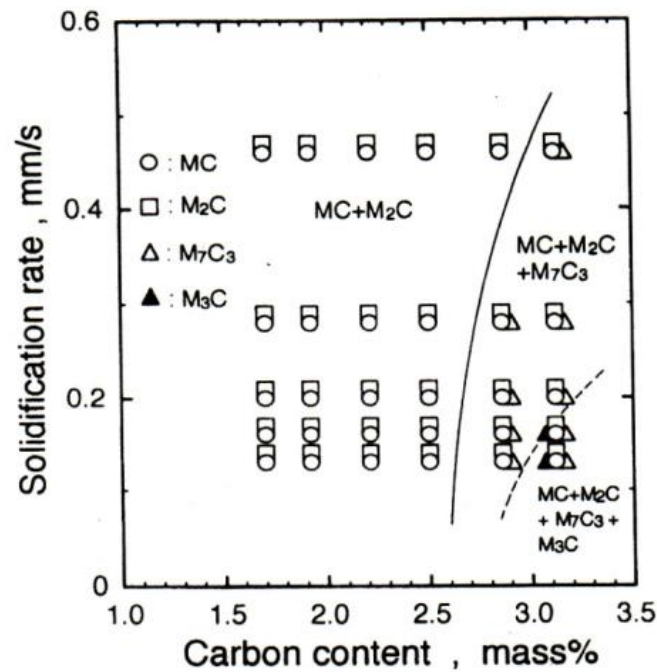
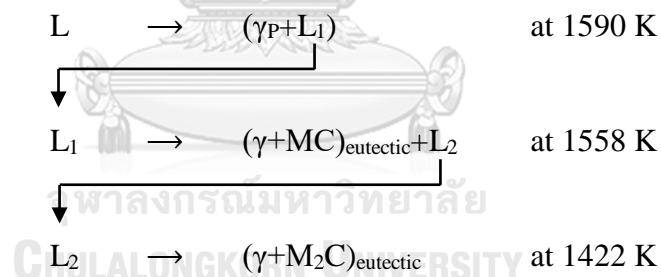


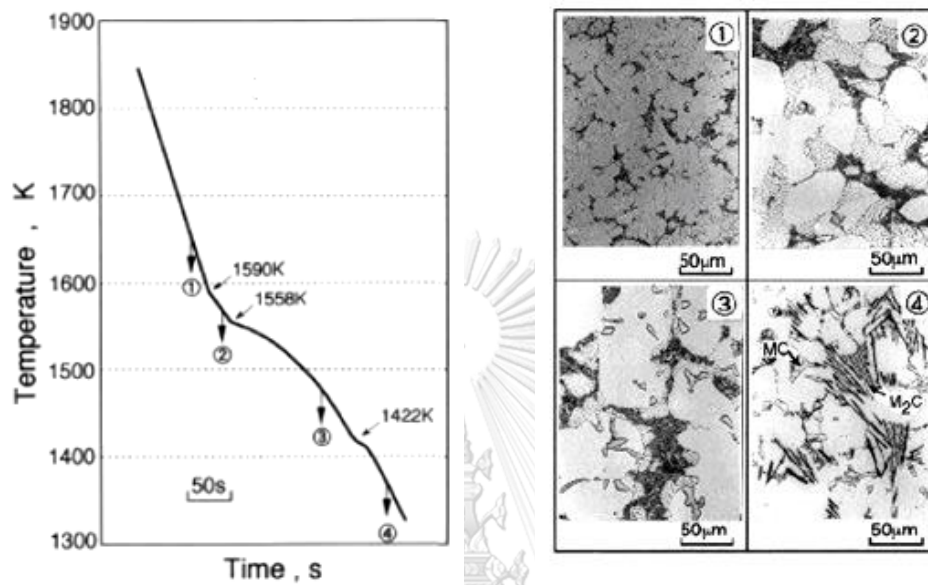
Fig.2-10 Type of carbide corresponding to solidification rate and C content [13].

2.4 Solidification sequence of multi-alloyed white cast iron

The solidification sequence of multi-alloyed white cast iron with basic chemical composition was explored by means of quenching during thermal analysis. A thermal analysis curve and transition of microstructure obtained by quenched tests of specimen with basic chemical composition (Fe-5%Cr-5%Mo-5%W-5%V-5%Co-2%C) were shown in Fig.2-11 (a) and (b), respectively [13, 29, 35]. A small amount of sample was quenched into water from at temperature before and after each freezing reaction [36]. First of all, the primary austenite dendrite forms at 1590K, follows by precipitation of $(\gamma+MC)$ eutectic at 1558 K, and finally $(\gamma+M_2C)$ eutectic solidifies at 1422 K as shown the solidification flow chart below.



It was reported that an increase in C content rose the crystallizing temperature of primary phase [14, 35]. Solidification sequences of multi-alloyed white cast irons with several chemical compositions are shown in Table 2-3.



(a) Thermal analysis curve (b) Transition of microstructures by quench test

Fig.2-11 Solidification of multi-alloyed white cast iron with basic chemical composition (Fe-5%Cr-5%Mo-5%W-5%V-5%Co-2%C) [29].

Table 2-3 Solidification sequence of multi-alloyed white cast irons with several chemical compositions [29].

Chemical composition	Combination of carbides	Solidification sequences
2% C-5% Cr -2% Mo-2% W -9% V-5% Co	Coral-like MC- Lamellar M ₂ C	L ₀ → γ _p + L ₁ at 1651 K L ₁ → (γ+MC) _E + L ₂ at 1631 K L ₂ → (γ+M ₂ C) _E at 1498 K
3% C-5% Cr -2% Mo-2% W -5% V-5% Co	Nodular MC- Rod-like M ₇ C ₃	L ₀ → γ _p + L ₁ at 1556 K L ₁ → (γ+MC) _E + L ₂ at 1515 K L ₂ → (γ+M ₇ C ₃) _E at 1452 K
3% C-5% Cr -2% Mo-2% W -9% V-5% Co	Chunky and coral-like MC- Rod-like M ₇ C ₃	L ₀ → γ _p + L ₁ at 1732 K L ₁ → (γ+MC) _E + L ₂ at 1550 K L ₂ → (γ+M ₇ C ₃) _E at 1453K

The quasi-binary phase diagram varying carbon content of multi-alloyed white cast iron with basic alloy composition (Fe-5%Cr-5%Mo-5%W-5%V-5%Co-2%C) is displayed in Fig.2-12 [35]. It is clear that the eutectic reaction appears near 2.8 %C. This phase diagram also tells that after the eutectic reaction of (L → γ+ MC), the melt is followed by two other eutectic reactions, L → γ+M₇C₃ and L → γ+M₂C continuously.

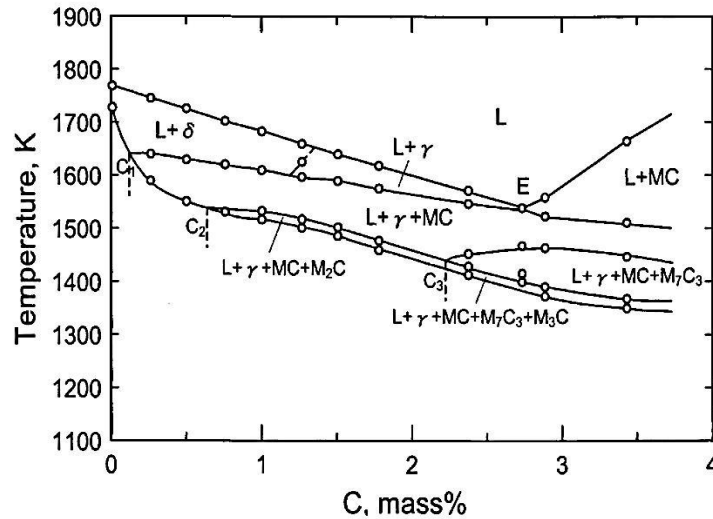


Fig.2-12 Quasi-binary section diagram of multi-alloyed white cast iron with alloy system of M (Fe-5%Cr-5%Mo-5%W-5%V-5%Co)-C [35].

2.5 Matrix of multi-alloyed white cast iron

The matrix plays an important role to support carbides against the deformation by loading. Therefore, the matrix should have not only high hardness or high strength but also high toughness. The matrix of multi-alloyed white cast iron in the as-cast state consists of bainite, martensite and some retained austenite which vary depending on the chemical composition [14, 20-22, 24, 26-33, 35]. The retained austenite is supposed to transform into the useful phases by heat treatment [14, 30]. Moreover, it is known that the retained austenite can be transformed to martensite during operation by stress-induced mechanism.

2.6 Matrix transformation of multi-alloyed white cast iron

Microstructure of multi-alloyed white cast iron in the as-cast state consists of ferrite, bainite, martensite and austenite. Volume fraction of retained austenite (V_{γ}) is 5 to 50% depending on the amount of C and alloying elements in the cast iron [14]. Because of the matrix microstructure, in the as-cast state the hardness is very low and shows poor wear resistance. Therefore, the cast iron must be heat-treated before service. The heat treatment process of multi-alloyed white cast iron is also in the same way as the heat treatment of high Cr cast iron and tool steel [14, 33], that is, general heat treatment of hardening and tempering. In hardening process, austenite is held at high temperature to destabilize the retained austenite. Then, the destabilized austenite transforms to martensite by quenching or by fan air cooling. The hardened specimens are tempered to reduce residual stress and amount of retained austenite from the viewpoint of wear resistance.

The continuous cooling transformation (CCT) curve of the basic multi-alloyed white cast irons with different C contents of 1.95% and 2.81 %C are shown in Fig.2-13. In spite of the difference in C content and austenitizing temperature, the pearlite and bainite transformations are independently separated. The nose temperatures of both the pearlite and bainite transformations range from 920 to 980K and 570 to 610K for 1.95%C cast iron, and 900 to 950K and 590 to 640K for 2.81%C cast iron, respectively. The nose of pearlite shifts to the short time side when the C content is increased. However, an increase in the austenitizing temperature postpones the pearlite transformation. This result tells that the pearlite transformation is hard to occur in the case of austenitizing at high temperature. Otherwise,

the Ms temperature is lowered by raising the austenitizing temperature because the solubility of alloys in austenite is increased.

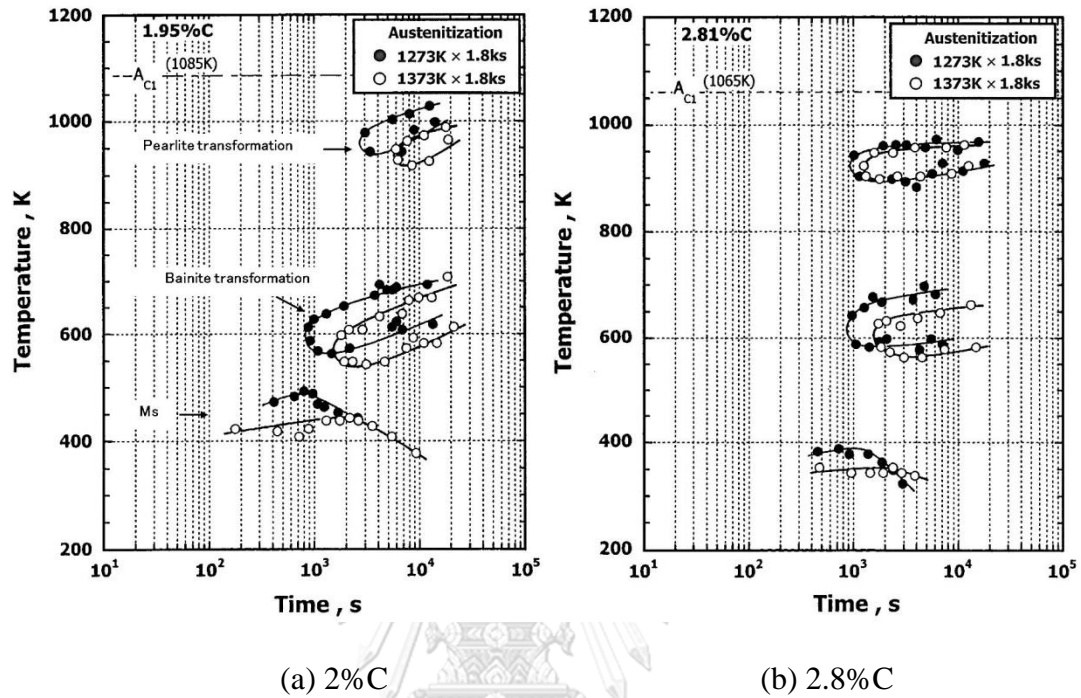


Fig.2-13 CCT diagrams of multi-alloyed white cast iron with different C contents in basic chemical composition (Fe-5%Cr-5%Mo-5%W-5%V-2%Co-C alloys) [33].

จุฬาลงกรณ์มหาวิทยาลัย
CHULALONGKORN UNIVERSITY

2.7 Heat treatment of multi-alloyed white cast iron

General heat treatment processes, which are annealing, hardening and tempering, are applied to multi-alloyed white cast iron. However, the transformation behavior is quite different from steel because plural kinds of alloying elements are dissolved in as-hardened matrix. Particularly, during tempering the hardness changes widely due to the decomposition of martensite and retained austenite to precipitate secondary carbides. The precipitation of carbides reduces alloy concentration in the

retained austenite and then, the M_s temperature rises. Finally, the rest of austenite transforms to martensite in the post cooling [3, 25, 37]. However, it was reported that the agglomeration or coarsening of secondary carbides could occur during tempering at high temperature and it reduces the hardness.

The heat treatment behavior of multi-alloyed white cast iron with basic chemical composition has been reported as shown in Fig.2-14. It is found that an evident secondary hardening is obtained in each specimen hardened from 1323 or 1373K austenitizing temperature. The maximum hardness appears at 800 K tempering. After that, the hardness drops remarkably due to the coarsening of precipitated carbides that is called over-tempering. On the other hand, the volume fraction of retained austenite decreases as tempering temperature increases.

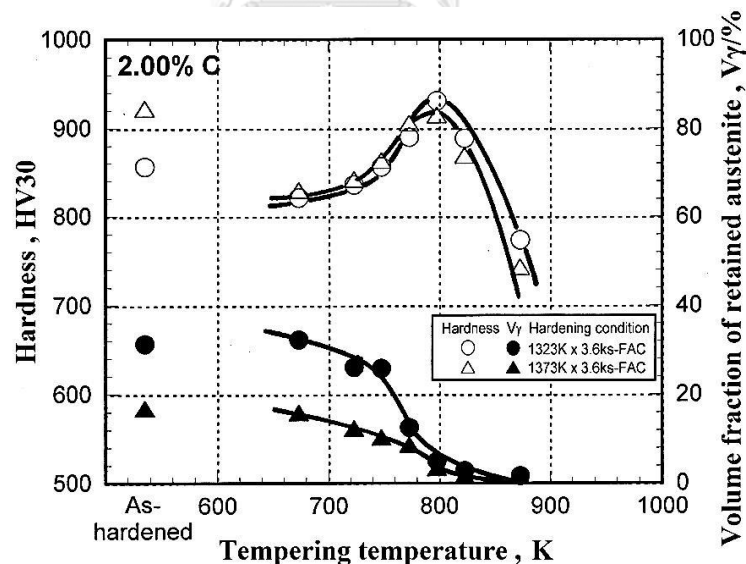


Fig.2-14 Tempered hardness curve and variation of volume fraction of retained austenite (V_γ) of multi-alloyed white cast iron with basic chemical composition [15].

2.8 Abrasive wear resistance

The wear resistance of cast iron depends on type, morphology, volume fraction and distribution of carbides and the matrix strength. The principal of abrasive wear resistance is shown in Fig.2-15. It can be defined according to how the materials resist the abrasives which contact or press repeatedly on the surface under the high load. Normally, the hardness of eutectic carbide should higher than abrasive materials. The morphology of carbides in the cast iron is one factor in the wear performance. The continuous morphology carbides in Fig.2-15 (c) are unfavorable because they do not protect the matrix against the abrasive materials. On the other side, if the matrix is too soft, the abrasives wear out hard carbides together with matrix [24, 38-41].

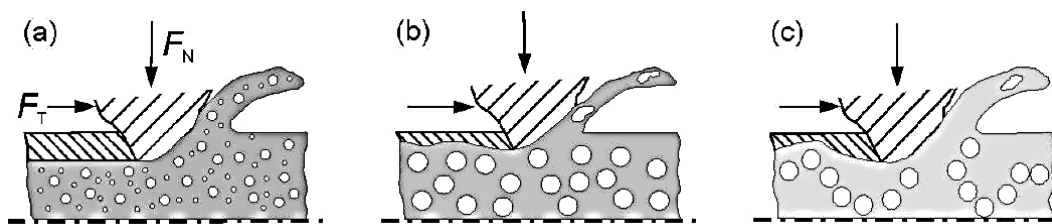


Fig.2-15 Schematic drawing of wearing of cast iron with too small carbides (a), carbides in effective size (b) and continuous carbides (c) [24].

It can be said that the carbides with high hardness improve the wear resistance of alloyed white cast iron. Nevertheless, the amount of eutectic carbide should be limited from the viewpoint of the toughness [37]. The abrasive wear resistance was expressed in terms of mass loss which could be measured by digital balance or in terms of volume loss which can be calculated by the equation (2-5) [42].

$$\text{Volume loss (mm}^3\text{)} = \frac{\text{mass loss (g)}}{\text{density (g/cm}^3\text{)}} \times 1000 \dots\dots\dots(2-5)$$

In the practical application, the mechanism of abrasive wear is very complicated. The abrasive wear can be classified into two types as shown in Fig.2-16; two-body and three-body-type wears. The concept of these wears is described by that the abrasive particles are bound (two-body) or move freely (three-body). Two-body-type abrasion is caused by friction between two surfaces in which hard particles are embedded. On the other side, three-body-type wear is caused by hard particles moving freely between contacting surface of wear resistant materials.

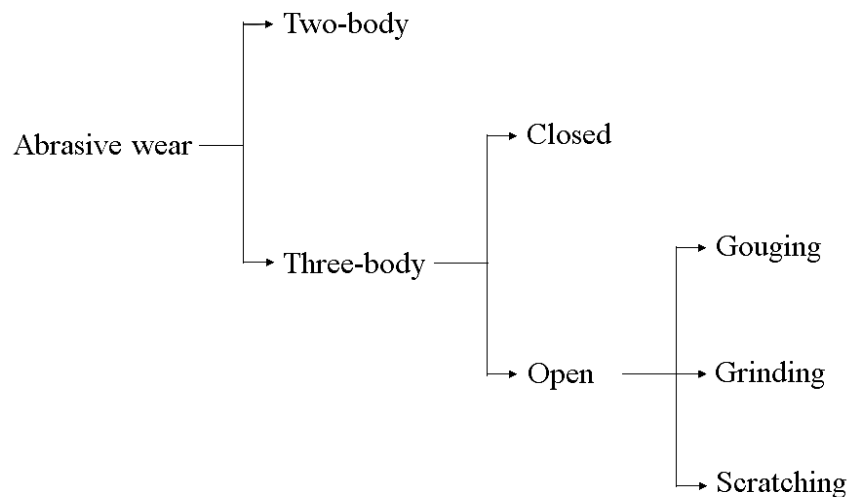


Fig.2-16 Classification of abrasive wear [43]

The hardness of some abrasive materials are shown in Table 2-4.

Table 2-4 Hardness of some abrasive materials and matrix phase [9, 44].

Abrasive materials	Hardness (HV)
SiC	2600
VC	2000-3000
Al ₂ O ₃	1800
SiO ₂ (Silica)	1430
High carbon martensite	500-1010

The specific situation of wear can be summarized as follows by Avery [45, 46].

1. Gouging abrasion: the machine parts are extremely received high forced and pressure from other large objects such as stones or minerals. Then, a large volume of surface is grooved away. Normally, it can be found in the hammers or crushers.

2. Grinding or high-stress abrasion: this mechanism occurs when small particles are forced to the surface of machine parts and then, the particles are crushed when the load is higher than that of fracture. The load in this abrasion seems to be

lower than gouging abrasion. However, it is difficult to separate the boundary between two models clearly.

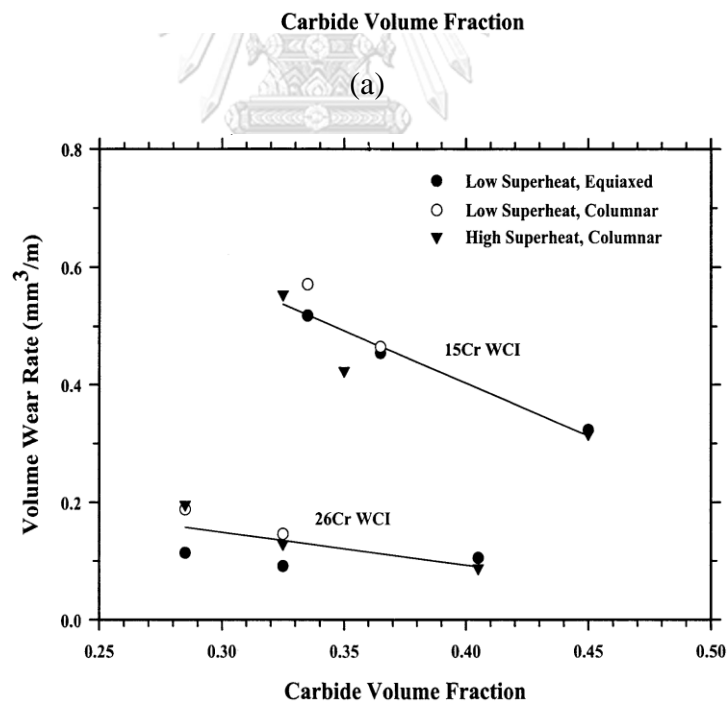
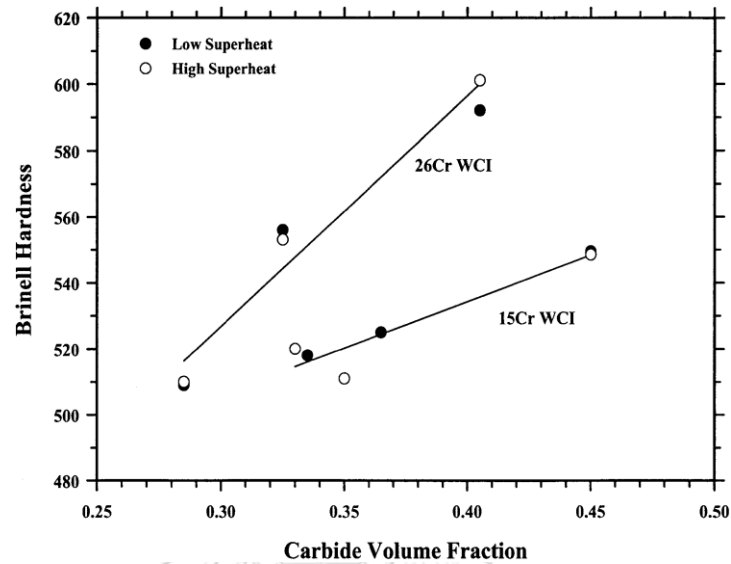
3. Scratching abrasion or low-stress abrasion is slight severe in abrasive wear. Small particles are freely moving throughout the surface of machine parts with less crushing. In this case, particles are not fractured. The difference between low-stress and high-stress abrasion is whether the abrasive particles are broken or not.

2.9 Abrasive wear resistance of alloyed white cast irons

Many researches on abrasive wear resistance of alloyed cast iron have been reported. The results showed that an increase in the amount and hardness of carbide could improve the abrasive wear resistance. Doğan and Hawk reported that the abrasive wear resistance differs depending on the orientation of carbides, surface appearance and direction of load. In pin-on-drum wear test, the abrasive wear resistance was reduced when the orientation of carbide is in parallel to the wear surface [40, 47]. Doğan et al also reported that the wear resistance of high Cr cast iron was improved by increasing the hardness and volume fraction of carbide as shown in Fig.2-17.

The abrasive wear resistance of multi-alloyed white cast irons being alloyed by total carbide forming elements of 20% was reported by Matsubara et al. [48]. The relationship between wear loss and testing time in each state are shown in Fig.2-18. It is found that the lowest wear resistance in the as-cast state was obtained in the cast iron alloyed with high Cr content ($M_{No.3}$). In as-hardened and tempered states, however, the highest wear resistance was obtained in the cast irons with high V content ($M_{No.2}$) because of the precipitation of MC carbides with very

high hardness. It is also found that the M_7C_3 carbide was worn by spalling. The similar results were obtained in the as-hardened and tempered specimens, that is, the highest wear resistance can be obtained in the cast iron with high V content.



(b)

Fig.2-17 Effect of carbide volume fraction on (a) hardness and (b) volume wear rate of high Cr white cast irons [40].

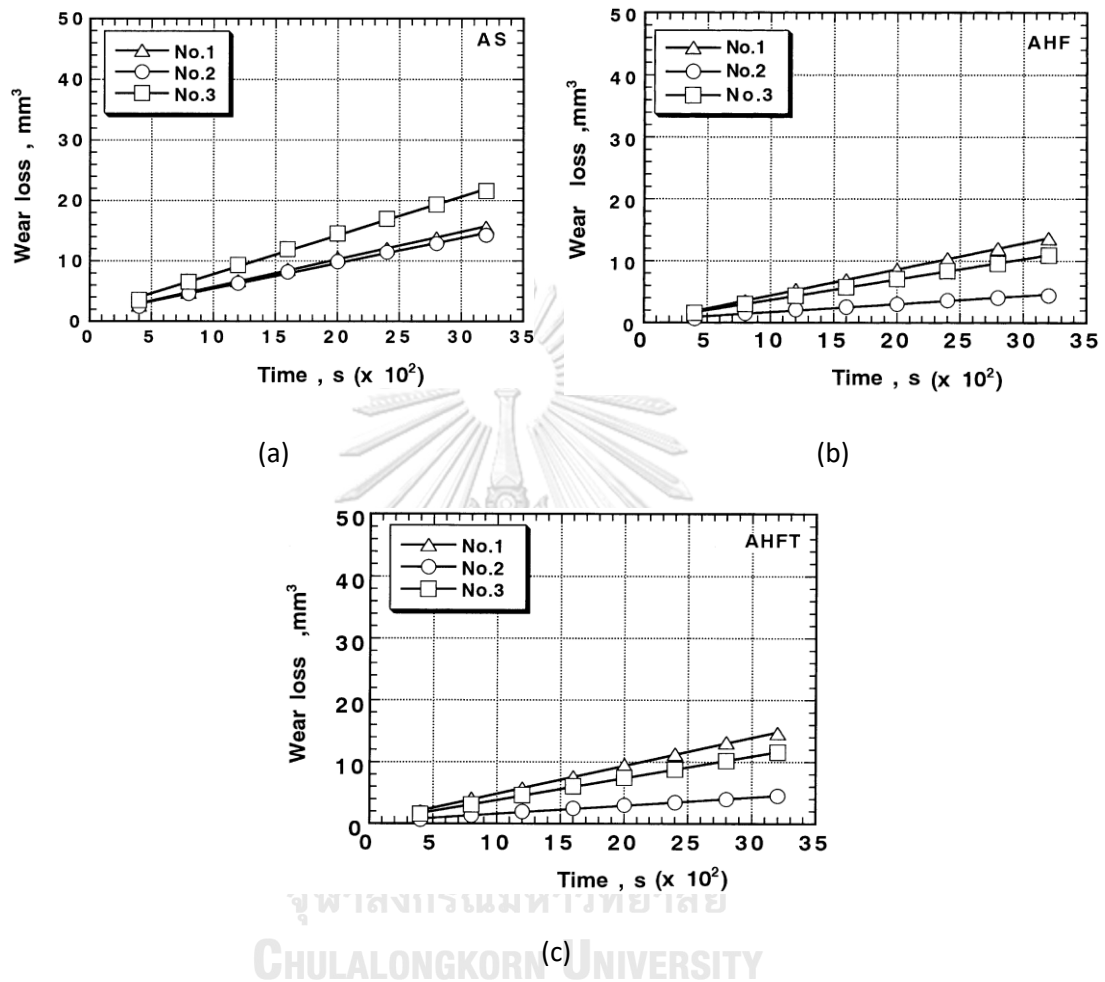


Fig.2-18 Relationship between wear loss and testing time of multi-alloyed white cast iron in Fe-M-C alloys in (a) as-cast, (b) as-hardened and (c) hardened-tempered states [48]. ($M_{No.1}$: 9.95%Cr-0.01%V-5.14%Mo-4.87%W, $M_{No.2}$: 0.04%Cr-10.21%V-5.21%Mo-4.84%W and $M_{No.3}$: 17.54%Cr-3.14%V-0.01%Mo-0.02%W).

The effect of Co on wear behavior of heat-treated multi-alloyed white cast iron was studied by Sasaguri et al. [23]. In Fig.2-19, it is found that the wear resistance in the as-hardened state was larger than those in the as-cast and annealed states. It is considered that the reason is due to the different in the matrix structure. However, the Co reduces the wear resistance in the as-cast and annealed states because Co promotes the pearlite transformation. The effect of Co content on the wear resistance in the tempered state is shown in Fig.2-20. It is clear that the highest wear resistance of each cast iron is obtained in the specimen tempered at around 800 K which has the highest hardness.

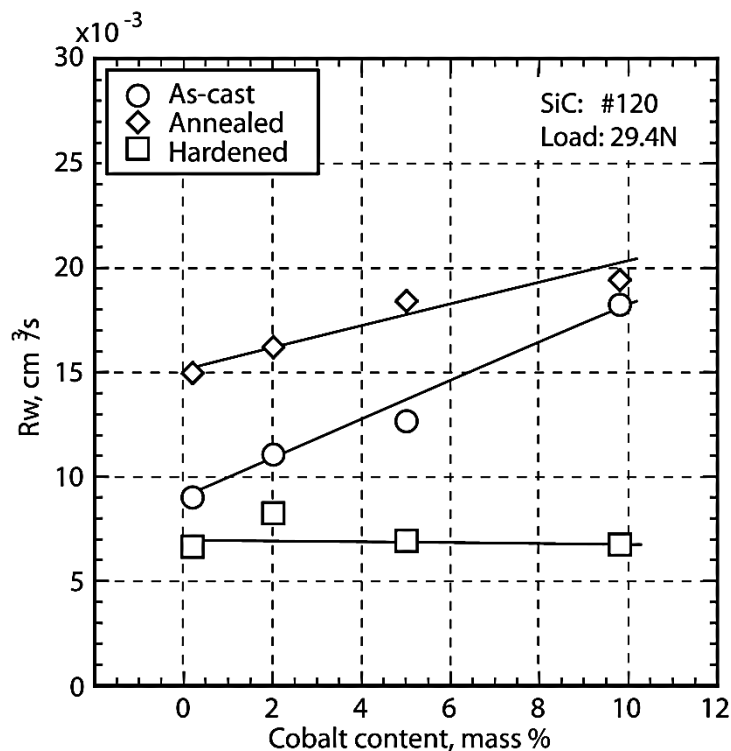


Fig.2-19 Effect of Co content on wear rate (R_w) of multi-alloyed white cast irons heat-treated with different conditions [23].

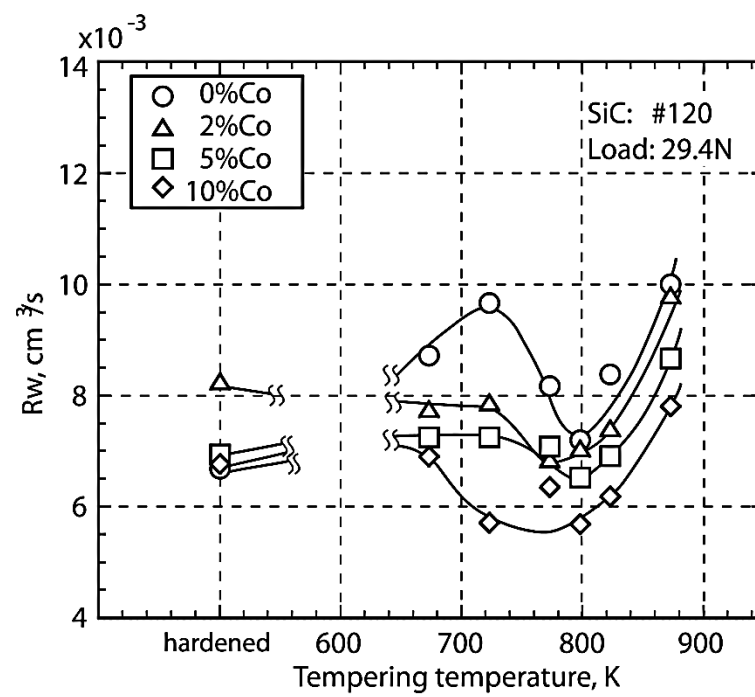


Fig.2-20 Effect of tempering temperature on wear rate (R_w) of multi-alloyed white cast irons heat-treated with different Cr content [23].

The effect of alloying elements on high temperature wear property of multi-alloyed white cast iron for hot rolling mill roll was studied using roll simulator by Hashimoto et al. [26]. The results are shown in Fig.2-21. The wear resistance is expressed by wear loss. The superior wear resistance is obtained in 1.5 to 2.5 %C specimens of which C_{bal} values are near 0% regardless of alloying elements. It was discussed that the combination of hard matrix with tempered martensite and a large amount of hard eutectic carbides showed better wear resistance. With respect to the effect of alloy content, it is clear that the highest wear resistance or lowest wear loss is obtained at 2% C and 7.5% of each V, Cr and Mo as well as 1.5 %C and 7.5 %W.

Fig.2-22 shows the relationship between wear depth of roll used in the finishing mill and tonnage of rolled product which is expressed as a parameter of the rolling load and the number of rolling cycles [1]. The wear of roll made of multi-alloyed white cast iron is very small compared with conventional rolls, less than 1/5 of an indefinite-chilled cast iron roll (Ni-hard roll) and less than 1/3 of a high Cr cast iron roll.

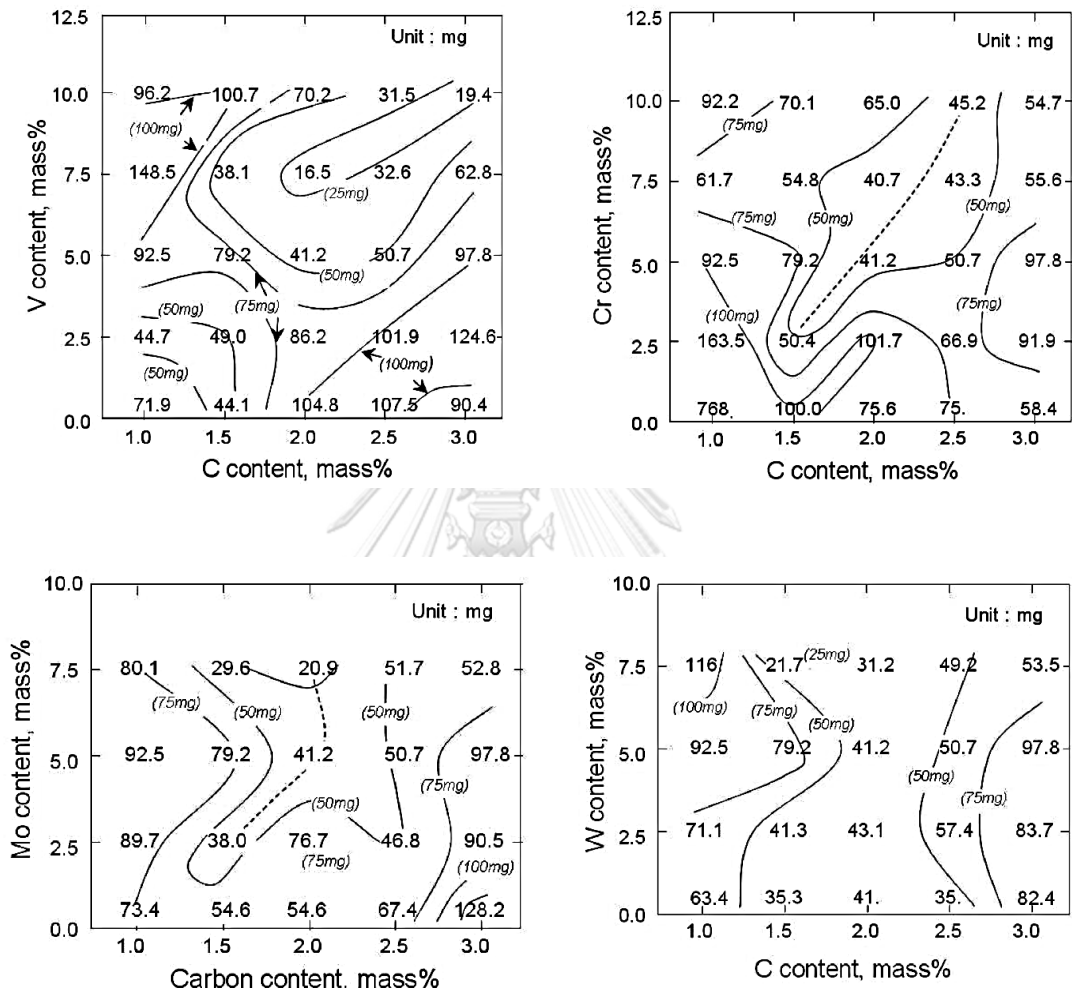


Fig.2-21 Effect of alloying elements content on hot abrasive wear resistance of multi-alloyed white cast iron with the basic chemical composition in relations of C and another carbide formers of V, Cr, Mo and W [26].

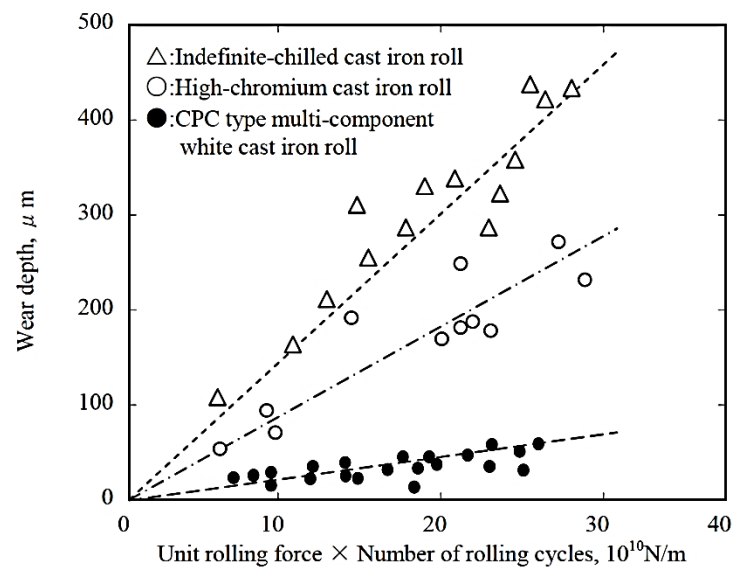


Fig.2-22 Relationship between wear depth and wear load of conventional rolls and CPC type roll made of multi-alloyed white cast iron [1].

Chapter III

Experimental Procedures

3.1 Preparation of test specimens

The charge calculations for test specimens with target chemical compositions are carried out. The raw materials such as mild steel, pig irons, ferro-alloys and pure-metals are used. The chemical composition of charge materials is shown in Table 3-1 while the target chemical compositions are shown in Table 3-2. Total weight of charge materials, 30 kg, is melted in a high-frequency induction furnace with alumina lining and the melt is superheated up to 1853K. After holding for 10 to 15 minutes, the melt is poured into preheated CO₂ mold with round bar with 25 mm in diameter and 65 mm in height as shown in Fig.3-1. To produce the specimen for abrasive wear test piece, the same melt is poured into Y-block mold with 50 mm in both of width and height and 200 mm in length shown in Fig.3-2 (a). The top of riser is immediately covered by an exothermic powder to prevent the melt from fast cooling and oxidation.

In order to investigate the heat treatment behavior, the risers of round bar and Y-block ingots are cut off by a wire-cutting machine to obtain the block of specimen. These blocks of specimen are supplied to annealing for the removal of casting stress and micro-segregation produced during solidification. The surface of each substantial body is coated with an anti-oxidation paste to prevent the block from oxidation and decarburization during annealing. The annealing condition is at 1223K for 18 ks holding and then, cooling in the furnace (FC). After annealing, the bodies are sectioned at 7 mm in thickness by a wire-cutting machine to obtain test pieces.

Table 3-1 Chemical composition of charge materials.

Charge materials	Elements (mass%)						
	C	Si	Mn	Cr	V	Mo	Fe
Mild steel scrap	0.12	0.02	0.28				bal
Pig iron	4.30	0.20	0.12				bal
Metallic Cr				98.6			
Metallic Mn			99.97				
Fe-Cr (HC)	8.12	1.80		60.54			bal
Fe-Cr (LC)	0.08	0.37		67.44			bal
Fe-Mo	0.05	0.70				62.87	bal
Fe-V	0.09	1.07			82.31		bal
Fe-Si	0.05	77.80					bal

Table 3-2 Target chemical compositions of test specimens.

Specimen No.	C	Si	Mn	Cr	Mo	W	V	Co
No.1	2.00	0.50	0.50	3.00	5.00	5.00	5.00	2.00
No.2	2.00	0.50	0.50	5.00	5.00	5.00	5.00	2.00
No.3	2.00	0.50	0.50	6.00	5.00	5.00	5.00	2.00
No.4	2.00	0.50	0.50	7.00	5.00	5.00	5.00	2.00
No.5	2.00	0.50	0.50	9.00	5.00	5.00	5.00	2.00

The chemical compositions of the ingot are shown in Table 3-3.

Table 3-3 Chemical compositions of the ingot.

Specimen No.	C	Si	Mn	Cr	Mo	W	V	Co
No.1	1.96	0.52	0.49	3.09	5.02	5.02	4.96	1.98
No.2	1.97	0.52	0.52	4.98	5.02	4.98	5.07	1.99
No.3	2.02	0.54	0.51	5.99	4.93	4.93	4.97	2.00
No.4	1.98	0.50	0.49	7.01	5.09	5.05	5.03	2.01
No.5	2.08	0.53	0.49	8.93	5.01	5.03	5.07	2.00

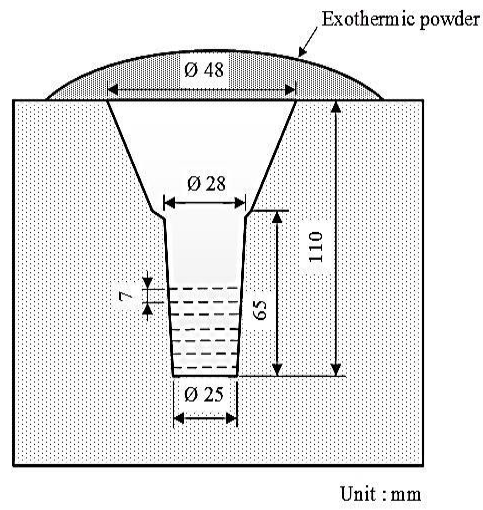


Fig.3-1 Schematic drawing of CO₂ mold for round-bar ingot.

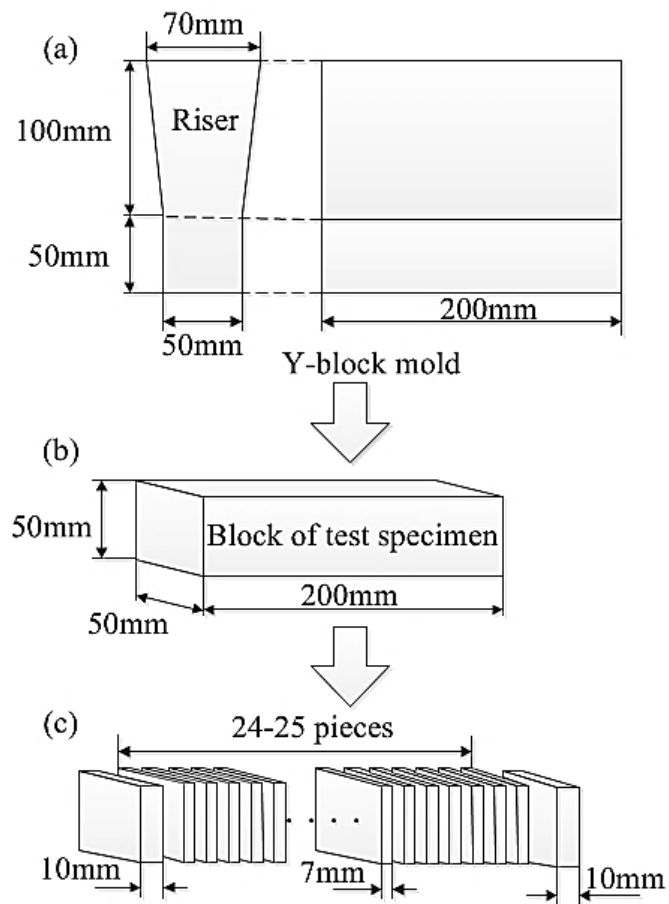


Fig.3-2 Schematic drawings of processes for making test pieces of abrasive wear tests from ingots.

3.2 Heat treatment process

3.2.1 Heat treatment condition to investigate heat treatment behavior

Before heat treatment, test specimens are coated by an anti-oxidation solution to prevent the specimens from oxidation and decarburization. The heat treatment conditions are summarized in Table 3-4. After annealing at 1223K for 18 ks, the test pieces are austenitized at 1323K (1050 °C) and 1373K (1100 °C) for 3.6 ks (1 hour). After holding, the test pieces are hardened by fan air cooling (FAC) to room temperature. The hardened test pieces are tempered at temperatures between 623 and 873K (400 to 600°C) by 50K intervals for 12 ks (200 minutes) and cooled by air (AC).

Table 3-4 Conditions of heat treatment.

Heat treatment	Temperature (K)	Holding Time (ks)	Cooling Condition
Annealing	1223	18	Furnace Cooling (FC)
Hardening	1323 1373	3.6	Fan Air Cooling (FAC)
Tempering	623 673 723 748 773 798 823 873	12	Air Cooling (AC)

3.2.2 Heat treatment condition of test piece to perform carry out abrasive wear test

The test pieces for abrasive wear test have to be heat-treated under the various conditions. The conditions of heat treatment are summarized in Table 3-5. As-hardened specimens are tempered at 3 levels between 673 and 873K. The three tempering temperatures are determined from the tempered hardness curve of each specimen which is already made by the experiment. The method is schematically illustrated in Fig.3-3. First of all, a temperature at which the maximum tempered hardness is obtained ($H_{T_{max}}$). Next, the temperatures lower and higher than temperature of $H_{T_{max}}$ ($L-H_{T_{max}}$ and $H-H_{T_{max}}$ respectively) at which same tempering hardness are expected. In this method, one test piece with the highest hardness and two test pieces with lower hardness than $H_{T_{max}}$ are made. However, there are reasonable differences among of matrix microstructures of three specimens, especially in the volume fraction of retained austenite ($V\gamma$) as shown in Fig.3-3. It can be understood that under the similar hardness in $L-H_{T_{max}}$ and $H-H_{T_{max}}$ specimens, the $V\gamma$ value differs greatly between both specimens. Using these three test pieces of $L-H_{T_{max}}$, $H_{T_{max}}$ and $H-H_{T_{max}}$, the effects of hardness and $V\gamma$ on the abrasive wear behaviors are evaluated, and additionally those results will be related to the Cr content of specimens. In the experiment, test pieces are held at the tempering temperature for 12 ks and cooled to room temperature in the air.

Table 3-5 Heat treatment conditions.

Heat treatment	Annealing	Hardening	Tempering
Temperature	1223K	1323 and 1373K	3 levels between 673 and 873K
Holding time	18 ks	3.6 ks	12 ks
Cooling condition	Furnace cooling (FC)	N ₂ quench	Air cooling (AC)

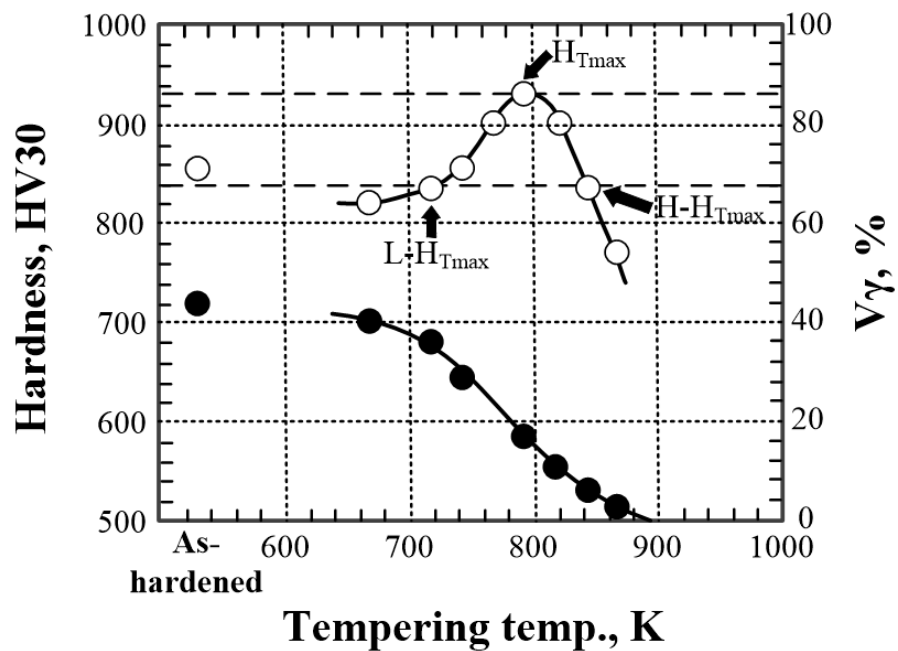


Fig.3-3 Schematic illustration showing how to determine three tempering temperatures from tempered hardness curve.

3.3 Observation of microstructure

3.3.1 Optical microscope (OM)

Two-dimensional microstructures of specimens are observed by optical microscope (OM). The test piece is polished using SiC emery paper in the order of 80, 120, 180, 320, 400 and 600 meshes, and then polished with alumina powder of 0.3 μm in grain size. Finally, it is etched by Groesbeck's reagent to reveal the types of carbide, Vilella's reagent to reveal between carbide and microstructure and Nital reagent to reveal matrix structure. The etchant, etching method and observation points are summarized in Table 3-6.

Table 3-6 Etchant, etching method and observation point.

Etchant	Etching method	Observation
<u>Groesbeck's reagent</u> – KMnO_4 4 g. – NaOH 4 g. Water 100 mL	Immersion at room temperature	Types of carbide
<u>Vilella's reagent</u> – Picric acid 1 g. – HCl 5 cc. – Ethanol 100 cc.	Immersion at room temperature	Carbide and matrix structures
<u>Nital reagent</u> – HNO_3 5 mL – Ethanol 95 mL	Immersion at room temperature	Matrix structure

3.3.2 Scanning electron microscope (SEM)

Three-dimensional microstructure or configuration of specimen is observed by scanning electron microscope (SEM) at high magnifications. The investigation focuses on the matrix microstructure or phases in matrix for discussion of wear behavior. The mirror polished surface etched a little deep is provided to investigate microstructure in detail. SEM operation is taken under the conditions of accelerating voltage with 25 kV and filament current of 80 mA.

3.4 Hardness measurement

Macro-hardness of specimen is measured using Vickers hardness tester with the load of 294.2 N (30 kgf). The hardness of matrix or micro-hardness is performed using Micro-Vickers hardness tester with the load of 0.98 N (100 gf). The measurement is accomplished randomly more than five times and the average value is adopted.

3.5 Measurement of volume fraction of austenite

Volume fraction of retained austenite (V_{γ}) of specimen is measured using X-ray diffraction method. The specialized goniometer set up an automatic rotating and swinging sample stage is used to reduce the influence of preferred orientation of austenite. The measurement condition is presented in Table 3-7. The Mo- $K\alpha$ beam with the wavelength of 0.007 nm, which is filtered through Zr foil, is used as the x-ray source and the test piece is scanned from 24 to 44 degrees of 2θ .

The basic equation of quantitative measurement of the volume fraction of retained austenite is expressed by equation as

$$I_{hkl} = K(FF^*)(LPF)me^{-2M}[A(\theta)](V_i/v_i^2) \dots \dots \dots (3-1)$$

- where
- I_{hkl} = integrated intensity per angular diffraction peak (hkl).
 - K = proportionality constant.
 - FF^* = structure factor of the unit cell of interested phase, it equal to $4f^2$ and $16f^2$ in diffraction line of α (ferrite or martensite) and γ (austenite), respectively.
 - LPF = Lorenz Polarization Factor which equal to $(1+\cos^2 2\theta)/\sin^2 \theta \cos \theta$.
 - m = multiplicity factor of the (hkl) plane reflection.
 - e^{-2M} = Debye-Waller or temperature factor which is function of θ , where $M = (B \sin^2 \theta)$ and B is material constant.
 - $A(\theta)$ = absorption factor which independent from θ if sample is flat.
 - V_i = volume fraction of the interested phase.
 - v_i = volume fraction of unit cell.

Assume, $K' = K * A(\theta) \dots \dots \dots (3-2)$

and $R_{hkl} = [(FF^*)(LPF)me^{-2M}]/v_i^2 \dots \dots \dots (3-3)$

Substitutes equation (3-2) and (3-3) in the equation (3-1), then

$$I_{hkl} = K'(R_{hkl})(V_i) \dots \dots \dots (3-4)$$

The calculation of numerous peaks in the diffraction pattern, equation (3-4) becomes

$$\Sigma I_{hkl} = K'(\Sigma R_{hkl})(V_i) \dots \dots \dots (3-5)$$

Therefore, peaks of ferrite or martensite (α) and austenite (γ) are considered. The integrated intensity equation is expressed as

$$\Sigma I_{\alpha} = K'(\Sigma R_{\alpha})(V_{\alpha}) \dots \dots \dots (3-6)$$

$$\Sigma I_{\gamma} = K'(\Sigma R_{\gamma})(V_{\gamma}) \dots \dots \dots (3-7)$$

Then, the pair of ferrite or martensite and austenite can be written as

$$\Sigma I_{\alpha} / \Sigma I_{\gamma} = [(\Sigma R_{\alpha} / \Sigma R_{\gamma})(V_{\gamma} / V_{\alpha})] \dots \dots \dots (3-8)$$

Beside, $V_{\alpha} + V_{\gamma} + V_c = 1 \dots \dots \dots (3-9)$

where V_c is the volume fraction of carbides. Assume only ferrite or martensite and austenite exist in the microstructure, so that, equation becomes

$$V_{\alpha} + V_{\gamma} = 1 \dots \dots \dots (3-10)$$

The volume fraction of austenite (V_{γ}) which relates to integrated intensity of ferrite and austenite peaks to R-value is

$$V_{\gamma} = 1 / [1 + (\Sigma I_{\alpha} \Sigma R_{\gamma} / \Sigma I_{\gamma} \Sigma R_{\alpha})] \dots \dots \dots (3-11)$$

The diffraction peaks for quantitative calculation are (200) and (220) planes for ferrite (α) or martensite (M) and (220) and (311) planes for austenite (γ). The main purpose to choose these peaks is the fact that every peak is independent or apart from other unnecessary peaks. Therefore, the overlapped peaks with plane of Cr carbide (M_7C_3) are not taken into account austenite plane (211).

The volume fraction of retained austenite (V_{γ}) is calculated from integrated area of the selected peaks measured by an image analysis software. The calculations

of V_γ are done from the ratio of the integrated areas in peak α_{200} vs. peak γ_{311} , that of peak α_{200} vs. peak $\Sigma\gamma_{(220,311)}$, and peak $\Sigma\alpha_{(200,220)}$ vs. peak γ_{311} . The values obtained from three calculations are averaged.

Table 3-7 X-ray diffraction conditions for measurement of volume fraction of retained austenite (V_γ).

Target metal	Mo
Tube voltage / current	50 kV / 30 mA
Slits	Divergence slit : 1°, Receiving slit : 1.5 mm, Scattering slit : 1°
Filter	Zr
Scanning range (2θ)	24-44 degree
Scanning speed	0.5 degree/min
Step/sampling	0.01 degree

3.6 Abrasive wear test

3.6.1 Mechanism of abrasive wear

The simplified model of abrasive wear is introduced to understand the wear mechanism. The model that material is worn by an abrasive particle or single grit is schematically shown in Fig.3-4. The relation of the hardness of material and the load on the grit is express by equation (3-12),

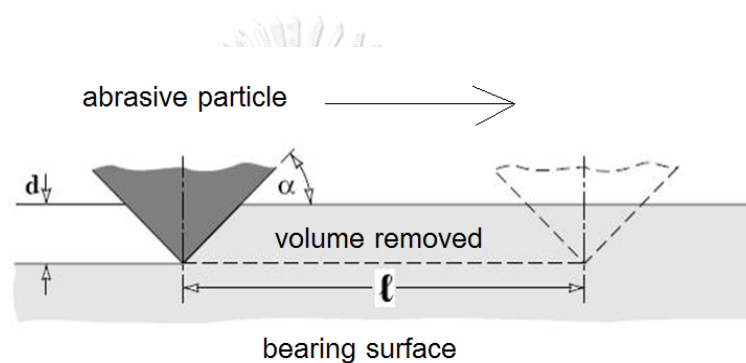


Fig.3-4 Schematic drawing of model showing abrasive wear by single grit with cone shape [49].

$$F = A \times H_v \dots\dots\dots(3-12)$$

here, F is the force applied to the grit, A is surface area of the indentation produced and H_v is the Vickers hardness of material. Then, the individual load on a grit (L_g) can be calculated using the following equation,

$$L_g = 0.5\pi(d \cot\alpha)^2 H_v \dots\dots\dots(3-13)$$

Where, d is the depth of indentation (m) and α is the slope angle (degree) of the cone. Since the approximate volume of the material removed by the cone is the product of

the cross-sectional area of indentation and the traversed distance, the relation is expressed by next equation,

$$V_g = \ell d^2 \cot \alpha \dots \dots \dots (3-14)$$

here, V_g is the volume of material removed by the cone (m^3) and ℓ is the distance travelled by the cone (m). Eliminating 'd' from equation (3-13) and equation (3-14), equation (3-15) which express the relationship between V_g and the shape of the grit, the sliding distance (ℓ) and L_g is obtained.

$$V_g = \frac{2\ell \tan \alpha}{\pi H} \times L_g \dots \dots \dots (3-15)$$

The total wear is the sum of volume of material removed by grids. Therefore, the total volume of wear loss (V_{tot}) can be given by following equation,

$$V_{tot} (m^3) = \frac{2\ell \tan \alpha}{\pi H} \times W_{tot} \dots \dots \dots (3-16)$$

where, W_{tot} is total load (N). It is found from equation (3-16) that the wear loss is closely connected to the applied load and the hardness of material. Because the load depends on the wear environment, it can be said that the hardness becomes very important barometer of the wear resistance.

3.6.2 Preparation of surface of wear test piece

The surface of test piece is ground using grindstone wheel machine for the surface roughness (Ra_{max}) to be controlled less than 3 μm . The surface roughness is measured using a roughness tester.

3.6.3 Suga abrasive wear tester

The Suga abrasive wear tester is used to evaluate a two-body-type abrasive wear test. The schematic drawing of Suga abrasive wear tester is shown in Fig.3-5. The abrading wheel with 44 mm in diameter and 12 mm in thickness is adhered to 180 mesh emery paper. The abrasive load of 1 kgf is applied to the surface of test piece. During test, the abrading wheel rotates intermittently synchronizing the movement of test piece back and forth in 30 mm distance on the same surface area. The abrading wheel moves once while the test piece reciprocates once in the fixed distance. Therefore, a new surface of emery paper can contact to the surface of test piece at every movement of the test piece. After test, the test piece is cleaned in ultrasonic acetone bath and then, dried. The amount of weight loss in the test piece is weighed by using a high precision digital balance with 0.1 mg accuracy before and after the test. The wear loss per one test is obtained as the difference between the weight before and that after one test. The wear test is repeated for eight times in the same area, and then, the total distance of test is 192 m.

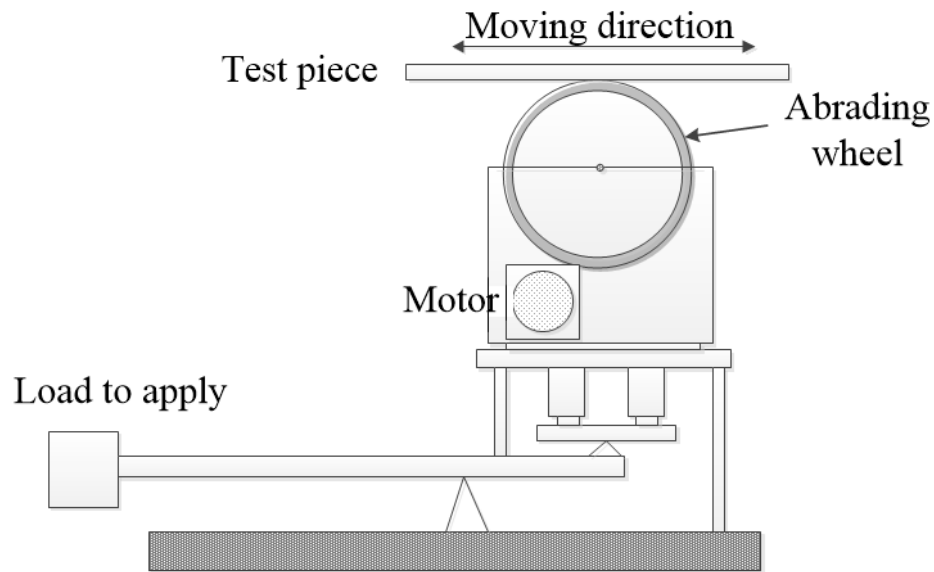


Fig.3-5 Schematic drawing of Suga abrasive wear tester.

3.6.4 Rubber wheel abrasive wear tester

The rubber wheel abrasive wear test is adopted to evaluate the three-body-type abrasive wear resistance and the outline of the equipment is shown in Fig.3-6. The silica sand of ASTM 60 grade is used as abrasive materials. The wheel has 125 mm in diameter and 15 mm in thickness. The test condition is shown in Table 3-6. The abrasives are fed through the nozzle to the contacting surface between rotating rubber wheel and test piece at the feeding rate of 250-300 g/min under the load of 8.7 kgf. The number of revolutions per one cycle test is 1000 revolutions and the rotating speed is 120 rpm. After finishing one cycle, test piece is cleaned in an ultrasonic acetone bath and dried. The weight of test piece before the test, and afterward, that after every test is measured by using high precision digital balance with 0.1 mg accuracy. The test is repeated four times in the same area.

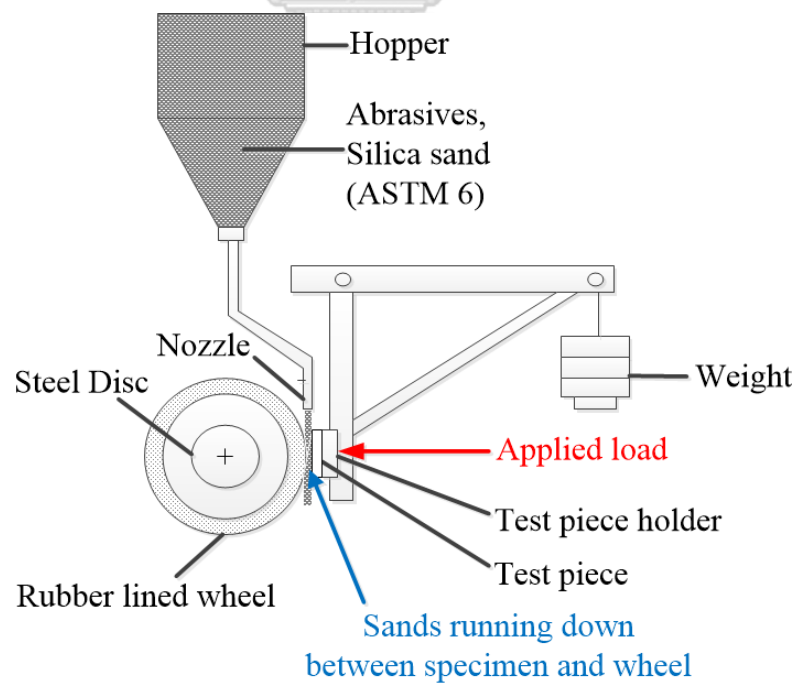


Fig.3-6 Photo and schematic drawing of rubber wheel abrasive wear tester.

Table 3-8 Test condition for Rubber wheel abrasive wear test.

Abrasives material	Silica sand of ASTM 6 grade
Feeding rate	250 - 300 g/min
Applied load	85.32 N (8.7 kgf)
Number of revolutions	1,000
Rotating speed	120 rpm

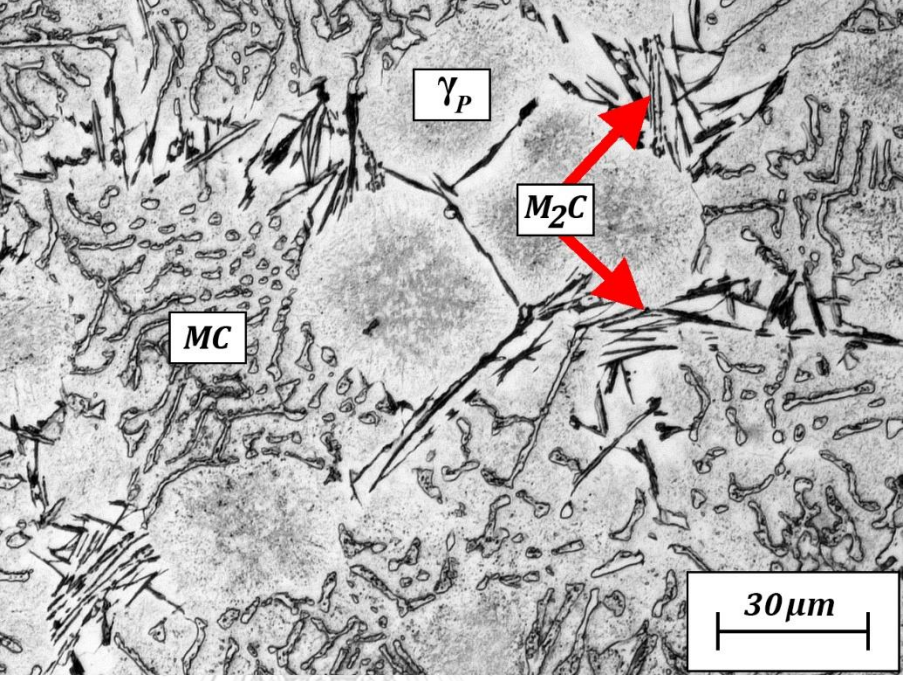
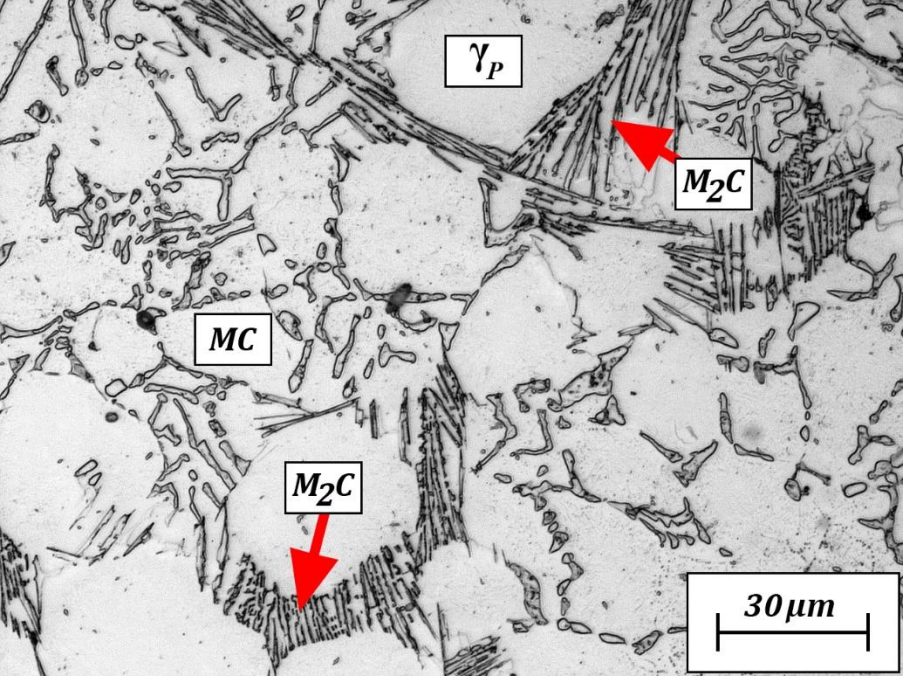
Chapter IV

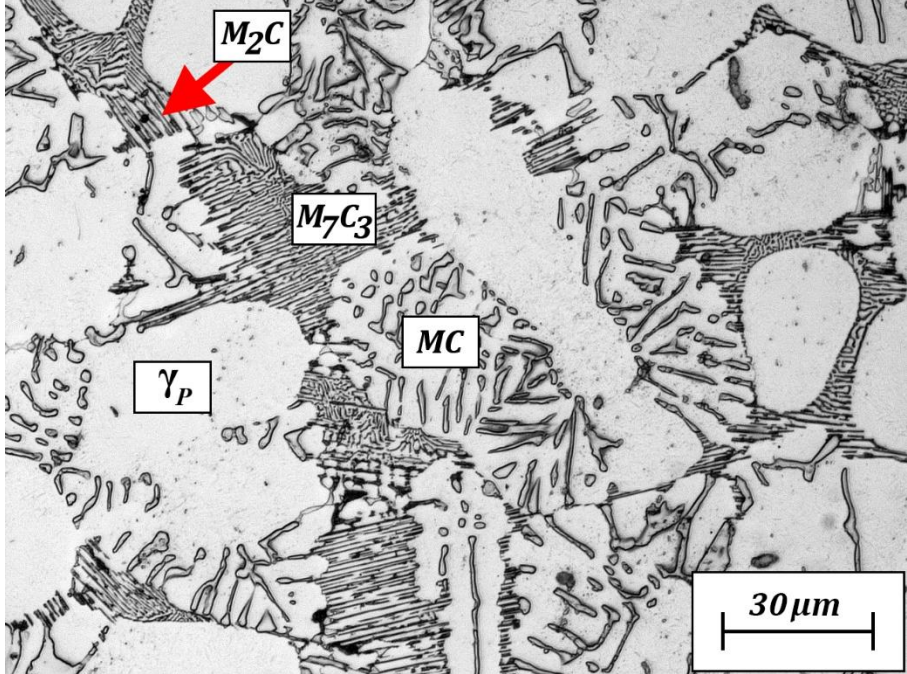
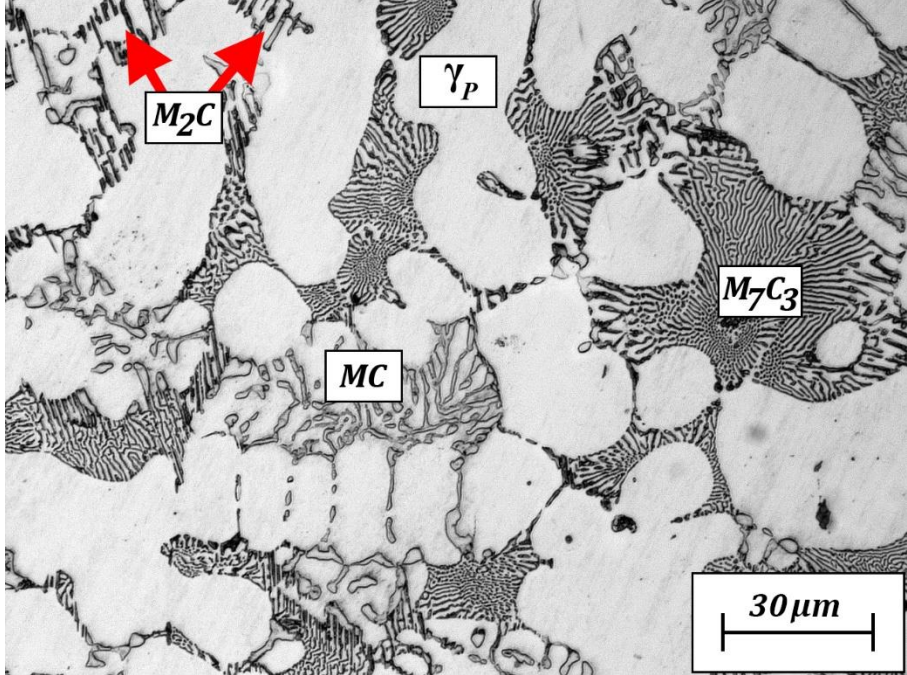
Experimental Results

4.1 Microstructures of specimens in as-cast state

4.1.1 Effect of Cr content on as-cast microstructure

The surface of as-cast specimens was polished by metallurgical method and etched by Groesbeck's reagent to distinguish M_2C and M_7C_3 carbides. The microstructures of as-cast specimens were observed using optical microscope (OM). The microphotograph of each specimen is shown in Fig.4-1. All the specimens show hypoeutectic structure consisting of primary austenite dendrite (γ_P) and eutectic structure (γ +eutectic carbide). In the freezing sequence, the γ_P solidifies first and the eutectic follows it at the boundary of γ_P . The eutectic carbides of MC type are in flaky and nodular, M_2C type in fine or coarse rod-like and M_7C_3 type in ledeburitic morphologies. The eutectics of (γ +MC) and (γ + M_2C) exist in the specimens with low Cr content such as No.1 and 2 with 3.09% and 4.98%Cr, respectively. In the specimen No.3 with 5.99%Cr, the eutectic of (γ + M_7C_3) begins to crystallize by taking place of (γ + M_2C) eutectic. As for specimen No.4 with 7.01%Cr, the (γ + M_2C) eutectic is very less and the amount of (γ + M_7C_3) eutectic increases. In the case of specimen No.5 with 8.93%Cr, the eutectic structure is mostly consisted of (γ +MC) and (γ + M_7C_3). The matrix structures are mainly composed of austenite and some martensite. This is because Cr suppresses pearlite transformation and lowers the M_s temperature. However, martensite could not be observed clearly by OM with low magnification.

Specimen	Microstructure
No.1 (3.09% Cr)	 <p>Micrograph showing the microstructure of specimen No.1 (3.09% Cr). The structure consists of primary γ_P (primary austenite), martensite (M_2C), and martensite carbide (MC). Red arrows point to M_2C regions. A scale bar indicates $30\ \mu\text{m}$.</p>
No.2 (4.98% Cr)	 <p>Micrograph showing the microstructure of specimen No.2 (4.98% Cr). The structure consists of primary γ_P (primary austenite), martensite (M_2C), and martensite carbide (MC). Red arrows point to M_2C regions. A scale bar indicates $30\ \mu\text{m}$.</p>

Specimen	Microstructure
No.3 (5.99% Cr)	 <p>Micrograph showing the microstructure of Specimen No.3 (5.99% Cr). The image displays a complex microstructure with various phases labeled: M_2C, M_7C_3, MC, and γ_P. A red arrow points to an M_2C phase. A scale bar indicates $30\ \mu\text{m}$.</p>
No.4 (7.01% Cr)	 <p>Micrograph showing the microstructure of Specimen No.4 (7.01% Cr). The image displays a microstructure with various phases labeled: M_2C, γ_P, M_7C_3, and MC. Two red arrows point to M_2C phases. A scale bar indicates $30\ \mu\text{m}$.</p>

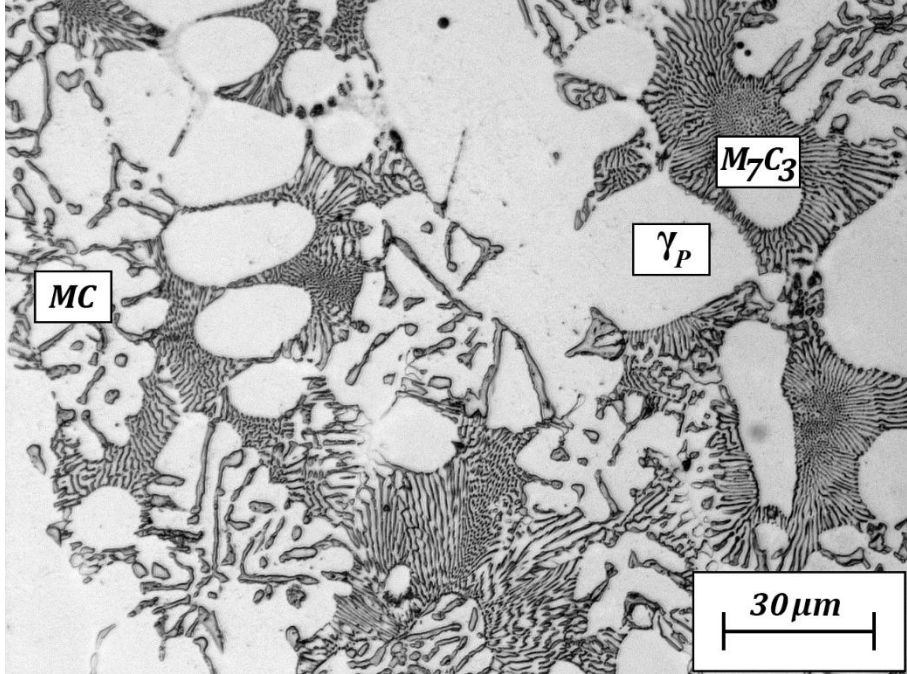
Specimen	Microstructure
No.5 (8.93% Cr)	 <p>The micrograph displays a complex microstructure of an as-cast specimen. It features several distinct regions: a matrix of fine, needle-like structures; larger, irregularly shaped regions labeled 'MC'; and a prominent, star-shaped region labeled 'M₇C₃'. A central region is labeled 'γ_P'. A scale bar in the bottom right corner indicates a length of 30 μm.</p>

Fig.4-1 Microstructures of as-cast specimens with different Cr contents.

4.1.2 Effect of Cr content on amount of primary austenite (γ_P) and eutectic structures

In order to clarify how Cr content affects the fraction of phases crystallized from the liquid, several microphotographs were taken in each as-cast specimen and primary austenite dendrite (γ_P) and each type of eutectic structure were outlined on the tracing paper. Then the area fractions of both phases were quantitatively measured by an image analysis software. The results are summarized in Table 4-1 and the relationship between both phases and Cr content is shown in Fig.4-2. Even if the Cr content increases, the γ_P values change only the range from 54% to 58%. The total area fraction of eutectic structures also changes a little between 41% and 45% to an increase in Cr content. When considering the effect of Cr content on individual eutectic structure, it is found that the area fraction of ($\gamma+MC$) eutectic decreases in the order from 40.56% in specimen No.1 with 3.09%Cr to 22.82% in No.5 with 8.93%Cr. The value of ($\gamma+M_2C$) eutectic increases to the highest value of 9.36% in specimen No.2 with 4.98%Cr, and then, it decreases to 5.97% in No.3 with 5.99%Cr. On the other side, the area fraction of ($\gamma+M_7C_3$) eutectic increases in order the from 3.87% in specimen No.3 to 21.50% in No.5 with 8.94%Cr.

Table 4-1 Area fractions of primary austenite (γ_p) and eutectic structures.

Specimen	Area fraction of primary austenite (%)	Total area fraction of eutectic structures (%)	Area fraction of eutectic structures (%)		
			$\gamma+MC$	$\gamma+M_2C$	$\gamma+M_7C_3$
No.1 (3.09%Cr)	58.27	41.73	40.56	1.17	
No.2 (4.98%Cr)	56.43	43.57	34.21	9.36	
No.3 (5.99%Cr)	58.14	41.86	32.02	5.97	3.87
No.4 (7.01%Cr)	54.75	45.25	27.51		17.74
No.5 (8.93%Cr)	55.68	44.32	22.82		21.50

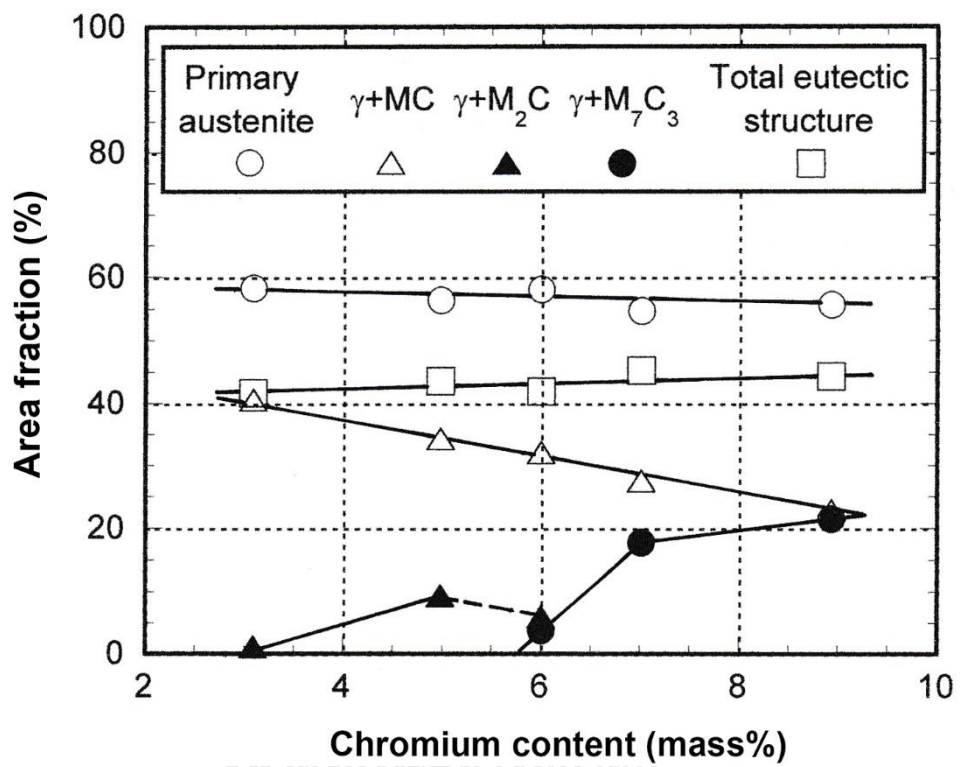


Fig.4-2 Effect of Cr content on area fraction of primary austenite and eutectic structures.

4.1.3 Effect of Cr content on macro- and micro-hardness in as-cast state

Macro- and micro-hardness of as-cast specimens are shown in Table 4-2. The hardness of specimen No.1 with 3.09%Cr are 537 HV30 and 499 HV0.1 whereas those of No.2 with 4.98%Cr specimen are 672 HV30 and 637 HV0.1, respectively. In the case of No.3 with 5.99%Cr specimen, the hardness are 784 HV30 and 745 HV0.1 and those of No.4 with 7.01%Cr shows the highest hardness values of 816 HV30 and 774 HV0.1, respectively. In specimen No.5 with highest Cr content of 8.93%, the hardness lower to be 761 HV30 and 725 HV0.1. It could be concluded that the hardness increased continuously to the highest value at Cr content of around 7%, and after that, it decreased as the Cr content increased.

Table 4-2 Macro- and micro-hardness of as-cast specimens.

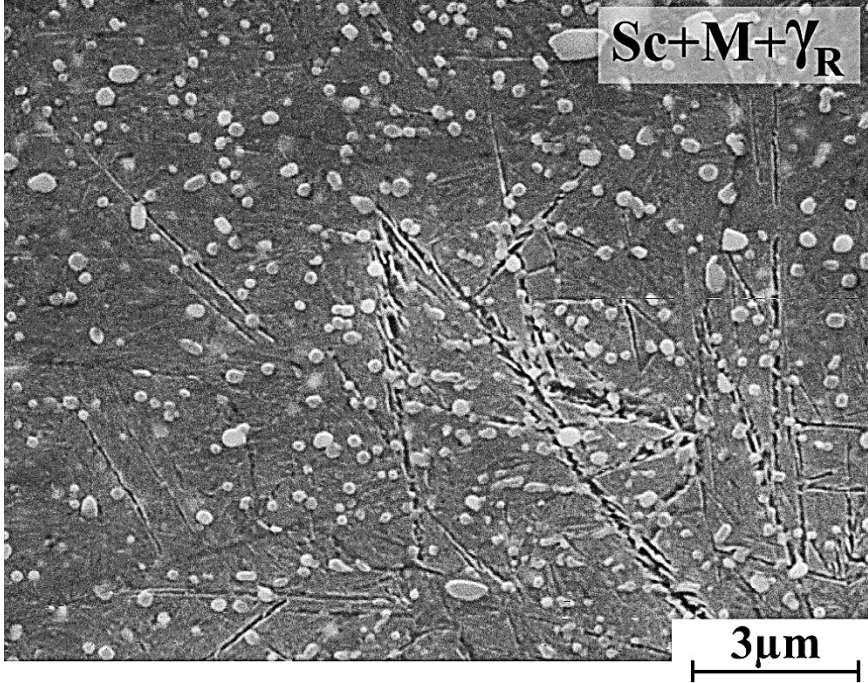
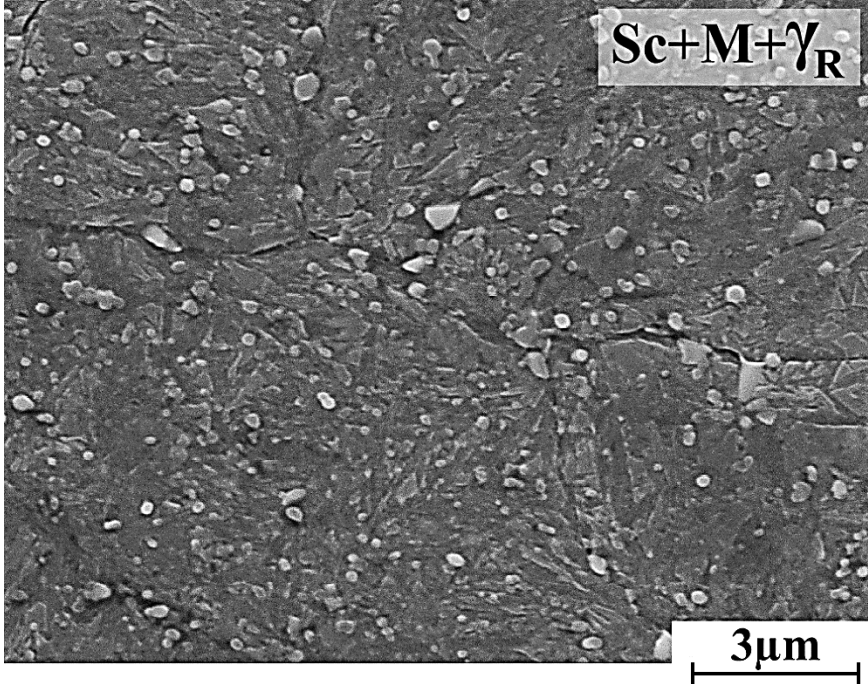
Specimen	Macro-hardness (HV30)	Micro-hardness (HV0.1)
No.1 (3.09%Cr)	537	499
No.2 (4.98%Cr)	672	637
No.3 (5.99%Cr)	784	745
No.4 (7.01%Cr)	816	774
No.5 (8.93%Cr)	761	725

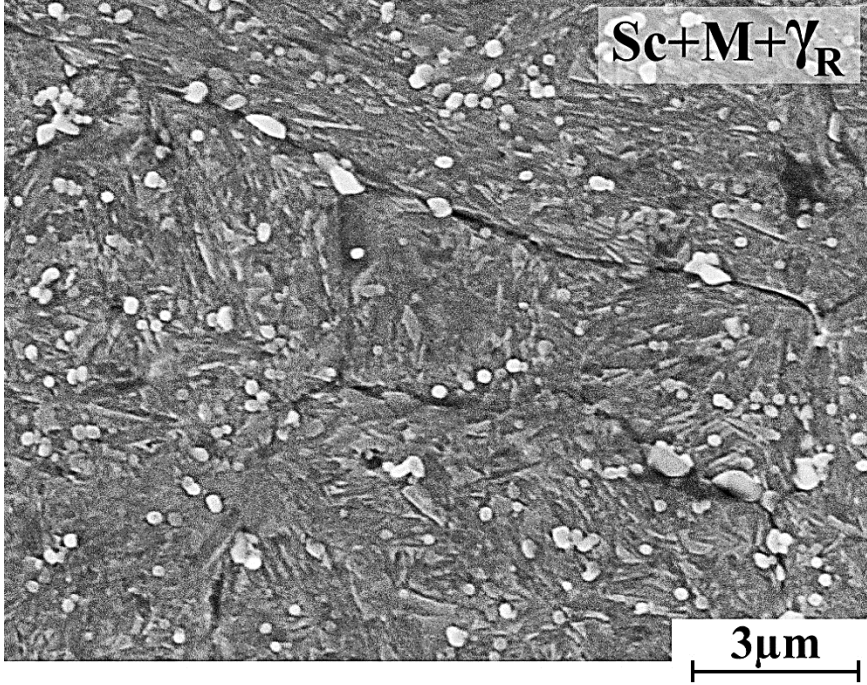
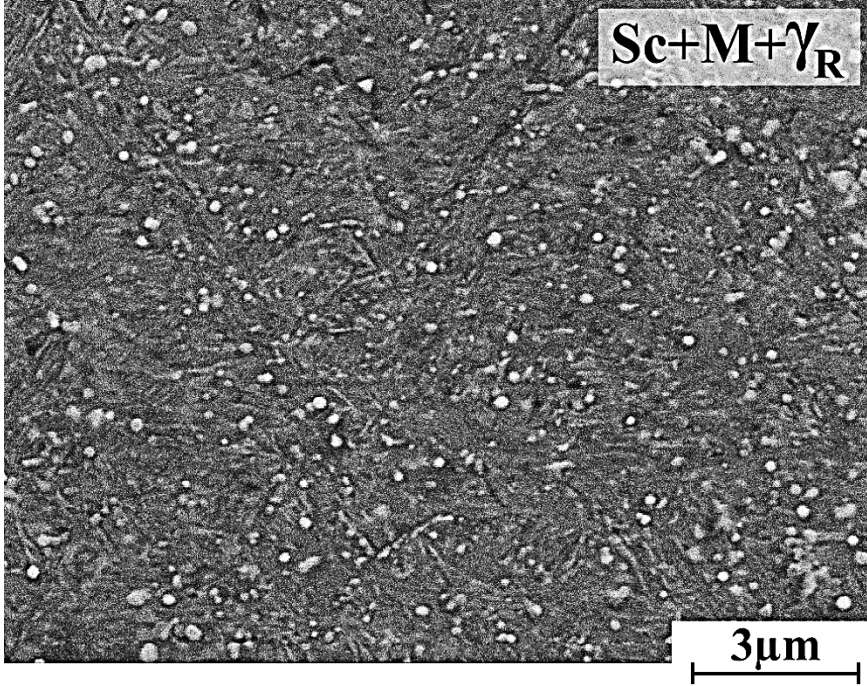
4.2 Effect of Cr content on heat treatment behavior

4.2.1 Relationship between heat treatment condition and variation of matrix structure

4.2.1.1 As-hardened state

It is well known that eutectic structure changes little by heat treatment from that in as-cast state except for M_2C carbide which decomposes to $(MC+M_6C+M_7C_3)$ during holding at high temperature for a long time. However, the matrix in specimen changes greatly depending on the heat treatment condition. The microphotographs focusing on matrix were taken using SEM and are shown in Fig.4-3 and 4-4 for 1323K and 1373K austenitizing, respectively. The retained austenite formed in the as-cast state is destabilized during austenitizing by precipitation of secondary carbide and martensite transformation. Therefore, the matrices in as-hardened specimens are mainly composed of secondary carbide (Sc), martensite (M) and some retained austenite (γ_R). The secondary carbide can be observed more clearly in SEM microphotograph. It is found that the amount of secondary carbides decreased with an increase in Cr content. Moreover, the microstructures of specimens hardened from low temperature of 1323K (Fig.4-3) show more secondary carbides compared with those hardened from high temperature of 1373K (Fig.4-4).

Specimen	Microstructure
No.1 (3.09%Cr)	 <p data-bbox="1093 421 1353 488">Sc+M+γ_R</p> <p data-bbox="1182 1025 1358 1086">3μm</p>
No.2 (4.98%Cr)	 <p data-bbox="1093 1137 1353 1205">Sc+M+γ_R</p> <p data-bbox="1182 1742 1358 1803">3μm</p>

Specimen	Microstructure
No.3 (5.99%Cr)	 <p data-bbox="1093 421 1353 488">$Sc+M+\gamma_R$</p> <p data-bbox="1182 1025 1358 1088">3 μm</p>
No.4 (7.01%Cr)	 <p data-bbox="1093 1137 1353 1205">$Sc+M+\gamma_R$</p> <p data-bbox="1182 1742 1358 1805">3 μm</p>

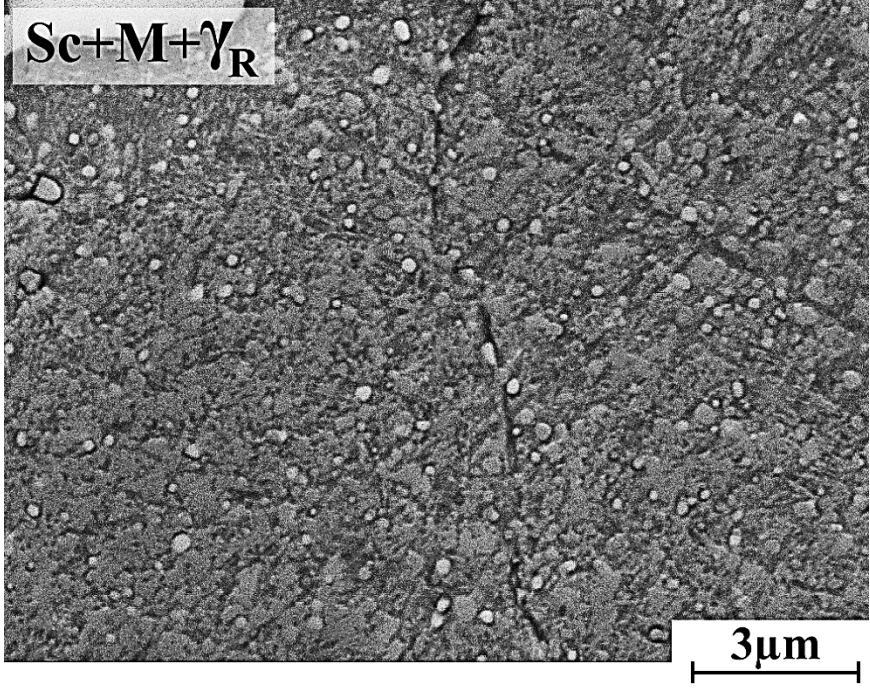
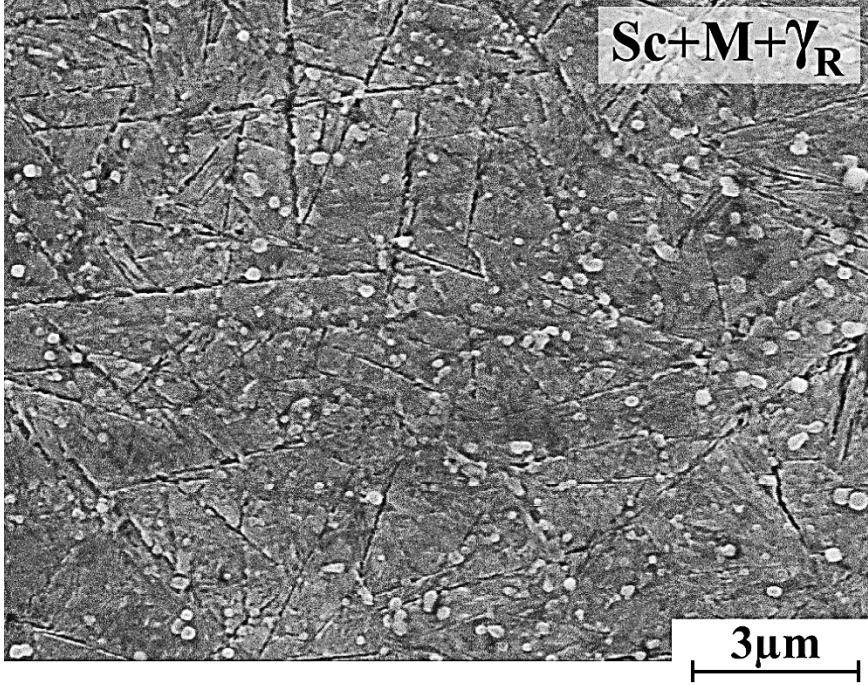
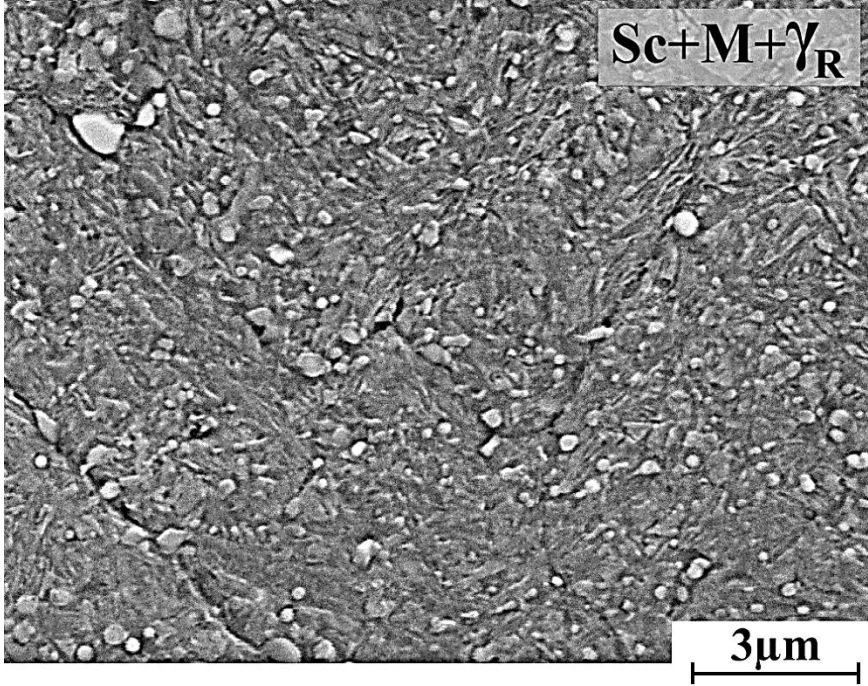
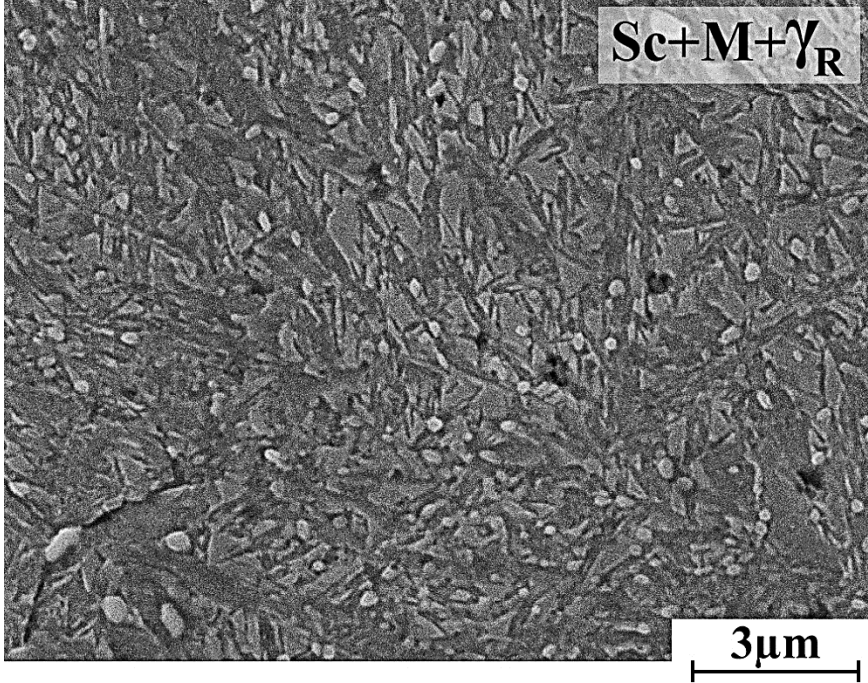
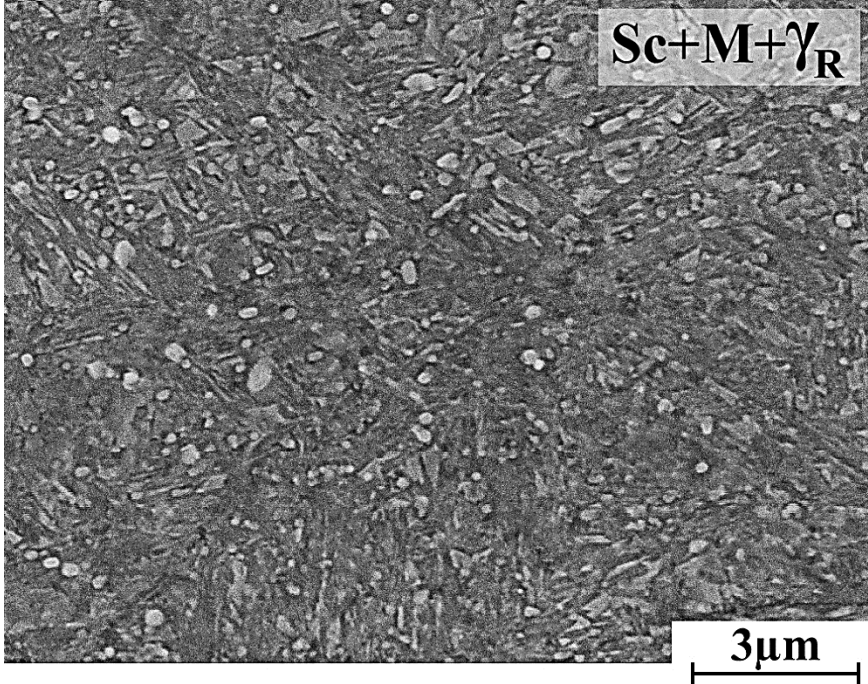
Specimen	Microstructure
No.5 (8.93%Cr)	 <p>Sc+M+γ_R</p> <p>3μm</p>

Fig.4-3 Matrix microstructures of as-hardened specimens with different Cr contents.
Austenitizing : 1323K.

Specimen	Microstructure
No.1 (3.09%Cr)	 <p data-bbox="1093 421 1353 488">$Sc+M+\gamma_R$</p> <p data-bbox="1177 1025 1353 1088">3 μm</p>
No.2 (4.98%Cr)	 <p data-bbox="1093 1137 1353 1205">$Sc+M+\gamma_R$</p> <p data-bbox="1177 1742 1353 1805">3 μm</p>

Specimen	Microstructure
No.3 (5.99%Cr)	 <p data-bbox="1093 414 1353 488">Sc+M+γ_R</p> <p data-bbox="1177 1019 1358 1086">3μm</p>
No.4 (7.01%Cr)	 <p data-bbox="1093 1131 1353 1205">Sc+M+γ_R</p> <p data-bbox="1177 1736 1358 1803">3μm</p>

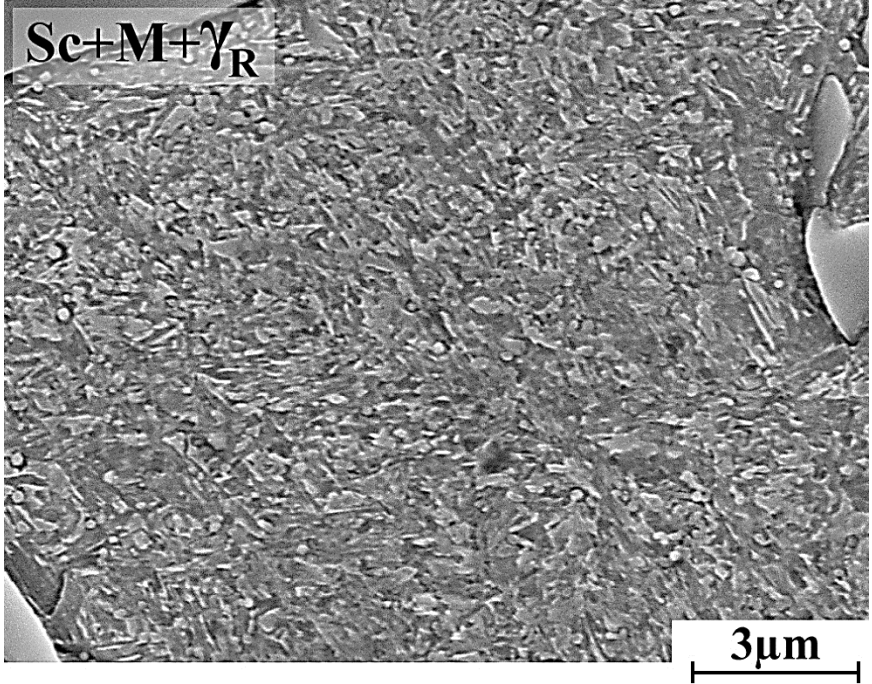
Specimen	Microstructure
No.5 (8.93%Cr)	 <p>Sc+M+γ_R</p> <p>3μm</p>

Fig.4-4 Matrix microstructures of as-hardened specimens with different Cr contents.

Austenitizing : 1373K.

4.2.2 Relationship between macro-hardness and volume fraction of retained austenite (V_γ)

4.2.2.1 As-hardened state

The macro-, micro-hardness and volume fraction of retained austenite (V_γ) in as-hardened specimens are summarized in Table 4-3.

Table 4-3 Macro-, micro-hardness and volume fraction of retained austenite (V_γ) of as-hardened specimens.

Specimen	Austenitizing temperature					
	1323K (1050°C)			1373K (1100°C)		
	Macro-hardness (HV30)	Micro-hardness (HV0.1)	V_γ (%)	Macro-hardness (HV30)	Micro-hardness (HV0.1)	V_γ (%)
No.1 (3.09%Cr)	919	858	14	901	841	12
No.2 (4.98%Cr)	931	872	18	909	853	24
No.3 (5.99%Cr)	922	860	16	900	844	23
No.4 (7.01%Cr)	913	851	11	897	840	20
No.5 (8.93%Cr)	887	840	7	870	826	12

The macro-hardness of specimens No.1 to No.4 hardened from 1323K austenitizing are overall higher than 900 HV30, i.e., 919 HV30 of specimen No.1 with 3.09%Cr, 931 HV30 of No.2 with 4.98%Cr, 922 HV30 of No.3 with 5.99%Cr and 913 HV30 of No.4 with 7.01%Cr. However, the macro-hardness of No.5 with highest Cr content of 8.93%Cr is 887 HV30 lower than the others.

In the case of hardening from 1373K austenitizing, macro-hardness of specimen No.1 to No.4 are almost same at about 900 HV30 except for No.5 with lower hardness of 870 HV30 for austenitizing temperatures of 1323K and 1373K, respectively.

The micro-hardness shows the same trend as macro-hardness, but the values are naturally lower than the macro-hardness. Moreover, the hardening from high temperature gives lower hardness than that from low temperature in all the specimens. The micro-hardness of specimen No.1 are 858 HV0.1 and 841 HV0.1 for hardening from 1323K and 1373K austenitizing, respectively. Hardness of 872 HV0.1 and 842 HV0.1 in No.2, 860 HV0.1 and 844 HV0.1 in No.3, 851 HV0.1 and 840 HV0.1 in No.4, and 840 HV0.1 and 826 HV0.1 in No.5 were also obtained for hardening from 1323K and 1373K, respectively.

On the other side, the V_γ values of specimen No.1 with 3.09%Cr are 14% and 12% for hardening from 1323 and 1373K austenitizing. The V_γ values of other specimens are 18 and 24% in No.2 with 4.98%Cr, 16 and 23% in No.3 with 5.99%Cr, 11 and 20% in No.4 with 7.01%Cr, 7 and 12% in specimen No.5 with 8.93%Cr for hardening from 1323K and 1373K, respectively. The largest V_γ values are obtained in 4.98%Cr specimen, regardless of the hardening temperatures. The reason why the amount of austenite showed the highest value at around 5%Cr can be supported by the results of Y. Yokomizo et., al., [50] i.e., the M_s temperature of multi-component white cast iron was lowest at 5% to 6%Cr.

4.2.2.2 Tempered state

After hardening from 1323K and 1373K austenitizing temperatures, the specimens were tempered between 673 and 873K with 50K interval and additional 25K interval where the highest hardness could be obtained. The relationship between macro-hardness, volume fraction of retained austenite (V_γ) and tempering temperature are shown in Fig.4-5 for specimen No.1, Fig.4-6 for No.2, Fig.4-7 for No.3, Fig.4-8 for No.4 and Fig.4-9 for No.5, respectively.

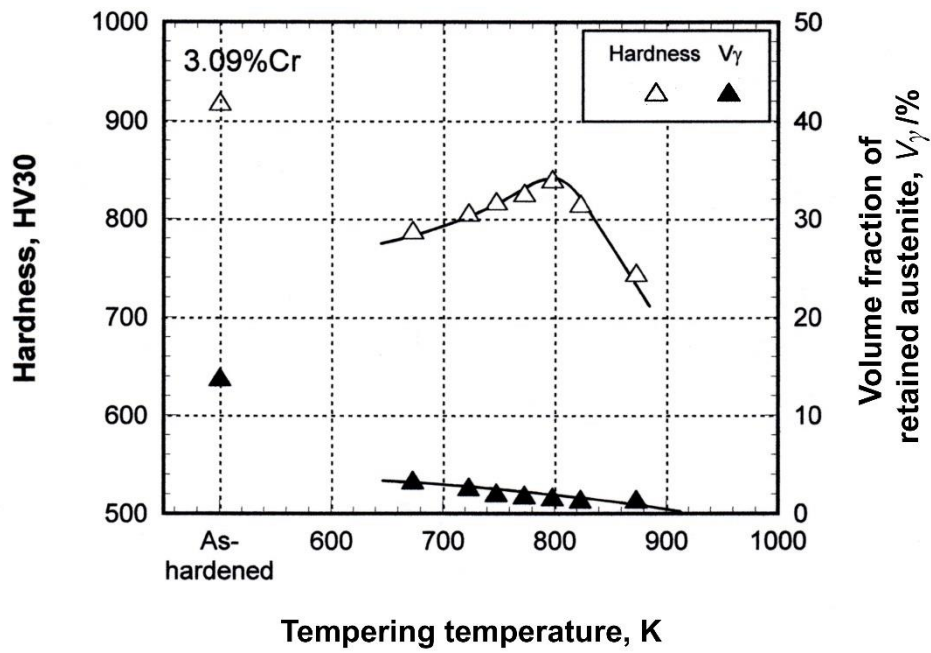
The results show that the macro-hardness drops greatly at first stage of low tempering temperature from that in as-hardened state because martensite is decomposed by C diffusion to pearlite with very fine carbides which is called as tempered martensite and formation of secondary carbide began to occur from the retained austenite. As the tempering temperature rises, the hardness continues to go up to the highest value at a certain temperature. When the tempering temperature gets over the highest point, the hardness decreases continuously. The increase in the hardness is due to an increase in the precipitation of secondary carbides, what is called, secondary hardening. The decrease in hardness over the maximum point could be due to the coarsening of secondary carbides and transformation of residual austenite to soft ferrite without transforming into martensite.

As shown in Fig.4-5, the macro-hardness of specimen No.1 increases continuously to the maximum tempered hardness (H_{Tmax}) of 841 HV30 (a) and 902 HV30 (b) at tempering temperature of 798K for 1323K and 1373K austenitizing, respectively. It is found that higher hardening temperature provides larger H_{Tmax} in

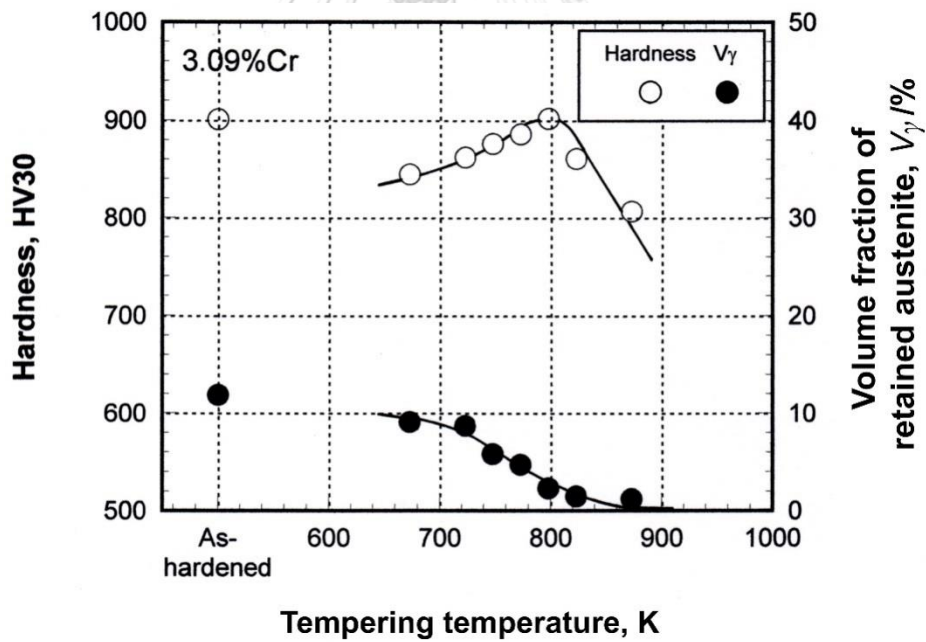
comparison with the case of low hardening temperature. On the other side, the V_γ in as-hardened state decreases continuously as tempering temperature rises.

In the case of specimen No.2 shown in Fig.4-6, the H_{Tmax} values of 913 HV30 and 933 HV30 for 1323K and 1373K austenitizing specimens are obtained at the same tempering temperature of specimen No.1. The tempered hardness curves are overall located at higher hardness side than those of specimen No.1 in both austenitizing temperatures. The V_γ values in as-hardened state show the highest compared with the other specimens in every tempering temperature. The reason why the V_γ values in as-hardened state is largest must be due to the fact that the M_s temperature decreased as the Cr content increased and the lowest M_s temperature was obtained at 5%Cr in the basic alloyed composition of multi-alloyed white cast iron.

As for the results of specimen No.3 shown in Fig.4-7, the H_{Tmax} of 909 HV30 and 928 HV30 are obtained by hardening at 1323K and 1373K, respectively. It is also clear that high austenitizing temperature gives higher hardness than low austenitizing temperature at all the tempering temperatures. However, it is noticeable that the tempering temperature at which H_{Tmax} is obtained shifted to the lower temperature side at 773K. This reason can be explained that the C concentration in austenite was reduced by increasing of Cr content and therefore, the lower tempering temperature was sufficient to complete the precipitation of secondary carbide and reach the H_{Tmax} . The V_γ values decrease slowly with an increase in tempering temperature but they begin to drop greatly when the tempering temperature get over 748K in both austenitizing temperatures.

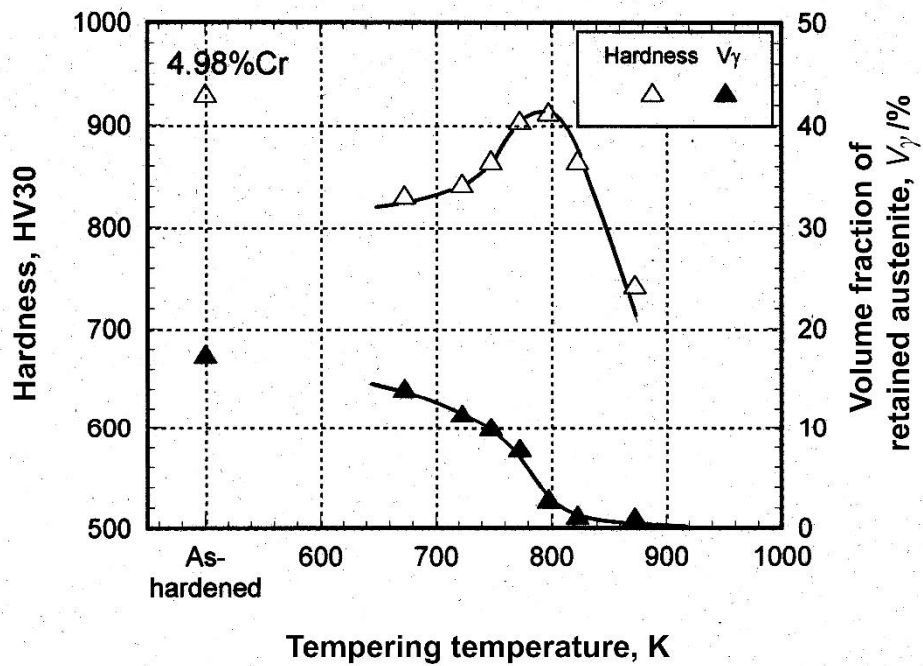


(a) Austenitizing temperature: 1323K.

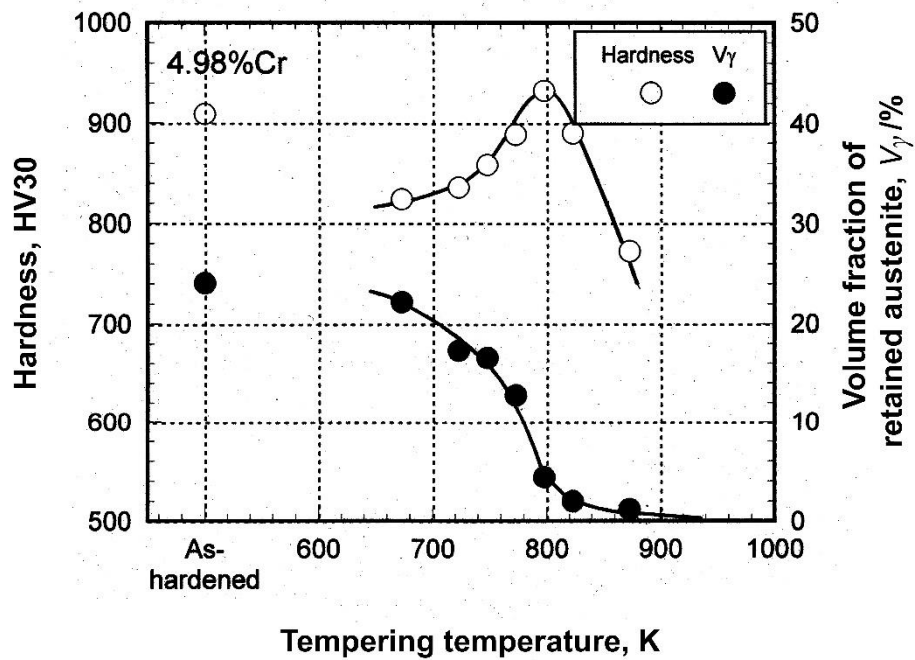


(b) Austenitizing temperature: 1373K.

Fig.4-5 Relationship between macro-hardness, volume fraction of retained austenite (V_γ) and tempering temperature of specimen No.1. Austenitizing : (a) 1323K and (b) 1373K.

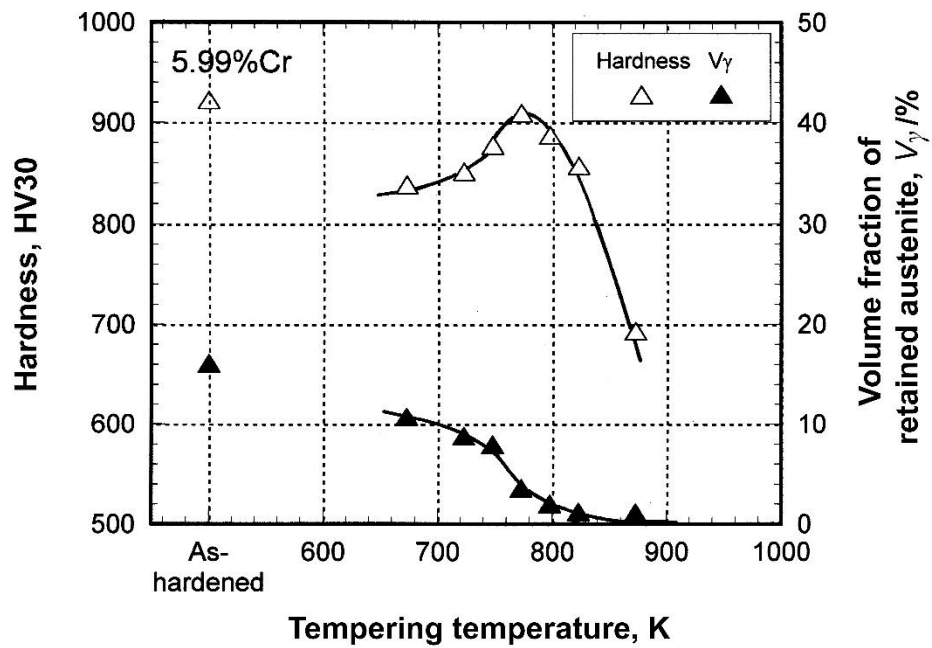


(a) Austenitizing temperature: 1323K.

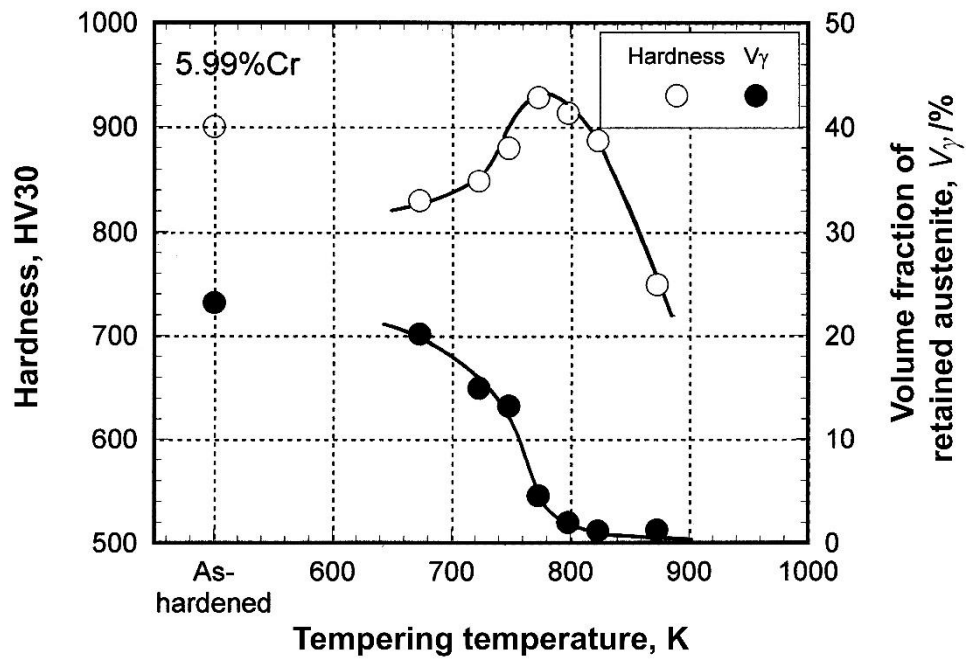


(b) Austenitizing temperature: 1373K.

Fig.4-6 Relationship between macro-hardness, volume fraction of retained austenite (V_γ) and tempering temperature of specimen No.2. Austenitizing : (a) 1323K and (b) 1373K.



(a) Austenitizing temperature: 1323K.

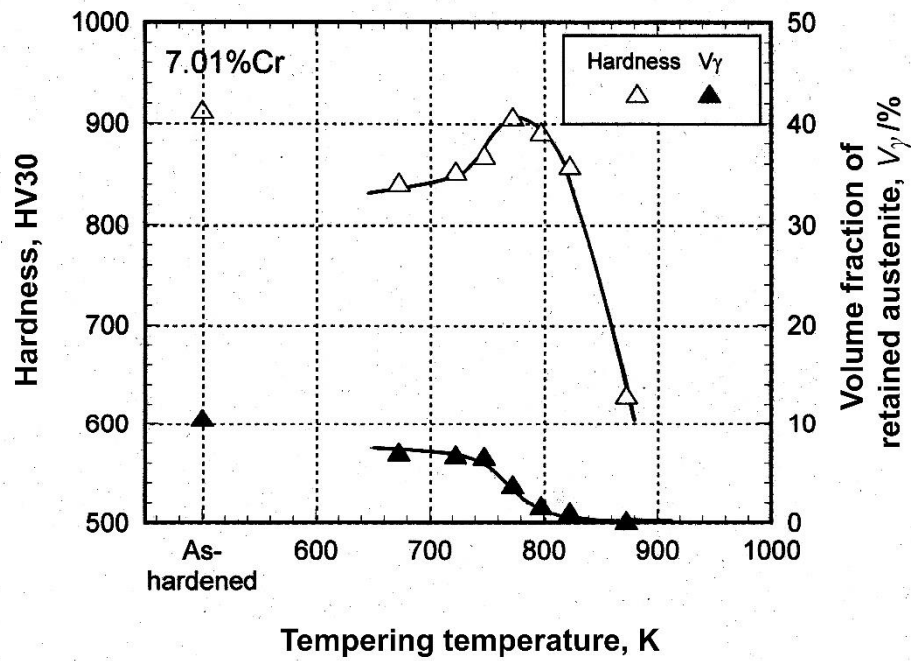


(b) Austenitizing temperature: 1373K.

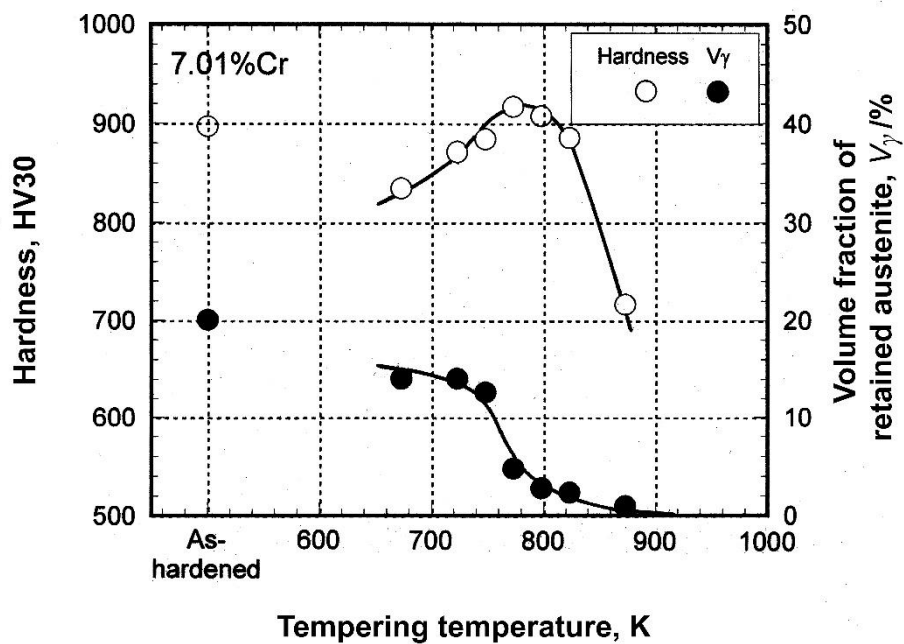
Fig.4-7 Relationship between macro-hardness, volume fraction of retained austenite (V_γ) and tempering temperature of specimen No.3. Austenitizing : (a) 1323K and (b) 1373K.

The results of specimen No.4 are shown in Fig.4-8. The locations of tempered hardness curves are quite similar to those of No.3. The H_{Tmax} is obtained at 773K tempering in both austenitizing temperature. The H_{Tmax} values are 906 HV30 and 918 HV30 in 1323K and 1373K austenitizing, respectively. The change in V_γ values by tempering showed similar tendency to those in specimen No.3.

Fig.4-9 shows the results of specimen No.5. It is found that the tempered hardness curves locate at the lowest hardness side, regardless of austenitizing temperatures. The H_{Tmax} values of both specimens are lowest in this group of specimens, i.e., 840 HV30 and 865 HV30 at 773K tempering for 1323K and 1373K austenitizing, respectively. The V_γ value decreases continuously as the tempering temperature increases and it begins to go down gradually where the tempering temperature exceeds 723K. The V_γ values are lower than those of other specimens except for specimen No.1 containing 3%Cr and the values at H_{Tmax} are quite few in the specimens hardened from both austenitizing temperatures.

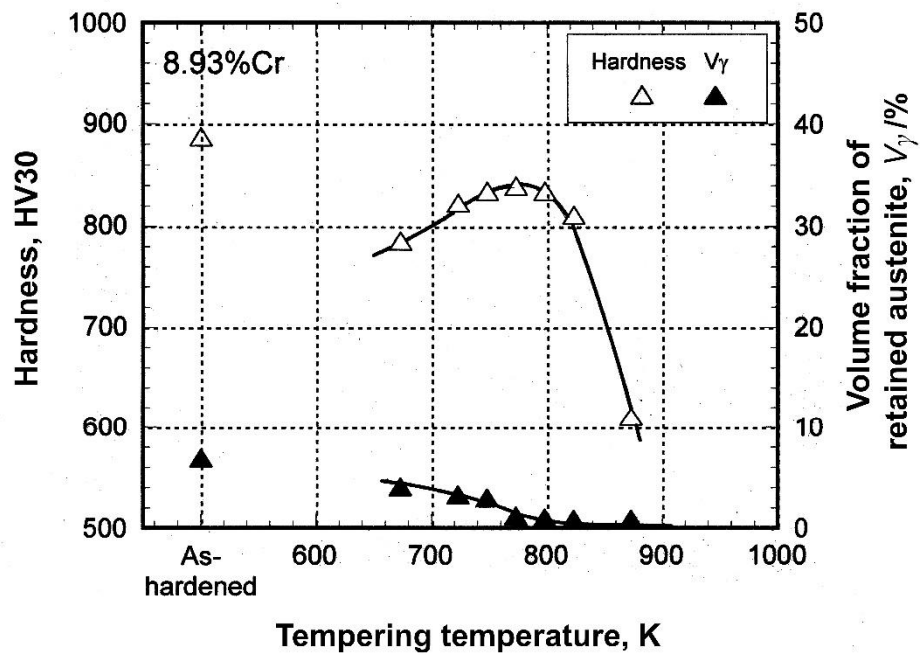


(a) Austenitizing temperature: 1323K.

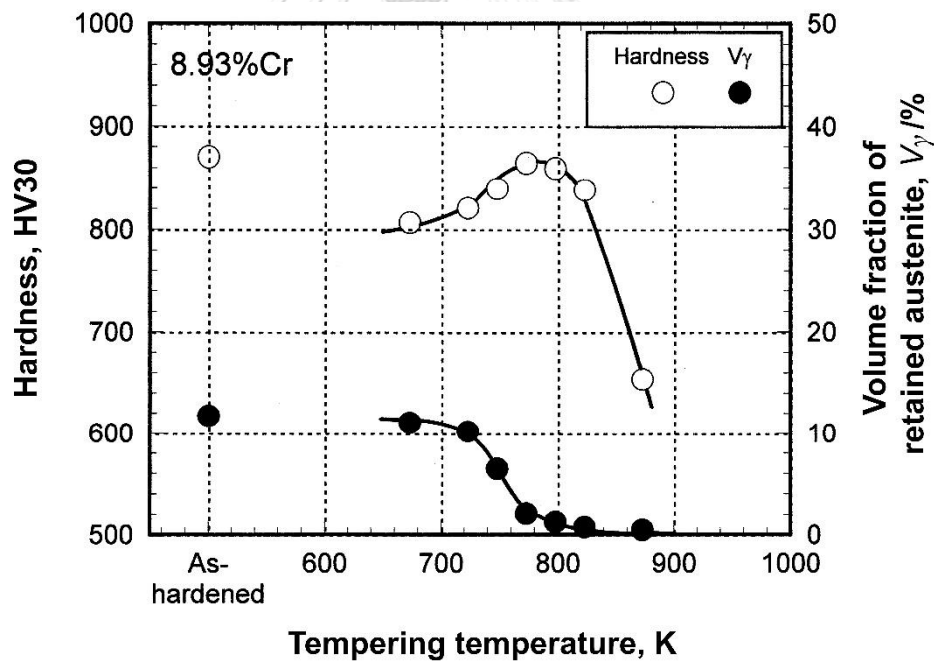


(b) Austenitizing temperature: 1373K.

Fig.4-8 Relationship between macro-hardness, volume fraction of retained austenite (V_γ) and tempering temperature of specimen No.4. Austenitizing : (a) 1323K and (b) 1373K.



(a) Austenitizing temperature: 1323K.



(b) Austenitizing temperature: 1373K.

Fig.4-9 Relationship between macro-hardness, volume fraction of retained austenite (V_γ) and tempering temperature of specimen No.5. Austenitizing : (a) 1323K and (b) 1373K.

4.3 Effect of Cr content and heat treatment conditions on abrasive wear resistance

In practical use, alloyed white cast irons have been used in heat-treated state. For this reason, the wear resistance of multi-alloyed white cast iron must be evaluated under the various heat treatment and wear conditions. In the previous sections, it was found that hardness and retained austenite (V_γ) of specimens changed extensively depending on the heat treatment conditions. Since Cr in the cast iron affects remarkably the phase transformation in the matrix, the constituents in the matrix such as retained austenite, martensite and secondary carbide are directly influenced by the Cr content. Resultantly, it can be said that the Cr content is involved with the wear resistance.

In this section, the effects of Cr content on the wear behavior under some different heat treatment conditions are described. The specimens were hardened from 1323K and 1373K austenitizing. The hardened specimens (As-H) were tempered at three levels of temperatures as shown in Fig.3-3, i.e., the temperatures lower than that at maximum hardness (L- $H_{T_{max}}$), at maximum hardness ($H_{T_{max}}$) and higher than that at $H_{T_{max}}$ (H- $H_{T_{max}}$), respectively. The actual tempering temperatures at three points illustrated in Fig.3-3 are shown in Table 4-4. Hardness of L- $H_{T_{max}}$ and H- $H_{T_{max}}$ are lower than those of $H_{T_{max}}$ but nearly same. However, the V_γ values are quite different in the three kinds of tempered specimen. With respect to the three kinds of test pieces of each specimen, Suga (two-body-type) and rubber wheel (three-body-type) abrasive wear tests were carried out to evaluate the wear behavior and finally wear resistance.

The macro-hardness and V_γ of test pieces are integrated into Table 4-5 for 1323K and 4-6 for 1373K austenitizing, respectively.

Table 4-4 Selected tempering temperatures for $L-H_{T_{max}}$, $H_{T_{max}}$ and $H-H_{T_{max}}$ in each specimen.

Specimen	Tempering temperature (K)					
	1323K austenitizing			1373K austenitizing		
	$L-H_{T_{max}}$	$H_{T_{max}}$	$H-H_{T_{max}}$	$L-H_{T_{max}}$	$H_{T_{max}}$	$H-H_{T_{max}}$
No.1 (3%Cr)	748	798	827	748	798	827
No.2 (5%Cr)	748	798	827	748	798	840
No.3 (6%Cr)	723	773	820	723	773	840
No.4 (7%Cr)	723	773	827	723	773	827
No.5 (9%Cr)	723	773	810	723	773	827

Table 4-5 Macro-hardness and volume fraction of retained austenite (V_γ) of heat-treated test pieces for abrasive wear test. Austenitizing : 1323K.

Specimens	Heat treatment condition	Macro-hardness (HV30)	V_γ , %
No.1 (3%Cr)	As-H	844	7.9
	L- $H_{T_{max}}$ (748K)	769	2.2
	$H_{T_{max}}$ (798K)	800	2.0
	H- $H_{T_{max}}$ (827K)	771	1.6
No.2 (5%Cr)	As-H	925	15.6
	L- $H_{T_{max}}$ (748K)	848	10.3
	$H_{T_{max}}$ (798K)	883	2.2
	H- $H_{T_{max}}$ (827K)	841	1.5
No.3 (6%Cr)	As-H	918	10.6
	L- $H_{T_{max}}$ (723K)	850	8.5
	$H_{T_{max}}$ (773K)	897	3.9
	H- $H_{T_{max}}$ (820K)	850	0.9
No.4 (7%Cr)	As-H	911	11.6
	L- $H_{T_{max}}$ (723K)	838	7.8
	$H_{T_{max}}$ (773K)	866	4.0
	H- $H_{T_{max}}$ (827K)	833	1.2
No.5 (9%Cr)	As-H	879	9.3
	L- $H_{T_{max}}$ (723K)	821	3.1
	$H_{T_{max}}$ (773K)	837	1.8
	H- $H_{T_{max}}$ (810K)	818	1.1

Table 4-6 Macro-hardness and volume fraction of retained austenite (V_γ) of heat-treated test pieces for abrasive wear test. Austenitizing : 1373K.

Specimens	Heat treatment condition	Macro-hardness (HV30)	V_γ , %
No.1 (3%Cr)	As-H	887	11.1
	L- $H_{T_{max}}$ (748K)	810	3.8
	$H_{T_{max}}$ (798K)	846	2.5
	H- $H_{T_{max}}$ (827K)	816	1.6
No.2 (5%Cr)	As-H	909	25.1
	L- $H_{T_{max}}$ (748K)	841	15.2
	$H_{T_{max}}$ (798K)	906	4.0
	H- $H_{T_{max}}$ (840K)	848	1.2
No.3 (6%Cr)	As-H	894	23.0
	L- $H_{T_{max}}$ (723K)	843	15.8
	$H_{T_{max}}$ (773K)	924	4.6
	H- $H_{T_{max}}$ (840K)	850	1.0
No.4 (7%Cr)	As-H	896	20.8
	L- $H_{T_{max}}$ (723K)	849	13.8
	$H_{T_{max}}$ (773K)	875	5.0
	H- $H_{T_{max}}$ (827K)	856	1.5
No.5 (9%Cr)	As-H	862	16.0
	L- $H_{T_{max}}$ (723K)	822	9.0
	$H_{T_{max}}$ (773K)	860	2.2
	H- $H_{T_{max}}$ (827K)	823	1.0

4.3.1 Suga abrasive wear test (two-body-type).

The data of wear loss (W_1) and wear distance (W_d) of test pieces in each specimen were plotted in diagram and the relation was expressed by the equation obtained from the method of least squares. The test results of specimens No.1 to No.5 hardened from 1323K and 1373K are shown in Fig.4-10 to 4-14 and Fig.4-15 to 4-19, respectively. The equations between W_1 and W_d are shown under the diagram. In all the figures, it is found that the W_1 increases in proportion to the W_d regardless of heat treatment conditions. It is one way to evaluate wear resistance by the total wear loss of test piece at the same distance where the abrasive wear test finished. As an example, the total wear losses of test pieces at the wear distance of 192 m are shown in Table 4-7 for the specimens hardened from 1323K.

Table 4-7 Total wear losses at wear distance of 192 m of specimens hardened from 1323K and tempered. Suga abrasive wear test under a load of 9.8N (1 kgf).

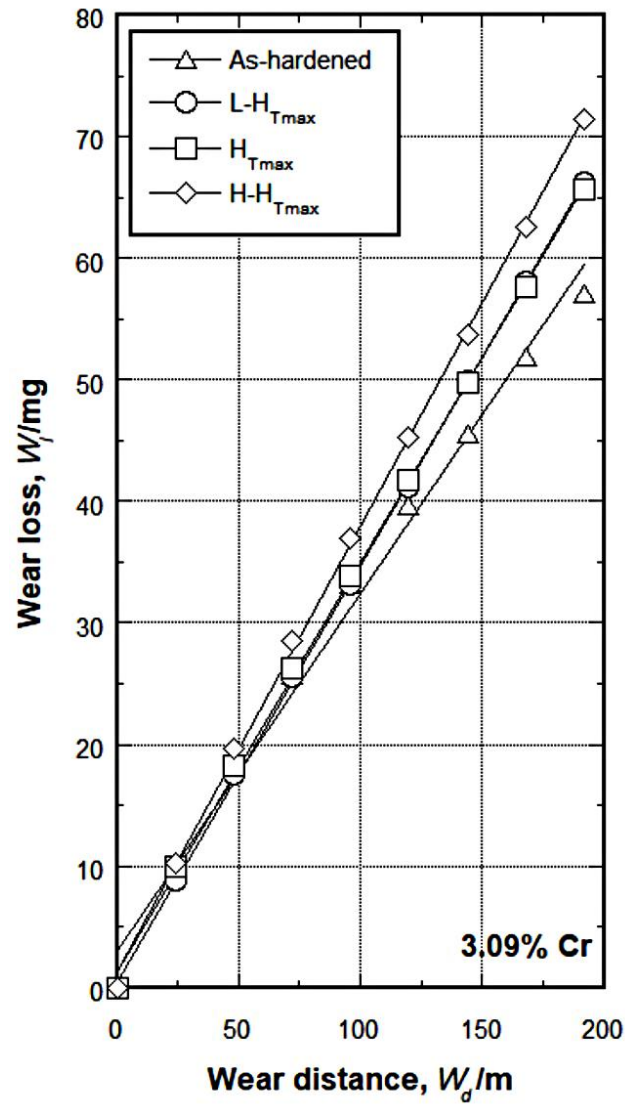
Specimen	Total wear loss (mg)			
	As-H	L-H _{Tmax}	H _{Tmax}	H-H _{Tmax}
No.1 (3%Cr)	57.0	66.2	65.7	71.4
No.2 (5%Cr)	51.9	55.5	52.1	57.2
No.3 (6%Cr)	50.0	56.2	51.1	55.4
No.4 (7%Cr)	49.7	57.1	52.0	52.9
No.5 (9%Cr)	54.6	61.0	54.8	56.6

These data may helpful to presume the degree of wear. However, it is not adequate to judge the wear properties of cast iron by means of the total wear loss at only one wear distance because the wear characteristics or wear resistance should be evaluated by the average wear rate through whole wear test. From above reason, it was decided that the total wear loss was not discussed any more. Instead, the wear rate (R_w : mg/m) which is expressed by the slope of each straight line of W_1 vs. W_d was introduced as a parameter.

4.3.1.1 Wear test results of specimens tempered after hardening from 1323K austenitizing.

Fig.4-10 shows the results of specimen No.1 with 3%Cr. The wear pattern of L- $H_{T_{max}}$ and $H_{T_{max}}$ test pieces are almost same. However, that of H- $H_{T_{max}}$ test piece lies at upper and that of As-H test piece at lower positions than them. The smallest R_w value of 0.294 mg/m or the highest wear resistance is obtained in the As-H test piece and the largest R_w of 0.366 mg/m or the smallest wear resistance is got in H- $H_{T_{max}}$ test piece. In addition, the R_w values of $H_{T_{max}}$ and L- $H_{T_{max}}$ test pieces are 0.336 and 0.342 mg/m, respectively.

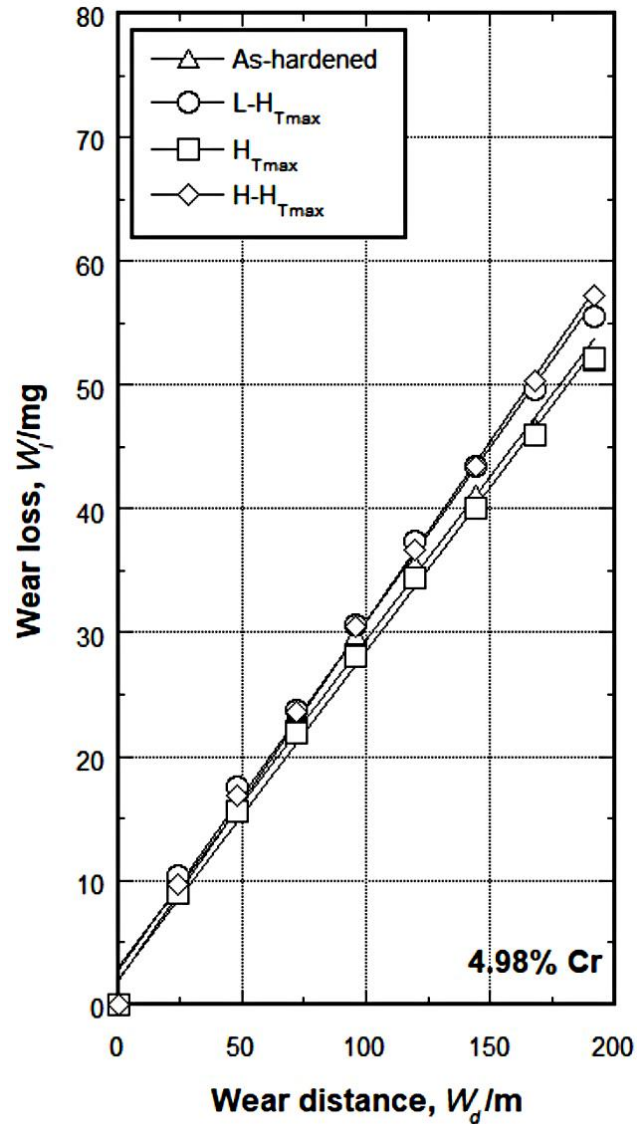
The results of specimen No.2 with 5%Cr are shown in Fig.4-11. Compared with specimen with 3%Cr, the difference in wear pattern due to the heat treatment condition is small. The wear patterns of $H_{T_{max}}$ and As-H test pieces are close and those of L- $H_{T_{max}}$ and H- $H_{T_{max}}$ test pieces are nearly same at upper side. The lowest R_w is 0.264 mg/m in As-H and $H_{T_{max}}$ specimens and it increases in the order of 0.282 in L- $H_{T_{max}}$ and 0.290 mg/m in H- $H_{T_{max}}$ specimens.



As-H	△	$W_1 = 0.294 * W_d + 3.02$	$(R^2 = 0.99)$
L-H_{Tmax}	○	$W_1 = 0.342 * W_d + 0.51$	$(R^2 = 0.99)$
H_{Tmax}	□	$W_1 = 0.336 * W_d + 1.38$	$(R^2 = 0.99)$
H-H_{Tmax}	◇	$W_1 = 0.366 * W_d + 1.31$	$(R^2 = 0.99)$

W_1 : Wear loss, W_d : Wear distance

Fig.4-10 Relationship between wear loss (W_1) and wear distance (W_d) of specimen No.1 with 3%Cr hardened from 1323K austenitizing. Suga abrasive wear test under a load of 9.8N (1 kgf).



As-H	△	$W_1 = 0.264 * W_d + 2.99$	$(R^2 = 0.99)$
L-H_{Tmax}	○	$W_1 = 0.282 * W_d + 2.74$	$(R^2 = 0.99)$
H-T_{max}	□	$W_1 = 0.264 * W_d + 2.08$	$(R^2 = 0.99)$
H-H_{Tmax}	◇	$W_1 = 0.290 * W_d + 1.97$	$(R^2 = 0.99)$

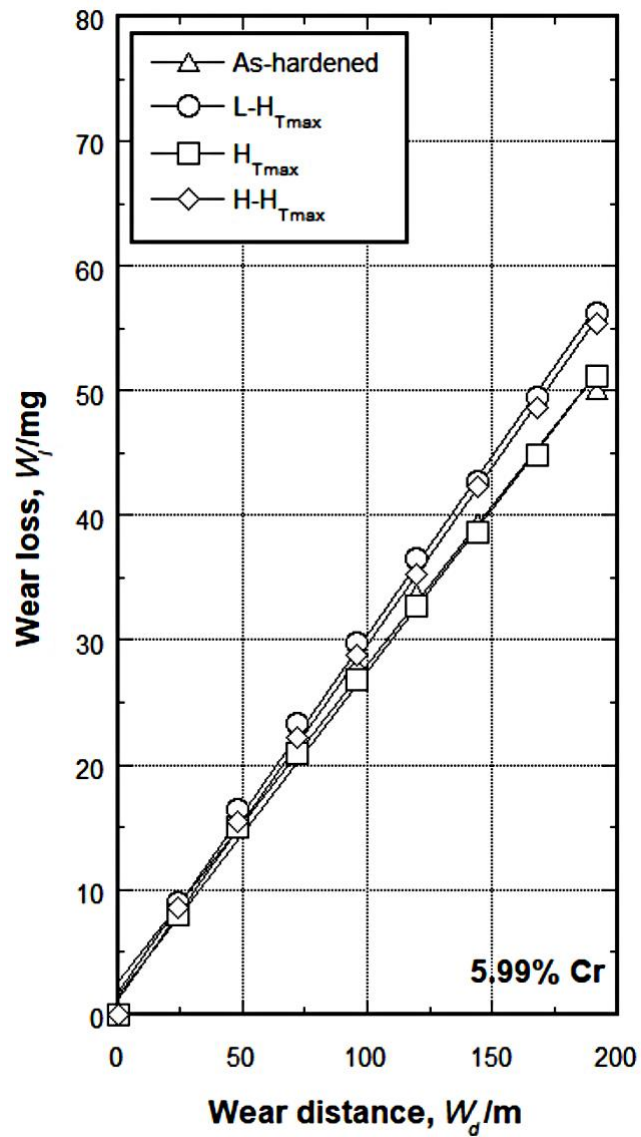
W_1 : Wear loss, W_d : Wear distance

Fig.4-11 Relationship between wear loss (W_1) and wear distance (W_d) of specimen No.2 with 5%Cr hardened from 1323K austenitizing. Suga abrasive wear test under a load of 9.8N (1 kgf).

The case of specimen No.3 with 6%Cr is shown in Fig.4-12. The variation of wear behaviors is also small. The wear patterns of As-H and $H_{T_{max}}$ test pieces are almost same and those of $L-H_{T_{max}}$ and $H-H_{T_{max}}$ test pieces are close. The former lies lower than the latter. The R_w values are 0.254 in As-H, 0.260 in $H_{T_{max}}$, 0.284 in $H-H_{T_{max}}$ and 0.287 mg/m in $L-H_{T_{max}}$ test pieces, respectively. It is clear that the highest wear resistance is obtained in the As-H and $H_{T_{max}}$ specimens whereas the lowest wear resistance is obtained in the $L-H_{T_{max}}$ specimen.

Fig.4-13 shows the results of specimen No.4 with 7%Cr. The wear trend is similar to those of 5% and 6% Cr specimens. The wear patterns of $H_{T_{max}}$ and $H-H_{T_{max}}$ test pieces are close. The wear pattern of As-H test piece lies at a little lower position and that of $L-H_{T_{max}}$, is in upper side than them. The R_w value is smallest of 0.255 mg/m in As-H test piece and it increases in the order of 0.261 in $H_{T_{max}}$, 0.271 in $H-H_{T_{max}}$ and the largest of 0.292 mg/m in $L-H_{T_{max}}$ test pieces. Therefore, the largest and the smallest wear resistances are obtained in As-H and $L-H_{T_{max}}$ specimens, respectively.

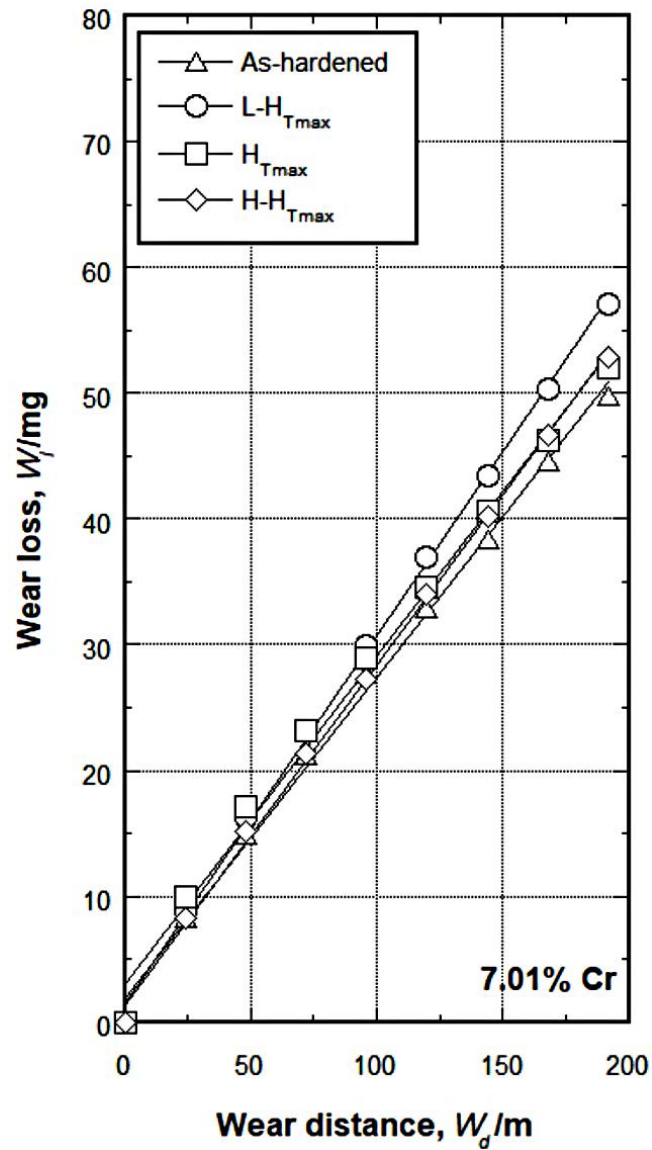
The results of specimen No.5 with 9%Cr are shown in Fig.4-14. The wear patterns of $H-H_{T_{max}}$, $H_{T_{max}}$ and As-H test pieces are closed each other but the $L-H_{T_{max}}$ test piece is isolated upper than them. The R_w values are 0.276 in $H_{T_{max}}$, 0.277 in As-H, 0.289 in $H-H_{T_{max}}$ and 0.312 mg/m in $L-H_{T_{max}}$ specimens, respectively. In 9%Cr specimen, therefore, the $H_{T_{max}}$ test piece has the highest and the $L-H_{T_{max}}$ test piece does the lowest wear resistances.



As-H	△	$W_1 = 0.254 * W_d + 2.60$	$(R^2 = 0.99)$
L-H_{Tmax}	○	$W_1 = 0.287 * W_d + 1.76$	$(R^2 = 0.99)$
H_{Tmax}	□	$W_1 = 0.260 * W_d + 1.51$	$(R^2 = 0.99)$
H-H_{Tmax}	◇	$W_1 = 0.284 * W_d + 1.25$	$(R^2 = 0.99)$

W_1 : Wear loss, W_d : Wear distance

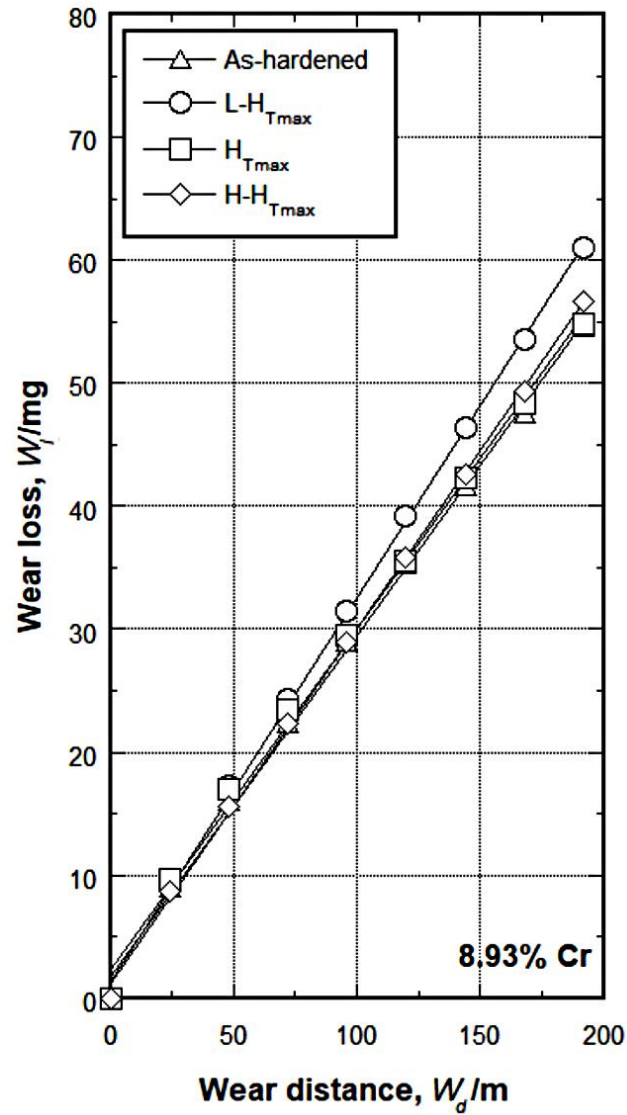
Fig.4-12 Relationship between wear loss (W_1) and wear distance (W_d) of specimen No.3 with 6%Cr hardened from 1323K austenitizing. Suga abrasive wear test under a load of 9.8N (1 kgf).



As-H	△	$W_l = 0.255 * W_d + 1.95$	$(R^2 = 0.99)$
L-H_{Tmax}	○	$W_l = 0.292 * W_d + 1.49$	$(R^2 = 0.99)$
H_{Tmax}	□	$W_l = 0.261 * W_d + 3.03$	$(R^2 = 0.99)$
H-H_{Tmax}	◇	$W_l = 0.271 * W_d + 1.32$	$(R^2 = 0.99)$

W_l : Wear loss, W_d : Wear distance

Fig.4-13 Relationship between wear loss (W_l) and wear distance (W_d) of specimen No.4 with 7%Cr hardened from 1323K austenitizing. Suga abrasive wear test under a load of 9.8N (1 kgf).



As-H	\triangle	$W_1 = 0.277 * W_d + 1.83$	$(R^2 = 0.99)$
L-H_{Tmax}	\circ	$W_1 = 0.312 * W_d + 1.40$	$(R^2 = 0.99)$
H-T_{max}	\square	$W_1 = 0.276 * W_d + 2.42$	$(R^2 = 0.99)$
H-H-T_{max}	\diamond	$W_1 = 0.289 * W_d + 1.16$	$(R^2 = 0.99)$

W_1 : Wear loss, W_d : Wear distance

Fig.4-14 Relationship between wear loss (W_1) and wear distance (W_d) of specimen No.5 with 9%Cr hardened from 1323K austenitizing. Suga abrasive wear test under a load of 9.8N (1 kgf).

Here, the R_w values of all the test pieces are summarized in Table 4-8.

Table 4-8 Wear rates (R_w) of specimens hardened from 1323K and tempered. Suga abrasive wear test under a load of 9.8N (1 kgf).

Specimen	Wear rate (mg/m)			
	As-H	L- $H_{T_{max}}$	$H_{T_{max}}$	H- $H_{T_{max}}$
No.1 (3%Cr)	0.294	0.342	0.336	0.366
No.2 (5%Cr)	0.264	0.282	0.264	0.290
No.3 (6%Cr)	0.254	0.287	0.260	0.284
No.4 (7%Cr)	0.255	0.292	0.261	0.271
No.5 (9%Cr)	0.277	0.312	0.276	0.289

4.3.1.2 Wear test results of specimens tempered after hardening from 1373K austenitizing

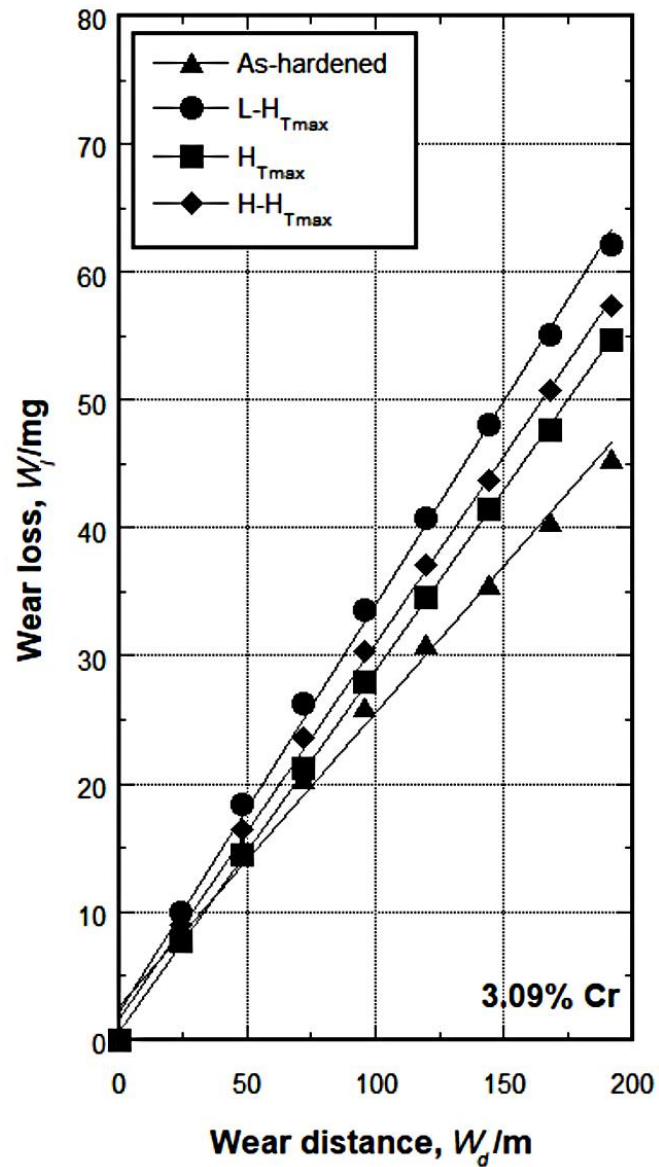
The relationships between wear loss (W_1) and wear distance (W_d) of specimens hardened from 1373K are displayed in Fig.4-15 for specimen No.1 with 3%Cr, Fig.4-16 for No.2 with 5%Cr, Fig.4-17 for No.3 with 6%Cr, Fig.4-18 for No.4 with 7%Cr and Fig.4-19 for No.5 with 9%Cr, respectively. As the same manner as the specimens hardened from 1323K austenitizing, the W_1 increases in proportion to the W_d .

Fig.4-15 shows the wear test results of specimen No.1 with 3%Cr. The wear patterns are separated clearly depending on the heat treatment conditions. The R_w value increases in the order of 0.229 in As-H, 0.282 in $H_{T_{max}}$, 0.293 in H- $H_{T_{max}}$ and 0.318 mg/m in L- $H_{T_{max}}$ specimens, respectively. It is understood that the As-H test

piece has the highest wear resistance and L-H_{Tmax} test piece does the lowest wear resistance.

The results of specimen No.2 with 5%Cr are illustrated in Fig.4-16. The relationships between W_1 and W_d are similar to those of 3%Cr specimen, i.e., the W_1 increases proportionally with an increase in the W_d in each heat treatment condition. Among the test pieces except for H-H_{Tmax} test piece which lies at upper side, however, the differences in the wear pattern corresponding to the difference of the heat treatment conditions are small compared with 3%Cr. The smallest R_w value of 0.226 mg/m is obtained in As-H specimen and it increases in the order of 0.237 in H_{Tmax}, 0.246 in L-H_{Tmax} and the largest of 0.272 mg/m in H-H_{Tmax} specimens. So, the As-H specimen has highest wear resistance while the H-H_{Tmax} specimen does the lowest wear resistance.

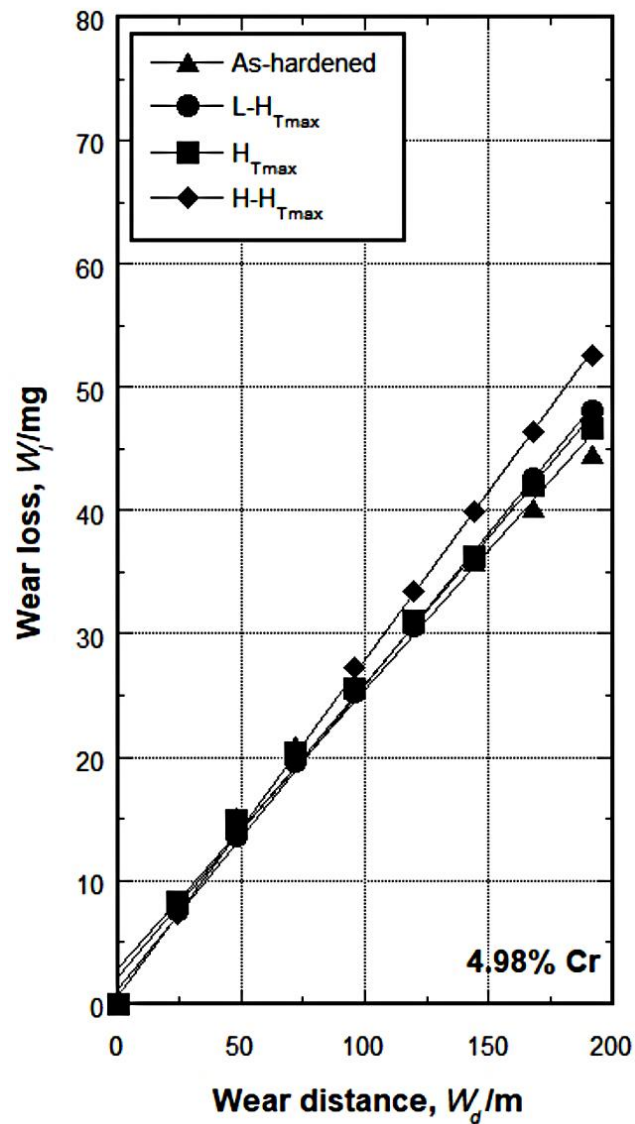
Fig.4-17 shows the results of specimen No.3 with 6%Cr. The amount of wear losses are small similar to the 5%Cr specimen. The wear patterns of test pieces can be distinguished individually by the difference of heat treatment conditions. The R_w values are smallest of 0.218 in As-H, 0.228 in H_{Tmax}, 0.244 in L-H_{Tmax} and the largest of 0.263 mg/m in H-H_{Tmax} specimens, respectively. Therefore, the As-H specimen has largest wear resistance and H-H_{Tmax} specimen does smallest wear resistance.



As-H	▲	$W_1 = 0.229 * W_d + 2.69$	$(R^2 = 0.99)$
L- H_{Tmax}	●	$W_1 = 0.318 * W_d + 2.17$	$(R^2 = 0.99)$
H_{Tmax}	■	$W_1 = 0.282 * W_d + 0.69$	$(R^2 = 0.99)$
H- H_{Tmax}	◆	$W_1 = 0.293 * W_d + 1.65$	$(R^2 = 0.99)$

W_1 : Wear loss, W_d : Wear distance

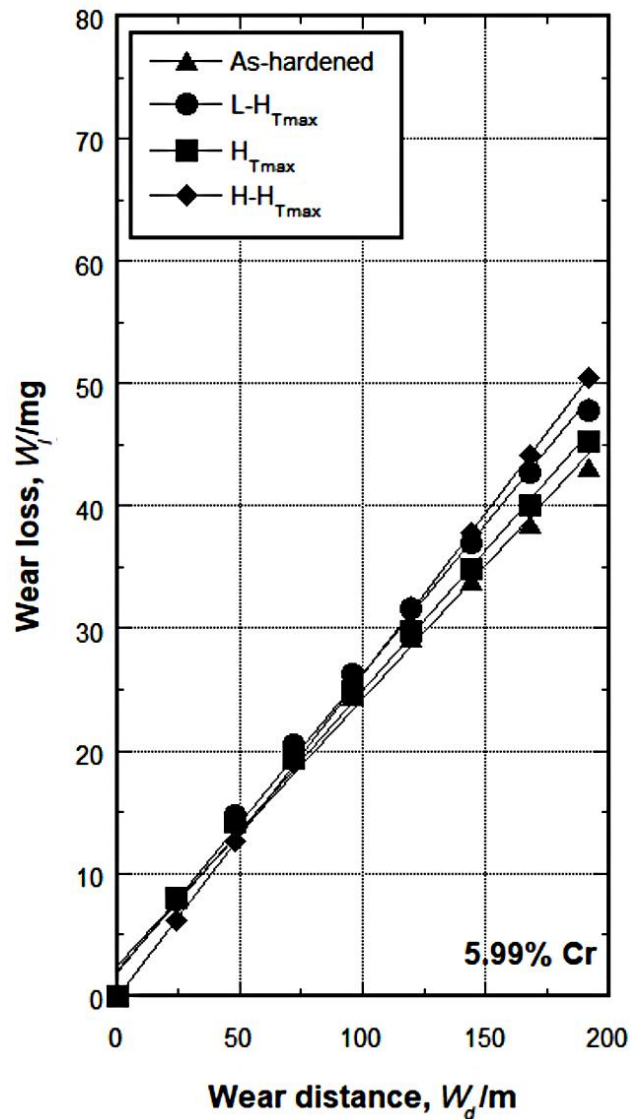
Fig.4-15 Relationship between wear loss (W_1) and wear distance (W_d) of specimen No.1 with 3%Cr hardened from 1373K austenitizing. Suga abrasive wear test under a load of 9.8N (1 kgf).



As-H	▲	$W_l = 0.226 * W_d + 2.91$	($R^2 = 0.99$)
L- H_{Tmax}	●	$W_l = 0.246 * W_d + 1.24$	($R^2 = 0.99$)
H- T_{max}	■	$W_l = 0.237 * W_d + 2.21$	($R^2 = 0.99$)
H- H_{Tmax}	◆	$W_l = 0.272 * W_d + 0.67$	($R^2 = 0.99$)

W_l : Wear loss, W_d : Wear distance

Fig.4-16 Relationship between wear loss (W_l) and wear distance (W_d) of specimen No.2 with 5%Cr hardened from 1373K austenitizing. Suga abrasive wear test under a load of 9.8N (1 kgf).



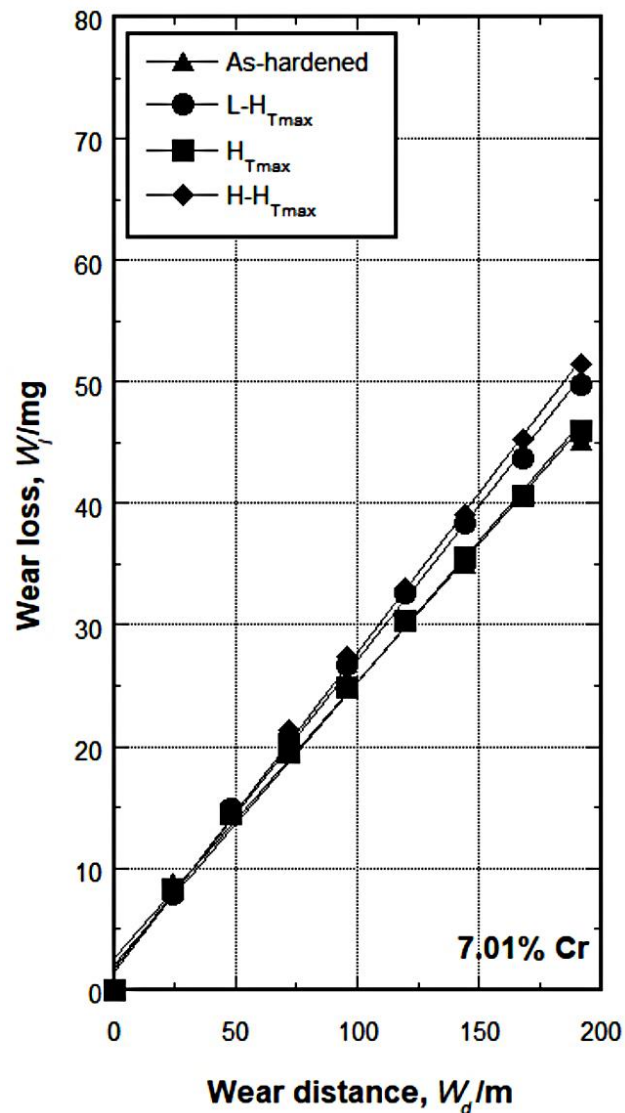
As-H	▲	$W_1 = 0.218 * W_d + 2.52$	$(R^2 = 0.99)$
L- H_{Tmax}	●	$W_1 = 0.244 * W_d + 1.94$	$(R^2 = 0.99)$
H- T_{max}	■	$W_1 = 0.228 * W_d + 2.13$	$(R^2 = 0.99)$
H- H_{Tmax}	◆	$W_1 = 0.263 * W_d - 0.08$	$(R^2 = 0.99)$

W_1 : Wear loss, W_d : Wear distance

Fig.4-17 Relationship between wear loss (W_1) and wear distance (W_d) of specimen No.3 with 6%Cr hardened from 1373K austenitizing. Suga abrasive wear test under a load of 9.8N (1 kgf).

Fig.4-18 shows the results of specimen No.4 with 7%Cr. The amount of wear losses are also small in all the test pieces with different heat treatment conditions and the wear patterns of As-H and $H_{T_{max}}$ test pieces are very close. The R_w values are 0.228 in As-H, 0.232 in $H_{T_{max}}$, 0.253 in L- $H_{T_{max}}$ and 0.262 mg/m in H- $H_{T_{max}}$ specimens, respectively. The As-H test piece has largest wear resistance and H- $H_{T_{max}}$ does smallest wear resistance as well as the case of 6%Cr specimen.

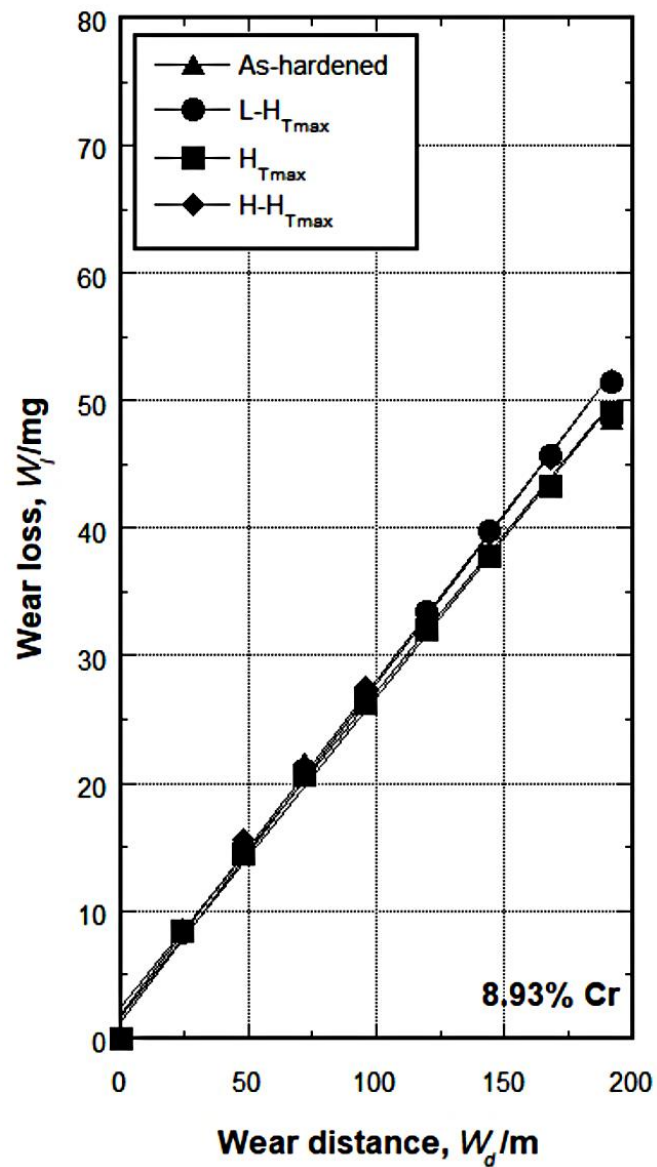
The results of specimen No.5 with the highest Cr content of 9% are displayed in Fig.4-19. The wear patterns of test pieces come near each other, i.e., the relationships between the W_l and the W_d show very little difference among test pieces with different heat treatment conditions. The R_w values range from the smallest of 0.247 in As-H test piece to the largest of 0.264 mg/m in L- $H_{T_{max}}$ test piece. As for the other test pieces, the R_w of $H_{T_{max}}$ test piece is 0.250 and that of H- $H_{T_{max}}$ one is 0.262 mg/m. Here, if the wear resistance dares to be ranked in these results, the largest wear resistance could be obtained in As-H specimen, whereas the smallest wear resistance in L- $H_{T_{max}}$ specimen.



As-H	▲	$W_l = 0.228 * W_d + 2.60$	($R^2 = 0.99$)
$L-H_{Tmax}$	●	$W_l = 0.253 * W_d + 1.75$	($R^2 = 0.99$)
H_{Tmax}	■	$W_l = 0.232 * W_d + 2.12$	($R^2 = 0.99$)
$H-H_{Tmax}$	◆	$W_l = 0.262 * W_d + 1.55$	($R^2 = 0.99$)

W_l : Wear loss, W_d : Wear distance

Fig.4-18 Relationship between wear loss (W_l) and wear distance (W_d) of specimen No.4 with 7%Cr hardened from 1373K austenitizing. Suga abrasive wear test under a load of 9.8N (1 kgf).



As-H	▲	$W_1 = 0.247 * W_d + 2.44$	$(R^2 = 0.99)$
$L-H_{T_{max}}$	●	$W_1 = 0.264 * W_d + 1.44$	$(R^2 = 0.99)$
$H_{T_{max}}$	■	$W_1 = 0.250 * W_d + 1.84$	$(R^2 = 0.99)$
$H-H_{T_{max}}$	◆	$W_1 = 0.262 * W_d + 1.89$	$(R^2 = 0.99)$

W_1 : Wear loss, W_d : Wear distance

Fig.4-19 Relationship between wear loss (W_1) and wear distance (W_d) of specimen No.5 with 9%Cr hardened from 1373K austenitizing. Suga abrasive wear test under a load of 9.8N (1 kgf).

The R_w values of all the test pieces are summarized in Table 4-9.

Table 4-9 Wear rates (R_w) of specimens hardened from 1373K and tempered. Suga abrasive wear test under a load of 9.8N (1 kgf).

Specimen	Wear rate (mg/m)			
	As-H	L- H_{Tmax}	H_{Tmax}	H- H_{Tmax}
No.1 (3%Cr)	0.229	0.318	0.282	0.293
No.2 (5%Cr)	0.226	0.246	0.237	0.272
No.3 (6%Cr)	0.218	0.244	0.228	0.263
No.4 (7%Cr)	0.228	0.253	0.232	0.262
No.5 (9%Cr)	0.247	0.264	0.250	0.262

4.3.2 Rubber wheel abrasive wear test (three-body-type)

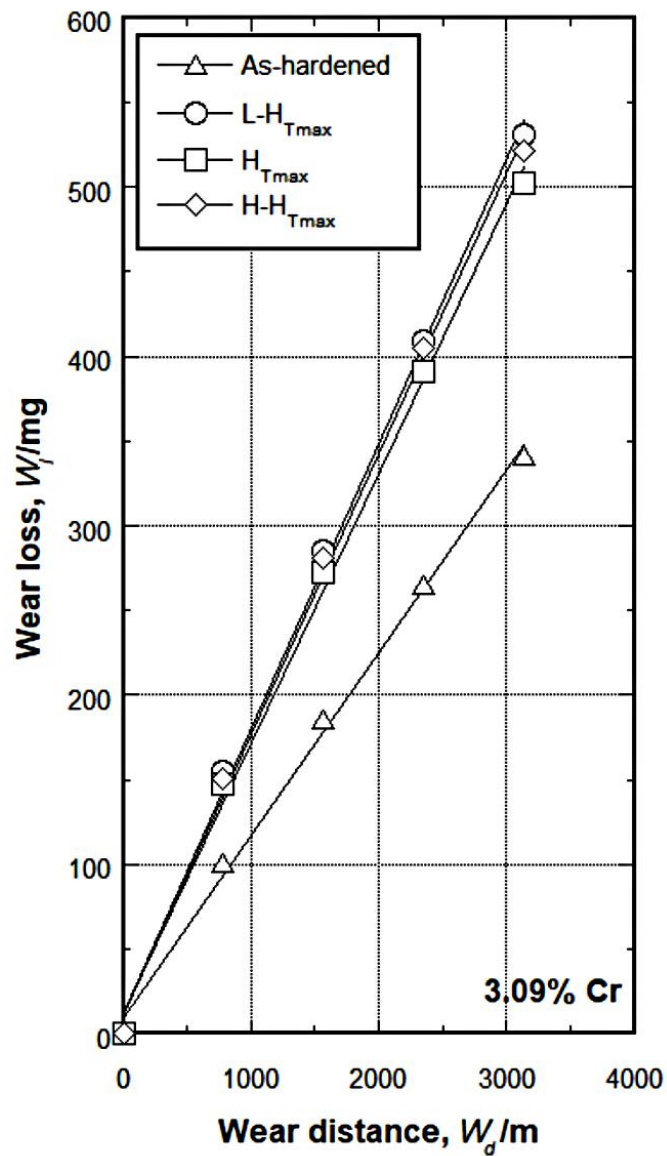
In order to investigate the wear behavior of three-body-type abrasion in the multi-alloyed white cast iron, the Rubber wheel abrasive wear test was selected. The test pieces heat-treated in the same way as those for Suga abrasive wear test were used. The results are demonstrated in Fig.4-20 to 4-24 for specimens hardened from 1323K and Fig.4-25 to 4-29 for those hardened from 1373K austenitizing. In each specimen, the linear relations are obtained between wear loss (W_l) and wear distance (W_d) as well as the results by Suga wear test. The wear patterns and R_w varied depending on the heat treatment conditions.

In every specimen, the R_w value was smaller compared with that by Suga abrasive wear test. It is because the load applying on the test piece is much smaller and wear mechanism is different between two types of wear tests.

4.3.2.1 Wear test results of specimens tempered after hardening from 1323K austenitizing

As for the specimen No.1 with 3%Cr, the relationships between W_1 and W_d is shown in Fig.4-20. The wear patterns of L- $H_{T_{max}}$, $H_{T_{max}}$ and H- $H_{T_{max}}$ test pieces are close regardless of heat treatment conditions and their wear losses are very high whereas the wear pattern of As-H test piece lies low far from the others. The R_w value in As-H test piece is 0.108 mg/m. The others are 0.168 in L- $H_{T_{max}}$, 0.159 in $H_{T_{max}}$ and 0.165 mg/m in H- $H_{T_{max}}$ test pieces, respectively. The As-H specimen has the largest wear resistance and the L- $H_{T_{max}}$ specimen does the smallest.

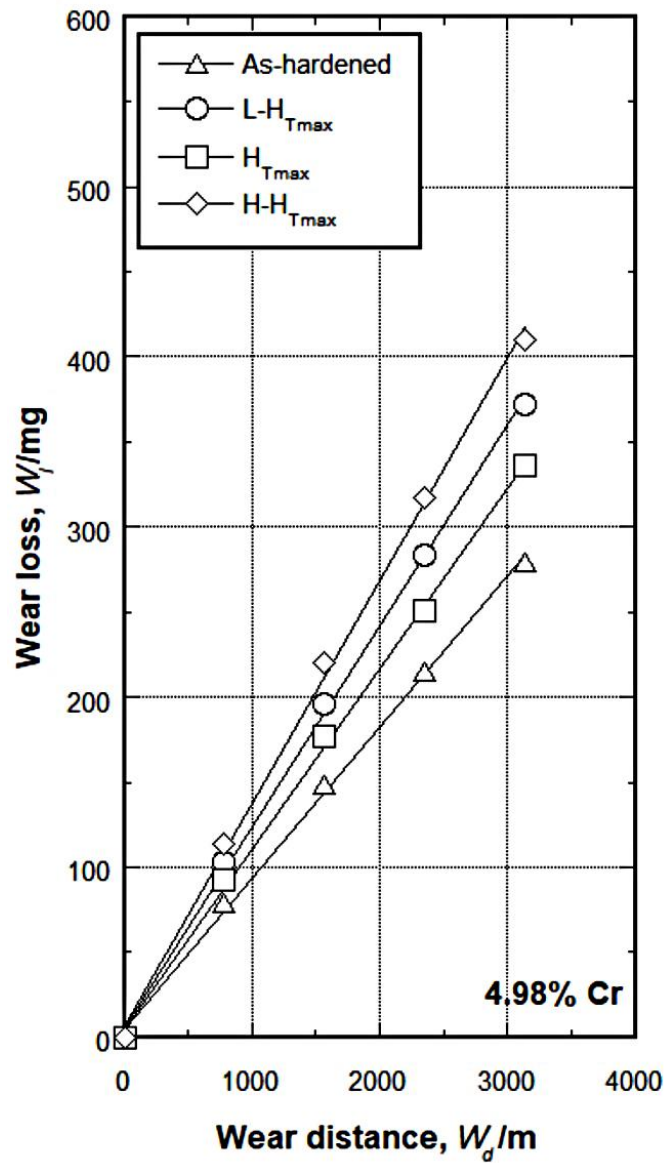
Fig.4-21 shows the results of specimen No.2 with 5%Cr. Each test piece has an individual wear pattern according to every heat treatment condition and linear relation is also obtained. The R_w value is the smallest of 0.088 in As-H test piece and it increases in the order of 0.106 in $H_{T_{max}}$, 0.118 in L- $H_{T_{max}}$ and 0.131 mg/m in the H- $H_{T_{max}}$ test pieces.



As-H	△	$W_l = 0.108 * W_d + 9.30$ ($R^2 = 0.99$)
L-H_{Tmax}	○	$W_l = 0.168 * W_d + 13.06$ ($R^2 = 0.99$)
H-T_{max}	□	$W_l = 0.159 * W_d + 13.04$ ($R^2 = 0.99$)
H-H-T_{max}	◇	$W_l = 0.165 * W_d + 12.44$ ($R^2 = 0.99$)

W_l : Wear loss, W_d : Wear distance

Fig.4-20 Relationship between wear loss (W_l) and wear distance (W_d) of specimen No.1 with 3%Cr hardened from 1323K. Rubber wheel abrasive wear test under a load of 85.3N (8.7 kgf).



As-H	△	$W_l = 0.088 * W_d + 5.30$	($R^2 = 0.99$)
L-$H_{T_{max}}$	○	$W_l = 0.118 * W_d + 5.82$	($R^2 = 0.99$)
$H_{T_{max}}$	□	$W_l = 0.106 * W_d + 5.18$	($R^2 = 0.99$)
H-$H_{T_{max}}$	◇	$W_l = 0.131 * W_d + 7.46$	($R^2 = 0.99$)

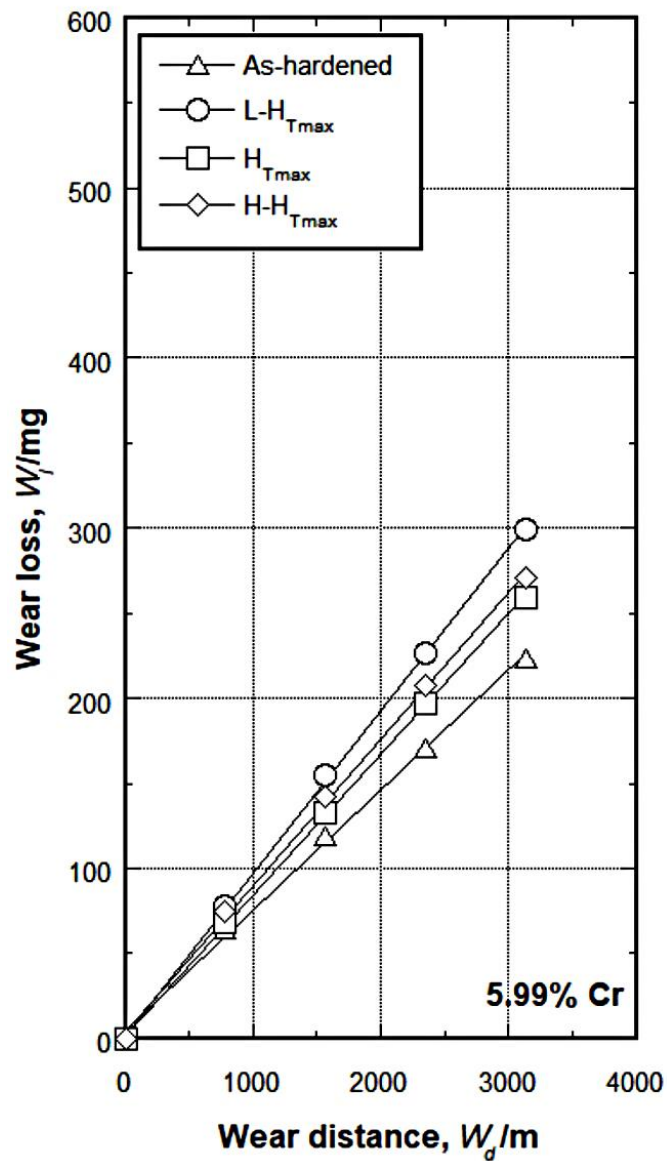
W_l : Wear loss, W_d : Wear distance

Fig.4-21 Relationship between wear loss (W_l) and wear distance (W_d) of specimen No.2 with 5%Cr hardened from 1323K. Rubber wheel abrasive wear test under a load of 85.3N (8.7 kgf).

The results of specimen No.3 with 6%Cr is shown in Fig.4-22, it is recognized that the wear pattern of each test piece appears separately according to its own heat treatment condition. This feature resembles to that of the 5%Cr specimen shown in Fig.4-20. However, the wear patterns are located in lower wear loss side than those of 5%Cr specimen. The R_w values are smallest in this group of specimens and they are 0.070 in As-H, 0.083 in $H_{T_{max}}$, 0.086 in $H-H_{T_{max}}$ and 0.095 mg/m in $L-H_{T_{max}}$ specimens, respectively.

Fig.4-23 shows the results of specimen No.4 with 7%Cr. It is notable that the difference among wear patterns is smallest. The patterns of $H_{T_{max}}$ and As-H and those of $L-H_{T_{max}}$ and $H-H_{T_{max}}$ test pieces are near. The former lies in lower position than the latter does. The smallest R_w of 0.085 mg/m is obtained in As-H test piece and the R_w value of other test pieces increases in the order of 0.088 in $H_{T_{max}}$, 0.095 in $H-H_{T_{max}}$ and the largest R_w of 0.098 mg/m is done in $L-H_{T_{max}}$ test pieces.

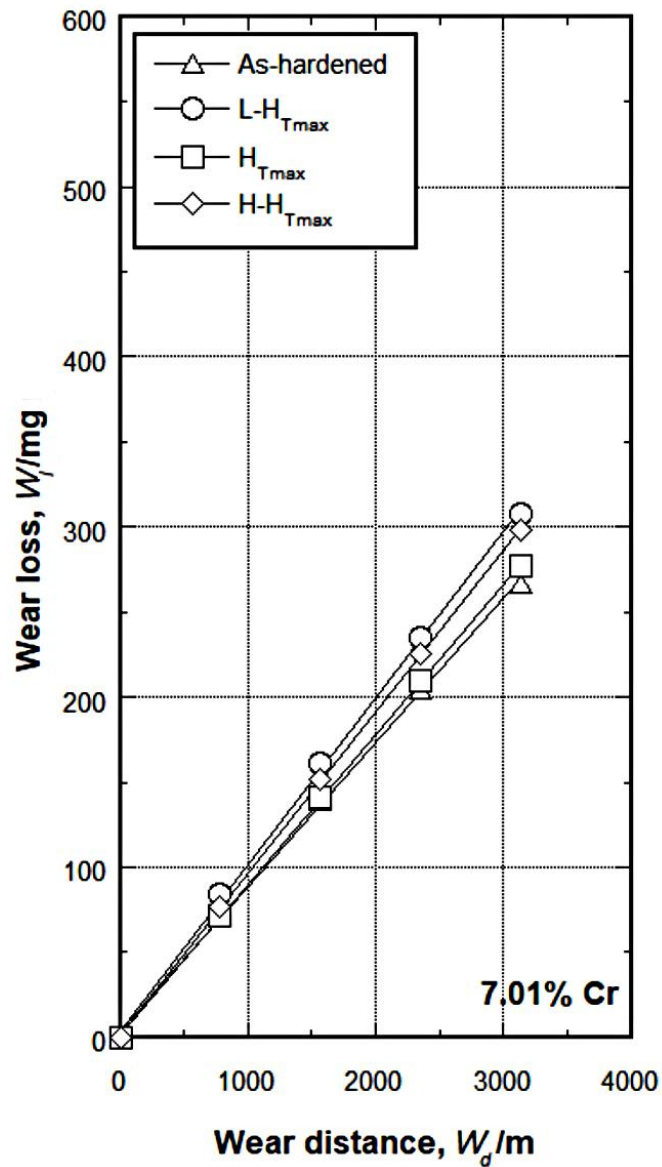
Fig.4-24 displays the results of specimen No.5 with 9%Cr. The wear pattern is very similar to that of specimen No.1 with 3% Cr shown in Fig.4-19, i.e., the patterns of $H-H_{T_{max}}$, $L-H_{T_{max}}$ and $H_{T_{max}}$ test pieces are close and that of As-H lies at lower position far from other three test pieces. However, the wear patterns locate in the very low side compared with 3%Cr specimens. The R_w value increases in the order of 0.085 in As-H, 0.100 in $H_{T_{max}}$, 0.105 in $L-H_{T_{max}}$ and 0.106 mg/m in $H-H_{T_{max}}$ test pieces. The As-H specimen has the largest wear resistance and $H-H_{T_{max}}$ specimen does the smallest wear resistance.



As-H	△	$W_l = 0.070 * W_d + 4.98$	($R^2 = 0.99$)
L-H_{Tmax}	○	$W_l = 0.095 * W_d + 2.04$	($R^2 = 0.99$)
H_{Tmax}	□	$W_l = 0.083 * W_d + 1.82$	($R^2 = 0.99$)
H-H_{Tmax}	◇	$W_l = 0.086 * W_d + 4.22$	($R^2 = 0.99$)

W_l : Wear loss, W_d : Wear distance

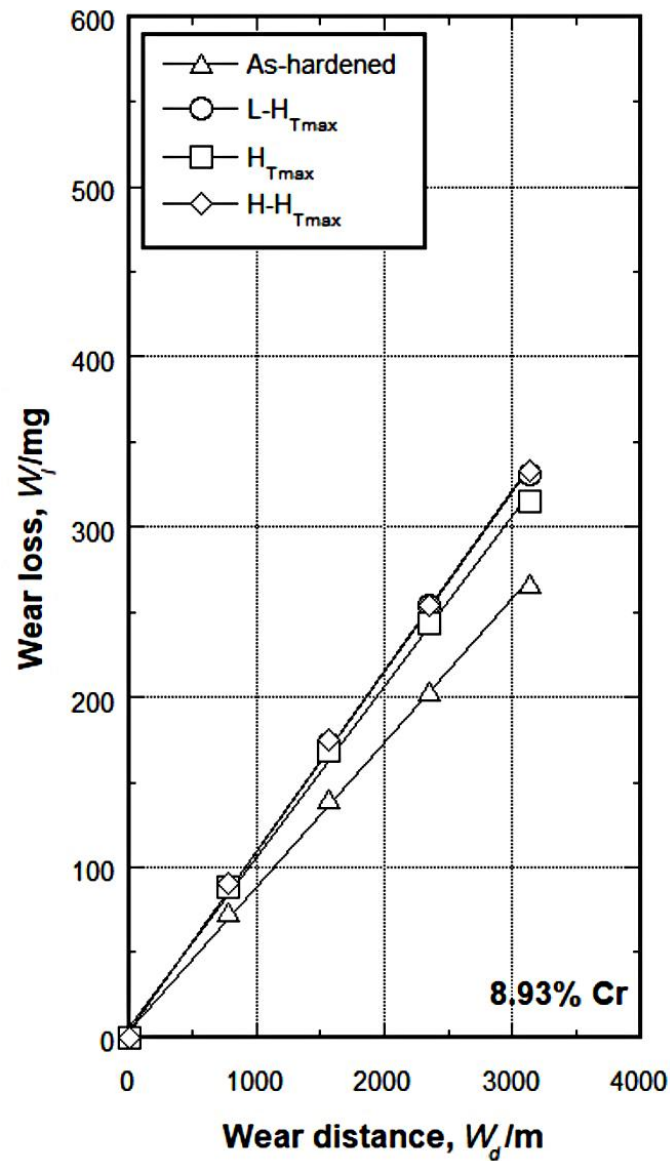
Fig.4-22 Relationship between wear loss (W_l) and wear distance (W_d) of specimen No.3 with 6%Cr hardened from 1323K. Rubber wheel abrasive wear test under a load of 85.3N (8.7 kgf).



As-H	△	$W_l = 0.085 * W_d + 3.58$	$(R^2 = 0.99)$
L-H_{Tmax}	○	$W_l = 0.098 * W_d + 4.50$	$(R^2 = 0.99)$
H_{Tmax}	□	$W_l = 0.088 * W_d + 1.40$	$(R^2 = 0.99)$
H-H_{Tmax}	◇	$W_l = 0.095 * W_d + 1.60$	$(R^2 = 0.99)$

W_l : Wear loss, W_d : Wear distance

Fig.4-23 Relationship between wear loss (W_l) and wear distance (W_d) of specimen No.4 with 7%Cr hardened from 1323K. Rubber wheel abrasive wear test under a load of 85.3N (8.7 kgf).



As-H	△	$W_l = 0.085 * W_d + 3.80$	$(R^2 = 0.99)$
L-H_{Tmax}	○	$W_l = 0.105 * W_d + 3.90$	$(R^2 = 0.99)$
H_{Tmax}	□	$W_l = 0.100 * W_d + 6.00$	$(R^2 = 0.99)$
H-H_{Tmax}	◇	$W_l = 0.106 * W_d + 4.48$	$(R^2 = 0.99)$

W_l : Wear loss, W_d : Wear distance

Fig.4-24 Relationship between wear loss (W_l) and wear distance (W_d) of specimen No.5 with 9%Cr hardened from 1323K. Rubber wheel abrasive wear test under a load of 85.3N (8.7 kgf).

The R_w values of all the test pieces are summarized in Table 4-10.

Table 4-10 Wear rates (R_w) of specimens hardened from 1323K and tempered.

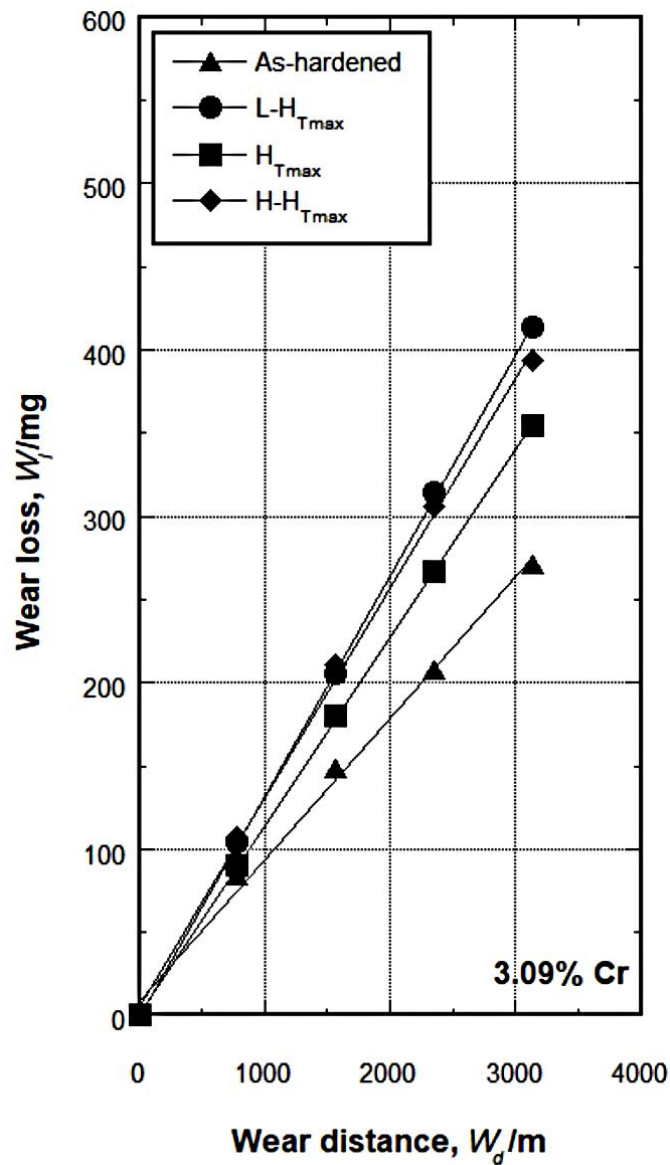
Rubber wheel abrasive wear test under a load of 85.3N (8.7 kgf).

Austenitizing : 1323K.

Specimen	Wear rate (mg/m)			
	As-H	L- $H_{T_{max}}$	$H_{T_{max}}$	H- $H_{T_{max}}$
No.1 (3%Cr)	0.108	0.168	0.159	0.165
No.2 (5%Cr)	0.088	0.118	0.106	0.131
No.3 (6%Cr)	0.070	0.095	0.083	0.086
No.4 (7%Cr)	0.085	0.098	0.088	0.095
No.5 (9%Cr)	0.085	0.105	0.100	0.106

4.3.2.2 Wear test results of specimens tempered after hardening from 1373K austenitizing

The relationships between wear loss (W_l) and wear distance (W_d) of specimen No.1 with 3%Cr are shown in Fig.4-25. The wear patterns change broadly depending on the heat treatment conditions but those of L- $H_{T_{max}}$ and H- $H_{T_{max}}$ test pieces are close while the $H_{T_{max}}$ and As-H test pieces are separated and sit in the lower positions. The smallest R_w value of 0.085 mg/m is obtained in As-H specimen and it increases in the order of 0.113 in $H_{T_{max}}$, 0.126 in H- $H_{T_{max}}$ and 0.132 mg/m in L- $H_{T_{max}}$ test pieces.



As-H	▲	$W_l = 0.085 * W_d + 9.20$	($R^2 = 0.99$)
L- H_{Tmax}	●	$W_l = 0.132 * W_d + 0.24$	($R^2 = 0.99$)
H- T_{max}	■	$W_l = 0.113 * W_d + 1.48$	($R^2 = 0.99$)
H- H_{Tmax}	◆	$W_l = 0.126 * W_d + 6.34$	($R^2 = 0.99$)

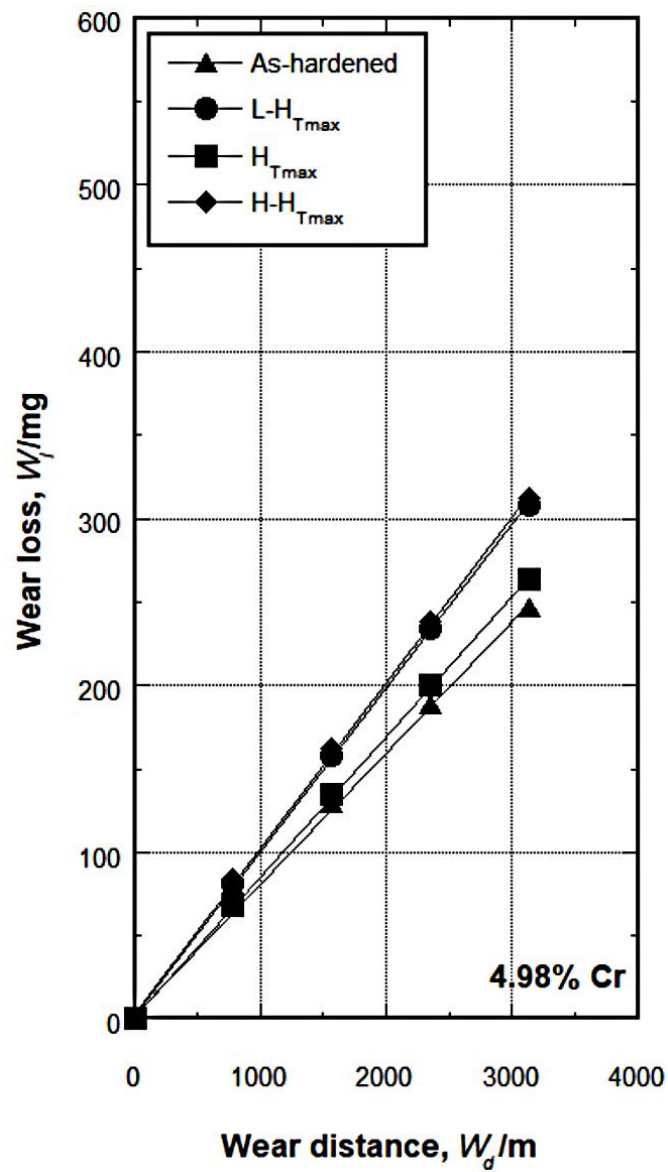
W_l : Wear loss, W_d : Wear distance

Fig.4-25 Relationship between wear loss (W_l) and wear distance (W_d) of specimen No.1 with 3%Cr hardened from 1373K. Rubber wheel abrasive wear test under a load of 85.3N (8.7 kgf).

Fig.4-26 shows the wear test results of specimen No.2 with 5%Cr. The wear pattern of test pieces are similar to 5%Cr specimen i.e., those of L-H_{Tmax} and H-H_{Tmax} test pieces are nearly same but those of H_{Tmax} and As-H are clearly separated. However, that of each test piece lies in much lower side compared with 3%Cr specimen. The R_w values are smallest of 0.078 in As-H, 0.084 in H_{Tmax}, 0.098 in L-H_{Tmax} and the largest of 0.099 mg/m in H-H_{Tmax} test pieces, respectively.

The results of specimen No.3 with 6%Cr is shown in Fig.4-27. The wear patterns of test pieces are separated according to their heat treatment conditions. The patterns are overall located in much lower site than those of 5%Cr specimen. The R_w values increases in the order of 0.065 in As-H, 0.073 in H_{Tmax}, 0.081 in H-H_{Tmax} and 0.085 mg/m in L-H_{Tmax} test pieces.

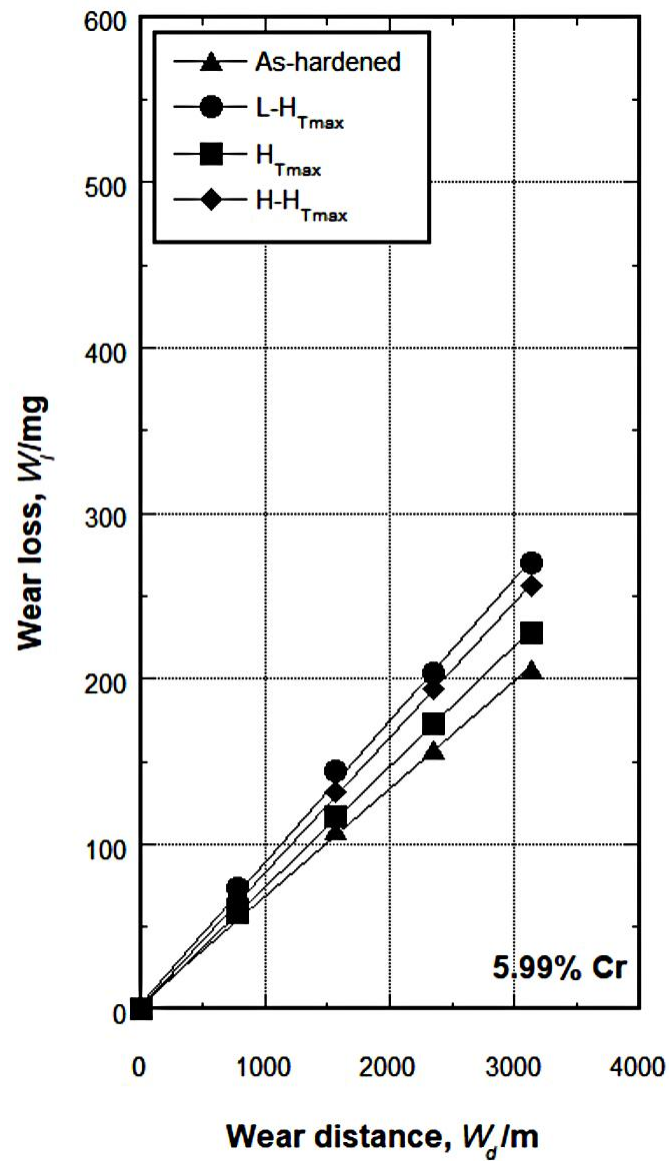
Fig.4-28 displays the results of specimen No.4 with 7%Cr. It is found that the wear pattern of every test piece is approximately same as that of the 6%Cr specimen but the difference in the wear patterns among test pieces is shrunk. The wear patterns of As-H and H_{Tmax} test pieces are almost same and those of L-H_{Tmax} and H-H_{Tmax} are individually separated each other. The smallest R_w value is 0.074 mg/m in As-H test piece and it rises in the order of 0.076 in H_{Tmax}, 0.081 in H-H_{Tmax} and the highest of 0.085 mg/m in L-H_{Tmax} test pieces.



As-H	▲	$W_1 = 0.078 * W_d + 3.18$	($R^2 = 0.99$)
$L-H_{T_{max}}$	●	$W_1 = 0.098 * W_d + 2.32$	($R^2 = 0.99$)
$H_{T_{max}}$	■	$W_1 = 0.084 * W_d + 2.02$	($R^2 = 0.99$)
$H-H_{T_{max}}$	◆	$W_1 = 0.099 * W_d + 3.76$	($R^2 = 0.99$)

W_1 : Wear loss, W_d : Wear distance

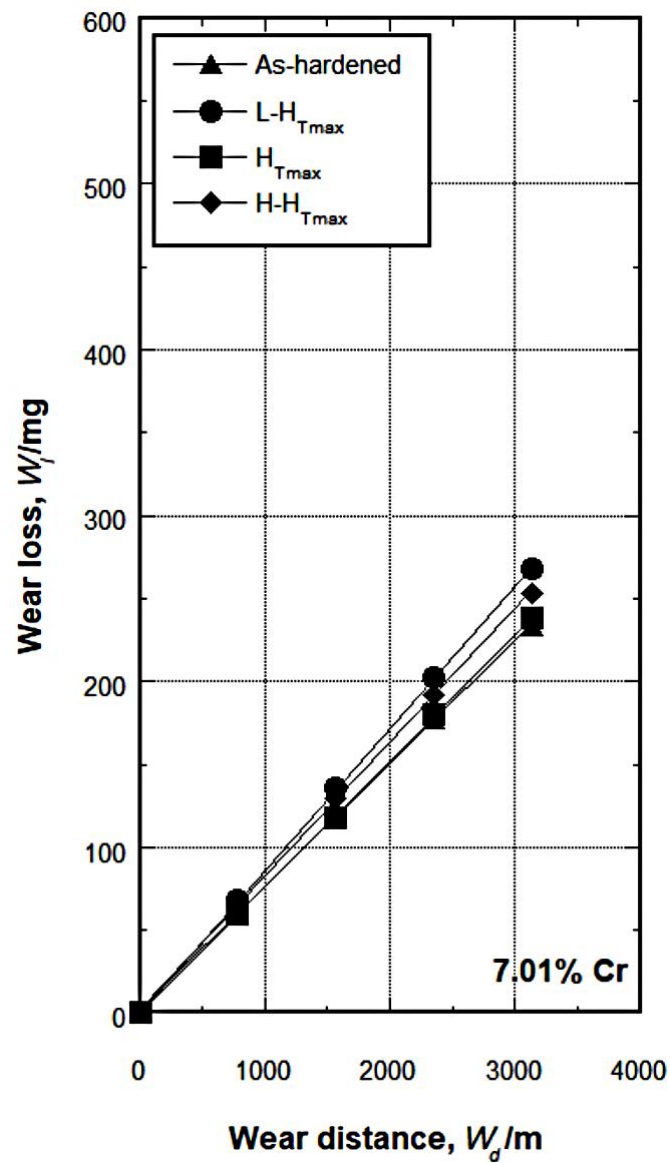
Fig.4-26 Relationship between wear loss (W_1) and wear distance (W_d) of specimen No.2 with 5%Cr hardened from 1373K. Rubber wheel abrasive wear test under a load of 85.3N (8.7 kgf).



As-H	▲	$W_l = 0.065 * W_d + 3.80$	$(R^2 = 0.99)$
$L-H_{T_{max}}$	●	$W_l = 0.085 * W_d + 4.16$	$(R^2 = 0.99)$
$H_{T_{max}}$	■	$W_l = 0.073 * W_d + 1.40$	$(R^2 = 0.99)$
$H-H_{T_{max}}$	◆	$W_l = 0.081 * W_d + 1.90$	$(R^2 = 0.99)$

W_l : Wear loss, W_d : Wear distance

Fig.4-27 Relationship between wear loss (W_l) and wear distance (W_d) of specimen No.3 with 6%Cr hardened from 1373K. Rubber wheel abrasive wear test under a load of 85.3N (8.7 kgf).



As-hardened	▲	$W_l = 0.074 * W_d + 2.64$	$(R^2 = 0.99)$
L-$H_{T_{max}}$	●	$W_l = 0.085 * W_d + 0.74$	$(R^2 = 0.99)$
$H_{T_{max}}$	■	$W_l = 0.076 * W_d - 0.12$	$(R^2 = 0.99)$
H-$H_{T_{max}}$	◆	$W_l = 0.081 * W_d + 2.08$	$(R^2 = 0.99)$

W_l : Wear loss, W_d : Wear distance

Fig.4-28 Relationship between wear loss (W_l) and wear distance (W_d) of specimen No.4 with 7%Cr hardened from 1373K. Rubber wheel abrasive wear test under a load of 85.3N (8.7 kgf).

The results of specimen No.5 with highest Cr content of 9% are shown in Fig.4-29. The wear patterns of test pieces are separated independently according to difference of their heat treatment conditions and the position of the wear patterns are similar to those of 7%Cr specimen. The R_w values increases in the order of 0.074 in As-H, 0.080 H_{Tmax} , 0.086 in H- H_{Tmax} and 0.093 mg/m in L- H_{Tmax} test pieces, respectively.

From all the results mentioned above, it can be said on the whole that the smallest R_w value or the highest wear resistance is obtained in As-H specimen and the largest R_w value or the lowest wear resistance is obtained in L- H_{Tmax} or H- H_{Tmax} specimens, regardless of hardening temperatures.

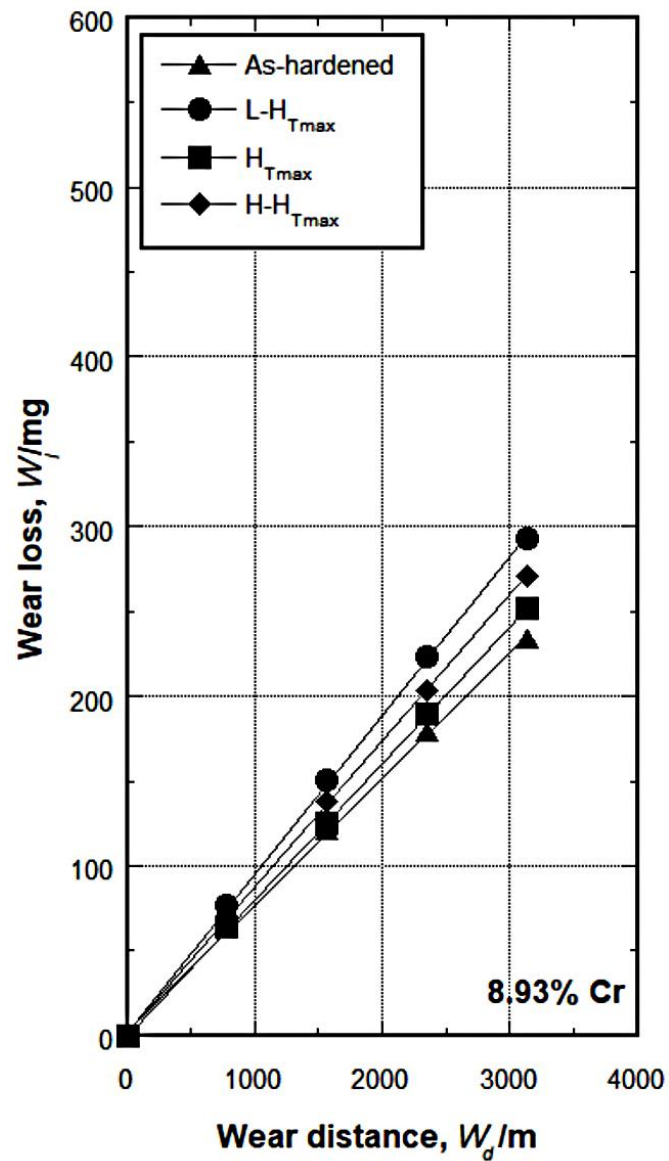
The R_w values of all the test pieces are summarized in Table 4-11.

Table 4-11 Wear rates (R_w) of specimens hardened from 1323K and tempered.

Rubber wheel abrasive wear test under a load of 85.3N (8.7 kgf).

Austenitizing : 1373K.

Specimen	Wear rate (mg/m)			
	As-H	L- H_{Tmax}	H_{Tmax}	H- H_{Tmax}
3%Cr	0.085	0.132	0.113	0.126
5%Cr	0.078	0.098	0.084	0.099
6%Cr	0.065	0.085	0.073	0.081
7%Cr	0.074	0.085	0.076	0.081
9%Cr	0.074	0.093	0.080	0.086



As-H	▲	$W_1 = 0.074 * W_d + 2.66$	$(R^2 = 0.99)$
L-HT_{max}	●	$W_1 = 0.093 * W_d + 2.28$	$(R^2 = 0.99)$
H_{Tmax}	■	$W_1 = 0.080 * W_d + 0.32$	$(R^2 = 0.99)$
H-HT_{max}	◆	$W_1 = 0.086 * W_d + 1.66$	$(R^2 = 0.99)$

W_1 : Wear loss, W_d : Wear distance

Fig.4-29 Relationship between wear loss (W_1) and wear distance (W_d) of specimen No.5 with 9%Cr hardened from 1373K. Rubber wheel abrasive wear test under a load of 85.3N (8.7 kgf).

Chapter V

Discussions

5.1 Effect of Cr content on heat treatment behavior

5.1.1 Effect of Cr content on hardness and volume fraction of retained austenite (V_γ)

5.1.1.1 As-hardened state

As mentioned in Chapter 4, it has been believed that eutectic carbides are little affected by the heat treatment. Therefore, the variation of hardness is practically influenced by the phase transformation of matrix during heat treatment. It is well known that hardness in heat-treated alloyed cast iron is closely related to the amount of retained austenite (V_γ), that is, the hardness decreases as the V_γ increases. In addition, the hardness of martensite itself affects the matrix hardness as well. It is the fact that the hardness of martensite rises with an increase in C concentration in martensite.

Before discussing the relation of macro-hardness vs. Cr content, the relationship between Cr content and micro-hardness which is one of factors to make up the macro-hardness was obtained and shown in Fig.5-1. As the Cr content of specimen increases from 3%, the micro-hardness rises to the maximum value at 5%Cr and then lowers, regardless of austenitizing temperatures. The micro-hardness of specimens hardened from 1323K lie at higher value than those hardened from 1373K. These results agree well with the behavior of macro-hardness corresponding to Cr content which is shown later in Fig.5-2. It is obvious that from these results the

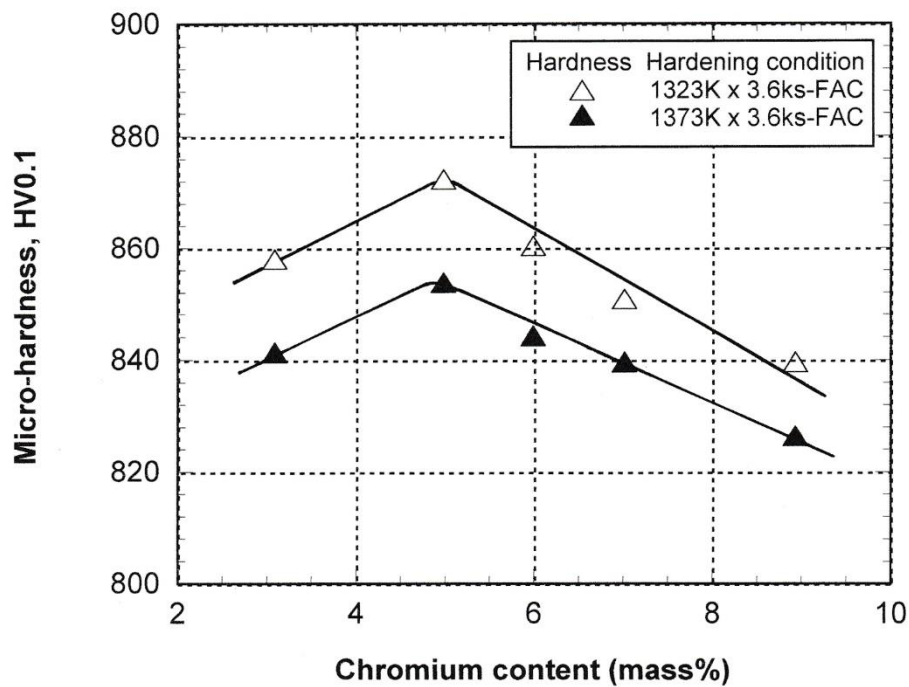


Fig.5-1 Relationship between micro-hardness and Cr content of as-hardened specimens.

macro-hardness changes coping with the micro-hardness. From now on, therefore, the macro-hardness is chiefly adopted because the macro-hardness is closely related to the wear resistance described in the future section on abrasive wear behavior.

The relationships between macro-hardness, V_H and Cr content of the specimens hardened from 1323 and 1373K austenitizing were conducted and they are shown in Fig.5-2.

It is found that the macro-hardness shows the same tendency corresponding to the Cr content even if the austenitizing temperature changes. The macro-hardness increases a little to the highest point at 5%Cr and then decreases gradually as Cr content increases. This tells that the hardness is significantly influenced by the Cr content. The reason of a rise in hardness is due to an increase in Cr dissolved in

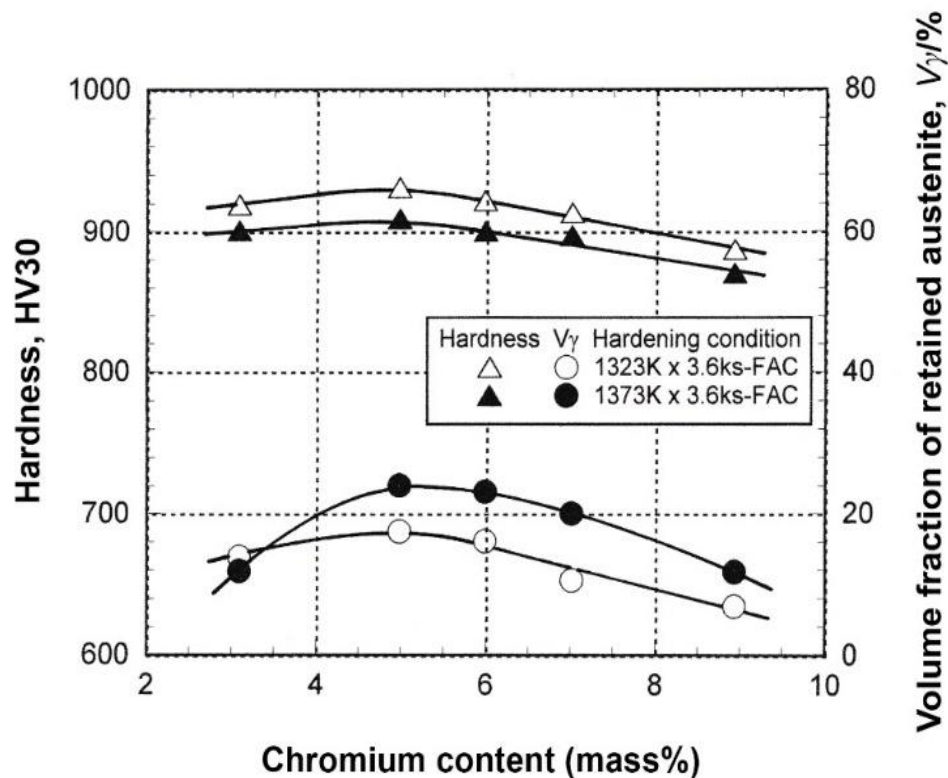


Fig.5-2 Relationship between macro-hardness, volume fraction of retained austenite (V_{γ}) and Cr content of as-hardened specimens.

matrix which strengthens the matrix and promotes the precipitation of secondary carbides. Another reason is that the Cr delays pearlite and bainite transformations and improves the hardenability of the cast iron.

The hardness lowers continuously when the Cr content gets over 5% because the ($\gamma+M_7C_3$) eutectic begins to solidify in the cast iron (section 4.1.2). It is known that the M_7C_3 carbide has lower hardness than MC and M_2C carbides. As mentioned in Fig.4-2, the amount of ($\gamma+M_7C_3$) eutectic rises while ($\gamma+MC$) and ($\gamma+M_2C$) eutectics reduce with increasing the Cr content over 5%. Another reason is that the hardness of martensite decreases due to a reduction of C concentration in martensite. Therefore, the total hardness of specimen continues to decrease. It is clear that the low

austenitizing temperature of 1323K provides higher macro-hardness than those hardened from high austenitizing temperature of 1373K. This is because the low austenitizing temperature produces less retained austenite than those hardened from higher austenitizing temperature.

The amount of retained austenite (V_γ) increases gradually to the highest at 5%Cr and then decreases little by little as Cr content rises in the cases of both hardening temperatures. This result is explained by the fact that M_s temperature of multi-alloyed white cast iron lowered to 5%Cr and rose over 5%Cr as Cr content increases [50]. Consequently, the V_γ values increases from 3 to 5%Cr and decreases from 5 to 9%Cr. It is considered that an increase in Cr content promotes C consumption to form eutectic carbides and resultantly reduces C dissolved in the matrix. From the behavior of such elements, it can be generally said that the amount of added alloying elements which dissolves in austenite during austenitizing affects directly the transformation behavior of matrix.

In the case of low-alloyed steel, the effect of alloying elements on M_s temperature has been expressed by the next equation [51] supposing that all the alloying elements dissolve in the matrix.

$$M_s(^{\circ}C) = 550 - 361(\%C) - 39(\%Mn) - 35(\%V) - 20(\%Cr) - 17(\%Ni) - 10(\%Cu) - 5(\%Mo + \%W) + 15(\%Co) + 30(\%Al) \dots \dots \dots (5-1)$$

Although the multi-alloyed white cast iron contains plural kinds of alloying elements, the transformation of matrix must depend on the concentration of total alloying elements including C in austenite. According to the equation 5-1, the M_s

temperature lowers in proportion to an increase in Cr content. So, the V_{γ} value should increase proportionally to Cr content. In this multi-alloyed white cast iron, however, the turning point of V_{γ} value appears at 5%Cr [50]. In the case of Cr content less than 5%, it is considered that the solubility of alloying elements in austenite could be less than saturation. When the Cr concentration in austenite increases in this state, the Ms temperature decreases and the V_{γ} value rises. In the case of Cr content more than 5%, on the other side, it could be considered that an excessive Cr shrinks the solubilities of not only C but also other alloying elements, and consequently, the precipitation of secondary carbides occurs. As a result, the Ms temperature is increased and the V_{γ} value decreases.

The specimens hardened from 1373K austenitizing show higher V_{γ} values than those hardened from 1323K except for 3%Cr specimen. This can be explained by that the solubilities of C and alloying elements in austenite are expanded by raising the austenitizing temperature. When these elements dissolve more in austenite, the Ms temperature is lowered as expressed by equation 5-1. In the case of 3%Cr specimen, particularly the solubility of Cr in austenite may not be influenced so much by the increase in austenitizing temperature. Therefore, the V_{γ} values in the cases of both austenitizing temperatures changed little.

As shown in Fig.5-1, the matrix hardness is remarkably varied by the Cr content of specimen. So, the relationship between micro-hardness and V_{γ} in as-hardened state was conducted and it is shown in Fig.5-3.

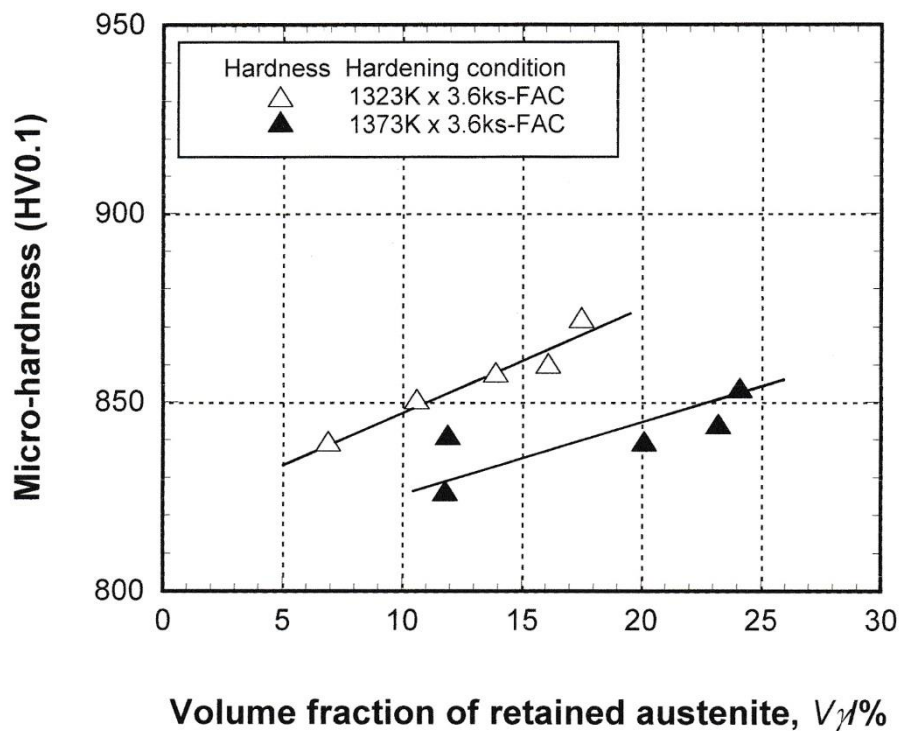


Fig.5-3 Relationship between micro-hardness and volume fraction of retained austenite (V_γ) of as-hardened specimens.

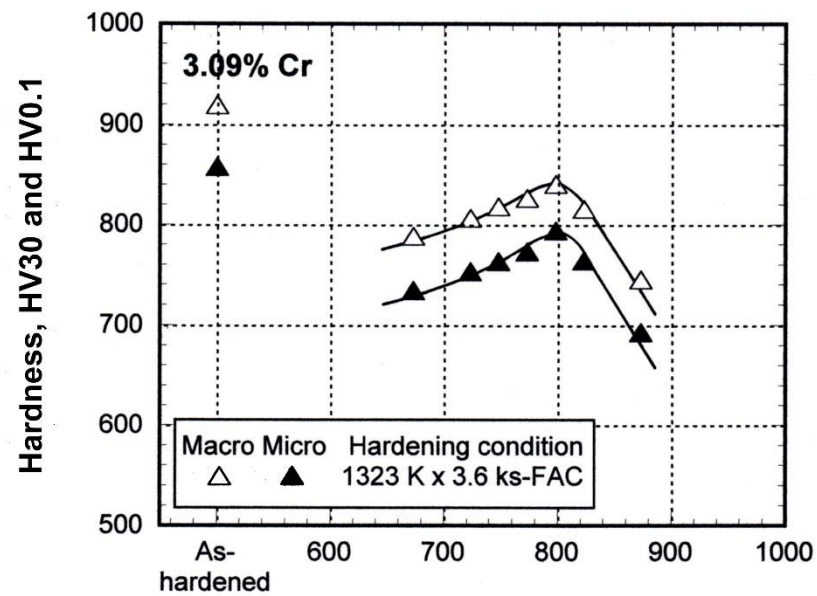
It is found that the matrix hardness increases gradually in proportion to an increase in V_γ value regardless of austenitizing temperatures. The reason of the increase in hardness is explained by that an increase in V_γ value due to more dissolution of C in matrix promotes not only the precipitation of secondary carbides but also rises the hardness of martensite itself. At the same V_γ value, the hardness in the case of hardening from 1323K is higher than that in the case of hardening from 1373K. This reason is considered due to the difference in the amount of secondary carbides which precipitated much greater in the matrix of specimen hardening from lower temperature as already mentioned in section 4.2.1.

5.1.1.2 Tempered state

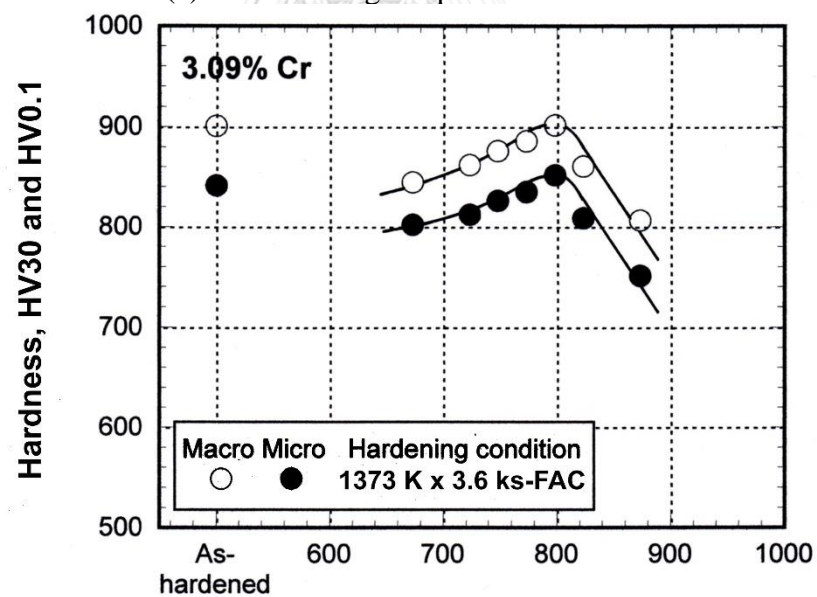
5.1.1.2.1 Relationship between hardness and tempering temperature

The strength of matrix can be widely varied by heat treatment and it influences the mechanical properties including wear resistance. Since the hardness changes mainly depending on the matrix structure, it is commendable to measure the micro-hardness relating to the condition of heat treatment. In order to clarify the behavior of matrix by heat treatment, the micro-hardness and macro-hardness were compared for all the specimens under the same tempering condition and they are shown in Fig.5-4 to 5-8.

It is found that the micro-hardness of each specimen shows similar behavior to the macro-hardness in all of the tempering temperatures and the peak of hardness is obtained at same tempering temperature. Naturally, the micro-hardness is lower than the macro-hardness regardless of austenitizing temperature. It is because the macro-hardness shows the comprehensive hardness of eutectic carbides and matrix while the micro-hardness does the hardness of only matrix in which plural phases are co-existing. The difference between macro-hardness and micro-hardness occurs due to the existence of eutectic carbides with higher hardness than the matrix. The average values of the differences between the macro-hardness and micro-hardness are summarized in Table 5-1.

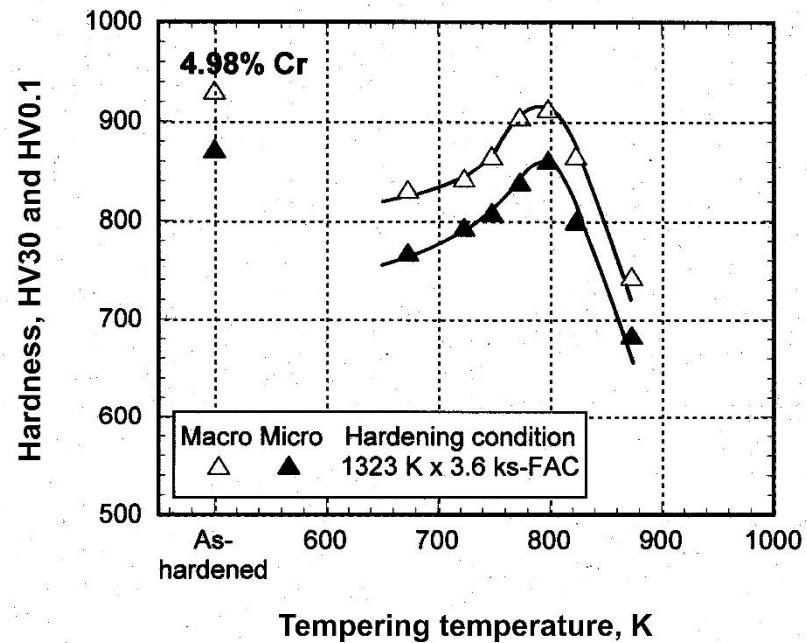


(a) Austenitizing temperature : 1323K.

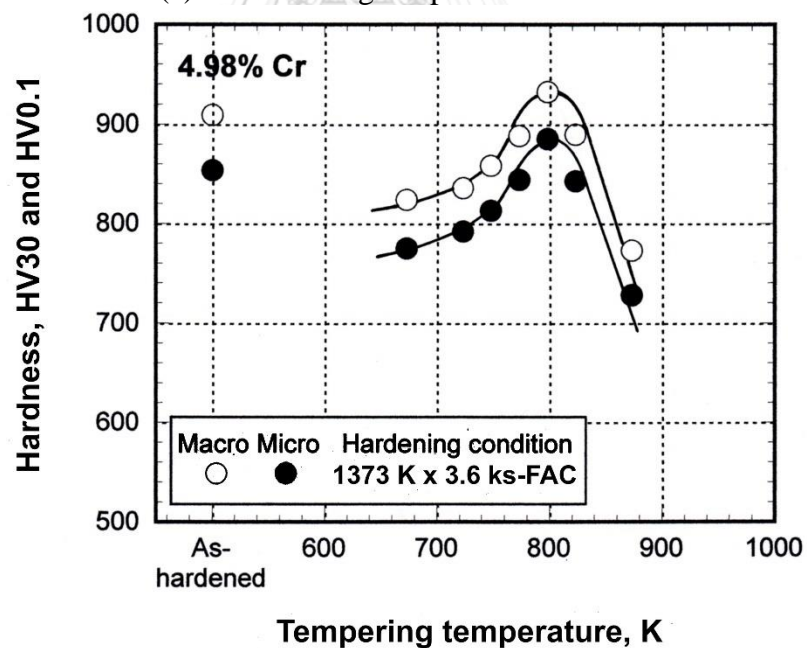


(b) Austenitizing temperature : 1373K.

Fig.5-4 Relationship between macro-hardness, micro-hardness and tempering temperature of 3%Cr specimens. Austenitizing : (a) 1323K and (b) 1373K.

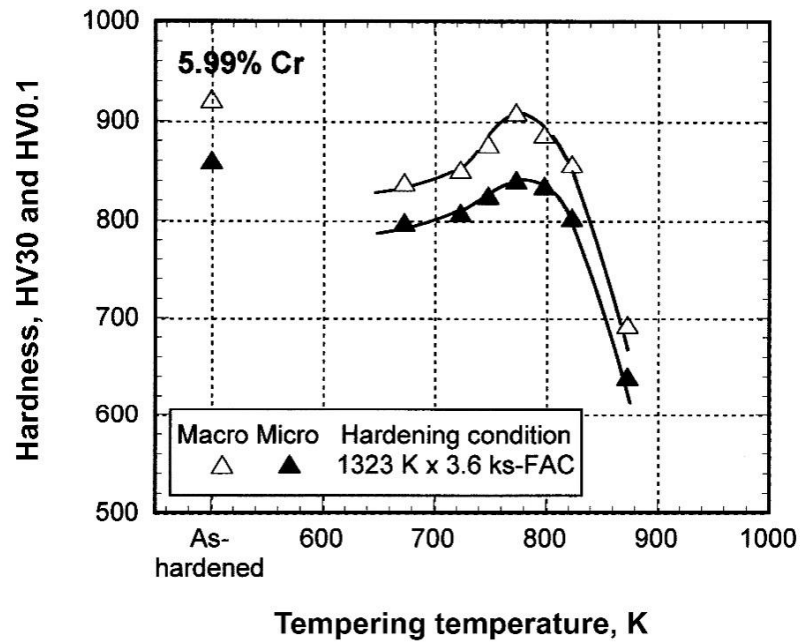


(a) Austenitizing temperature : 1323K.

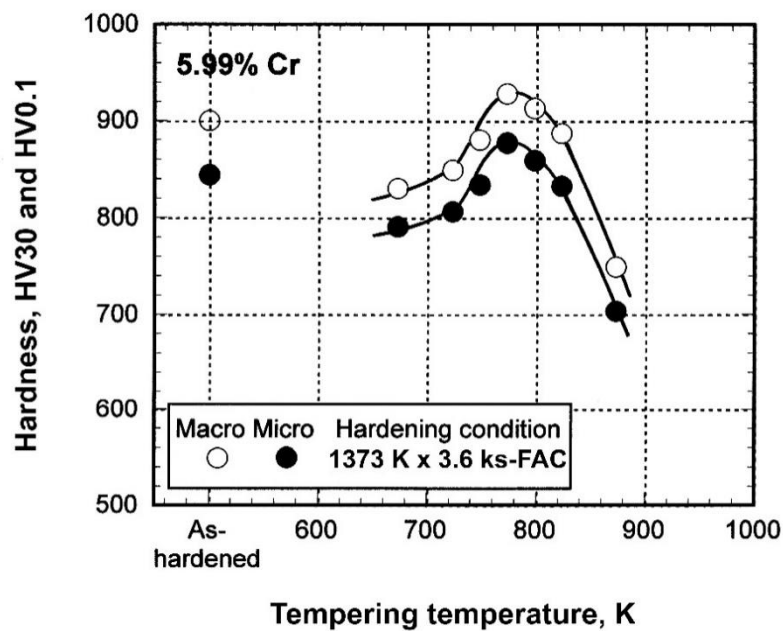


(b) Austenitizing temperature : 1373K.

Fig.5-5 Relationship between macro-hardness, micro-hardness and tempering temperature of 5%Cr specimens. Austenitizing : (a) 1323K and (b) 1373K.

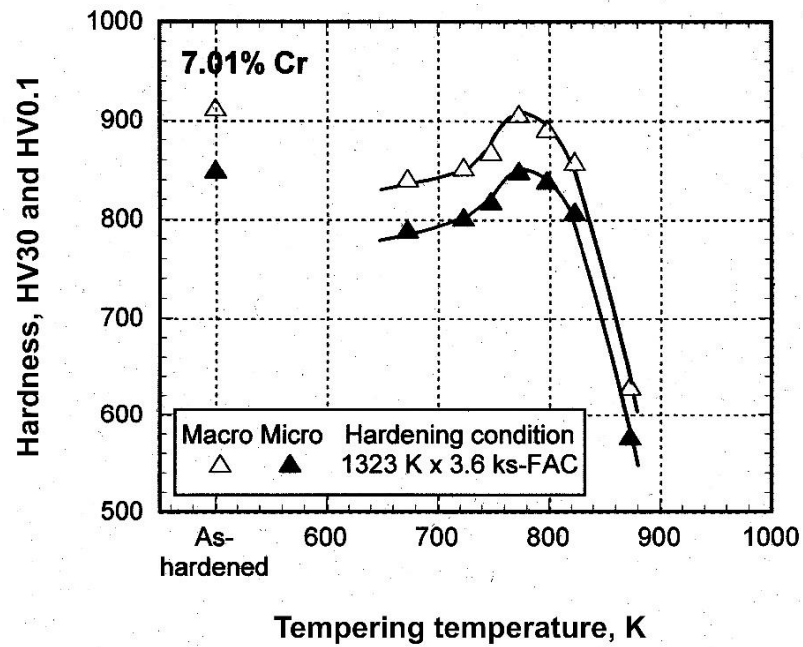


(a) Austenitizing temperature : 1323K.

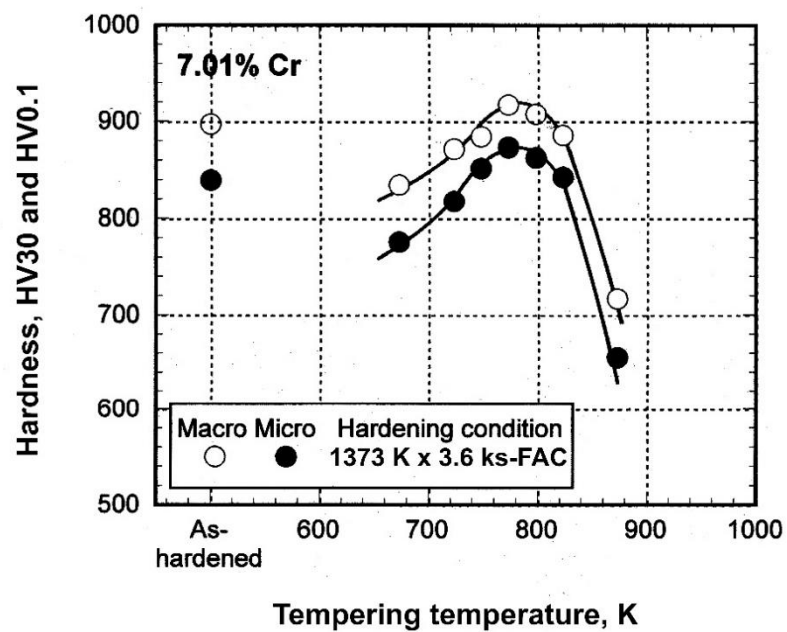


(b) Austenitizing temperature : 1373K.

Fig.5-6 Relationship between macro-hardness, micro-hardness and tempering temperature of 6%Cr specimens. Austenitizing : (a) 1323K and (b) 1373K.

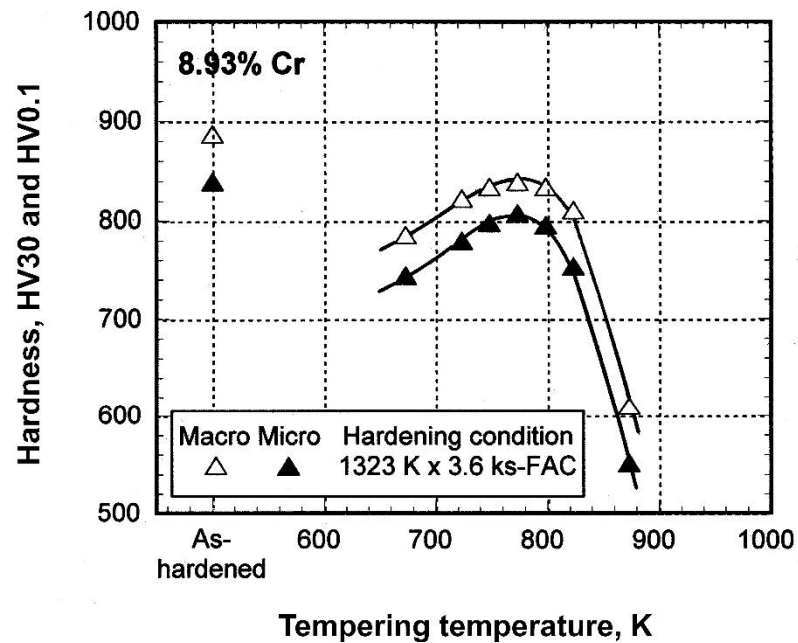


(a) Austenitizing temperature : 1323K.

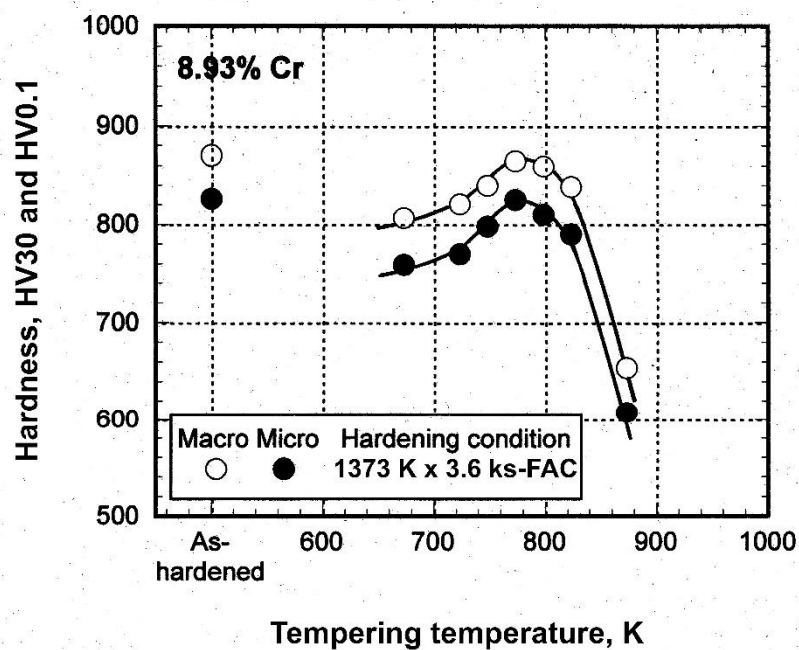


(b) Austenitizing temperature : 1373K.

Fig.5-7 Relationship between macro-hardness, micro-hardness and tempering temperature of 7%Cr specimens. Austenitizing : (a) 1323K and (b) 1373K.



(a) Austenitizing temperature : 1323K.



(b) Austenitizing temperature : 1373K.

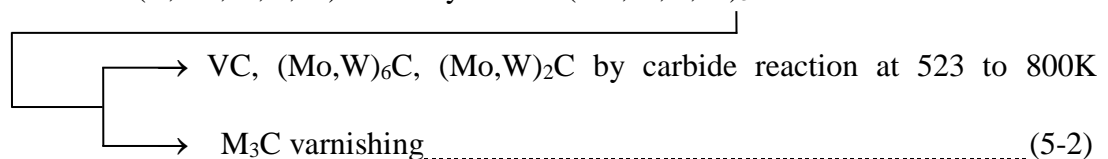
Fig.5-8 Relationship between macro-hardness, micro-hardness and tempering temperature of 9%Cr specimens. Austenitizing : (a) 1323K and (b) 1373K.

Table 5-1 The difference in hardness between macro-hardness and micro-hardness in tempered state.

Specimen	Difference in hardness (HV)	
	1323K austenitizing	1373K austenitizing
No.1 (3%Cr)	53.6	51.2
No.2 (5%Cr)	59.0	48.7
No.3 (6%Cr)	53.2	48.7
No.4 (7%Cr)	53.4	49.5
No.5 (9%Cr)	44.5	45.9

In each micro-hardness curve, the secondary hardening appears in the same manner as in the macro-hardness curve. When the specimen was tempered at 673K, the micro-hardness drops largely from that in as-hardened state chiefly due to the tempering of martensite, that is, the very fine $M(\text{Mo}, \text{W}, \text{V}, \text{Cr})_3\text{C}$ formed in martensite crystal lattice. As the tempering temperature increases, the precipitation of very fine carbides continues and grows. Resultantly, the hardness rises. On the other side, the retained austenite is decomposed by precipitation of secondary carbides combined with alloying elements. Then, the alloying elements in residual austenite decrease and the M_s temperature goes up. Resultantly, martensite formed during post cooling. Since this phenomenon continues up to near 800K where the carbide reaction starts, the hardness continues to rise greatly. When the temperature is increased, the progress of carbide reaction in martensite is expressed as follows,

Martensite (C,Mo,W,V,Cr) \rightarrow Very fine $M(\text{Mo}, \text{W}, \text{V}, \text{Cr})_3\text{C}$ formation in martensite



In the tempering approximately near 800K, the carbide reaction almost finishes. Each alloying elements form their own special carbides like VC, (Mo,W)₆C or (Mo,W)₂C and they are dispersed in the matrix. These carbides have much higher hardness compared with those of MC, M₆C and M₂C carbides. Therefore, the total hardness increases to the maximum micro-hardness ($H_{T_{max-M}}$) at around 773-800K tempering. When the tempering temperature rises over 800K, however, the agglomeration or coarsening of secondary carbides takes place due to the Ostwald ripening effect. This reaction makes the hardness low remarkably.

The reduction of retained austenite (V_γ) in matrix contributes to an increase in hardness reasonably. As shown in section 4.2.2, the V_γ begins to decrease markedly over 748-823K. This means that the decomposition rate of austenite to secondary carbides and martensite is accelerated at this temperature. It can be understood that an increase in the precipitated carbides reduces stability of retained austenite and the unstable austenite transforms into martensite easily.

In Table 5-1, the difference values between the macro-hardness and micro-hardness in the case of hardening from 1323K are almost same except for specimen No.2 (5%Cr) with larger value and No.5 (9%Cr) with lower value. In the case of hardening from 1373K, the differences of specimens No.1 (3%Cr) to No.4 (7%Cr) are approximately same except for specimen No.5 (9%Cr) with lower value. It can be said on the whole that there is not so large difference in the hardness among the specimens under the same austenitizing temperature. However, the differences are lower in the case of hardening from 1373K. It can be presumed that the secondary

hardening of matrix could be greater in the specimens hardened from higher austenitizing temperature.

From all of the results, it is clear that the variation of macro-hardness follows that of the matrix hardness or micro-hardness. Therefore, it must be suitable to discuss the behavior of heat treatment and especially abrasive wear resistance which is described later by the macro-hardness.

5.1.1.2.2 Relationship between hardness and volume fraction of retained austenite (V_γ) in tempered state

Macro-hardness is a comprehensive hardness of eutectic carbides and matrix. Therefore, the macro-hardness is also significantly affected by the V_γ in the tempered matrix also affects. In alloyed white cast iron, it is known that the tempering alters the hardness and reduces the quantity of retained austenite. In addition, the hardness in tempered state increases due to the precipitation of carbides and/or special carbides with extremely high hardness as mentioned in section 5.1.2. The relation of hardness vs. V_γ is obtained for all the tempered specimens, and it is shown in Fig.5-9 (a) for macro-hardness and (b) for micro-hardness, respectively.

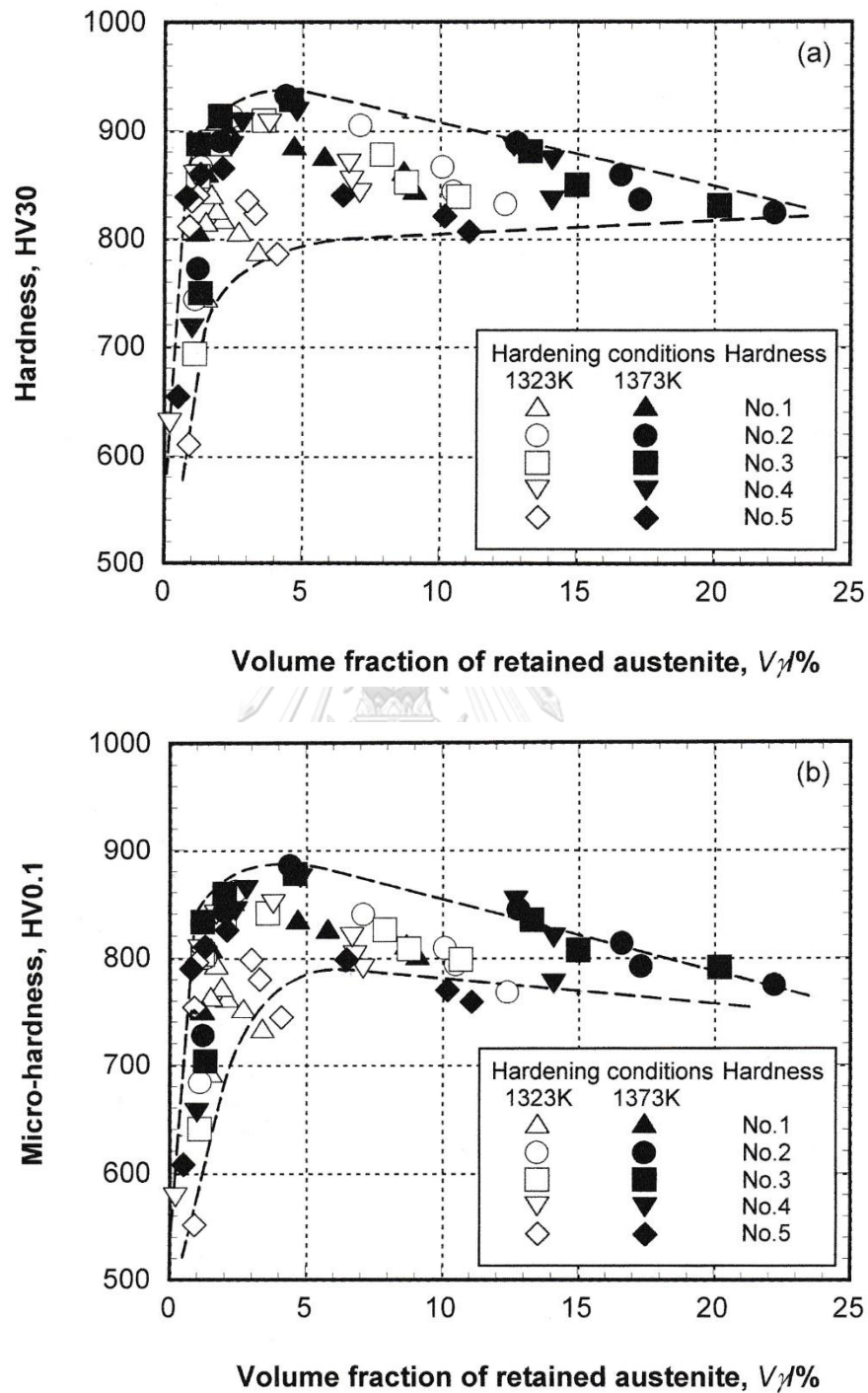


Fig.5-9 Relationship between hardness and volume fraction of retained austenite (V_γ) in tempered state. (a) Macro-hardness and (b) Micro-hardness.

From Fig.5-9 (a), it is found that the macro-hardness of specimens with less than 2% V_γ ranges widely. In the case of hardening from 1373K austenitizing, the hardness seems to show higher values than those of from 1323K. Over 3% V_γ , the scattering of hardness decreases as the V_γ value increases. The reasons are due to an increase in V_γ value and a reduction of martensite. It is found that the V_γ value at most 10% is allowed to remain to obtain the hardness over 900HV30.

With respect to the relationship between micro-hardness and V_γ value as shown in Fig.5-9 (b), the tendency is quite similar to that of the macro-hardness but as a whole, the micro-hardness is lower. The micro-hardness ranges from 550 to 890 HV0.1 depending on the Cr content and austenitizing temperature. It is clear from the diagram that the matrix hardness of specimens hardened from 1373K austenitizing is higher than those hardened from 1323K. The reason can be same as mentioned in the case of macro-hardness. The maximum values of around 890 HV0.1 is obtained at the 4% V_γ in the specimen with 5%Cr which is same the Cr content as the case of macro-hardness. The low micro-hardness in low V_γ region is because of over-tempering. There, the retained austenite has fully transformed to pearlite with low hardness. High micro-hardness in the same region, on the other side, the retained austenite transformed to martensite with high hardness. A large difference in hardness near 2% V_γ is considered to be due to the difference in the matrix structure. The highest hardness value about 940 HV30 is obtained at 4% V_γ in specimen with 5%Cr irrespective of austenitizing temperature. Over 4% V_γ , the macro-hardness seems to decrease roughly in proportion to an increase in V_γ value. Here, the relationship

between hardness and V_γ value was tried to express as an equation. The following formula for the macro-hardness is obtained by the method for least squares.

$$\text{Macro-hardness (HV30)} = -2.91 * \%V_\gamma + 890 \dots\dots\dots(5-3)$$

The relationship between micro-hardness and V_γ in the region over the maximum micro-hardness is obtained by the same method. The relation is expressed by the next equation.

$$\text{Micro-hardness (HV0.1)} = -2.56 * \%V_\gamma + 837 \dots\dots\dots(5-4)$$

By comparing the micro-hardness with the macro-hardness, it is evident that the decreasing rate of micro-hardness is smaller than that of macro-hardness.

In the region of V_γ values less than 2%, the macro-hardness and micro-hardness scatter widely. Since the tempering temperature does not vary the morphology of eutectic carbides, the scattering of hardness is mainly due to the difference in matrix structure or micro-hardness. In order to clarify this, the relationship between micro-hardness and tempering temperature was obtained for specimens with V_γ values less than 2% and it is shown in Fig.5-10.

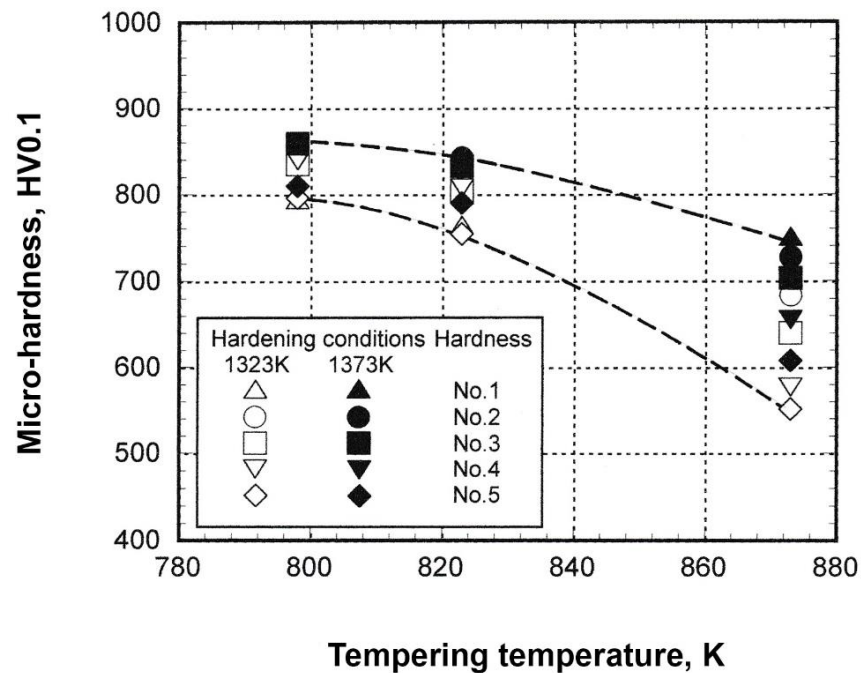


Fig.5-10 Relationship between micro-hardness and tempering temperature of tempered specimens with volume fraction of retained austenite (V_γ) less than 2%.

In even this small region, it is clear that the micro-hardness decreases continuously with scattering, as the tempering temperature rises. It is presumed that the decrease in hardness is due to the coarsening of secondary carbide and the transformation of austenite to pearlite or ferrite. It is noted that in the specimens tempered at 873K, the coarsening of carbides and other transformation were completed, and the micro-hardness lowers in order of Cr content. The reason could be that the concentration of C and other alloying elements in the matrix was reduced with an increase in Cr content, and then, the matrix hardness decreased by the precipitation of secondary chromium carbides with lower hardness like of M_7C_3 or $M_{23}C_6$.

5.1.2 Variation of maximum tempered hardness (H_{Tmax}), volume fraction of retained austenite (V_γ) and Cr content

5.1.2.1 Effect of Cr content on maximum tempered hardness (H_{Tmax}) and volume fraction of retained austenite at H_{Tmax} ($V_{\gamma-HTmax}$)

In application of alloyed white cast iron to the part and component satisfied with abrasive wear resistance, the heat treatment is usually introduced so that the cast iron can have higher hardness and appropriate toughness. As for the rolling mill roll, the amount of retained austenite must be limited to prevent the cracking which produces during operation by the transformation of strain-induced martensite and spalling wear. Therefore, it is necessary to clarify the factors obtains the maximum hardness by tempering.

The relationship between H_{Tmax} , V_γ at H_{Tmax} ($V_{\gamma-HTmax}$) and Cr content is shown in Fig.5-11. The H_{Tmax} values show similar pattern in specimens hardened from different austenitizing temperatures. The H_{Tmax} rises until 5%Cr and then goes down gradually as the Cr content increases. The H_{Tmax} in the case hardened from 1373K is larger than that from 1323K austenitizing at the overall Cr content. The highest H_{Tmax} values are 913 and 933 HV30 for hardening from 1323K and 1373K, respectively. The reason why the H_{Tmax} rises in the former stage up to 5%Cr is due to the decrease in M_s temperature by increasing the Cr content. The decrease in M_s temperature makes the V_γ increase in as-hardened state. During tempering, more secondary carbides are produced, and more martensite transforms from destabilized retained austenite as well. In the latter stage, over 5%Cr, the H_{Tmax} decreases

gradually because eutectic M_7C_3 carbide with low hardness begins to solidify and this situation progresses with an increase in Cr content.

The $V_{\gamma-HT_{max}}$ values are less than 5% at overall Cr content. It increases a little to 6%Cr and then, continues to decrease slightly as the Cr content rises. This suggests that even if the test piece shows the maximum hardness by tempering, a certain amount of austenite is remained. The $V_{\gamma-HT_{max}}$ is high in the case of hardening from higher austenitizing temperature of 1373K. This is because the hardening from high temperature produces more retained austenite in as-hardened state. Under the same tempering condition, therefore, the more austenite remains in the matrix.

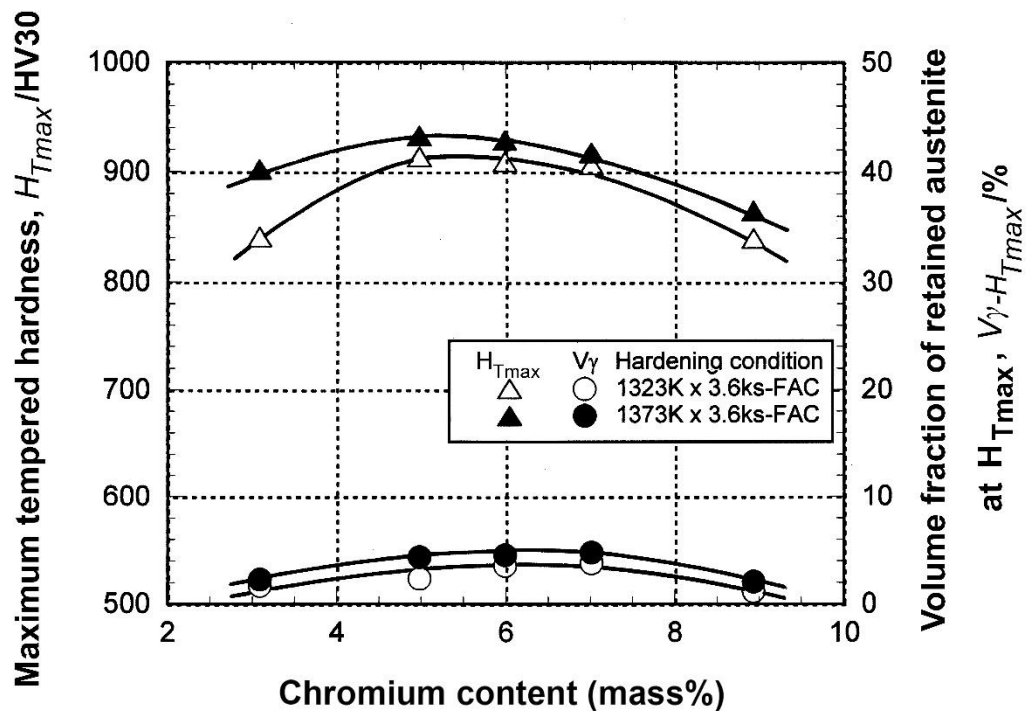
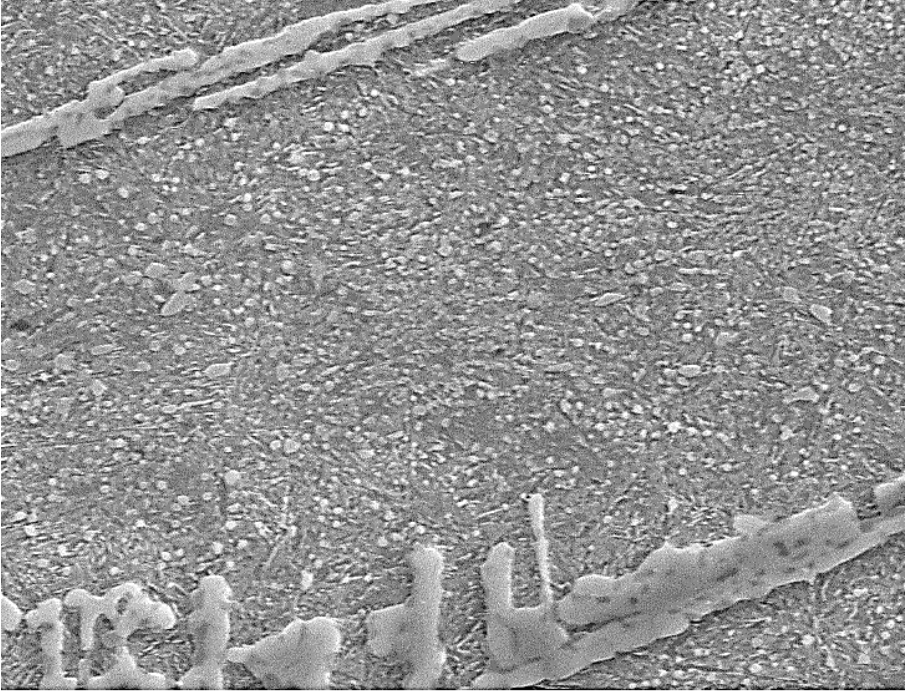
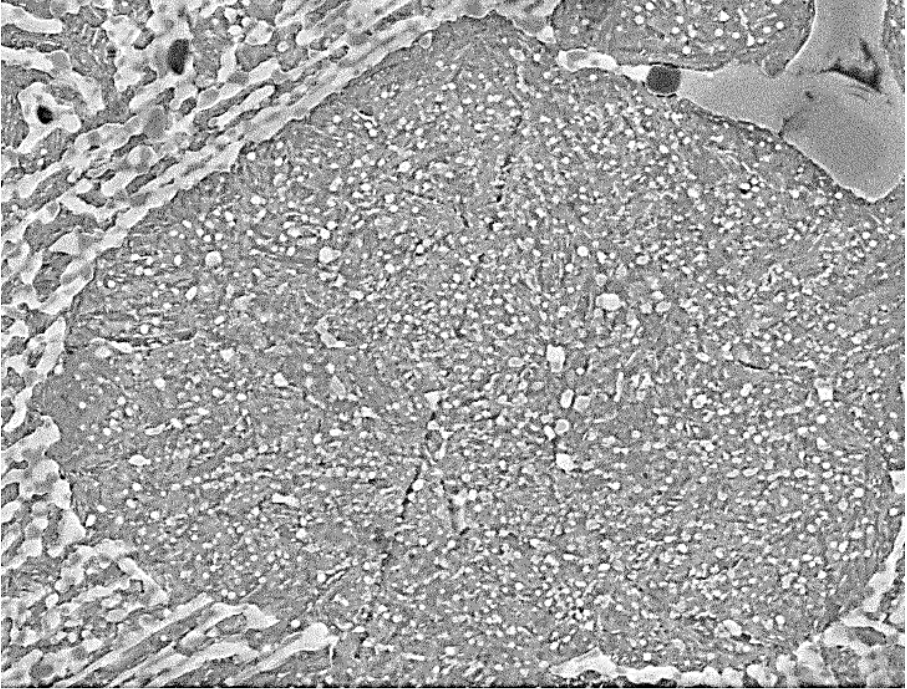
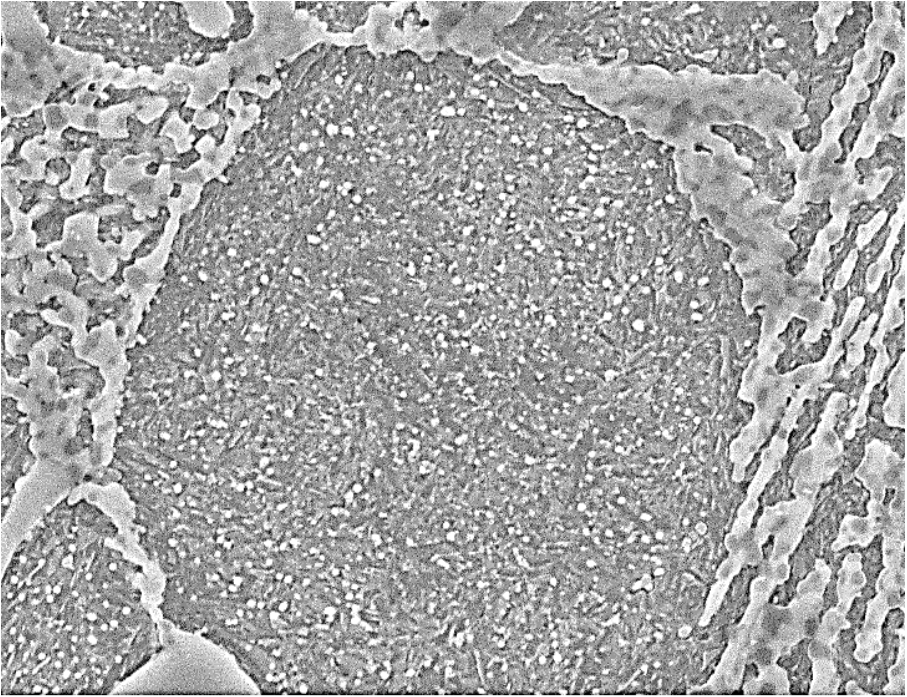
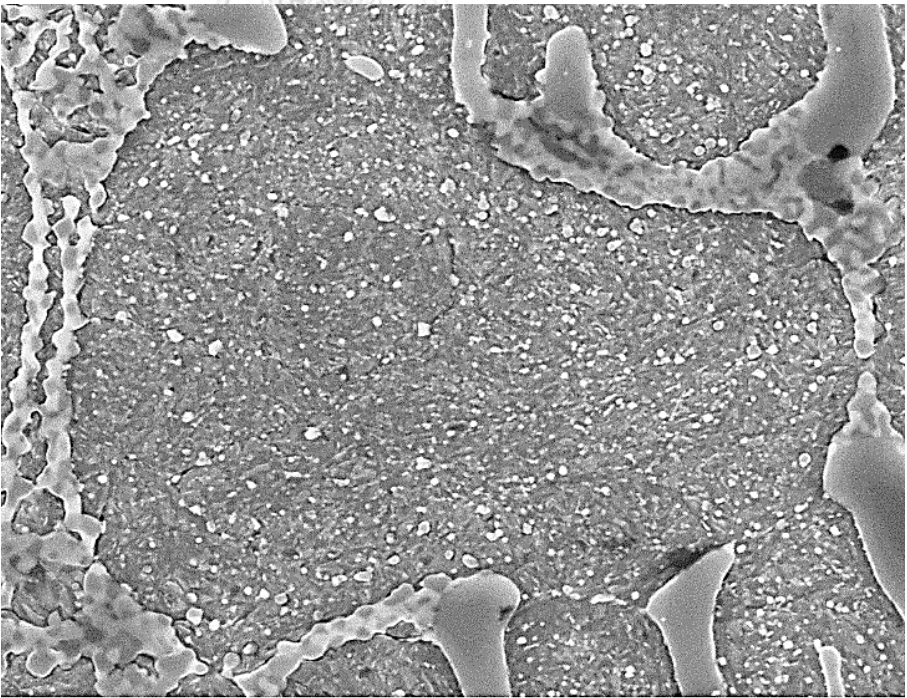


Fig.5-11 Relationship between maximum tempered hardness ($H_{T_{max}}$), volume fraction of retained austenite at $H_{T_{max}}$ ($V_{\gamma-HT_{max}}$) and Cr content.

From above results, it is convinced that the Cr affects the $H_{T_{max}}$ drastically. To demonstrate the variation of $H_{T_{max}}$, the specimens at $H_{T_{max}}$ were observed by SEM focusing on the matrix area and the microphotographs are representatively displayed in Fig.5-12 (a)-(e). The matrix microstructures of all specimens consist of secondary carbide, martensite and retained austenite. It is recognized that the size and the amount of secondary carbides vary depending on the Cr content of specimen, but it is difficult to distinguish the amount of retained austenite from SEM photographs. The difference in size and amount of secondary carbides can be distinguished among the specimens. The secondary carbides seem to increase in number as Cr content increases. However, it is found that the specimens with 7 and 9%Cr have coarse and less amount of secondary carbides compared with other specimens. It would be understood that Cr promotes the crystallization of eutectic carbides as well as the precipitation of secondary carbides in the matrix. At high Cr content, since more C is consumed to form M_7C_3 eutectic carbides, the C content in the matrix is reduced and resultantly, the formation of secondary carbides is decreased.

Specimen	Microstructure
No.1 (3.09%Cr)	 <p>15kV 6 μm</p>
No.2 (4.98%Cr)	 <p>15kV 6 μm</p>

Specimen	Microstructure
No.3 (5.99%Cr)	 <p>15kV 6 μm</p>
No.4 (7.01%Cr)	 <p>15kV 6 μm</p>

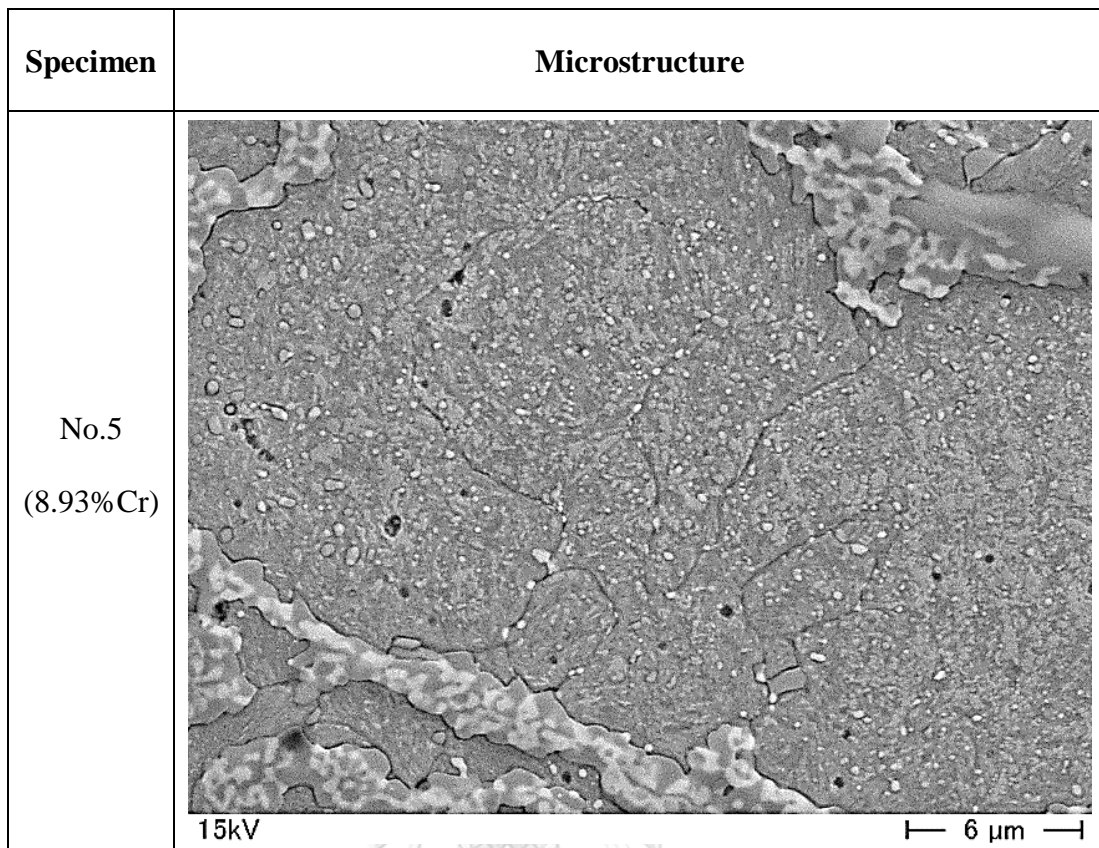


Fig.5-12 SEM microphotographs of specimens with H_{Tmax} . Austenitizing : 1323K.

5.1.2.2 Relationship between maximum tempered hardness (H_{Tmax}) and volume fraction of retained austenite (V_{γ})

From previous results, it is found that a certain amount of retained austenite existed in the H_{Tmax} specimen. It is well known that austenite has low hardness compared with other phases such as pearlite, martensite and secondary carbide and so, it reduces the matrix hardness. In order to clarify the effect of retained austenite on the maximum tempered hardness, the relation of H_{Tmax} vs $V_{\gamma-H_{Tmax}}$ was obtained and it is shown in Fig.5-13. The H_{Tmax} increases gradually until $V_{\gamma-H_{Tmax}}$ value of approximate 4% and after that, decreases as the $V_{\gamma-H_{Tmax}}$ rises. This tells that too much austenite left at H_{Tmax} reduces the hardness possibly. This result is suggesting that the $V_{\gamma-H_{Tmax}}$

value between 2.5 to 5% should be left in the matrix to get the H_{Tmax} value over 900 HV30 by tempering.

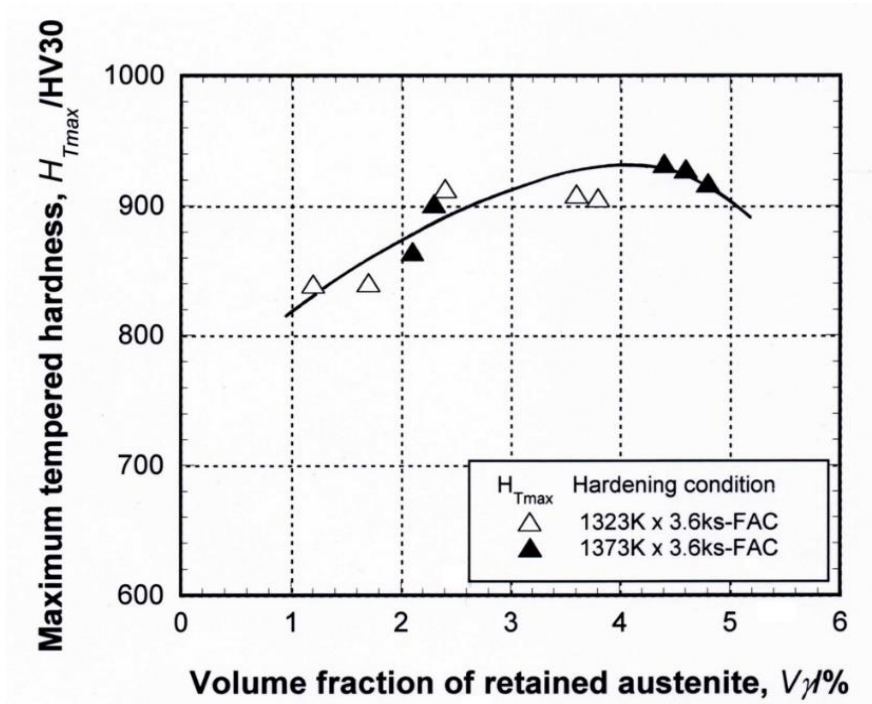


Fig.5-13 Relationship between maximum tempered hardness (H_{Tmax}) and volume fraction of retained austenite at H_{Tmax} ($V_{\gamma-H_{Tmax}}$).

Here, the V_γ in as-hardened state should be taken into account to obtain a target hardness in tempered state. The H_{Tmax} values are connected to the V_γ in as-hardened state and the relation is shown in Fig.5-14. When the austenite in as-hardened state increases, the H_{Tmax} increases proportionally as the V_γ in as-hardened state rises from 5 to 25%. This shows that the V_γ in as-hardened state contributes indirectly but additionally to the secondary hardening caused for the precipitation of secondary carbides and the transformation of austenite to martensite. Besides, it is understood that the V_γ value more than 17% in as-hardened state is necessary to get the H_{Tmax} over 900 HV30. However, the H_{Tmax} value must be lowered when the V_γ

value in as-hardened state is too much because the excessive retained austenite remains after tempering. In such a situation, the decrease in matrix hardness by V_γ is more effective than the increase in matrix hardness by the precipitation of carbides and the transformation of martensite.

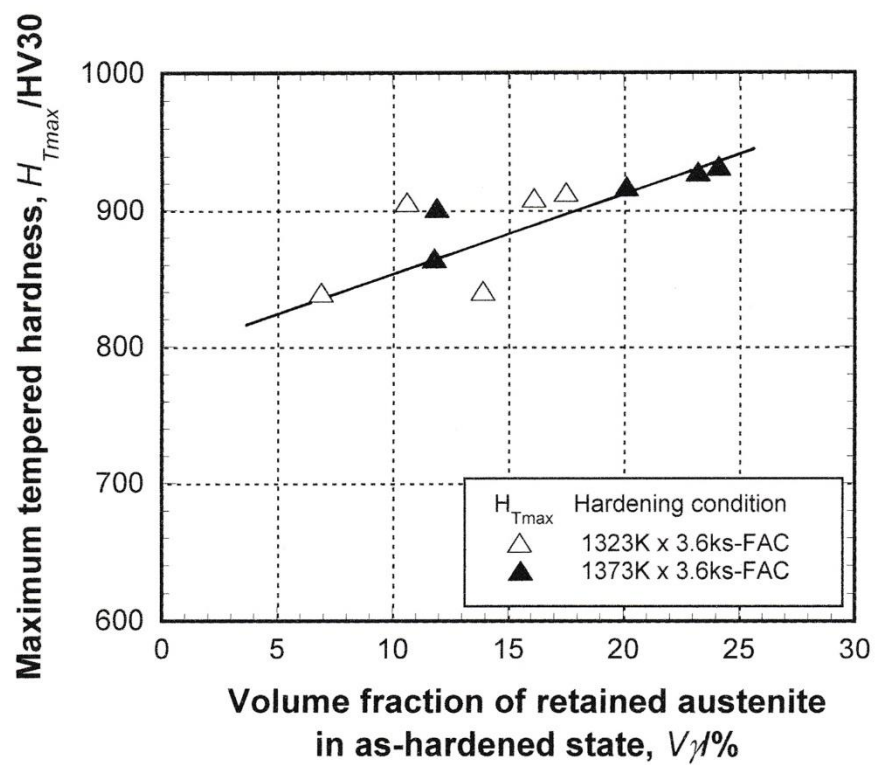


Fig.5-14 Relationship between maximum tempered hardness (H_{Tmax}) and volume fraction of retained austenite (V_γ) in as-hardened state.

5.1.3 Degree of secondary hardening (ΔH_s)

In the tempered hardness curve of each specimen displayed in Fig.4-5 to 4-9, the secondary hardening is recognized evidently. The secondary hardening occurred during tempering is explained by the following reactions;

- (1) Precipitation of secondary carbides from martensite or carbide reaction
- (2) Precipitation of carbides from austenite remained in matrix after hardening
- (3) Martensite formation that the retained austenite destabilized during tempering transforms to martensite by post cooling

Every reaction takes a certain part of an increase in hardness. However, the degree of the increase is considered to be covered by the reactions (1) and (3). From now, therefore, the details of the reactions (1) and (3) are discussed in the following.

To consider the mechanism of secondary hardening, the degree of secondary hardening (ΔH_s), of which parameter is defined as the difference in hardness between the maximum tempered hardness ($H_{T_{max}}$) and the hardness which begins to rise, was introduced. The ΔH_s values were calculated from all the macro-hardness curves in Fig.4-5 to 4-9 and they are summarized in Table 5-2. The ΔH_s values vary greatly depending on the Cr content in both austenitizing temperatures. It is clear that the ΔH_s is larger in the specimens hardened from higher austenitizing temperature of 1373K. In addition, the large ΔH_s value is obtained in the 5%Cr specimen and small ΔH_s value is in 3% and 9%Cr specimens irrespective of austenitizing temperature.

Table 5-2 Degree of secondary hardening (ΔH_s) of tempered specimens.

Specimen	Degree of secondary hardening (ΔH_s , HV30)	
	1323K austenitizing	1373K austenitizing
No.1 (3%Cr)	34.4	39.8
No.2 (5%Cr)	70.0	96.6
No.3 (6%Cr)	57.4	79.4
No.4 (7%Cr)	53.2	45.8
No.5 (9%Cr)	16.6	44.2

5.1.3.1 Effect of Cr content on degree of secondary hardening (ΔH_s)

From Table 5-2, it is considered that the Cr content of specimen affects the secondary hardening significantly. The effect of Cr content on the ΔH_s is shown in Fig.5-15. The ΔH_s value increases remarkably as the Cr content rises from 3 to 5% and over 5% it decreases in proportion to Cr content regardless of austenitizing temperatures. The largest ΔH_s values, 70 HV30 for 1323K and 97 HV30 for 1373K austenitizing, are obtained at 5%Cr. At the same Cr content, the ΔH_s of specimen hardened from 1373K is greater than that hardened from 1323K austenitizing. This proves that specimen hardened from high temperature provides greater ΔH_s value than that hardened from low temperature. In other words, the specimen with more austenite in as-hardened state gives more ΔH_s value.

From above results, it is certain that the secondary hardening occurs more or less depending on the kind and amount of precipitated secondary carbides accompanying with martensite transformed from residual austenite after tempering.

The ΔH_s increases up to 5%Cr because Cr improves in the hardenability and more retained austenite in as-hardened state is obtained to promote the precipitation of secondary carbides. Over 5%Cr, however, the ΔH_s decreases progressively due to a reduction of retained austenite obtained in as-hardened state and resultantly, precipitation of secondary carbides from retained austenite decreased. The former reason is proved by SEM microphotographs displayed in Fig.4-3 in section 4.2.1.1 and the latter reason is also proved by those illustrated in Fig.5-11.

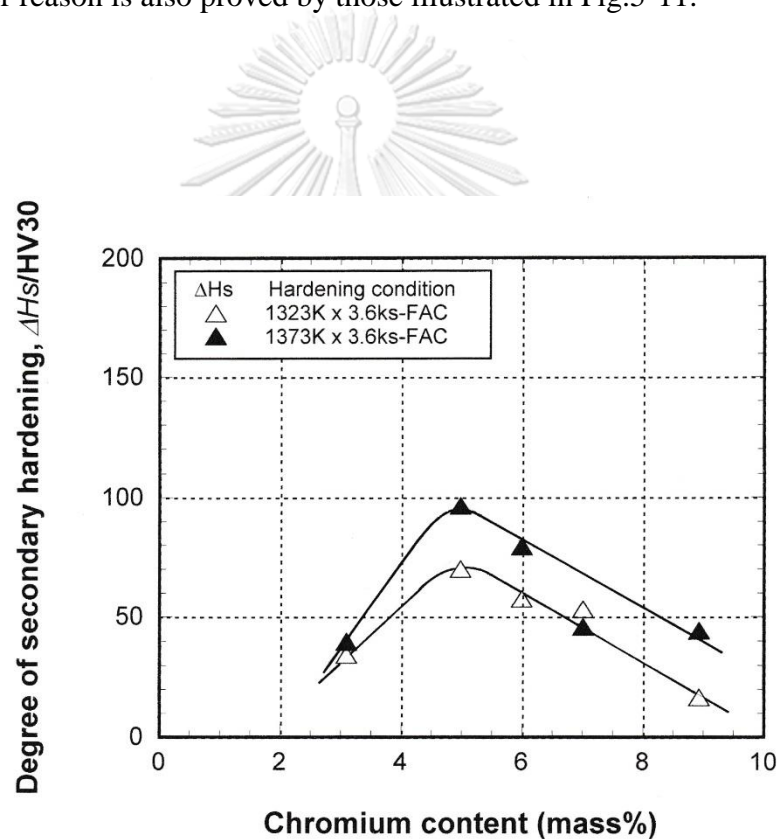


Fig.5-15 Relationship between degree of secondary hardening (ΔH_s) and Cr content.

5.1.3.2 Effect of volume fraction of retained austenite (V_γ) in as-hardened state on degree of secondary hardening (ΔH_s)

In the previous section, 5.1.4.1, it is found that the ΔH_s is closely related to the V_γ in as-hardened state. The relationship between ΔH_s and V_γ in as-hardened state is shown in Fig.5-16.

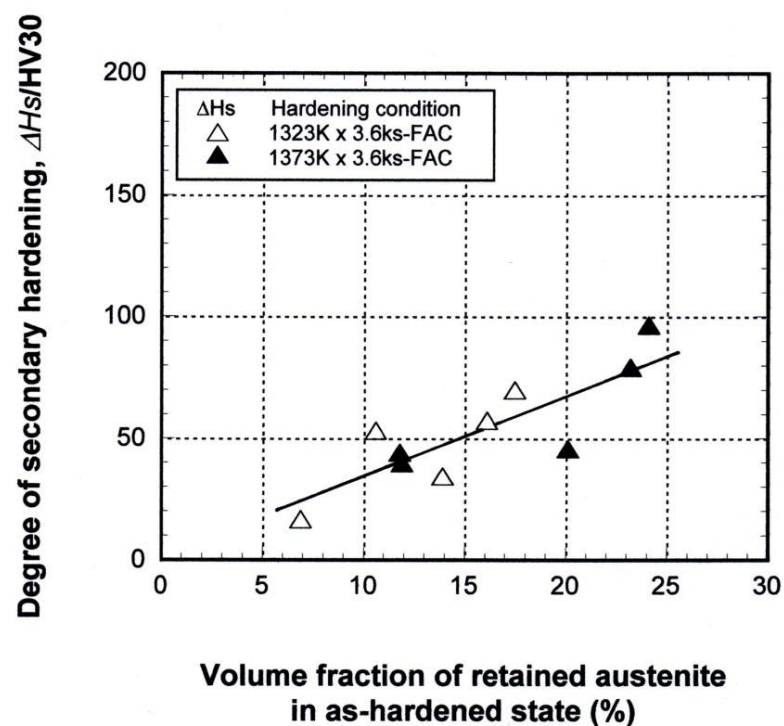


Fig.5-16 Relationship between degree of secondary hardening (ΔH_s) and volume fraction of retained austenite (V_γ) in as-hardened state.

In the range from 5 to 25% V_γ , the ΔH_s increases proportionally to the V_γ value in as-hardened state, regardless of austenitizing temperatures. The relation is expressed by the next equation;

$$\Delta H_s (HV30) = 4.1 * \%V_\gamma + 2.47 (R^2 = 0.68) \dots \dots \dots (5-5)$$

It is clear that the greater V_γ in as-hardened state provides the higher ΔH_s value.

It can be said that the difference between V_γ in as-hardened state and that at H_{Tmax} means the amount of austenite was consumed to provide the secondary hardening during tempering. To clarify how the retained austenite affects the secondary hardening, the relationship between ΔH_s and difference between V_γ in as-hardened state and that at H_{Tmax} ($\Delta V_{\gamma-HTmax}$) was obtained and it is shown in Fig.5-17.

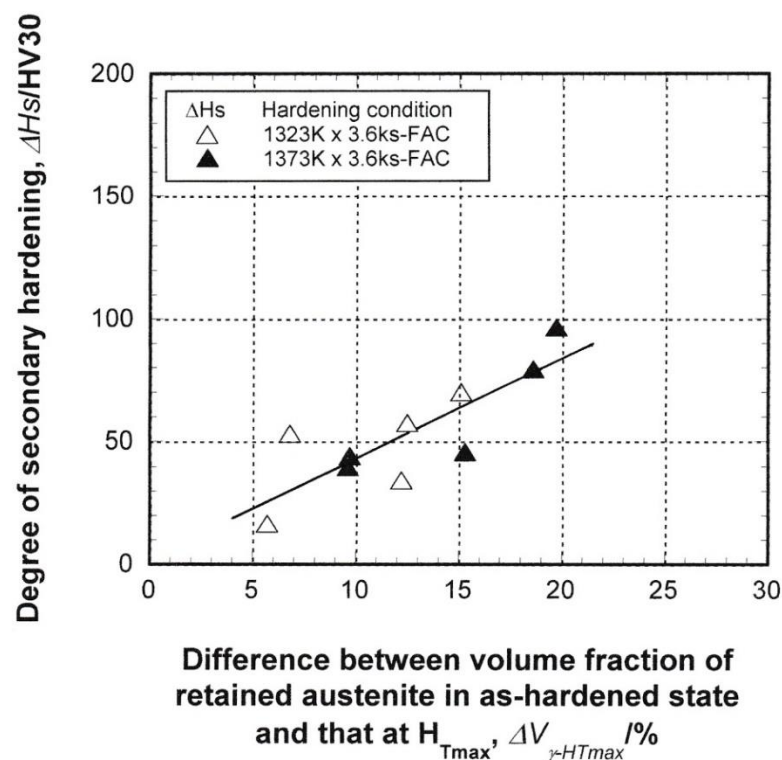


Fig.5-17 Relationship between degree of secondary hardening (ΔH_s) and difference between volume fraction of retained austenite in as-hardened state and that at H_{Tmax} ($\Delta V_{\gamma-HTmax}$).

The ΔH_s value increases in proportion to an increase in $\Delta V_{\gamma-HTmax}$ value, that is to say, the $\Delta V_{\gamma-HTmax}$ relates directly to the ΔH_s value in all of specimens irrespective of austenitizing temperatures. This suggests that relatively large amount of ΔV_γ must be needed to get a large degree of secondary hardening. Therefore, it can

be concluded that the decomposition of austenite during tempering determines the degree of secondary carbide. However, it must not be overlooked the kind and amount of constituents precipitated during tempering because they influence directly the matrix hardness.

5.1.3.3 Relationship between maximum tempered hardness (H_{Tmax}) and degree of secondary hardening (ΔH_s)

The relationship between H_{Tmax} and ΔH_s is shown Fig.5-18. The H_{Tmax} increases continuously with an increase in ΔH_s value. The result suggests that a large amount of ΔH_s provides high H_{Tmax} value. Generally, the multi-alloyed rolls used for hot rolling mill maintain the hardness of 800 to 880 HV30. When the target of hardness is laid down to 850 HV30, therefore, the ΔH_s value more than about 28 HV30 is necessary to get the H_{Tmax} over this value. In the case of pulverizing mill rolls, on the other side, the ΔH_s value more than approximate 50 HV30 is necessary to obtain the target H_{Tmax} over 900 HV30, the hardness is requested as high as possible. According to Fig.5-17, when the ΔH_s values are greater than 28 and 50 HV30, the $\Delta V_{\gamma-HTmax}$ values more than 6 and 12% are obtained, respectively. As mentioned in section 5.1.4.2, the $\Delta V_{\gamma-HTmax}$ is the difference between the V_{γ} in as-hardened state and that at H_{Tmax} . The V_{γ} values at H_{Tmax} are overall less than 5% as shown in Fig.5-11. Suppose that the $V_{\gamma-HTmax}$ is 5% in all the specimens, therefore, the V_{γ} value in as-hardened state must be needed over 11% for hot rolling mill and 17% for pulverizing mill rolls to get H_{Tmax} higher than 850 and 900 HV30 each by tempering. Both values are in close accordance with the V_{γ} values in as-hardened state shown in Fig.5-14. As for the pulverizing mill rolls, the high Cr cast irons are still used popularly. In the case

of high Cr cast iron, it is very difficult to get the hardness like 900 HV30 by heat treatment. So, it can be expected to promote the more use of this multi-alloyed white cast iron in future.

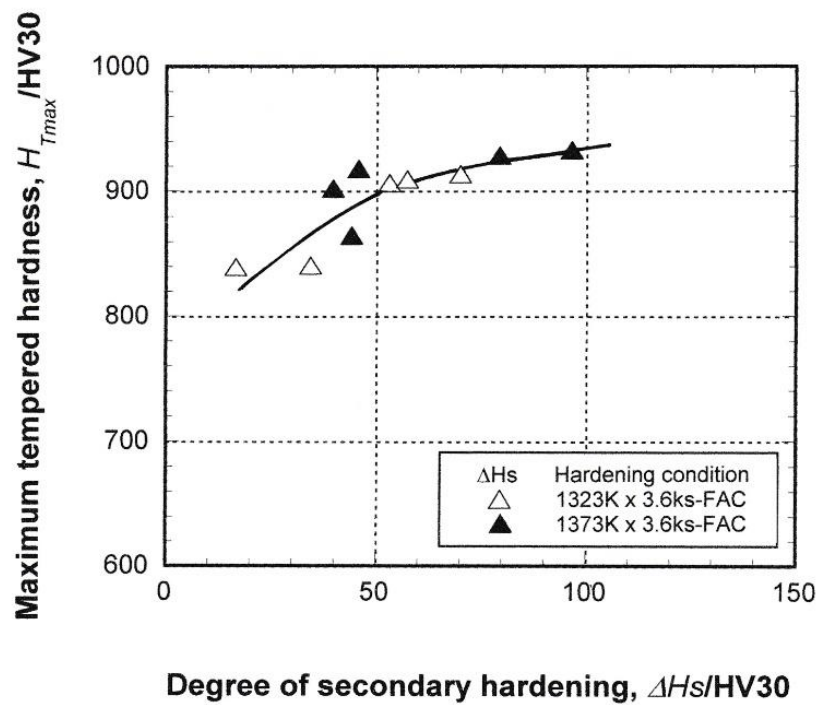


Fig.5-18 Relationship between maximum tempered hardness (H_{Tmax}) and degree of secondary hardening (ΔH_s).

5.2 Abrasive wear resistance

5.2.1 Severity of abrasive wear between Suga and rubber wheel abrasive wear tests

In Suga abrasive wear test, the abrasive material is SiC particles which is fixed on the emery paper by glue as shown in Fig.5-19. Under the test, the test piece is reciprocated in one stroke of 30 mm contacting with the abrasive wheel, and then, the wear distance for one cycle is 60 mm. The aluminum wheel, on which circumference is stuck by the emery paper with SiC particles, is rotated by 0.9 degrees/cycle to provide new surface of the abrasive paper. After 400 stokes, therefore, the total wear distance for one test is 24 m. The test was repeated for eight times using new abrasive wheel in the same test piece, and therefore, the total wear distance is 192 m and the total worn area is 2.304 m².

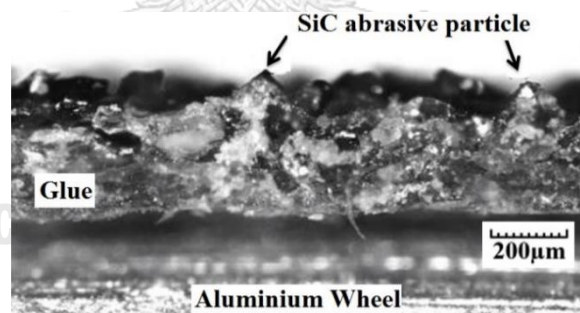


Fig.5-19 Cross-sectional structure of SiC abrasive paper fixed on aluminum wheel in Suga abrasive wear test [52].

In the rubber wheel abrasive wear test, the test piece is worn by silica sand particles (SiO₂) as shown in Fig.5-20. The sands are fed through the gap between the test piece and the rubber wheel which is rotating with 120 rpm. While testing, the silica particles move freely throughout the gap. The one test at 1000 revolutions of the

wheel per test is repeated for four times in the same worn area of test piece. Therefore, the total wear distance is 3,142 m and the total worn area is 47.12 m².

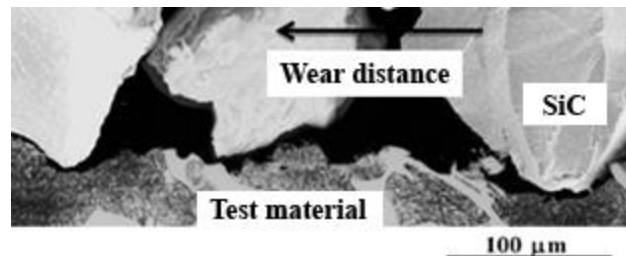


Fig.5-20 Schematic explanation of wear mechanism by rubber wheel abrasive wear test [52].

In order to clarify the severity of abrasive wear, the results of 5%Cr specimen hardening from 1373K austenitizing was selected for discussion. The results of the calculation of total wear loss per unit area and the ratio between Suga and rubber wheel abrasive wear tests are summarized in Table 5-3. In each heat treatment condition, the total wear loss of Suga abrasive wear test is much higher than that of rubber wheel abrasive wear test. It is found that the wear condition of Suga abrasive wear test is 3.5 time on average as severe as that of rubber wheel abrasive wear test. This result agrees with the work in reference [53].

Table 5-3 Wear loss per unit area of 5%Cr specimen with different heat treatment condition (Hardening : 1373K austenitizing).

Heat treatment condition	Wear loss per unit area (mg/m ²) (Total wear loss/Total worn area)		Ratio of tests (Suga/Rubber wheel)
	Suga abrasive wear test	Rubber wheel abrasive wear test	
As-H	19.4	5.2	3.7
L-H _{Tmax}	20.9	6.5	3.2
H _{Tmax}	20.3	5.6	3.6
H-H _{Tmax}	22.8	6.6	3.4
Average			3.5

5.2.2 Effect of Cr content on wear rate (R_w)

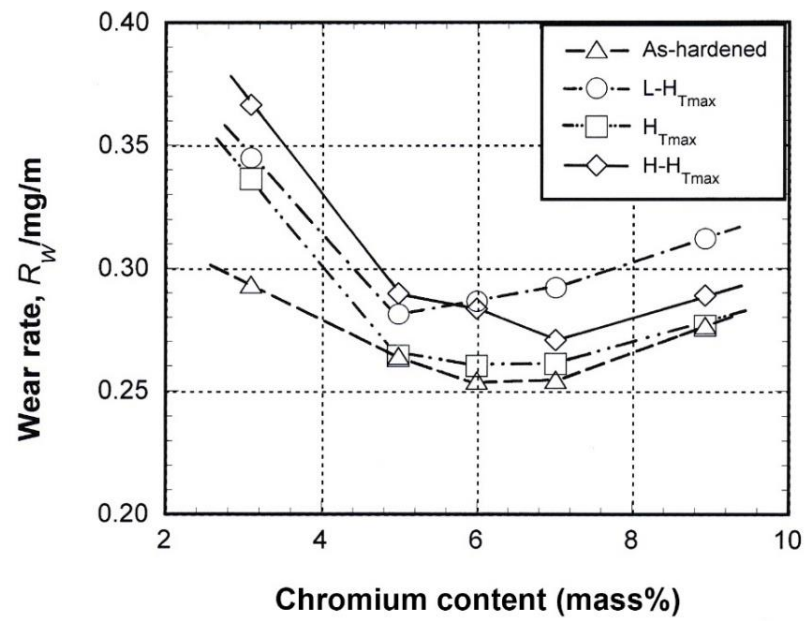
The wear resistance of alloyed white cast iron is related not only to the types and amounts of eutectic carbides but also to the matrix structure. It is known that the matrix offers a role to support the eutectic and secondary carbides, and it affects both of carbides to resist the wear by abrasive particles. On the other hand, if the matrix hardness is low and the matrix is preferentially worn by abrasive particles, not only eutectic but also secondary carbides may be worn out by spalling. Therefore, the wear resistance in other words, the strength, of the matrix is also very important barometer to the wear resistance of the materials.

From the experimental results shown in 4.2.2, it was clear that the Cr affected the matrix micro-structure, say, hardness and volume fraction of retained austenite (V_γ). Therefore, it is considered that the Cr is significant element to affect the wear behavior. As mentioned in section 4.3.1, the R_w is represented by the slope of straight line of relationship between wear loss and wear distance. The relationship between Cr

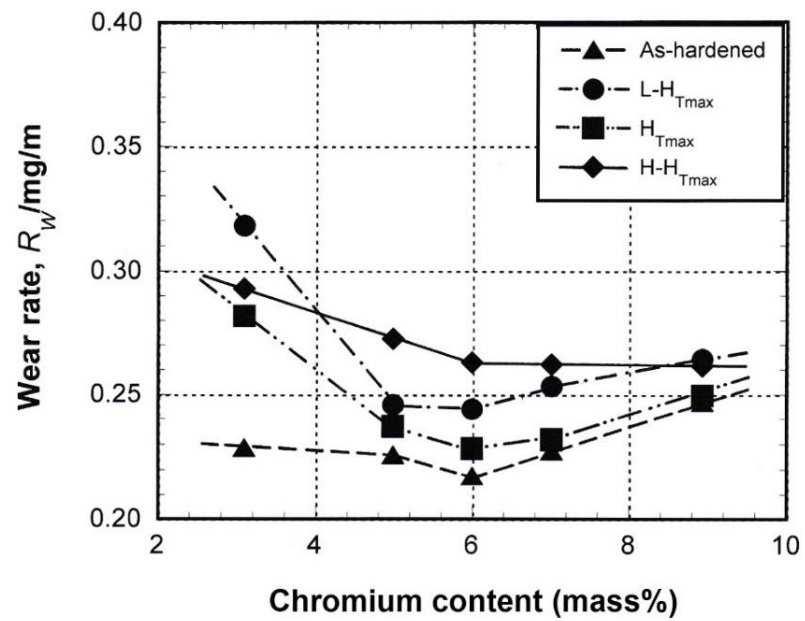
content and R_w of specimen is shown in Fig.5-21 for Suga abrasive wear test and Fig.5-22 for rubber wheel abrasive wear test, respectively.

As for Suga (two-body-type) abrasive wear test in Fig.5-21, the R_w values decrease with an increase in Cr content until 6%Cr, regardless of hardening and tempering conditions. Over 6%Cr, by contrast, the R_w increases gradually. This means that the wear resistance increases with an increasing the Cr content up to 6%. The reason can be explained by the fact that the Cr improves the hardenability and lowers the M_s temperature until 5~6%Cr [50]. As the M_s temperature lowers, the amount of retained austenite (V_γ) in the as-hardened state increases. The increasing of V_γ in as-hardened state contributes more to the precipitation of secondary carbides, i.e., more secondary hardening in the tempered state is obtained. Simultaneously, an increase in the V_γ in as-hardened state could promote more transformation of martensite from residual austenite after tempering.

When the Cr content gets over 6%, on the contrary, the opposite trend appears for R_w , i.e., the R_w values rise gradually with an increase in Cr content. This reason could be due to a reduction of hardness. An increase in Cr content promotes the crystallization of eutectic M_7C_3 and precipitation of secondary $M_{23}C_6$ carbides with lower hardness than those of MC , M_2C and M_6C carbides. In addition, the retained austenite in the as-hardened state decreases because the M_s temperature rises with an increase in the Cr content over 6% [50]. Consequently, the ratio of secondary hardening is low during tempering. The R_w showed almost the same tendency in both austenitizing temperatures. However, the R_w values of specimens hardened from high



(a) 1323K austenitizing



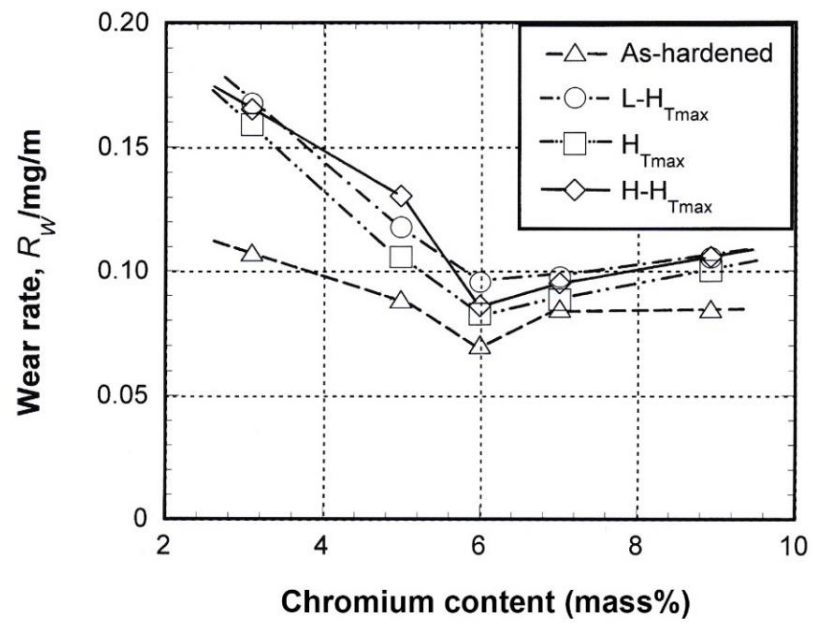
(b) 1373K austenitizing

Fig.5-21 Relationship between wear rate (R_w) and Cr content of specimens by Suga abrasive wear test. Load : 9.8N (1 kgf).

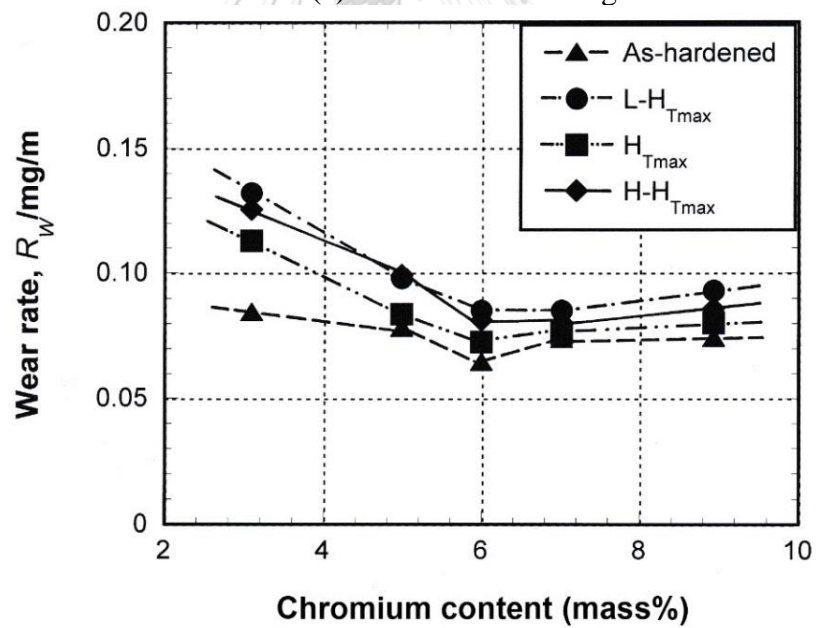
austenitizing temperature of 1373K are located at the lower site than those hardened from low austenitizing temperature of 1323K. It can be understood that the hardening from high austenitizing temperature produced greater retained austenite in as-hardened state and it promoted the secondary hardening in the tempered state. Therefore, the higher hardness decreased the R_w values.

In the case of rubber wheel abrasive wear test, as shown in Fig.5-22, the R_w values show similar behavior to those of Suga abrasive wear test. The R_w decreases gradually until Cr content reaches 6%, and after that, it increases slightly with a rise of Cr content. In addition, specimens hardened from high austenitizing temperature of 1373K show smaller R_w values than those hardened from low austenitizing temperature of 1323K. By comparing with the Suga abrasive wear test, it is clear that the R_w values in rubber wheel abrasive wear test are much lower. The reason why the R_w values in rubber wheel (three-body-type) abrasive wear test are less than those in Suga (two-body-type) abrasive wear test can be explained as follows.

The stress concentration on the worn surface in this test is quite low because the abrasive material of SiO_2 particles are moving freely throughout the surface of test pieces. Besides, the hardness of silica with about 1100 HV is lower than that of eutectic M_7C_3 carbide (1500-1800 HV). Therefore, the matrix with lower hardness is worn by silica preferentially. From these viewpoints, the matrix hardness affected the R_w greatly in this three-body type abrasive wear test.



(a) 1323K austenitizing



(b) 1373K austenitizing

Fig.5-22 Relationship between wear rate (R_w) and Cr content of specimens by rubber wheel abrasive wear test. Load : 85.3N (8.7 kgf).

It is found that the lowest R_w or the highest wear resistance is obtained in 6%Cr specimen in both kinds of abrasive wear tests. As for the hardness, the macro-hardness in as-hardened and tempered states are highest at 5 to 6%Cr (section 4.2.2), and so, this should give the lowest R_w or largest wear resistance. However, the test results showed the lowest R_w or the highest wear resistance at 6%Cr specimen. It could be because M_7C_3 eutectic carbide, which is tougher and had more resistance to the abrasive wear due to the interconnected morphology, coexists in the specimen with 6%Cr. When the micro-hardness of test pieces with each heat treatment are taken notice of, on the other hand, the matrix hardness are overall highest in 6%Cr specimen (Table 5-4) and this also makes the R_w value lower and the wear resistance increase.

The reason why the R_w values increase with an increase in the Cr content over 6%, on the contrary, is due to more increase in M_7C_3 eutectic carbide with low hardness and resultant decrease in the wear resistance.

When focusing on the effect of heat treatment condition on the wear behavior, the As-H specimen shows better wear resistance than tempered specimens in both the Suga and rubber wheel abrasive wear tests. This must be due to the difference in the matrix structure of specimen. The phases existing in the matrix are quite different between as-hardened and tempered states. In the as-hardened specimen, the matrix consists of secondary carbides precipitated during austenitizing, high carbon martensite produced by quenching and austenite remained without transformation. In the tempered state, on the other hand, the matrix of H_{Tmax} specimen has very fine tempered martensite, secondary carbides and some residual austenite. The H- H_{Tmax} specimens have coarse carbides caused by tempering of martensite and cohesion of

secondary carbides and very less residual austenite. By contrast, the L-H_{Tmax} specimens have secondary carbides, tempered martensite and more retained austenite compared with H-H_{Tmax} specimens.

The matrix hardness of all the specimens are listed in Table 5-4. In each Cr specimens, the highest matrix hardness is on the whole obtained in As-H specimen and followed by H_{Tmax} specimen. The lowest matrix hardness is obtained in L-H_{Tmax} or H-H_{Tmax} specimen. Therefore, it is not surprising that the R_w of As-H specimen with higher matrix hardness was lower than those in tempered specimens in each Cr content. In the tempered state, it is reasonable that the H_{Tmax} specimens show the lowest R_w value or highest wear resistance, followed by H-H_{Tmax} and L-H_{Tmax} specimens. It is noted that the difference in matrix structure between them determined the difference in matrix hardness and finally the difference of abrasive wear resistance. The matrix with higher hardness can fix the eutectic carbides sufficiently even under high abrasive load and resultantly, the wear resistance is improved.

Table 5-4 Micro-hardness of matrix in heat-treated specimens used for abrasive wear test.

Specimen	Micro-hardness (HV0.1)							
	1323K austenitizing				1373K austenitizing			
	As-H	L-H _{Tmax}	H _{Tmax}	H-H _{Tmax}	As-H	L-H _{Tmax}	H _{Tmax}	H-H _{Tmax}
No.1 (3%Cr)	801	722	756	722	841	765	811	765
No.2 (5%Cr)	862	792	831	774	851	801	862	811
No.3 (6%Cr)	851	811	831	801	842	801	872	811
No.4 (7%Cr)	851	792	811	783	841	801	831	821
No.5 (9%Cr)	841	774	801	774	823	774	821	783

5.2.3 Effect of macro-hardness on wear rate (R_w)

It is well known that the hardness determines mostly the wear resistance. Generally, the wear resistance is high in the white cast irons with high hardness compared with steel. There is correlation among the hardness, the type and amount of eutectic and matrix microstructure. Since the R_w varied depending on the heat treatment condition and Cr content as shown in the previous section, the wear resistance must as well be directly connected to the hardness of heat-treated test pieces.

The relationship between R_w and macro-hardness is shown in Fig.5-23 for Suga abrasive wear test and Fig.5-24 for rubber wheel abrasive wear test, respectively.

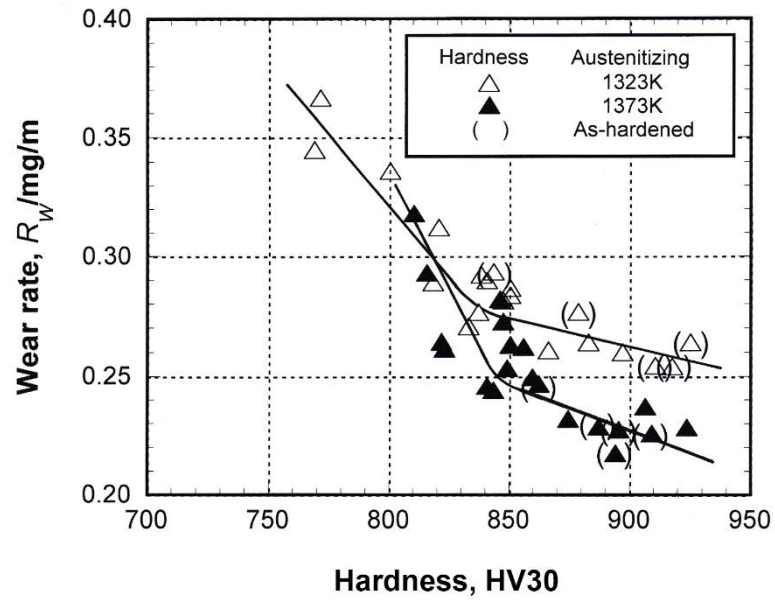


Fig.5-23 Relationship between wear rate (R_w) and macro-hardness of specimens for Suga abrasive wear test.

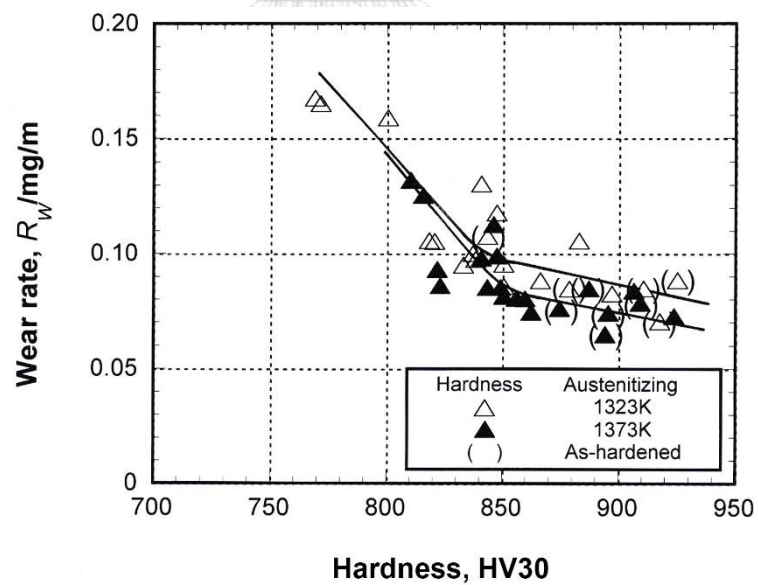


Fig.5-24 Relationship between wear rate (R_w) and macro-hardness of specimens for rubber wheel abrasive wear test.

The test pieces with low hardness are almost in tempered state but those with high hardness are in as-hardened state. Overall, the R_w decreases as the macro-hardness increases. It is found in both of abrasive wear tests that the R_w shows two slopes regardless of austenitizing temperature. The R_w value decreases steeply until the hardness goes up to 840 HV30 in the case of hardening from 1323K and 850 HV30 in the case of hardening from 1373K austenitizing, respectively. At over the hardness, the R_w decreases gradually in the Suga abrasive wear test and decreases slightly in the rubber wheel abrasive wear test. The relations by Suga abrasive wear test are expressed by the next equations,

For 1323K austenitizing,

$$R_w \text{ (mg/m)} = -(12 \times 10^{-4}) \times (\text{HV30}) + 1.245 \text{ (below 840 HV30)}$$

$$R_w \text{ (mg/m)} = -(4 \times 10^{-4}) \times (\text{HV30}) + 0.626 \text{ (over 840 HV30)}$$

For 1373K austenitizing,

$$R_w \text{ (mg/m)} = -(10 \times 10^{-4}) \times (\text{HV30}) + 1.112 \text{ (below 850 HV30)}$$

$$R_w \text{ (mg/m)} = -(5 \times 10^{-4}) \times (\text{HV30}) + 0.677 \text{ (over 850 HV30)}$$

The same relations of by rubber wheel abrasive wear test are as follows,

For 1323K austenitizing,

$$R_w \text{ (mg/m)} = -(11 \times 10^{-4}) \times (\text{HV30}) + 1.026 \text{ (below 840 HV30)}$$

$$R_w \text{ (mg/m)} = -(4 \times 10^{-4}) \times (\text{HV30}) + 0.428 \text{ (over 840 HV30)}$$

For 1373K austenitizing,

$$R_w \text{ (mg/m)} = -(7 \times 10^{-4}) \times (\text{HV30}) + 0.644 \text{ (below 850 HV30)}$$

$$R_w \text{ (mg/m)} = -(0.6 \times 10^{-4}) \times (\text{HV30}) + 0.133 \text{ (over 850 HV30)}$$

Steep decreasing of R_w values in the former stage is mostly due to the decreasing in the hardness. The hardness of tempered specimen rises because of matrix transformation, i.e., precipitation of special secondary carbides with high hardness from martensite and retained austenite together with simultaneous reduction of residual austenite. In the latter state, on the other side, an increase in hardness gives smaller effect on the R_w . In these test pieces, it is possible that work-hardening of retained austenite could take place and it made the macro-hardness rise. As mentioned earlier, the specimens with high hardness are mainly As-H specimens. In the as-hardened state, the retained austenite is stabilized by saturating with alloying elements., and therefore, the work hardening of retained austenite should be hard to occur. With respect to wear behavior, an increase in the retained austenite tends to promote the pitting and scratching wear on the matrix and too high hardness caused by work-hardening can make the matrix brittle to pose the risk of spalling wear additionally. According to these reasons, the R_w decreases slowly even if the hardness is increased. It is found that the higher austenitizing temperature provides a lower R_w value, because the higher austenitizing temperature gives the higher matrix hardness by tempering.

5.2.4 Relationship between wear rate (R_w) and volume fraction of retained austenite (V_γ) in heat-treated state

From the previous section, it became clear that the wear rate (R_w) is influenced by not only the macro-hardness but also the state of matrix or matrix structure. It is well known that retained austenite has high toughness and it can be work-hardened by strain induced martensite transformation. Therefore, the volume fraction of retained austenite (V_γ) should affect the R_w as well. In this section, the effect of V_γ on the R_w is clarified. The relationship between V_γ and R_w of specimens is shown in Fig.5-25 for Suga abrasive wear test and Fig.5-26 for rubber wheel abrasive wear test, respectively.

In the Suga test, the R_w is separated into two groups at 5% V_γ . In the V_γ values less than 5%, the R_w values spread in wide range from 0.23 to 0.37 mg/m. In other words, it seems that even the small difference in the amount of retained austenite influences the R_w . However, this scattering of R_w values is considered to be the other reason, except for the retained austenite, that is, the difference in matrix structure. Since the phases in the matrix microstructure cannot be analyzed quantitatively, the other main factor can be the matrix hardness. The relationship between R_w and macro-hardness of specimens with V_γ less than 5% is obtained and it is displayed in Fig.5-27. It is clear that the R_w varies depending on the hardness and that the R_w decreases with an increase in the hardness. It can be said that the hardness is main factor to decrease the R_w value or to increase the abrasive wear resistance when the V_γ values of test pieces less than 5%.

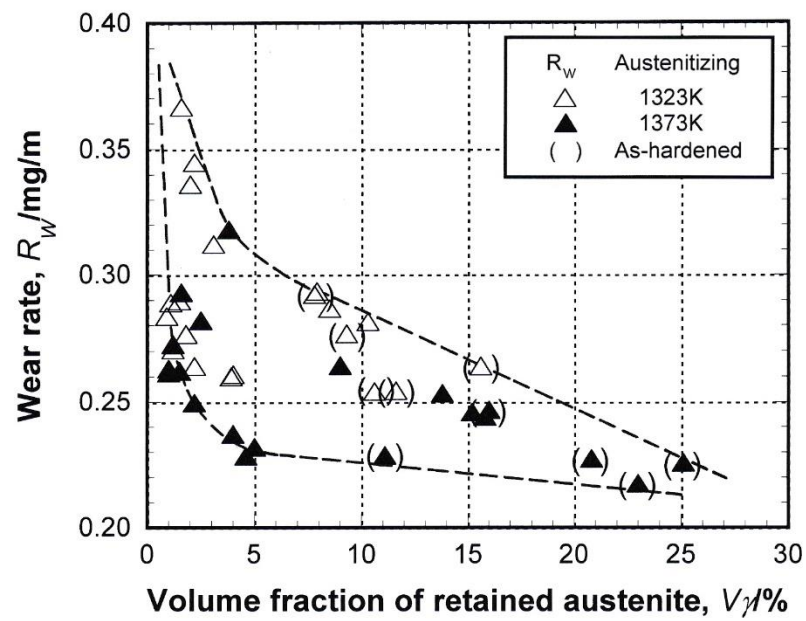


Fig.5-25 Relationship between wear rate (R_w) and volume fraction of retained austenite (V_γ) of all the specimens (Suga abrasive wear test).

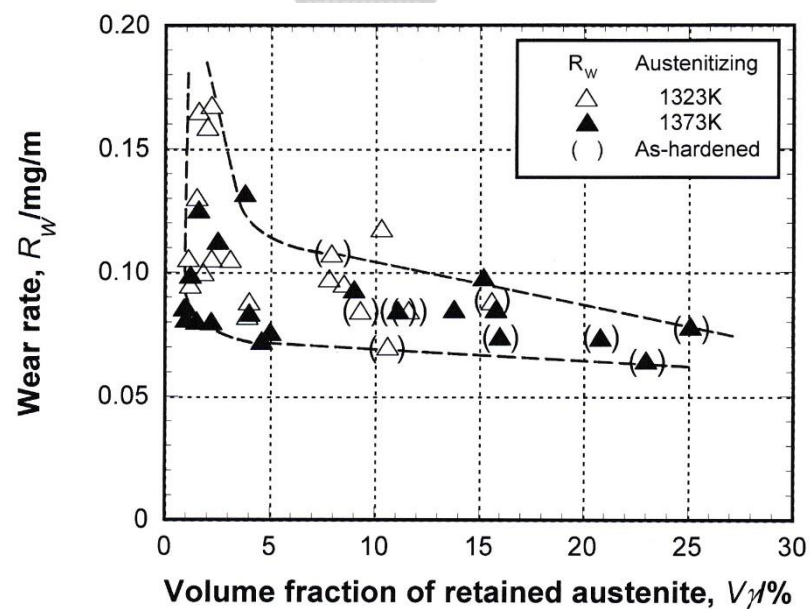


Fig.5-26 Relationship between wear rate (R_w) and volume fraction of retained austenite (V_γ) of all the specimens (Rubber wheel abrasive wear test).

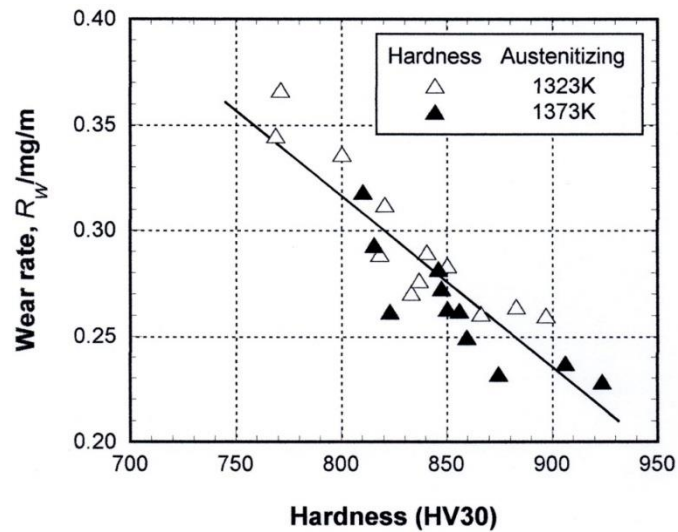


Fig.5-27 Relationship between wear rate (R_w) and macro-hardness of specimens with volume fraction of retained austenite (V_γ) less than 5% (Suga abrasive wear test).

In the V_γ values more than 5%, the R_w values decreases progressively as the V_γ value increases. The reason could be due to the greater load or stress applying the wearing surface in Suga abrasive wear test. In this region, the increase in R_w value by increasing of retained austenite in the matrix is compensated by the decrease in R_w value due to an increase of work hardening involving martensite transformation. From this result, it can be concluded that the work hardening in this wear test is sufficient to increase the wear resistance.

As shown in Fig.5-26 for rubber wheel abrasive wear test, the relation of R_w vs. V_γ shows similar behavior to that of the Suga abrasive wear test, that is, it is separated into two groups at 5% V_γ . In the range less than 5% V_γ , the R_w values cover wide range from 0.07 to 0.17 mg/m. The reason for the widely spreading of R_w can be considered because of the difference in hardness as same manner as Suga abrasive

wear test. As shown in Fig.5-28, it is evident that the R_w lowers with an increase in hardness of specimen. It can be concluded that in the specimens with such low V_γ values less than 5%, the wear resistance varies depending on the matrix hardness which is controlled by microstructure, the higher hardness promotes the larger wear resistance.

In the specimens with V_γ more than 5%, however, the R_w decreases very slightly as the V_γ value rises. This reason should be a small degree of work-hardening compared with Suga abrasive wear test. However, such work-hardening is enough to compensate the decrease in hardness due to the increasing of V_γ . As a result, the R_w decreases a little even if the V_γ value rises over 5%. Within these austenite levels in the specimens, the compensation effects on the matrix hardness between a decrease by an increase in V_γ and an increase by work-hardening must not be so large. If the retained austenite is contained much more than in the specimens for this experiment, the hardness should decrease and the R_w value must rise.

With respect to the effect of austenitizing temperature, it is found that the R_w values of specimens hardened from 1373K austenitizing are lower than those hardened from 1323K austenitizing. It can be explained that the matrix of specimen hardened from high austenitizing temperature contains more concentration of C and other alloying elements and such a condition improves the hardenability and promotes the precipitation of secondary carbides. At the same V_γ value, therefore, the higher matrix hardness is obtained and then, the R_w is lowered or the wear resistance is increased.

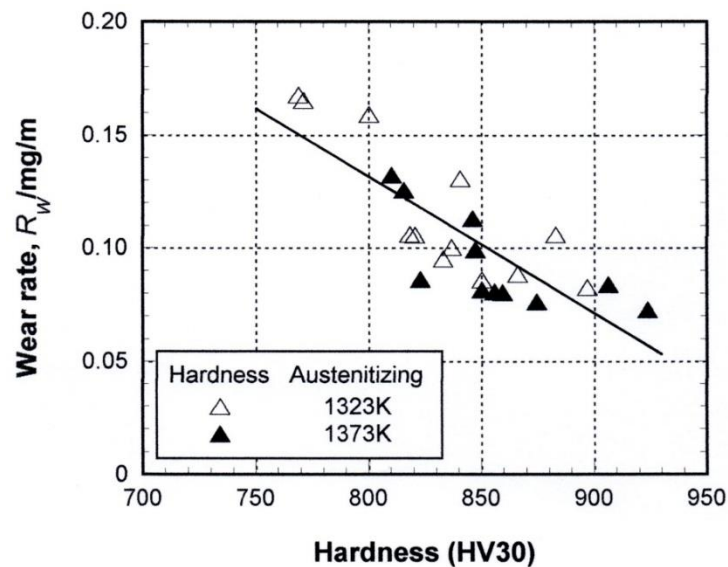


Fig.5-28 Relationship between wear rate (R_w) and macro-hardness of specimens with volume fraction of retained austenite (V_γ) less than 5% (Rubber wheel abrasive wear test).

From the results mentioned above, it is found that the highest wear resistance or low R_w value is obtained in As-H specimens irrespective of Cr content and austenitizing temperatures. Here, the effect of V_γ on R_w in the as-hardened state is discussed in detail. The relationship between R_w and V_γ of all the As-H specimens is shown in Fig.5-29 for the Suga abrasive wear test and Fig.5-30 for the rubber wheel abrasive wear test, respectively. In both wear tests, the R_w drops abruptly in a small region to $12\%V_\gamma$ and decreases very little until $25\%V_\gamma$. In the range of less than $12\%V_\gamma$, the R_w is greatly influenced by the matrix hardness. The higher matrix hardness gives the lower R_w value. When the V_γ gets over 12% , however, the decreasing rate of R_w corresponding to an increase in V_γ becomes very low. This suggests that the work-hardening by strain induced martensite transformation

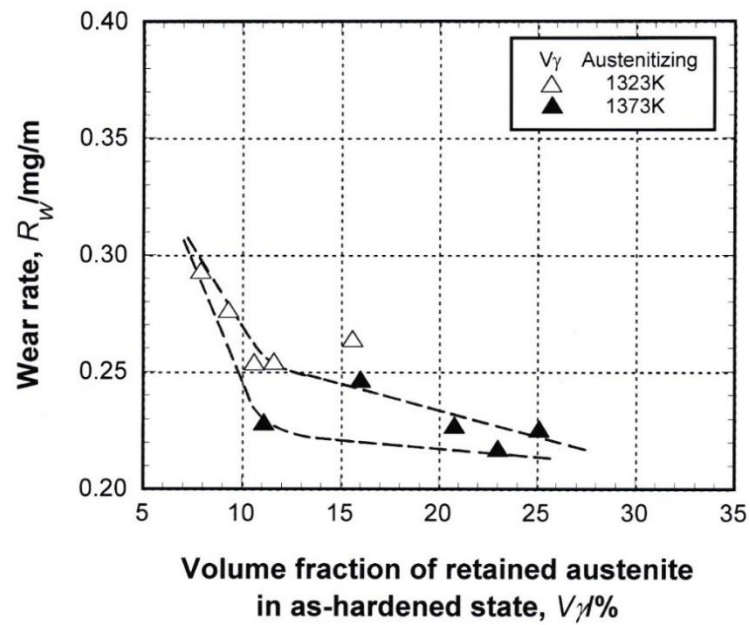


Fig.5-29 Relationship between wear rate (R_w) and volume fraction of retained austenite (V_γ) in as-hardened state (Suga abrasive wear test).

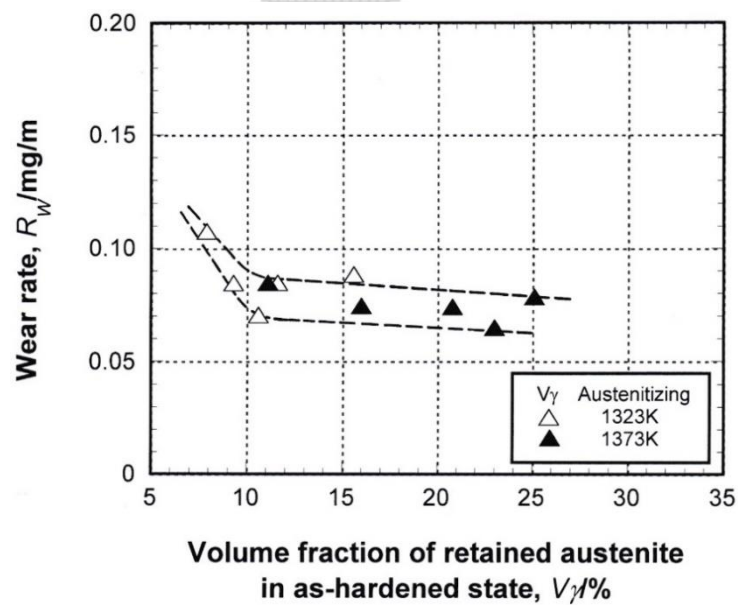


Fig.5-30 Relationship between wear rate (R_w) and volume fraction of retained austenite (V_γ) in as-hardened state (Rubber wheel abrasive wear test).

decreases because the retained austenite is getting more stability as the saturation of alloying elements increases in the as-hardened state. Also, a large amount of V_γ could lower the matrix hardness. In both wear tests, the lowest R_w value is obtained at 11% V_γ in 1323K and 23% V_γ in 1373K austenitizing, respectively.

From the viewpoint of results obtained until now, it may be thought that this kind of multi-alloyed white cast iron can be used in as-hardened state for the practical rolls and the parts or components. The answer is No because there is a large risk that under servicing a large amount of retained austenite transforms into martensite involving a great deal of expansion and it may cause to cracking or destructing of the products. Therefore, the cast irons have to be tempered in order to reduce austenite. In the tempered state, the H_{Tmax} specimen shows the highest wear resistance regardless of Cr content and hardening temperature of specimens. When focusing on the microstructure of H_{Tmax} specimen, the matrix structure composes of secondary carbides, fine martensite and retained austenite less than 5%. Here, the relationship between R_w and V_γ value of specimen at H_{Tmax} ($V_{\gamma-H_{Tmax}}$) is obtained and it is illustrated in Fig.5-31 for Suga abrasive wear test and Fig.5-32 for rubber wheel abrasive wear tests, respectively.

In Suga abrasive wear test, the R_w drops suddenly as the V_γ increases to 2.5%. After that, it decreases continuously as the V_γ value increases. In the rubber wheel abrasive wear test, on the other side, the similar behavior for R_w is observed. The R_w value gets down to 2.5% V_γ and after that, it keeps constant value even when the V_γ value increases. In the range of very less V_γ , the R_w is determined by hardness of specimen as mentioned before. However, it seems that the 2.5-5% V_γ has some effect on the R_w . The reasons can be explained as followed,

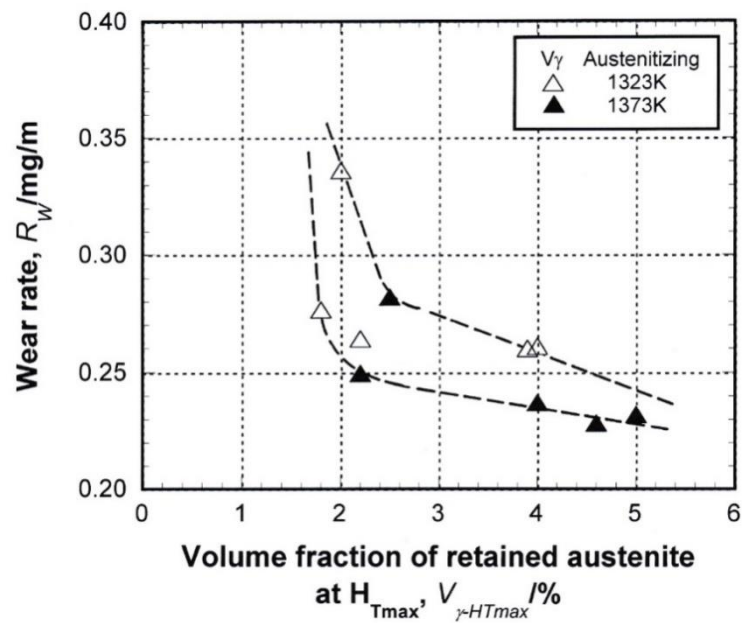


Fig.5-31 Relationship between wear rate (R_w) and volume fraction of retained austenite at H_{Tmax} ($V_{\gamma-HTmax}$) (Suga abrasive wear test).

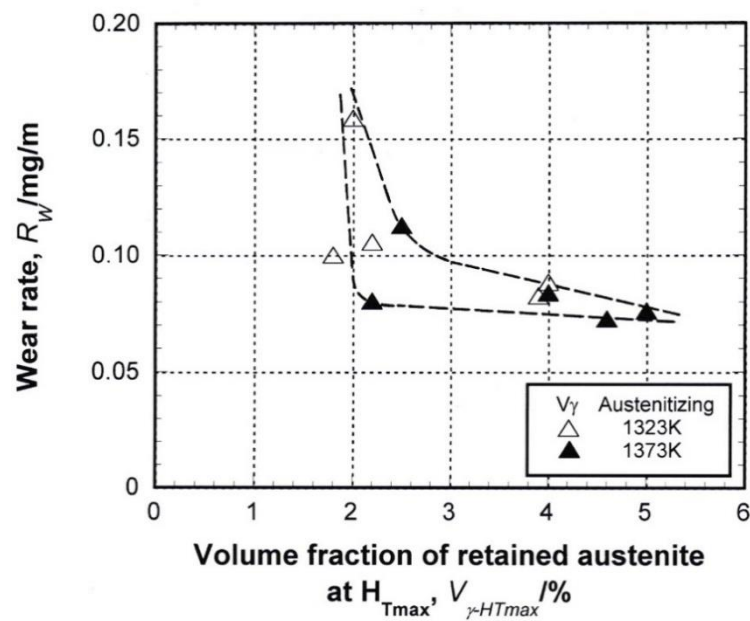
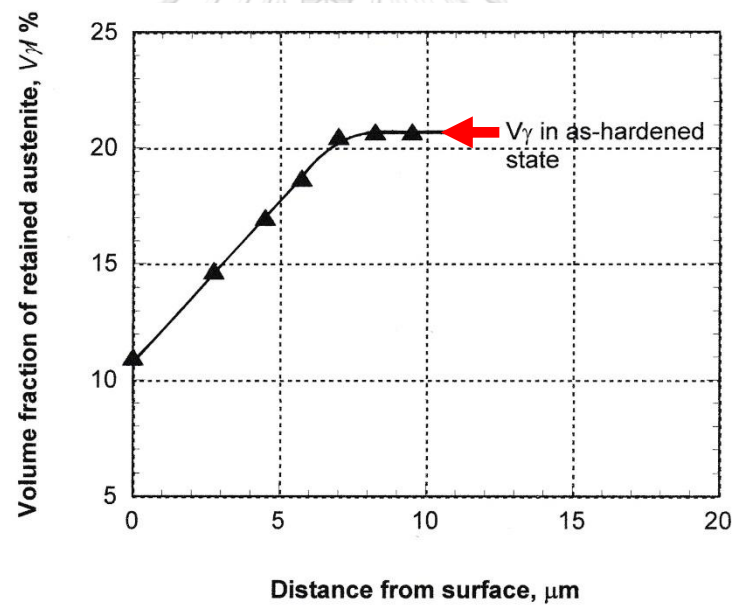
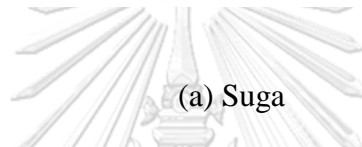
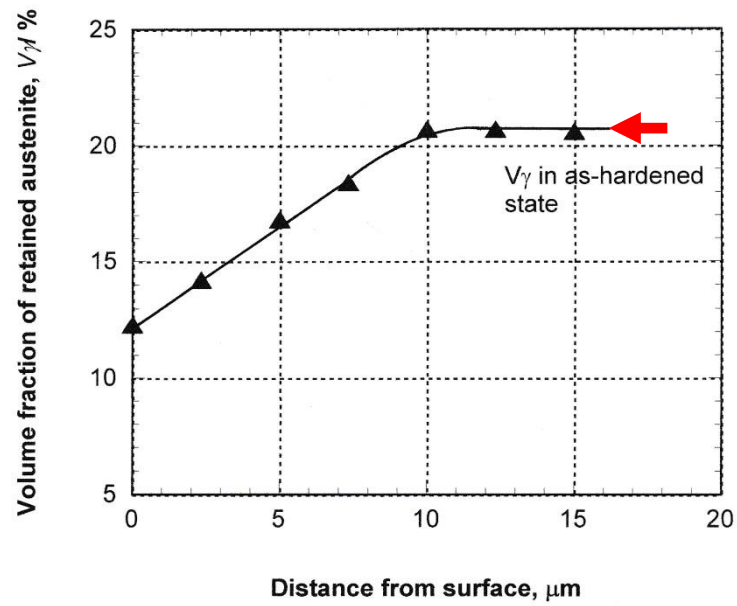


Fig.5-32 Relationship between wear rate (R_w) and volume fraction of retained austenite at H_{Tmax} ($V_{\gamma-HTmax}$) (Rubber wheel abrasive wear test).

In Suga abrasive wear test, the strained induced of transformation martensite occurs usually in the austenite. The stability of residual austenite at $H_{T_{max}}$ is relieved by tempering and therefore, the work-hardening by martensite transformation occurs easily while testing. As a result, the wear resistance is improved. In the rubber wheel abrasive wear test, the degree of work-hardening is rather small due to the low wearing stress. When $V_{\gamma-H_{T_{max}}}$ increases over 5%, it is possible that the residual austenite does not transform into martensite sufficiently by wearing. Then, the R_w does not lower contrary to the expectation. From these results, it can be said that 5% V_{γ} is required for $H_{T_{max}}$ specimen to obtain the lowest R_w value in Suga test and the 2.5 to 5% V_{γ} in rubber wheel test, respectively.

In the discussions on abrasive wear resistance, it was often mentioned that the work-hardening took place possibly on the worn surface by wear stress and it improved the wear resistance in each wear test. In order to make it sure, two ways are considered. One is to measure the volume fraction of retained austenite (V_{γ}) from the worn surface toward the inside and another is to measure the hardness from worn surface perpendicularly to the inside at the cross-section of specimen. Here, the measurement of V_{γ} was chosen by means of chosen by using the electropolishing technique. The worn surface is eliminated by electropolishing method every 2-3 μ m and measurement of the V_{γ} value is repeated. The relationships between the V_{γ} and distance from the surface of specimen were obtained using specimen of No.3 with 6%Cr, and it is shown in Fig.5-33 (a) for Suga and (b) for rubber wheel abrasive wear tests, respectively. The results show that the V_{γ} is lowest at the worn surface because



(b) Rubber wheel

Fig.5-33 Relationship between volume fraction of retained austenite (V_γ) and distance from surface of specimen No.3 in as-hardened state for (a) Suga and (b) rubber wheel abrasive wear tests (Austenitizing: 1373K).

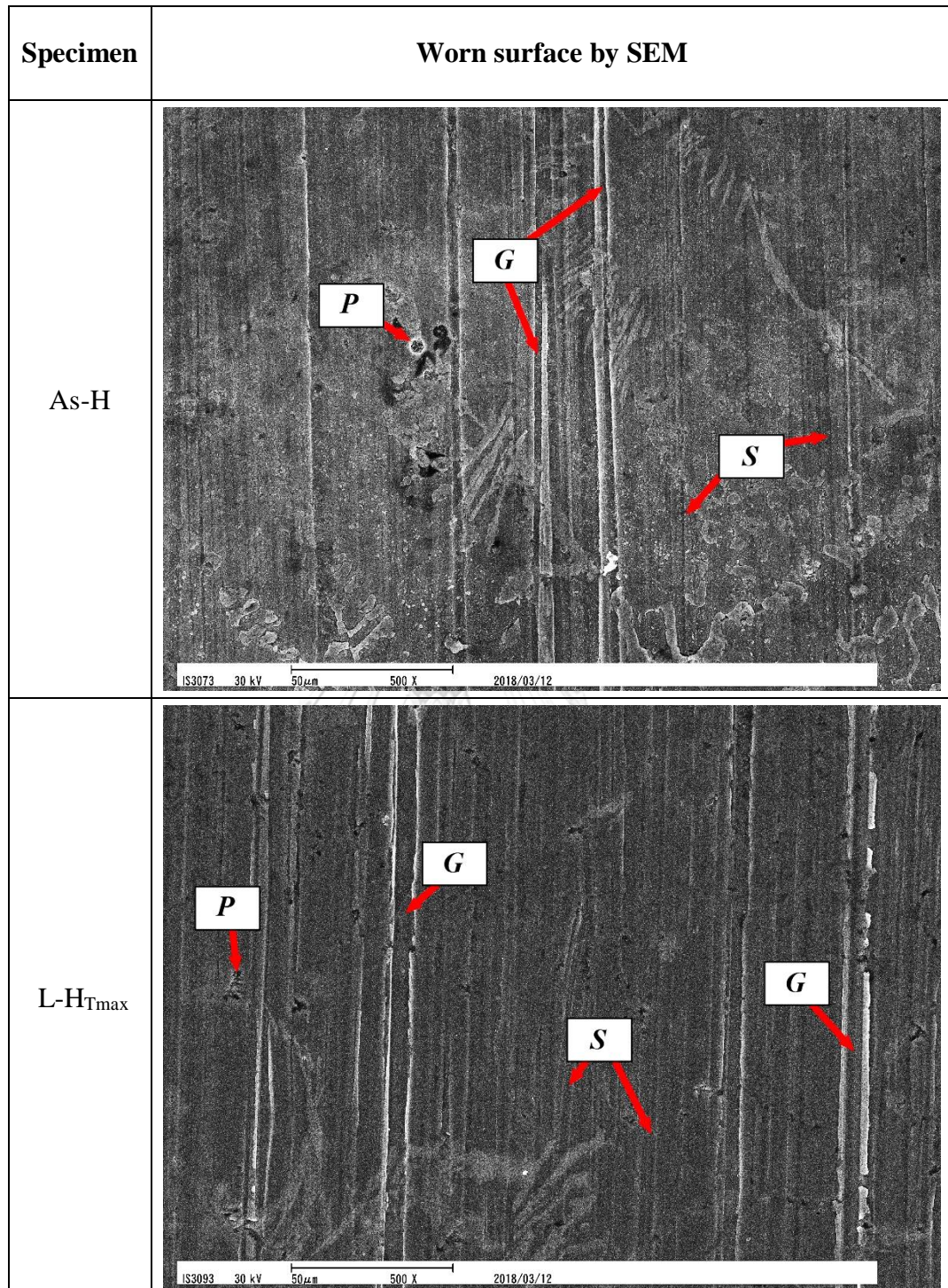
martensite transformation from retained austenite occurred greatly, and it increases gradually toward the initial value in as-hardened state as the distance from surface increases. This tells that the work-hardening was occurring inside the specimen, and that this phenomenon is same in both wear tests. It is also clear that depth from worn surface is influenced by the wear methods. It can be explained that the difference distance to reach the original value of $21\% V_\gamma$ in as-hardened state, $11\mu\text{m}$ in Suga and $7\mu\text{m}$ in rubber wheel tests, are due to the difference in the degrees of wear stresses applied on the worn surface, greater in Suga test than in rubber wheel test.

5.2.5 Observation of worn surface

As examples, the worn surface appearances of 3%, 6% and 9%Cr specimens were observed by SEM and they are shown in Fig.5-34 to 5-36 for Suga test specimens and Fig.5-37 to 5-39 for rubber wheel test specimens, respectively. In Suga abrasive wear test, the worn surface shows many scars parallel to the wear direction. The wear consists of grooving (G), pitting (P) and scratching (S). Overall, the pitting is observed in the eutectic area and their rougher surface can be recognized. The obvious wear by grooving is also recognized in both the primary dendrite and eutectic regions. The degree of wear in matrix is much more aggressive than that in eutectic regions. This reason is that the matrix is generally soft and does not resist so strong to wearing as carbides. It is clear that the $H_{T_{\max}}$ specimen shows less damage because of strong matrix in which fine secondary carbides, tempered martensite and moderate amount of retained austenite. The heavy damage is found in $H-H_{T_{\max}}$ specimen where the retained austenite is almost nil and coarse secondary carbides are dispersed in the matrix.

In rubber wheel abrasive wear test, the scratching, pitting and grooving types of wear are observed. The pitting is caused in the eutectic area and the grooving or scratching are in the matrix. It is natural that the matrix is preferably worn more than eutectic area because the eutectic carbides have higher hardness. It was reported that the wear rate of the matrix is related to the fracture rate of carbide. The matrix is removed first and followed by the fracture of carbides [54]. The smooth worn surface is obtained in H_{Tmax} specimen and the rough surface is in $H-H_{Tmax}$ specimen regardless of the Cr content.

With respect to the effect of Cr content on the worn surface appearance, the worn surface of 6%Cr specimen is smoother than those of other specimens. In addition, the worn surface of As-H and H_{Tmax} specimens has smaller damage than those of L- H_{Tmax} and $H-H_{Tmax}$ specimens overall the Cr content. These results are in good agreement with the wear test results.



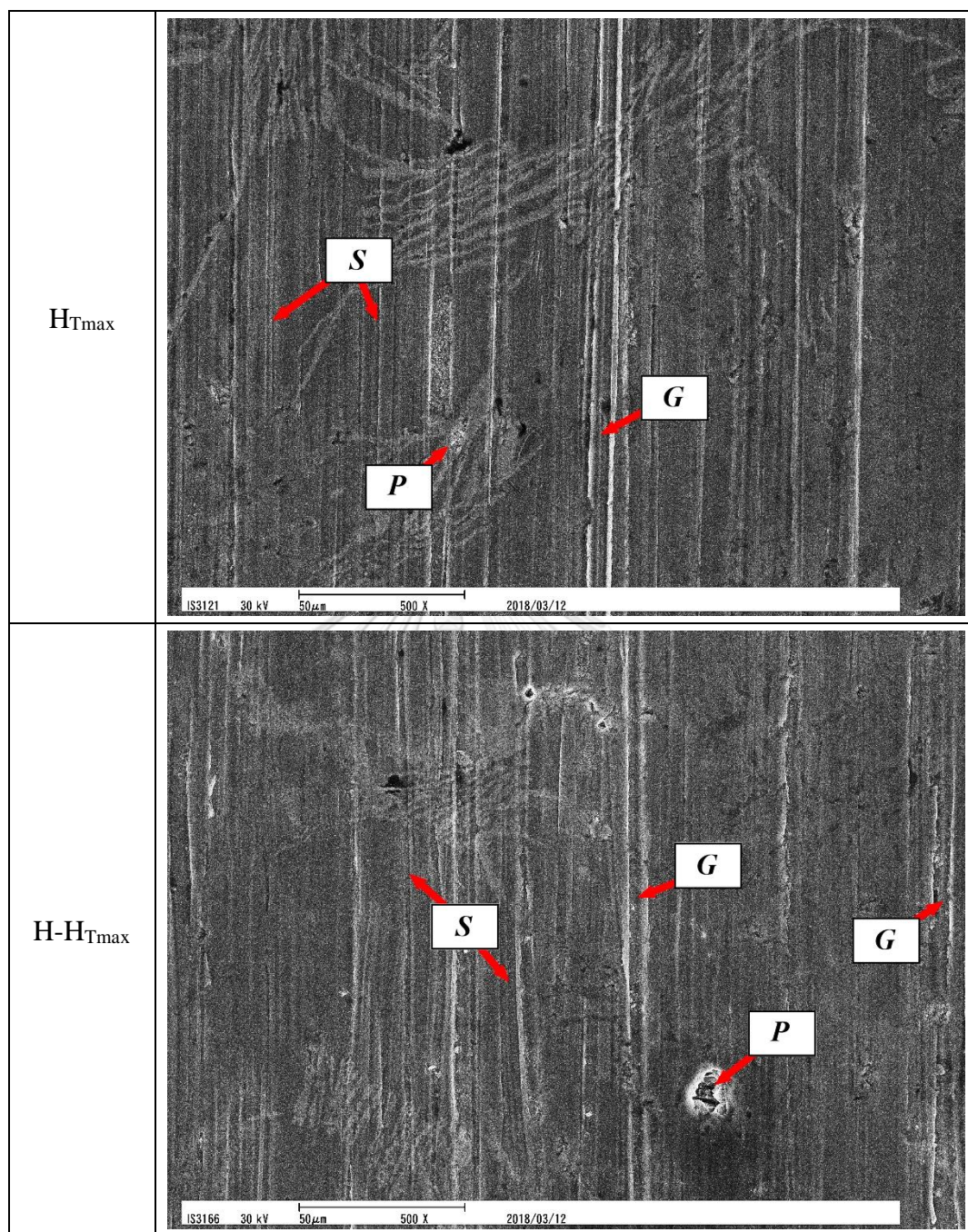
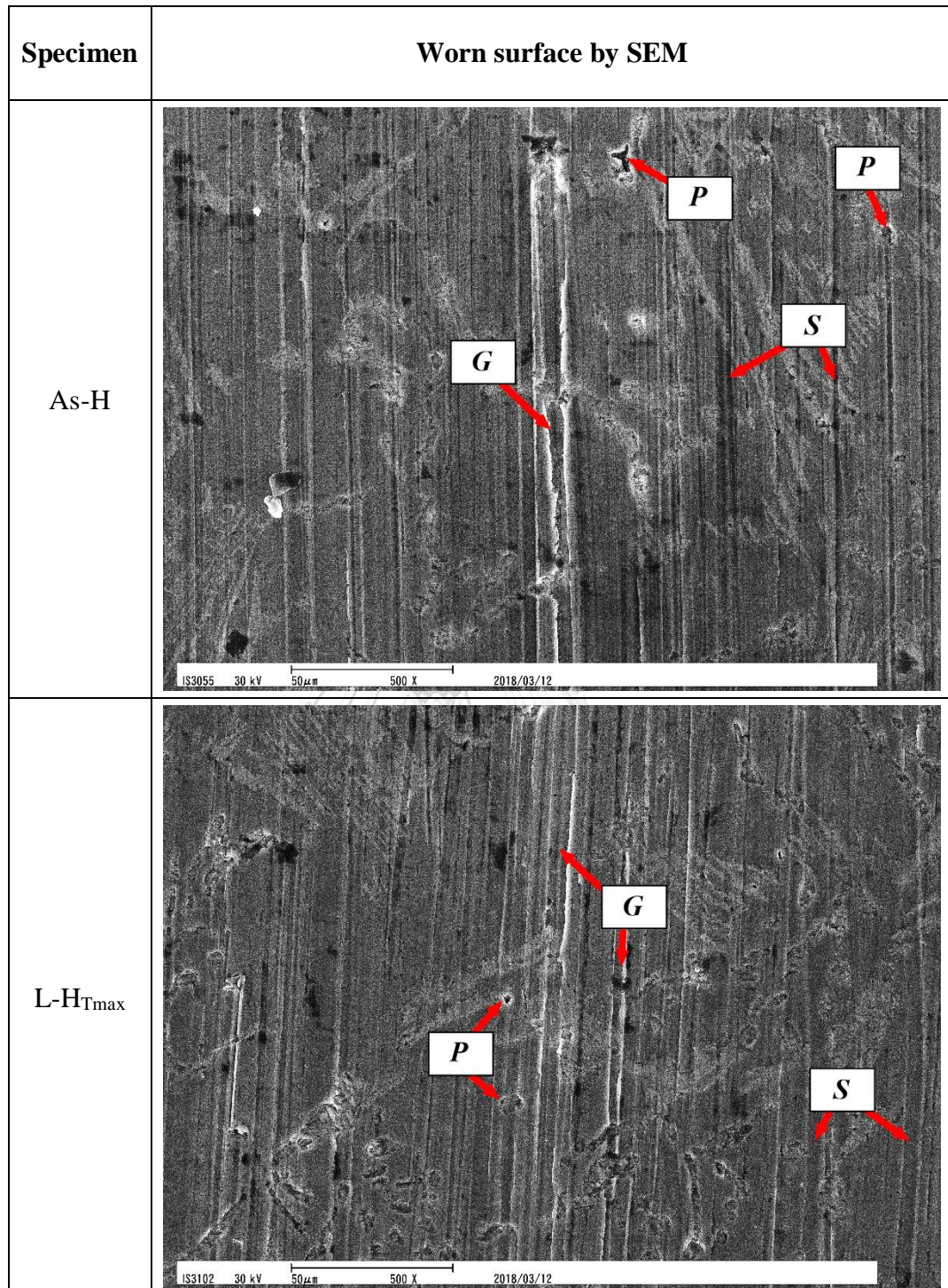


Fig.5-34 SEM microphotographs of worn surface after Suga abrasive wear test in 3%Cr specimen hardened from 1373K austenitizing.



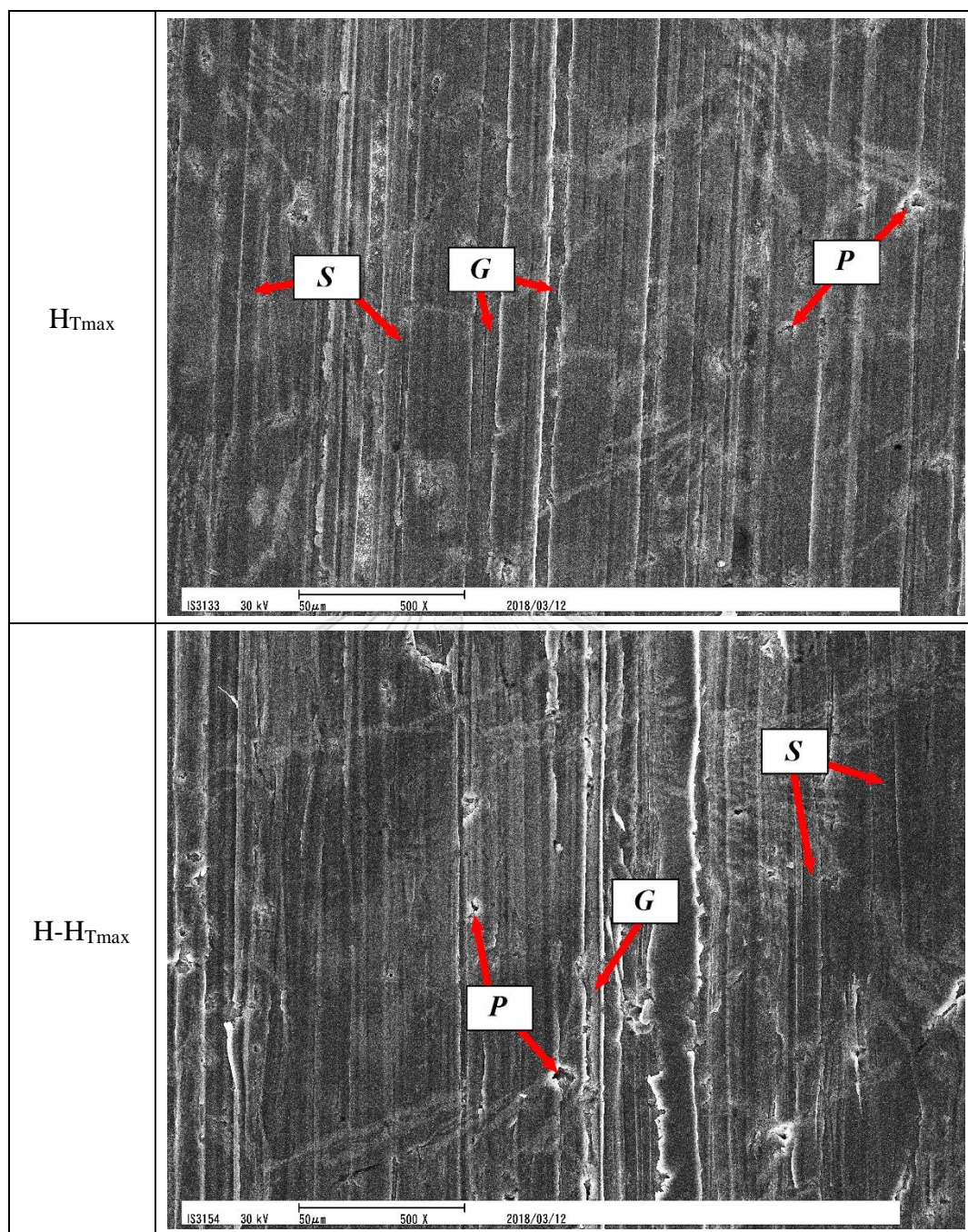
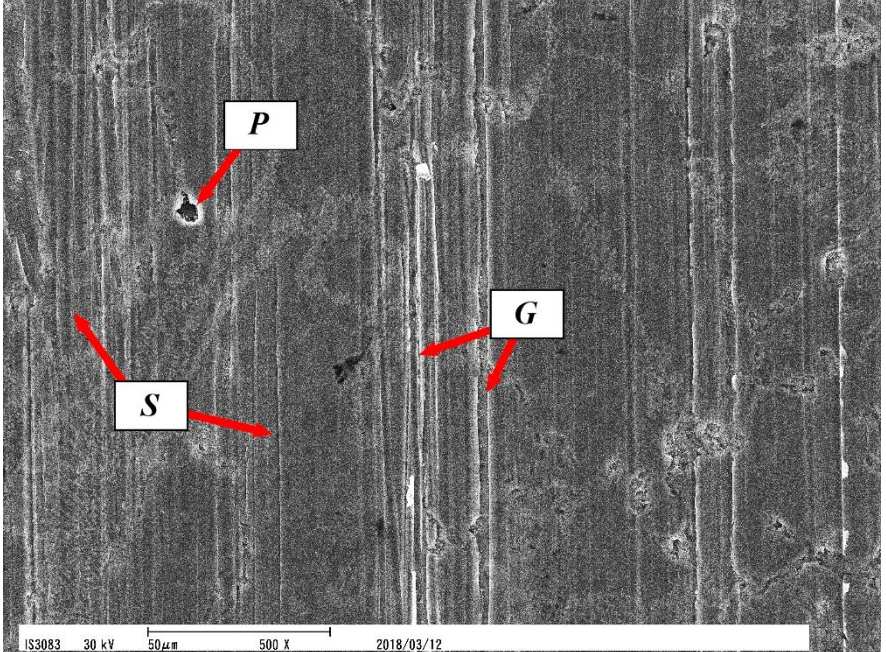
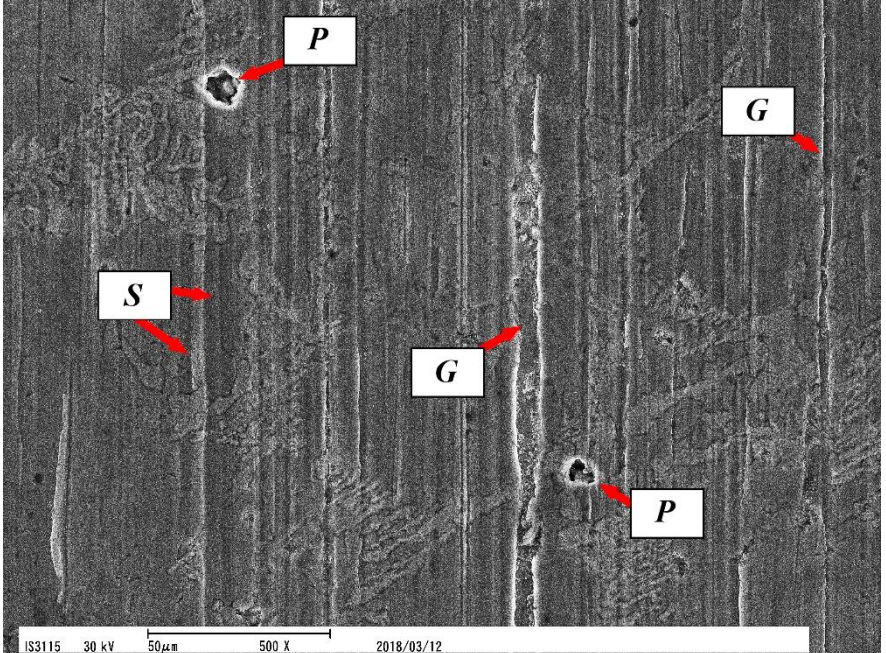


Fig.5-35 SEM microphotographs of worn surface after Suga abrasive wear test in 6%Cr specimen hardened from 1373K austenitizing.

Specimen	Worn surface by SEM
As-H	 <p>SEM image showing the worn surface of the As-H specimen. The surface exhibits vertical striations and several circular pits. Three features are labeled with red arrows and white boxes: 'P' (pit) at the top center, 'S' (scratch) on the left side, and 'G' (groove) on the right side. A scale bar at the bottom indicates 50 μm, 500 X magnification, and the date 2018/03/12. Technical parameters include IS3083, 30 kV, and 50 μm.</p>
L-H _{Tmax}	 <p>SEM image showing the worn surface of the L-H_{Tmax} specimen. The surface exhibits vertical striations and several circular pits. Three features are labeled with red arrows and white boxes: 'P' (pit) at the top center, 'S' (scratch) on the left side, and 'G' (groove) on the right side. A scale bar at the bottom indicates 50 μm, 500 X magnification, and the date 2018/03/12. Technical parameters include IS3115, 30 kV, and 50 μm.</p>

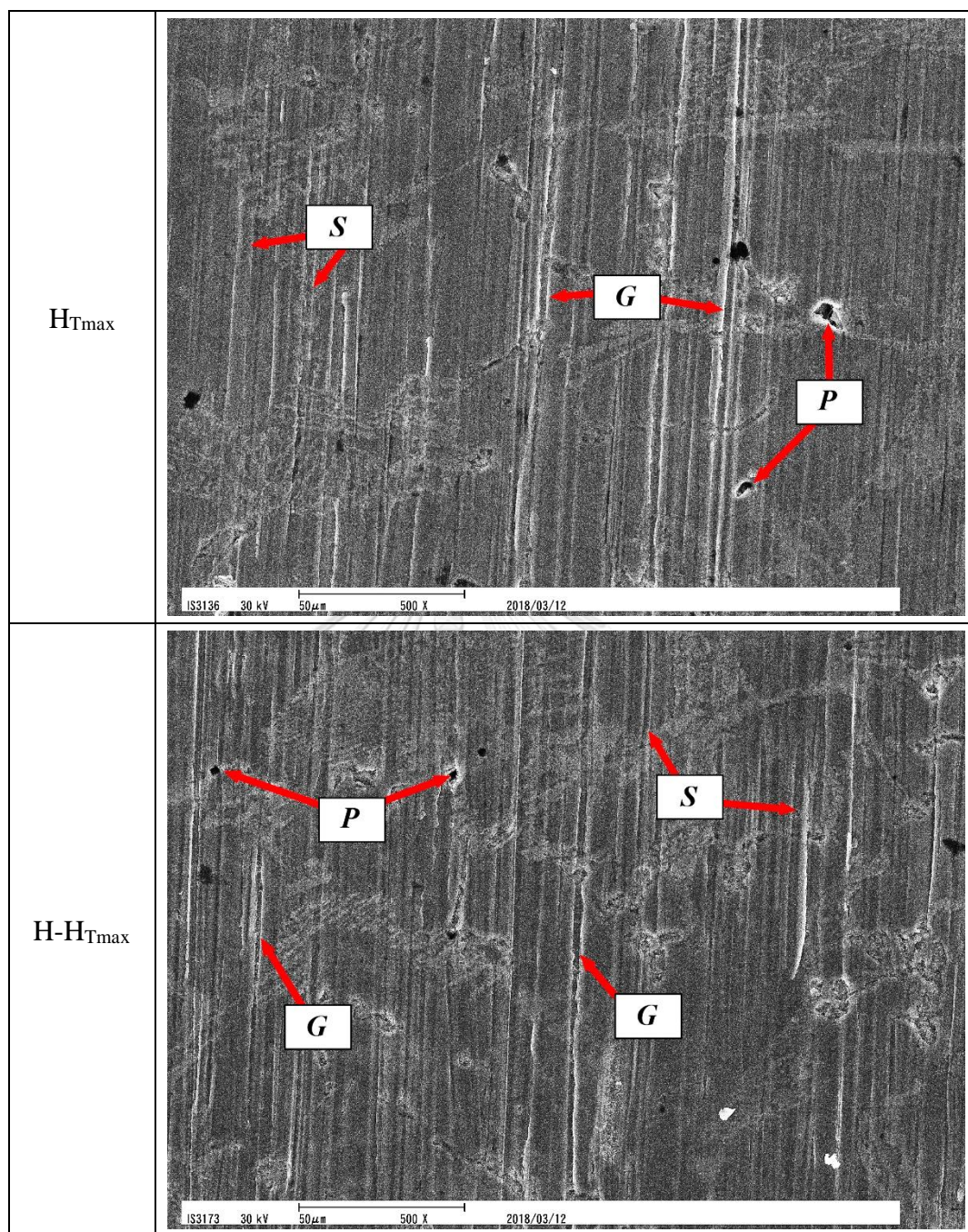
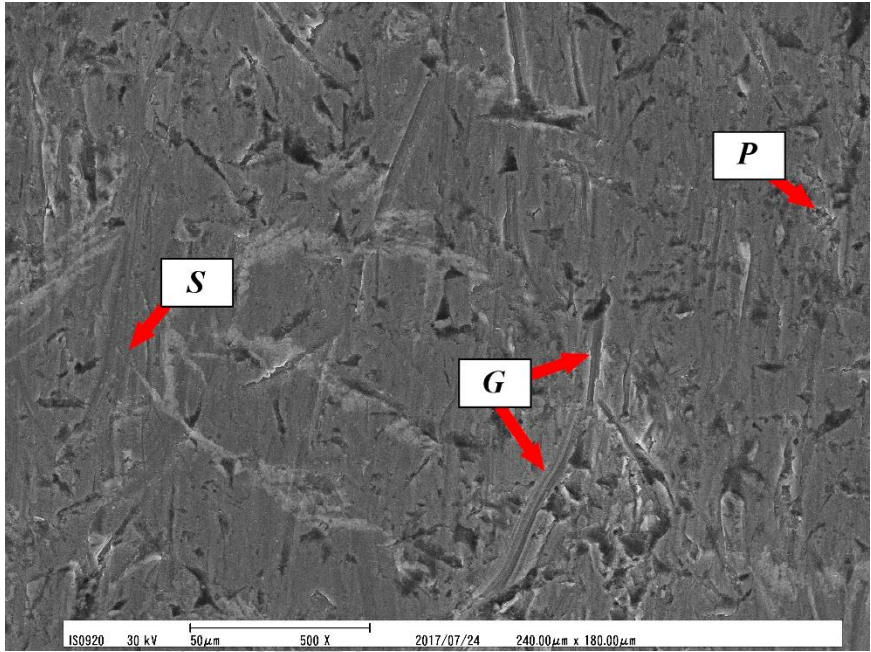
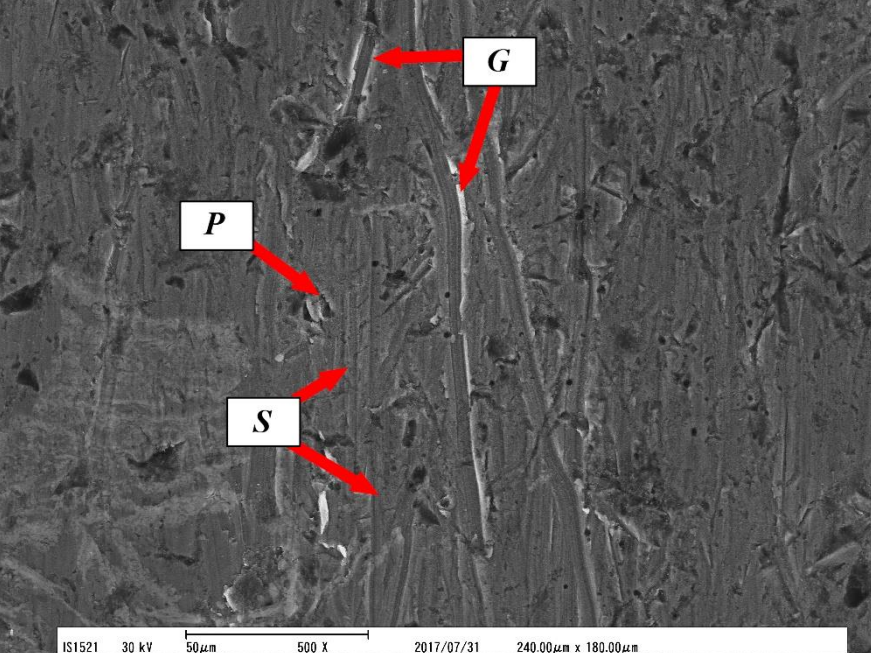


Fig.5-36 SEM microphotographs of worn surface after Suga abrasive wear test in 9%Cr specimen hardened from 1373K austenitizing.

Specimen	Worn surface by SEM
As-H	 <p>SEM image showing the worn surface of the As-H specimen. The surface exhibits a complex, textured morphology with various features. Three specific features are highlighted with red arrows and labeled: 'S' (Scratch), 'G' (Groove), and 'P' (Pit). The image includes a scale bar at the bottom indicating 50 μm, 500 X magnification, and technical parameters: IS0920, 30 kV, 240.00 μm x 180.00 μm, and a date of 2017/07/24.</p>
L-H _{Tmax}	 <p>SEM image showing the worn surface of the L-H_{Tmax} specimen. The surface exhibits a complex, textured morphology with various features. Three specific features are highlighted with red arrows and labeled: 'G' (Groove), 'P' (Pit), and 'S' (Scratch). The image includes a scale bar at the bottom indicating 50 μm, 500 X magnification, and technical parameters: IS1521, 30 kV, 240.00 μm x 180.00 μm, and a date of 2017/07/31.</p>

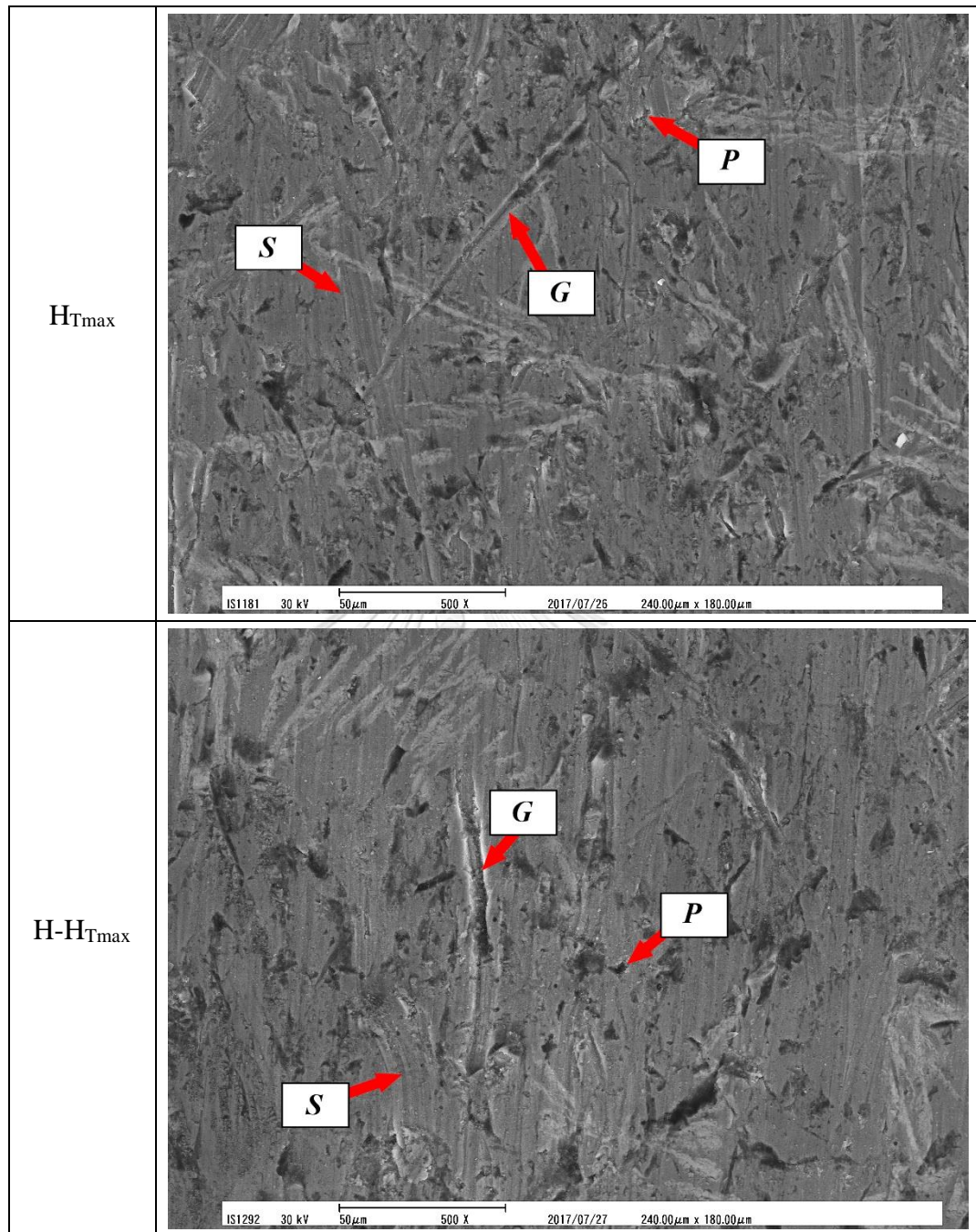
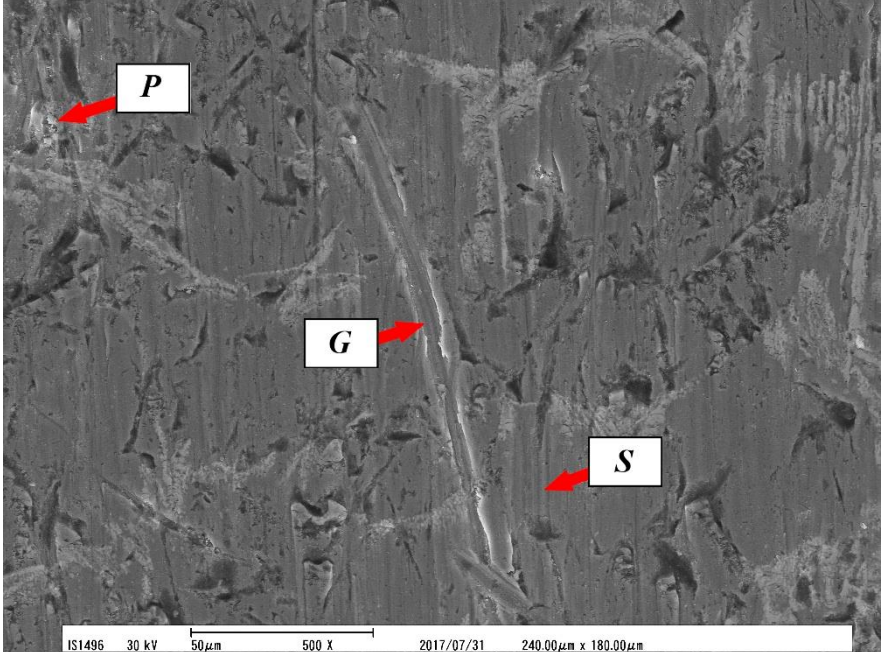
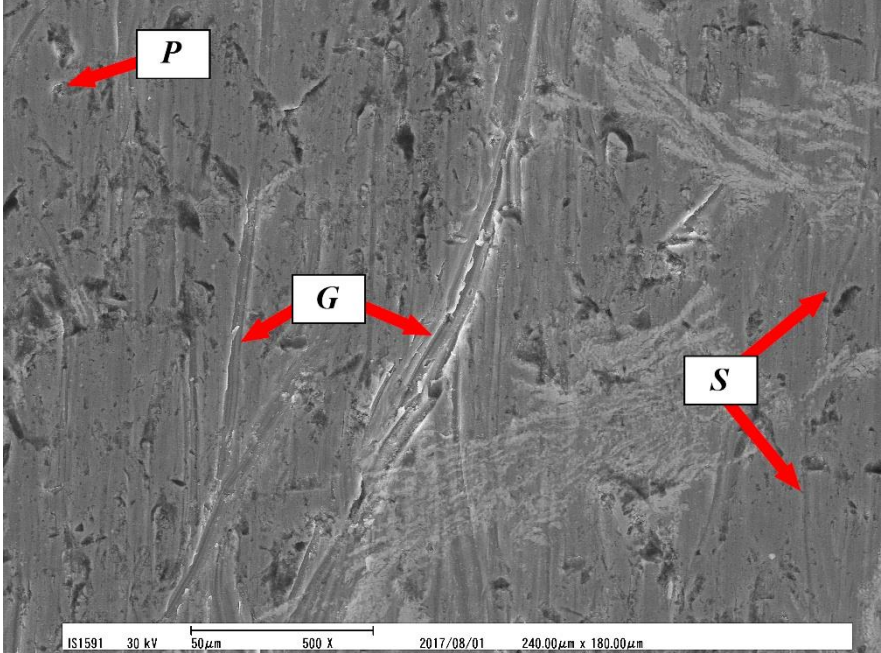


Fig.5-37 SEM microphotographs of worn surface after rubber wheel abrasive wear test in 3%Cr specimen hardened from 1373K austenitizing.

Specimen	Worn surface by SEM
As-H	 <p>SEM image showing the worn surface of the As-H specimen. The image displays a complex, textured surface with various features. Three red arrows point to specific regions labeled <i>P</i>, <i>G</i>, and <i>S</i>. <i>P</i> is located in the upper left, <i>G</i> is in the center, and <i>S</i> is in the lower right. A scale bar at the bottom indicates 50 μm, 500 X magnification, and a date of 2017/07/31. Technical parameters include IS1496, 30 kV, and a field of view of 240.00 μm x 180.00 μm.</p>
L-H _{Tmax}	 <p>SEM image showing the worn surface of the L-H_{Tmax} specimen. The image displays a complex, textured surface with various features. Three red arrows point to specific regions labeled <i>P</i>, <i>G</i>, and <i>S</i>. <i>P</i> is located in the upper left, <i>G</i> is in the center, and <i>S</i> is in the lower right. A scale bar at the bottom indicates 50 μm, 500 X magnification, and a date of 2017/08/01. Technical parameters include IS1591, 30 kV, and a field of view of 240.00 μm x 180.00 μm.</p>

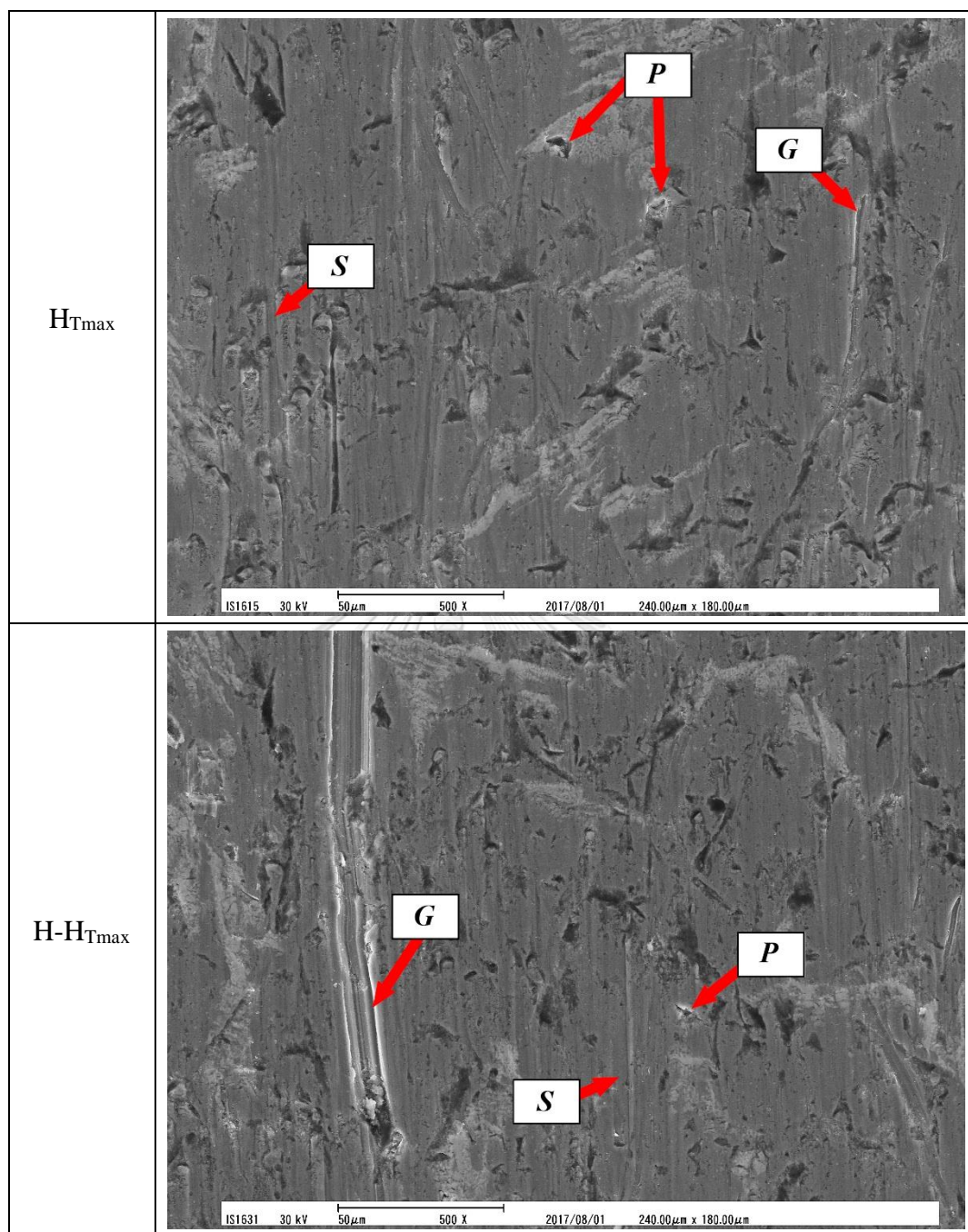
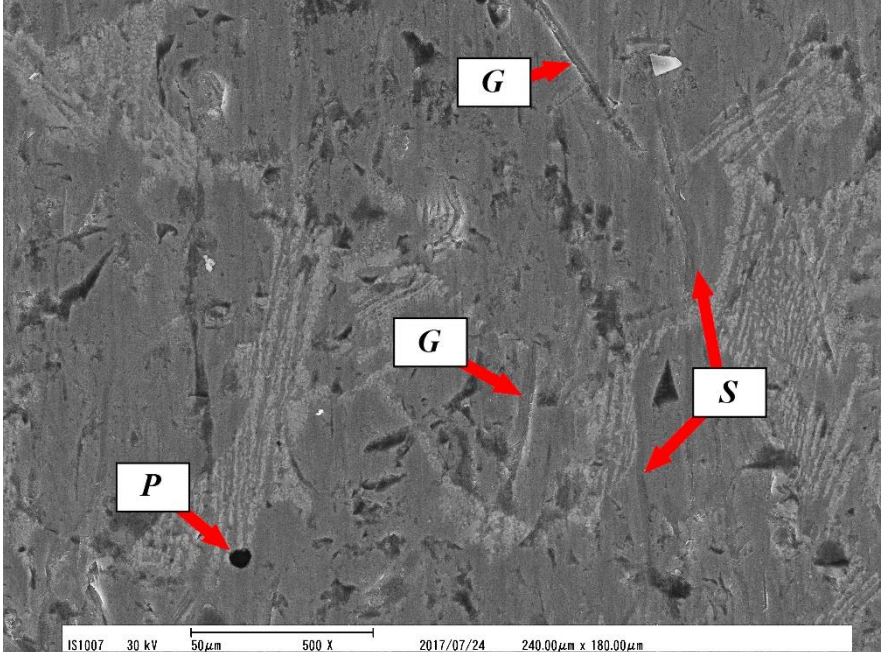
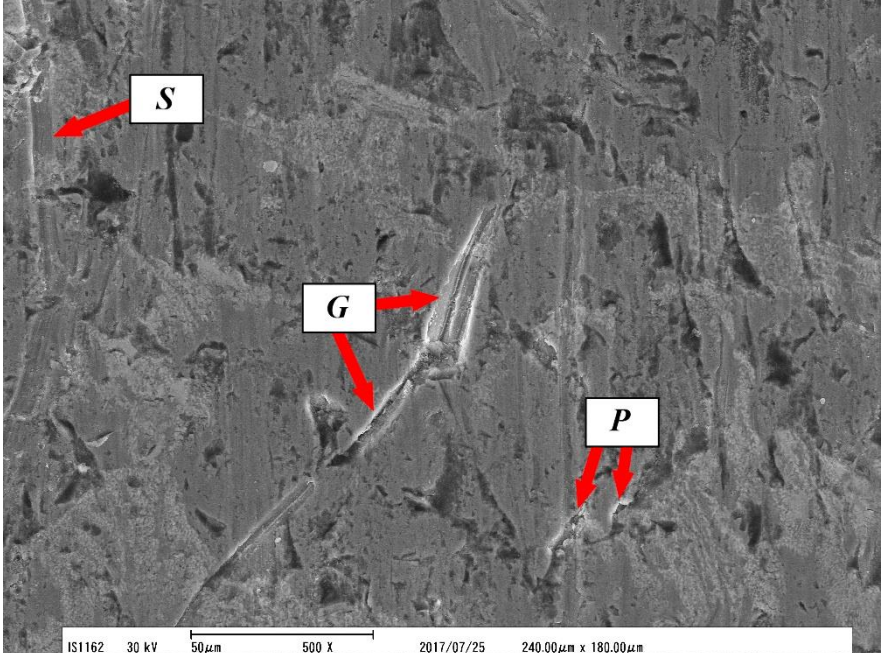


Fig.5-38 SEM microphotographs of worn surface after rubber wheel abrasive wear test in 6%Cr specimen hardened from 1373K austenitizing.

Specimen	Worn surface by SEM
As-H	 <p>SEM image showing the worn surface of the As-H specimen. The surface exhibits a complex, textured morphology with various features. Three features are highlighted with red arrows and labeled: 'P' (a small dark spot), 'G' (a linear feature), and 'S' (a triangular feature). A scale bar at the bottom indicates 50 μm, 500 X magnification, and a date of 2017/07/24. Technical parameters include IS1007, 30 kV, and a field of view of 240.00 μm x 180.00 μm.</p>
L-H _{Tmax}	 <p>SEM image showing the worn surface of the L-H_{Tmax} specimen. The surface exhibits a complex, textured morphology with various features. Three features are highlighted with red arrows and labeled: 'S' (a triangular feature), 'G' (a linear feature), and 'P' (a small dark spot). A scale bar at the bottom indicates 50 μm, 500 X magnification, and a date of 2017/07/25. Technical parameters include IS1162, 30 kV, and a field of view of 240.00 μm x 180.00 μm.</p>

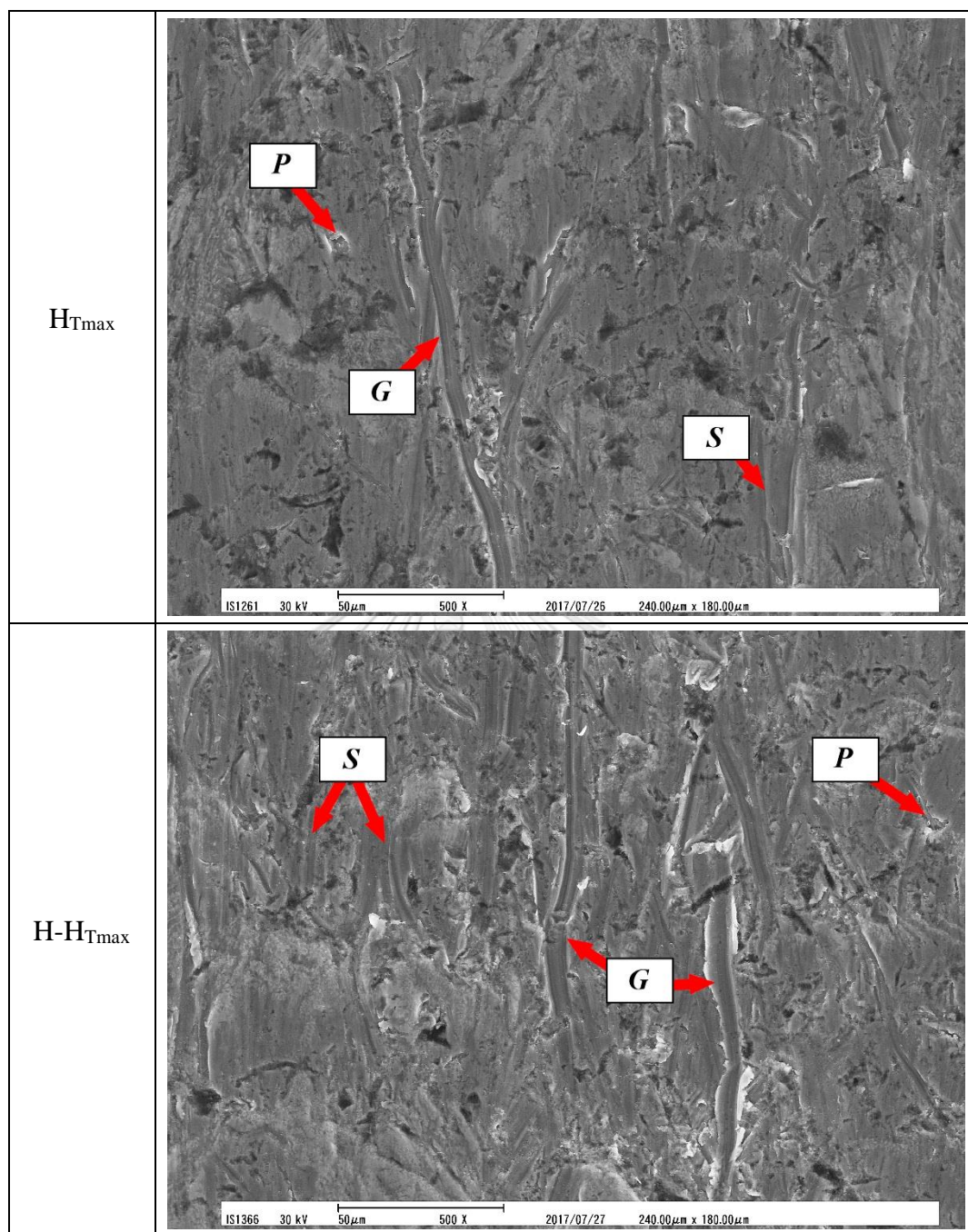


Fig.5-39 SEM microphotographs of worn surface after rubber wheel abrasive wear test in 9%Cr specimen hardened from 1373K austenitizing.

Chapter VI

Conclusions

Multi-alloyed white cast irons with varying Cr content from 3 to 9% in basic chemical composition of 2%C-5%Mo-5%W-5%V-2%Co were prepared and effect of Cr content on heat treatment behavior and abrasive wear resistance were investigated.

6.1 Effect of Cr content on heat treatment behavior

To clarify the heat treatment behavior, specimens were annealed at 1223K for 18 ks and then hardened by fan air cooling from 1323 and 1373K austenitizing for 3.6 ks. Hardened specimens were tempered between 673 and 873K for 12 ks with 50K intervals. The hardness and volume fraction of retained austenite (V_{γ}) were measured and they were related to the Cr content of specimens. In order to support the results and discussions, the microstructures of test pieces in as-cast and heat-treated states were observed by microscopes.

6.1.1 Effect of Cr content on microstructure

6.1.1.1 As-cast state

- 1) The microstructure of each specimen consisted of primary austenite dendrite (γ_P) and ($\gamma+MC$) and ($\gamma+M_2C$) eutectics in specimens with 3 and 5%Cr. By contrast, ($\gamma+M_7C_3$) eutectic appeared additionally in specimens with 6%Cr and more.
- 2) Within the chemical compositions of specimens in this research, the area fraction of γ_P decreased slightly and that of ($\gamma+MC$) eutectic decreased

progressively as the Cr content increased. However, the amount of $(\gamma+M_2C)$ eutectic increased up to 5%Cr and at 6%Cr, the crystallization of $(\gamma+M_2C)$ eutectic was inhibited and that of $(\gamma+M_7C_3)$ eutectic began to crystallize and it continued to increase in the amount as the Cr content increase over 6%, on the other side, $(\gamma+M_7C_3)$ eutectic increased.

6.1.1.2 As-hardened state

- 1) Matrix of all the specimens was composed of precipitated secondary carbide, martensite and retained austenite.
- 2) The amount of secondary carbides decreased with increasing the Cr content.
- 3) The high austenitizing temperature of 1373K provided less secondary carbide but it produced more retained austenite than those hardened from low austenitizing temperature of 1323K.

6.1.2 Effect of Cr content on hardness and volume fraction of retained austenite (V_γ)

6.1.2.1 As-hardened state

- 1) The macro-hardness increased slightly to the highest value at 5%Cr and thereafter, it decreased continuously as the Cr content rose. Hardening from low austenitizing temperature of 1323K resulted in higher hardness than that from high austenitizing temperature of 1373K.
- 2) The micro-hardness was naturally lower than macro-hardness in all the specimens but the effect of Cr content on the micro-hardness showed same tendency as that on the macro-hardness.

- 3) The V_γ increased gradually to the highest value at 5%Cr and then, decreased progressively as Cr content rose. The higher hardening temperature of 1373K produced larger amount of V_γ in specimens while the Cr content was increasing.

6.1.2.2 Tempered state

- 1) The moment tempering began to carry out, the hardness dropped abruptly from that in as-hardened state. After that, it went up to the maximum tempered hardness (H_{Tmax}) as the tempering temperature was elevated. These reasons are due to the precipitation of secondary carbides during tempering and the transformation of retained austenite to martensite in cooling after holding. When the tempering temperature increased over the temperature at H_{Tmax} , the hardness dropped steeply due to the coarsening of fine secondary carbides and the transformation of retained austenite to ferrite.
- 2) The H_{Tmax} was obtained by tempering between 773 and 798K and it shifted to the lower temperature side when the Cr content was more than 6%. Higher H_{Tmax} value was obtained by hardening from higher austenitizing temperature.
- 3) The micro-hardness showed similar behavior to the macro-hardness in all the specimens but the values were low regardless of austenitizing temperature. In addition, the peaks of micro-hardness were located at the same tempering temperature as macro-hardness.
- 4) The H_{Tmax} increased to the highest value at 5 to 6%Cr. The highest values of H_{Tmax} , 913.4 HV30 and 861.6 HV0.1 for hardening from 1323K and 932.6

HV30 and 885.6 HV0.1 for hardening from 1373K were obtained in 5%Cr specimen.

- 5) The V_γ value began to decrease greatly when the tempering temperature got over between 723 to 798K, regardless of austenitizing temperatures. The V_γ values in the specimens with H_{Tmax} were overall less than 5%.
- 6) The hardness increased to the maximum value at about 4% V_γ and decreased gradually as the V_γ value increased. Macro-hardness over 900 HV30 was obtained in the specimens with 2-10% V_γ .
- 7) The H_{Tmax} value increased proportionally as the V_γ in the as-hardened state rose. The V_γ value more than 17% in as-hardened state was necessary to achieve the H_{Tmax} over 900 HV30.
- 8) The degree of secondary hardening (ΔH_s) decreased progressively as the Cr content increased but it increased as the V_γ value in as-hardened state rose. Eventually, it was found that the ΔH_s value more than 50HV30 in tempered state, on the other words, the V_γ value more than 17% in as-hardened state was necessary to obtain H_{Tmax} over 900HV30.

6.2 Effect of Cr content on abrasive wear behavior

In order to clarify the wear behavior, the as-hardened specimens (As-H) were tempered at three temperatures which were chosen from tempered hardness curves obtained in the chapter on heat treatment behavior, i.e., temperature providing the maximum tempered hardness (H_{Tmax}), lower and higher temperatures than that at H_{Tmax} (L- H_{Tmax} and H- H_{Tmax}). The abrasive wear resistance of specimens was

evaluated by the barometer of wear rate (R_w) obtained using Suga abrasive wear test (two-body-type) and rubber wheel abrasive wear test (three-body-type).

6.2.1 Behavior of abrasive wear

- 1) Linear relationship between wear loss (W_l) and wear distance (W_d) was obtained in both the Suga and rubber wheel abrasive wear tests. The wear rate (R_w) which was expressed by a slope of each straight line varied depending on the Cr content and heat treatment condition.
- 2) In both of the abrasive wear tests, the R_w decreased continuously until 6%Cr and after that, it increased gradually as the Cr content rose. In all the Cr content, the hardening from high temperature provided low R_w value compared with that hardening from low temperature.
- 3) The R_w decreased steeply as the hardness increased up to 840-850 HV30, and over that hardness, it decreased gradually in Suga and slightly in rubber wheel abrasive wear tests.
- 4) In the specimens with V_γ value less than 5%, the R_w value scattered widely but it decreased regularly with an increase in the hardness. When the V_γ rose over 5%, the R_w value lowered continuously.
- 5) The macro-hardness gave a strong effect on the wear resistance in Suga abrasive wear test. Contrastively, the micro-hardness did a great effect on the wear resistance in the rubber wheel abrasive wear test.
- 6) Eventually, the lowest R_w or the highest wear resistance was obtained in the As-H specimen followed by H_{Tmax} specimen. The largest R_w or the lowest

wear resistance was obtained in L-H_{Tmax} or H-H_{Tmax} specimen, regardless of the Cr content and austenitizing temperature.

- 7) The 6%Cr specimens provided best wear resistance regardless of heat treatment conditions. This reason is due to the solidification of M₇C₃ eutectic carbide with tougher and high abrasive wear resistance.

6.2.2 Observation of worn surface

- 1) Suga abrasive wear test was carried out under more severe condition than rubber wheel abrasive wear test. In Suga test, the abrasive particles cut through both the eutectic carbides and matrix. In rubber wheel abrasive wear test, however, the matrix was preferentially worn out ahead of the eutectic areas.
- 2) The worn surface consisted of grooving, scratching and pitting wears in all of specimens. The pitting wear was found mainly in eutectic area while the grooving and scratching wears were intensively observed in matrix.
- 3) The 6%Cr specimens showed smoother worn surface than those of other specimens. Moreover, the damage on worn surface was smaller in As-H and H_{Tmax} specimens than those of L-H_{Tmax} and H-H_{Tmax} specimens in all range of the Cr content. This evident supports that specimens with 6%Cr had best abrasive wear resistance.

REFERENCES

- [1] M. Hashimoto, "Development of multi-component White Cast Iron (HSS) rolls and Rolling technology in steel rolling," *Abrasion Wear Resistant Alloyed White Cast Iron for Rolling and Pulverizing Mills*, pp. 1-23, 2008.
- [2] M. Boccalini Jr., "Overview : High speed steels for hot rolling mill rolls," *Abrasion Wear Resistant Alloyed White Cast Iron for Rolling and Pulverizing Mills*, pp. 123-142, 2011.
- [3] G. Walmag, X. Vanden Eynde, M. Sinnaeve, and V. Lecomte, "Mechanisms of work rolls degradation in HSM," *ABRASION WEAR RESISTANT ALLOYED WHITE CAST IRON FOR ROLLING AND PULVERIZING MILLS*, pp. 24-34, 2008.
- [4] G. Gevelmann and W. Theisen, "New wear resistant cast alloys for use at elevated temperatures," *Abrasion Wear Resistant Alloyed White Cast Iron for Rolling and Pulverizing Mills*, pp. 171-181, 2011.
- [5] G. Powell, "Improved wear-resistant high-alloyed white irons-A historical perspective," *International congress on abrasion wear resistance alloyed white cast iron for rolling and pulverizing mills*, 2002.
- [6] S. Ma *et al.*, "Microstructure and crystallography of M7C3 carbide in chromium cast iron," *Materials Chemistry and Physics*, vol. 161, pp. 65-73, 2015.
- [7] I. R. Sare and B. K. Arnold, "The influence of heat treatment on the high-stress abrasion resistance and fracture toughness of alloy white cast irons," *Metallurgical and*

Materials Transactions A, vol. 26, no. 7, pp. 1785-1793, 1995.

[8] Y. Matsubara, N. Sasaguri, and M. Hashimoto, "The history and development of cast rolls for hot working mill," *The 4th Asian Foundry Congress-Australia*, pp. 251-261, 1996.

[9] G. Laird, R. Gundlach, and K. Rohrig, *Abrasion-Resistance Cast Iron Handbook*. USA: American Foundry Society, 2000.

[10] J. D. Watson, P. J. Mutton, and I. R. Sare, "Abrasive Wear of White Cast Irons," *Australian Institute of Metals Forum*, vol. 3, pp. 74-88, 1980.

[11] K.-H. Zum Gahr and D. V. Doane, "Optimizing fracture toughness and abrasion resistance in white cast irons," *Metallurgical Transactions A* vol. 11, no. 4, pp. 613-620, 1980.

[12] O. Kubo, M. Hashimoto, and Y. Matsubara, "Influence of microstructure on wear resistance and crack propagation characteristics required for white iron rolling mill rolls," *Proceedings of The Science of Casting and Solidifications*, 2001.

[13] H.-Q. Wu, N. Sasaguri, Y. Matsubara, and M. Hashimoto, "Solidification of Multi-Alloyed White Cast Iron : Type and Morphology of Carbides," *AFS Transactions*, vol. 140, pp. 103-108, 1996.

[14] W. Khanitnantharak, M. Hashimoto, K. Shimizu, K. Yamamoto, N. Sasaguri, and Y. Matsubara, "Effects of Carbon and Heat Treatment on the Hardness and Austenite Content of a Multi-Component White Cast Iron," *AFS Transactions*, vol. 117,

pp. 435-444, 2009.

[15] J. Opapaiboon, P. Sricharoenchai, S. Inthidech, and Y. Matsubara, "Effect of Carbon Content on Heat Treatment Behavior of Multi-Alloyed White Cast Iron for Abrasive Wear Resistance," *MATERIALS TRANSACTIONS*, vol. 56, no. 5, pp. 720-725, 2015.

[16] S. Karagoz, R. Riedl, M. R. Gregg, and H. Fischmeister, "The role of M₂C carbides in high speed steels," *Sonderbande der Praktischen Metallographie*, vol. 14, pp. 389-362, 1983.

[17] J. T. H. Pearce;, "Wear of abrasion resisting materials," Ph.D. dissertation, Dept. Metallurgy & Materials Engineering, Aston University, Birmingham, 1982.

[18] J. T. H. Pearce;, "High chromium irons to resist wear," *The 6th Asian Foundry Congress*, pp. 120-134, 1999.

[19] D. Kopyciński, S. Piasny, M. Kawalec, and A. Madizhanova, "The Abrasive Wear Resistance of Chromium Cast Iron," *Archives of Foundry Engineering*, vol. 14, no. 1, pp. 63-66, 2014.

[20] G. V. Raynor and V. G. Rivlin, *Phase equilibria in iron ternary alloys*. London The Institute of Metals, 1988, pp. 177-191 and 201-212.

[21] V. Raghavan, *Phase Diagrams of Ternary Iron Alloys*. Indian Institute of Metals, 1987, pp. 111-125.

[22] G. Steven, A. E. Nehrenberg, and T. V. Philip, "High-performance high-speed

steels by design," *Transactions of the ASM*, vol. 57, pp. 925-948, 1964.

[23] N. Sasaguri, Y. Yokomizo, K. Yamamoto, and Y. Matsubara, "Influence of Cobalt Content on Heat Treatment Behavior and Abrasive Wear Characteristics of Multi-Component White Cast Iron," *Abrasion Wear Resistant Alloyed White Cast Iron for Rolling and Pulverizing Mills*, pp. 77-87, 2011.

[24] W. Theisen, "Design of wear resistant alloys against abrasion," *Abrasion Wear Resistant Alloyed White Cast Iron for Rolling and Pulverizing Mills*, pp. 128-138, 2008.

[25] W.-S. Chang, Y.-N. Pan, N. Sasaguri, and Y. Matsubara, "Effects of C and W contents and heat treatment condition on microstructure and wear resistance of multi-component white cast irons," *ABRASION WEAR RESISTANT ALLOYED WHITE CAST IRON FOR ROLLING AND PULVERIZING MILLS*, pp. 35-48, 2008.

[26] M. Hashimoto, "Effects of Alloying Element on Compressive and Wear Properties of Multi-component White Cast irons for Steel Rolling Mill Rolls," *Abrasion Wear Resistant Alloyed White Cast Iron for Rolling and Pulverizing Mills*, pp. 183-192, 2011.

[27] J. Tchoufang Tchoundjang, M. Sinnaeve, and J. Lecomte-Beckers, "Influence of High Temperature Heat Treatment on in situ Transformation of Mo-rich Eutectic Carbides in HSS and Semi-HSS Grades," *Abrasion Wear Resistant Alloyed White Cast Iron for Rolling and Pulverizing Mills*, pp. 61-75, 2011.

[28] M. Boccalini Jr., A. Vicente De O Corrêa, and A. Sinatora, "Niobium in multi-component white cast iron," *Abrasion Wear Resistant Alloyed White Cast Iron for*

Rolling and Pulverizing Mills, pp. 49-64, 2008.

[29] H.-Q. Wu, M. Hashimoto, N. Sasaguri, and Y. Matsubara, "Solidification Sequence of Multi-Component White Cast Iron," *Journal of Japan Foundry Engineering Society*, vol. 68, no. 8, pp. 637-643, 1996.

[30] J.D.B. De Mello and E. Canizza, "Influence of microstructural parameters on the tribological behaviour of multicomponent ferrous alloys," *Abrasion Wear Resistant Alloyed White Cast Iron for Rolling and Pulverizing Mills*, pp. 185-211, 2008.

[31] M. Radulovic, M. Fiset, K. Peev, and M. Tomovic, "The influence of vanadium on fracture toughness and abrasion resistance in high chromium white cast irons," *Journal of Materials Science* vol. 29, no. 19, pp. 5085-5094, 1994.

[32] O. Joos, C. Boher, C. Vergne, C. Gaspard, T. Nylén, and F. Rezaï-Aria, "Laboratory study of the wear and oxidation behavior of High Chromium Cast Iron and HSS material used for HSM work rolls," *Abrasion Wear Resistant Alloyed White Cast Iron for Rolling and Pulverizing Mills*, pp. 102-114, 2008.

[33] Y. Matsubara, N. Sasaguri, Y. Yokomizo, and H.-Q. Wu., "Continuous cooling transformation behavior of multi-alloyed white cast iron," *Journal of Japan Foundry Engineering Society*, vol. 71, pp. 183-189, 1999.

[34] E.S. Lee, W.J. Park, J.Y. Jung, and S. Ahn, "Solidification microstructure and M₂C carbide decomposition in a spray-formed high-speed steel," (in English), *Metallurgical and Materials Transactions A*, vol. 29, no. 5, pp. 1395-1404, 1998.

- [35] H.-Q. Wu, N. Sasaguri, M. Hashimoto, and Y. Matsubara, "Practical Phase Diagram of Multi-Component White Cast Iron," *Journal of Japan Foundry Engineering Society*, vol. 69, no. 11, pp. 917-923, 1997.
- [36] Y. Matsubara, K. Ogi, and K. Matsuda, "Eutectic solidification of high chromium cast iron-Eutectic structures and their quantitative analysis," *AFS Transactions*, vol. 89, pp. 183-196, 1981.
- [37] S. Inthidech, P. Sricharoenchai, and Y. Matsubara, "Effect of Alloying Elements on Heat Treatment Behavior of Hypoeutectic High Chromium Cast Iron," *MATERIALS TRANSACTIONS*, vol. 47, no. 1, pp. 72-81, 2006.
- [38] E. Albertin and A. Sinatoro, "Effect of carbide fraction and matrix microstructure on the wear of cast iron balls tested in a laboratory ball mill," *Wear*, vol. 250, no. 1-12, pp. 492-501, 2001.
- [39] I. R. Sare, *Abrasion resistance and fracture toughness of white cast irons* (Metals Technology). Maney Publishing, 1979, pp. 412-419.
- [40] Ö. N. Doğan, J. A. Hawk, and G. Laird II, "Solidification structure and abrasion resistance of high chromium white irons," *Metallurgical and Materials Transactions A* vol. 28, no. 6, pp. 1315-1328, 1997.
- [41] R. J. Chung, X. Tang, D. Y. Li, B. Hinckley, and K. Dolman, "Effects of titanium addition on microstructure and wear resistance of hypereutectic high chromium cast iron Fe-25wt.%Cr-4wt.%C," *Wear*, vol. 267, no. 1-4, pp. 356-361, 2009.

- [42] X. H. Tang, R. Chung, C. J. Pang, D. Y. Li, B. Hinckley, and K. Dolman, "Microstructure of high (45 wt.%) chromium cast irons and their resistances to wear and corrosion," *Wear*, vol. 271, no. 9–10, pp. 1426-1431, 2011.
- [43] A. Misra and I. Finnie, "A classification of three-body abrasive wear and design of a new tester," *Wear*, vol. 60, no. 1, pp. 111-121, 1980.
- [44] C. P. Tabrett, I. R. Sare, and M. R. Ghomashchi, "Microstructure-property relationships in high chromium white iron alloys," *International Materials Reviews*, vol. 41, no. 2, pp. 59-82, 1996.
- [45] H.S. Avery, *Surface protection against wear and corrosion*. American Society for Metals, 1954.
- [46] H.S. Avery, "The measurement of wear resistance," *Wear*, vol. 4, no. 6, pp. 427-449, 1961.
- [47] Ö. N. Doğan and J. A. Hawk, "Effect of carbide orientation on abrasion of high Cr white cast iron," *Wear*, vol. 189, no. 1–2, pp. 136-142, 1995.
- [48] Y. Matsubara, N. Sasaguri, K. Shimizu, S. Yu, and K. Yu, "Solidification and abrasion wear of white cast irons alloyed with 20% carbide forming elements," *Wear*, vol. 250, no. 1–12, pp. 502-510, 2001.
- [49] E.R. Booser, *Tribology Data Handbook: An Excellent Friction, Lubrication, and Wear Resource*. CRC Press, 1997.
- [50] Y. Yokomizo, N. Sasaguri, K. Nanjo, and Y. Matsubara, "Relationship between

Continuous Cooling Transformation Behavior and Chromium Content of Multi-component White Cast Iron," *Journal of Japan Foundry Engineering Society*, vol. 74, no. 11, pp. 691-698, 2002.

[51] H. Yamagata, "The crankshaft," in *The Science and Technology of Materials in Automotive Engines*, H. Yamagata, Ed.: Woodhead Publishing, 2005, pp. 165-206.

[52] P. Aungsupaitoon, "Abrasion wear behavior of hypoeutectic 16 mass% chromium cast iron containing molybdenum," Master's Degree, Metallurgical Engineering, Chulalongkorn University, 2008.

[53] M. Izciler and H. Çelik, *Two- and three-body abrasive wear behaviour of different heat-treated boron alloyed high chromium cast iron grinding balls*. 2000, pp. 237-245.

[54] S. Inthidech, A. Chooprajong, P. Sricharoenchai, and Y. Matsubara, "Two-Body and Three-Body Types Abrasive Wear Behavior of Hypoeutectic 26 mass% Cr Cast Irons with Molybdenum," *MATERIALS TRANSACTIONS*, vol. 53, no. 7, pp. 1258-1266, 2012.



Appendix

จุฬาลงกรณ์มหาวิทยาลัย
CHULALONGKORN UNIVERSITY

Macro-hardness, micro-hardness and volume fraction of retained austenite (V_γ) of specimens at 1323K austenitizing temperature.

Specimen No.	Tempering temperature, K	Macro-hardness, HV30	Micro-hardness, HV0.1	Volume fraction of retained austenite, %
Specimen No.1 (3.09%Cr)	As-hardened	919.4	858.0	13.9
	673	788.4	734.2	3.4
	723	806.4	753.0	2.7
	748	818.2	763.0	2.1
	773	826.6	773.0	1.9
	798	840.8	794.0	1.7
	823	815.6	764.0	1.5
	873	745.0	692.8	1.5
Specimen No.2 (4.98%Cr)	As-hardened	931.2	872.4	17.5
	673	831.8	768.0	14.1
	723	843.4	794.0	11.5
	748	866.2	809.0	10.1
	773	905.0	839.6	7.9
	798	913.4	861.6	2.9
	823	866.2	800.2	1.3
	873	744.0	684.2	1.1
Specimen No.3 (5.99%Cr)	As-hardened	922.2	860.4	16.1
	673	838.4	798.0	10.7
	723	851.8	807.8	8.8
	748	877.4	825.2	7.9
	773	909.2	840.6	3.6
	798	887.2	835.2	2.0
	823	857.2	803.2	1.2
	873	693.0	640.2	1.1

Specimen No.	Tempering temperature, K	Macro-hardness, HV30	Micro-hardness, HV0.1	Volume fraction of retained austenite, %
Specimen No.4 (7.01%Cr)	As-hardened	913.4	850.8	10.6
	673	842.0	790.0	7.1
	723	853.2	802.2	6.8
	748	869.0	818.8	6.7
	773	906.4	849.6	3.8
	798	891.4	839.8	1.7
	823	858.4	807.8	1.1
	873	630.0	577.4	0.2
Specimen No.5 (8.93%Cr)	As-hardened	887.2	839.6	6.9
	673	786.0	744.4	4.1
	723	823.0	780.0	3.3
	748	834.6	798.2	3.0
	773	839.6	807.8	1.2
	798	834.6	796.0	1.0
	823	811.4	754.0	0.9
	873	610.8	551.6	0.9

Macro-hardness, micro-hardness and volume fraction of retained austenite (V_γ) of specimens at 1373K austenitizing temperature.

Specimen No.	Tempering temperature, K	Macro-hardness, HV30	Micro-hardness, HV0.1	Volume fraction of retained austenite, %
Specimen No.1 (3.09%Cr)	As-hardened	901.0	841.3	11.9
	673	844.8	802.2	9.1
	723	862.0	812.2	8.7
	748	876.0	826.4	5.8
	773	885.8	835.2	4.7
	798	901.8	852.0	2.3
	823	860.8	808.8	1.5
	873	806.4	751.0	1.2
Specimen No.2 (4.98%Cr)	As-hardened	909.2	853.8	24.1
	673	824.2	775.0	22.2
	723	836.0	792.0	17.3
	748	858.4	813.2	16.6
	773	888.6	844.0	12.8
	798	932.6	885.6	4.4
	823	890.0	842.8	2.0
	873	772.6	727.8	1.2
Specimen No.3 (5.99%Cr)	As-hardened	900.2	844.2	23.2
	673	830.4	791.0	20.2
	723	849.0	806.6	15.0
	748	880.2	834.2	13.3
	773	928.4	877.2	4.6
	798	913.4	859.2	2.0
	823	887.2	833.0	1.2
	873	749.6	703.6	1.3

Specimen No.	Tempering temperature, K	Macro-hardness, HV30	Micro-hardness, HV0.1	Volume fraction of retained austenite, %
Specimen No.4 (7.01%Cr)	As-hardened	897.2	839.6	20.1
	673	834.6	776.0	14.1
	723	871.8	817.8	14.1
	748	884.4	852.0	12.7
	773	917.6	873.6	4.8
	798	907.8	862.8	2.8
	823	885.8	842.8	2.4
	873	717.0	655.4	1.0
Specimen No.5 (8.93%Cr)	As-hardened	870.4	826.4	11.8
	673	806.4	759.0	11.1
	723	820.6	770.0	10.2
	748	839.6	798.2	6.5
	773	864.8	825.2	2.1
	798	859.6	810.0	1.3
	823	838.4	790.0	0.8
	873	654.0	608.0	0.5

Wear loss (W_l) and wear distance (W_d) of specimen at 1323K austenitizing temperature. Suga abrasive wear test.

Specimen No.	Wear distance (W_d), m	Wear loss (W_l), mg			
		As-hardened	L- H_{Tmax}	H_{Tmax}	H- H_{Tmax}
Specimen No.1 (3.09%Cr)	24	9.5	8.8	10.0	10.2
	48	18.6	17.5	18.2	19.7
	72	25.7	25.5	26.2	28.5
	96	33.1	33.2	33.8	37.0
	120	39.6	41.2	41.7	45.2
	144	45.6	49.9	49.7	53.7
	168	51.9	58.0	57.6	62.6
	192	57.0	66.2	65.7	71.4
Specimen No.2 (4.98%Cr)	24	9.3	10.3	9.0	9.6
	48	16.9	17.5	15.6	16.8
	72	23.6	23.7	21.9	23.6
	96	29.8	30.6	28.1	30.5
	120	35.6	37.3	34.4	36.6
	144	41.2	43.5	40.1	43.5
	168	46.5	49.6	45.9	50.3
	192	51.9	55.5	52.1	57.2

Specimen No.	Wear distance (W _d), m	Wear loss (W _i), mg			
		As-hardened	L-H _{Tmax}	H _{Tmax}	H-H _{Tmax}
Specimen No.3 (5.99%Cr)	24	8.8	8.9	8.0	8.5
	48	16.1	16.4	15.0	15.4
	72	22.2	23.3	20.9	22.2
	96	28.0	29.8	26.8	28.8
	120	33.7	36.5	32.7	35.3
	144	39.3	42.8	38.7	42.3
	168	44.8	49.5	44.8	48.6
	192	50.0	56.2	51.1	55.4
Specimen No.4 (7.01%Cr)	24	8.2	8.8	9.9	8.2
	48	14.9	16.3	17.1	15.1
	72	21.2	23.2	23.2	21.4
	96	27.7	29.9	29.0	27.2
	120	32.9	37.0	34.5	34.0
	144	38.4	43.5	40.6	40.2
	168	44.6	50.3	46.3	46.6
	192	49.7	57.1	52.0	52.9

Specimen No.	Wear distance (W _d), m	Wear loss (W _i), mg			
		As-hardened	L-H _{Tmax}	H _{Tmax}	H-H _{Tmax}
Specimen No.5 (8.93%Cr)	24	9.0	9.3	9.6	8.7
	48	16.0	17.3	17.0	15.6
	72	22.3	24.3	23.5	22.3
	96	29.0	31.4	29.5	29.0
	120	35.3	39.2	35.6	35.8
	144	41.6	46.4	42.3	42.5
	168	47.5	53.5	48.3	49.4
	192	54.6	61.0	54.8	56.6

Wear loss (W_l) and wear distance (W_d) of specimen at 1373K austenitizing temperature. Suga abrasive wear test.

Specimen No.	Wear distance (W_d), m	Wear loss (W_l), mg			
		As-hardened	L- H_{Tmax}	H_{Tmax}	H- H_{Tmax}
Specimen No.1 (3.09%Cr)	24	8.3	9.9	7.7	9.0
	48	15.0	18.4	14.5	16.5
	72	20.4	26.3	21.2	23.6
	96	26.0	33.6	28.0	30.3
	120	30.9	40.8	34.6	37.1
	144	35.6	48.1	41.4	43.7
	168	40.4	55.1	47.7	50.7
	192	45.4	62.1	54.7	57.3
Specimen No.2 (4.98%Cr)	24	8.2	7.5	8.2	7.3
	48	15.2	13.6	14.8	14.0
	72	20.9	19.6	20.4	20.6
	96	25.8	25.3	25.6	27.2
	120	30.8	30.6	31.0	33.4
	144	35.8	36.3	36.3	39.9
	168	40.2	42.6	42.0	46.4
	192	44.6	48.1	46.7	52.6

Specimen No.	Wear distance (W _d), m	Wear loss (W _i), mg			
		As-hardened	L-H _{Tmax}	H _{Tmax}	H-H _{Tmax}
Specimen No.3 (5.99%Cr)	24	7.8	7.8	8.0	6.1
	48	14.2	14.7	14.2	12.6
	72	19.6	20.5	19.4	19.1
	96	24.5	26.3	24.9	24.6
	120	29.2	31.6	29.8	31.7
	144	33.9	37.0	34.8	37.8
	168	38.5	42.7	40.1	44.1
192	43.1	47.8	45.2	50.4	
Specimen No.4 (7.01%Cr)	24	8.8	7.9	8.2	8.1
	48	14.5	14.9	14.4	14.8
	72	20.1	20.8	19.5	21.4
	96	25.3	26.7	24.9	27.4
	120	30.4	32.6	30.4	33.0
	144	35.0	38.3	35.5	39.0
	168	40.8	43.7	40.6	45.3
192	45.1	49.7	45.9	51.5	

Specimen No.	Wear distance (W _d), m	Wear loss (W _i), mg			
		As-hardened	L-H _{Tmax}	H _{Tmax}	H-H _{Tmax}
Specimen No.5 (8.93%Cr)	24	8.3	8.2	8.4	8.6
	48	15.4	14.7	14.4	15.6
	72	21.7	21.1	20.7	21.4
	96	27.2	27.1	26.3	27.5
	120	32.8	33.4	32.1	33.3
	144	38.2	39.7	37.8	39.5
	168	43.3	45.7	43.3	45.4
	192	48.5	51.5	49.1	51.6

Wear loss (W_l) and wear distance (W_d) of specimen at 1323K austenitizing temperature. Rubber wheel abrasive wear test.

Specimen No.	Wear distance (W_d), m	Wear loss (W_l), mg			
		As-hardened	L- $H_{T_{max}}$	$H_{T_{max}}$	H- $H_{T_{max}}$
Specimen No.1 (3.09%Cr)	785	101.1	155.2	147.2	150.9
	1570	185.4	285.7	273.0	281.4
	2355	264.7	409.3	391.1	404.9
	3140	341.1	530.8	502.2	521.0
Specimen No.2 (4.98%Cr)	785	78.9	102.7	92.4	114.0
	1570	148.1	195.7	177.0	219.7
	2355	214.4	283.9	250.7	317.4
	3140	279.4	372.0	335.9	410.4
Specimen No.3 (5.99%Cr)	785	64.4	77.7	67.9	75.0
	1570	119.1	154.7	132.9	141.9
	2355	171.1	227.0	196.5	207.3
	3140	223.0	299.9	259.6	270.8

Specimen No.	Wear distance (W_d), m	Wear loss (W_l), mg			
		As-hardened	L- H_{Tmax}	H_{Tmax}	H- H_{Tmax}
Specimen No.4 (7.01%Cr)	785	72.7	84.5	71.8	77.2
	1570	139.5	161.2	141.0	152.0
	2355	204.2	235.2	209.6	225.9
	3140	267.0	307.7	277.6	298.4
Specimen No.5 (8.93%Cr)	785	73.2	88.8	88.8	90.5
	1570	139.6	172.9	168.1	174.7
	2355	203.6	253.8	243.1	254.4
	3140	267.0	331.0	315.7	333.3

Wear loss (W_l) and wear distance (W_d) of specimen at 1373K austenitizing temperature. Rubber wheel abrasive wear test.

Specimen No.	Wear distance (W_d), m	Wear loss (W_l), mg			
		As-hardened	L- H_{Tmax}	H_{Tmax}	H- H_{Tmax}
Specimen No.1 (3.09%Cr)	785	84.2	104.4	90.6	107.0
	1570	148.7	205.9	180.6	211.0
	2355	207.5	315.0	267.5	305.6
	3140	271.1	413.5	354.4	393.3
Specimen No.2 (4.98%Cr)	785	66.8	80.6	69.5	84.4
	1570	129.2	158.1	134.9	162.0
	2355	188.3	234.6	199.8	238.0
	3140	246.9	307.7	263.8	312.0
Specimen No.3 (5.99%Cr)	785	58.0	73.5	59.4	67.0
	1570	108.2	143.9	116.4	131.5
	2355	157.3	203.0	173.0	194.2
	3140	205.2	270.1	228.2	256.0

Specimen No.	Wear distance (W_d), m	Wear loss (W_l), mg			
		As-hardened	L- H_{Tmax}	H_{Tmax}	H- H_{Tmax}
Specimen No.4 (7.01%Cr)	785	62.5	68.0	60.2	67.0
	1570	121.1	135.4	117.7	129.9
	2355	177.6	202.1	180.4	191.7
	3140	232.9	267.7	238.7	253.5
Specimen No.5 (8.93%Cr)	785	63.1	76.9	63.9	71.0
	1570	121.3	150.4	125.8	137.4
	2355	178.6	223.2	190.0	203.6
	3140	234.2	292.8	252.0	271.1

VITA

NAME Jatupon Opapaiboon

DATE OF BIRTH 31 January 1989

PLACE OF BIRTH Lopburi

HOME ADDRESS 91/1384 Soi.Nuanchan56/1 Nuanchan rd., Nuanchan,
Bungkum, Bangkok 10230 Thailand

PUBLICATION

1. Effect of Chromium Content on Heat Treatment Behavior of Multi-alloyed White Cast Iron for Abrasive Wear Resistance
2. Effect of chromium content on the three-body-type abrasive wear behavior of multi-alloyed white cast iron



จุฬาลงกรณ์มหาวิทยาลัย
CHULALONGKORN UNIVERSITY